Characterisation and Engineering of Alkene Producing P450 Peroxygenases for Bioenergy Applications

A thesis submitted to the University of Manchester for the degree of Doctor of Philosophy in the Faculty of Science and Engineering

2016

Sarah Matthews

School of Chemistry

Table of Contents

List of Figures……..……6

List of Tables……..……9

Abbreviations……..……...10

Declaration……..……13

Copyright statement……..……14

Acknowledgements……..……15

Preface to the alternative thesis……..……16

Abstract……..……20

1.0 Chapter 1: Introduction……..21

1.1 The Biofuels Industry……..……..21

1.2 Hydrocarbon Biosynthesis In Microorganisms……..…21

1.3 Cytochromes P450: An Overview……..25

1.4 History of Cytochromes P450……..……..25

1.5 Cytochrome P450 Structure……..……..26

1.6 Redox Partners……..…28

1.7 The Cytochrome P450 Catalytic Cycle……..……30

1.7a Substrate Binding……31

1.7b Reduction of Ferric (Fe^{III}) to Ferrous (Fe^{II}) Heme Iron……..……31

1.7c Binding of Dixoxygen to Fe^{II} Heme Iron ……..……32

1.7d Second Electron Transfer to the Ferric-Superoxy Complex……..33

1.7e Protonation of the Ferric-Peroxy Species……33

1.7f Protonation of the Ferric-Hydroperoxy Intermediate Resulting in the .Formation of the Ferryl-Oxo Intermediate (Compound I)……..……34

1.7g Spectroscopic Properties of the Ferryl-Hydroxo Compound II……35

1.7h Ineffeciency in the P450 Catalytic Cycle and the Peroxide Shunt……..…36

1.8 P450 Peroxygenases……..…37

1.9 P450 Peroxygenases and P450 Evolution……..…….37

1.10 Homolytic and Heterolytic Cleavage of the Peroxy O-O Bond……..38

1.11 P450 Peroxygenase Structure……39

1.12 The Discovery of $OleT_{JE}$, a Fatty Acid Decarboxylase……..……..43

1.13 Mechanistic Analysis of $OleT_{JE}$……..……..48

1.14 Engineering of $OleT_{JE}$.....51

1.15 References……..……52

2.0 Chapter Two: Structure and Biochemical Properties of the Alkene Producing $OleT_{JE}$ (CYP152L1) from *Jeotgalicoccus* sp. 8456…..67

2.1 Abstract……..68

2.2 Introduction……..……..86

2.3 Experimental Procedures……71

2.3.1 Bioinformatics……..71

2.3.2 Expression and Purification of $OleT_{JE}$……72

2.3.3 UV-Visible Spectroscopy……74

2.3.4 Fatty Acid and Inhibitor Binding Titrations with $OleT_{JE}$.....74

2.3.5 Stopped-Flow Analysis of Substrate Turnover……..……75

2.3.6 Redox Potentiometry…… 76

2.3.7 EPR/ENDOR Analysis of $OleT_{JE}$.....76

2.3.8 Crystallography of $OleT_{JE}$……..78

2.3.9 Analysis of Products Formed by $OleT_{JE}$ in reactions with H_2O_2 and Fatty Acids……..…78

2.4 Results……78

2.4.1 Classification of $OleT_{JE}$ as CYP152L1……..……..78

2.4.2 Expression and Purification of $OleT_{JE}$……..79

2.4.3 UV-Visible Absorption Properties of $OleT_{JE...}$……..……..81

2.4.4 Analysis of Substrate and Inhibitor Binding to $OleT_{JE}$……83

2.4.5 Determination of the Heme Iron Redox Potentials of Substrate-Free and Substrate-Bound $OleT_{JE}$……86

2.4.6 Stopped-Flow Analysis of $OleT_{JE}$ Turnover Kinetics……..88

2.4.7 EPR Analysis of $OleT_{JE}$……..89

2.4.8 $OleT_{JE}$ Catalysed Substrate Turnover……..……91

2.4.9 Crystal Structure of $OleT_{JE}$……..……..92

2.5 Discussion……..……95

2.6 References……..100

3.0 Chapter Three: Interrogation of the Fatty Acid Carboxylate-Binding Site in the Alkene Producing Cytochrome P450 Peroxygenase $OleT_{JE}$……...107

3.1 Abstract……108

3.2 Introduction…….....108

3.3 Experimental Procedures……..114

3.3.1 Expression and Purification of $OleT_{JE}$ and $OleT_{JE}$ Mutants……114

3.3.2 UV-Vis Spectroscopy of WT and Mutant $OleT_{JE}$ hemoproteins....116

3.3.3 Fatty Acid Binding Titrations with $OleT_{JE}$ Mutants……..……116

3.3.4 Stopped-Flow Kinetic Analysis of Substrate Oxidation by $OleT_{JE}$ WT and Mutant Enzymes……..……..117

3.3.5 EPR Analysis of $OleT_{JE}$ Mutants……117

3.3.6 Crystallography of the $OleT_{JE}$ H85Q and $OleT_{JE}$ F79A Mutants...118

3.3.7 Fatty Acid Substrate Conversion Reactions with WT and Mutant $OleT_{JE}$ Enzymes……...118

3.3.8 Characterization of Fatty Acid Oxidation Products using GC/MS.120

3.4 Results……120

3.4.1 Expression and Purification of $OleT_{JE}$ and $OleT_{JE}$ Mutants…....120

3.4.2 UV-Visible Absorbance Properties of $OleT_{JE}$ Mutants……..122

3.4.3 Interactions of WT and Mutant $OleT_{JE}$ proteins with Fatty Acid Substrates……..……124

3.4.4 Stopped-Flow and Kinetic Analysis of Fatty Acid Oxidation by WT and Mutant $OleT_{JE}$ P450s……127

3.4.5 Characterisation of $OleT_{JE}$ WT and Mutant P450 Heme Coordination by EPR……128

3.4.6 Products Formed by Novel $OleT_{JE}$ Mutants……..……131

3.4.7 Structural Properties of $OleT_{JE}$ Mutant Enzymes……..……..135

3.5 Discussion……...136

3.6 References……...…141

4.0 Chapter Four: Driving Alkene Production in the Peroxygenase P450 $OleT_{JE}$ Using a Novel Hydrogen Peroxide-Producing Fusion Protein System……..146

4.1 Abstract……147

4.2 Introduction……..147

4.3 Materials and methods……..151

4.3.1 Gene Cloning……151

4.3.2 Gene Expression and Protein Purification……152

4.3.3 Purification of $OleT_{JE}$, $OleT_{JE}$-HRV3C-AldO, $OleT_{JE}$-αhelix-AldO and P450 BM3……..…152

4.3.4 Hydrogen Peroxide Tolerance of P450 Enzymes……153

4.3.5 *In Vitro* Substrate Turnover Reactions with Fusion Proteins…….154

4.3.6 *In Vitro* $OleT_{JE}$ Enzymatic Reactions with Products……...155

4.3.7 GC/Q-TOF……..155

4.3.8 Fusion Protein Kinetics……155

4.4 Results……..156

4.4.1 Hydrogen Peroxide Tolerance……156

4.4.2 Construction of $OleT_{JE}$-HRV3C-AldO and $OleT_{JE}$-αhelix-AldO Fusion Proteins……..156

4.4.3 Driving Decarboxylation of Fatty Acids With Different AldO Substrates……..158

4.4.4 Time-Dependent Oxidation of Fatty Acids using Fusion Proteins.160

4.4.5 Optimising Glycerol Concentration……..…162

4.4.6 Secondary Turnover of 2-OH Myristic Acid and 3-OH Myristic Acid Products……163

4.5 Discussion……164

4.6 References……166

5.0 Chapter Five: Catalytic and Structural Properties of the Peroxygenase Cytochrome P450 KR from *Kocuria rhizophila*……170

5.1 Abstract……171

5.2 Introduction……171

5.3 Materials and Methods……175

5.3.1 P450 KR Gene Expression……175

5.3.2 Protein Purification……176

5.3.3 UV-Visible Spectroscopy……177

5.3.4 Fatty Acid Inhibitor Binding Titrations……177

5.3.5 Redox Potentiometry……178

5.3.6 EPR Analysis of P450 KR……179

5.3.7 Fatty Acid Biotransformation by P450 KR……179

5.3.8 Analysis of Products using GC/MS……180

5.4 Results……181

5.4.1 Expression and Purification of P450 KR……181

5.4.2 UV-Visible Spectroscopic Analysis of P450 KR……182

5.4.3 Fatty Acid Substrate Binding Analysis……185

5.4.4 Heme Iron Redox Potential of P450 KR……187

5.4.5 EPR Analysis of P450 KR……188

5.4.6 Fatty Acid Conversion by P450 KR……190

5.5 Discussion……192

5.6 References……194

6.0 Chapter 6: Conclusions……200

6.1 Summary……200

6.2 Further Work……213

6.3 References……215

List of figures

Figure 1.1 Pathways for Fatty Acid-Based Alkene Production……22

Figure 1.2 Structural Similarity of Cytochrome P450 Enzymes……..…27

Figure 1.3 P450 Catalytic Cycle……..….30

Figure 1.4 Oxygen Rebound Mechanism of Substrate Hydroxylation by Cytochromes P450 ……...35

Figure 1.5 Catalytic Pathways of $OleT_{JE}$……50

Figure 2.1 The Cytochrome P450 Catalytic Cycle……69

Figure 2.2 Phylogenetic Tree of $OleT_{JE}$ and Other Members of the CYP152 P450 Family...79

Figure 2.3 Purification of $OleT_{JE}$……...80

Figure 2.4 UV-Visible Spectroscopic Features of $OleT_{JE}$……81

Figure 2.5 Analysis of Fatty Acid and Dithiothreitol to $OleT_{JE}$……84

Figure 2.6 Determination of the $OleT_{JE}$ Heme Iron Reduction Potential in its Substrate-Free and Arachidic Acid-Bound Forms……86

Figure 2.7 Stopped-Flow Kinetics of H_2O_2-dependent Oxidation of Substrate-Bound $OleT_{JE}$……...88

Figure 2.8 EPR Spectroscopic Analysis of $OleT_{JE}$…….....89

Figure 2.9 Oxidative Decarboxylation of Arachidic Acid and Lauric Acid by $OleT_{JE}$……90

Figure 2.10 Comparison Between the $OleT_{JE}$ and $P450_{BS\beta}$ P450 Structures……..……92

Figure 2.11 Comparison of the $OleT_{JE}$ and $P450_{BS\beta}$ Fatty Acid Binding Modes……..93

Figure 2.12 Detailed View of the $OleT_{JE}$ Active Site……..……..93

Figure 2.13 Proposed Mechanism for $OleT_{JE}$…….....……..96

Figure 3.1 The $OleT_{JE}$ Catalytic Cycle……..……109

Figure 3.2 Alignment of $OleT_{JE}$ with other Bacterial Peroxygenase P450s……111

Figure 3.3 Purification of WT and Active Site Mutants of $OleT_{JE}$……121

Figure 3.4 UV-Visible Spectroscopy of $OleT_{JE}$ and Key Active Site Mutants……122

Figure 3.5 Fatty Acid Binding Titrations with WT and Mutant $OleT_{JE}$ Proteins……..124

Figure 3.6 EPR Spectroscopic Properties of WT and Mutant Forms of $OleT_{JE}$……..…130

Figure 3.7 Products of Fatty Acid Turnover from WT and Mutant $OleT_{JE}$ Enzymes……..…132

Figure 3.8 Active Site Structures for WT and Mutant $OleT_{JE}$ Proteins……135

Figure 4.1 P450 Catalytic Cycle and Active Site Structure of $OleT_{JE}$……..148

Figure 4.2 Schematic of $OleT_{JE}$/AldO Constructs……...150

Figure 4.3 P450 H_2O_2 Tolerance…… ..156

Figure 4.4 SDS-PAGE Analysis of Purified $OleT_{JE}$ Fusion Proteins……158

Figure 4.5 GC/MS Chromatogram Showing Products Formed by the $OleT_{JE}$-αhelix-AldO Fusion Protein with Myristic Acid Substrate……159

Figure 4.6 Time Dependence of Myristic Acid Conversion and Product Formation at 1% Glycerol……..161

Figure 4.7 Secondary Turnover of Primary Hydroxylated Products from $OleT_{JE}$-mediated Myristic Oxidation……163

Figure 5.1 The Cytochrome P450 Catalytic Cycle……..171

Figure 5.2 Purification and UV-Visibile Spectroscopic Characterisation of P450 KR ……181

Figure 5.3 Titration of Imidazole into Capric Acid-Bound P450 KR…… ……182

Figure 5.4 Fatty Acid Binding to P450 KR…… ……...184

Figure 5.5 Heme Iron Redox Potentials For Substrate-Free and Capric Acid-Bound Forms of P450 KR…… ……186

Figure 5.6 EPR Spectroscopy of P450 KR…… 189

Figure 5.7 Fatty Acid Conversion by P450 KR……190

List of Tables

Table 2.1 Data Reduction and Final Structural Refinement Statistics for the Substrate-Free $OleT_{JE}$ P450 and for its Arachidic Acid Substrate Complex……77

Table 2.2 Determination of the affinity of $OleT_{JE}$ for long chain fatty acids……...83

Table 3.1 Data Reduction and Final Structural Refinement Statistics for $OleT_{JE}$ WT and Mutant Crystal……..…119

Table 3.2 Binding Affinity of Saturated Fatty Acids for WT and Mutant Forms of $OleT_{JE}$..126……126

Table 3.3 EPR g-Values for Substrate-Free and Fatty Acid-Bound Forms of WT and Mutant $OleT_{JE}$ Proteins ……131

Table 3.4 Conversion of Fatty Acid Substrates into Alkene and Hydroxylated Fatty Acid Products by WT and Mutant $OleT_{JE}$ Enzymes……133

Table 4.1 Rates of Oxidative Modification of $OleT_{JE}$ and P450 BM3 Heme by H_2O_2……157

Table 4.2 $OleT_{JE}$-Dependent Oxidation of Myristic Acid with Different Substrates……...160

Table 4.3 Myristic Acid Conversion of $OleT_{JE}$ Fusion Enzymes and Products Formed……162

Table 5.1 Dissociation Constants (K_d values) for the Binding of P450 KR to fatty acids….185

Table 5.2 P450 Conversion of Myristic Acid (0.5mM) using Different Hydrogen Peroxide Delivery Systems……..191

List of Abbreviations

A – Absorbance

Å – Ångstrom

AldO – Alditol Oxidase from *Streptomyces coelicor*

BSTFA – N,O-bis(trimethylsilyl)trifluoroacetamide containing 1% trimethylchlorosilane

Cpd 0 – Compound 0

Cpd I – Compound I

Cpd II – Compound II

CPR – Cytochrome P450 Reductase

CT- Charge Transfer

ΔALA – δ-aminolevulinic acid

DCM – Dicholormethane

DFT – Density Functional Theory

DT – Dithionite

DTT – Dithiothreitol

EDTA – Ethylenediamineetetraacetate

ENDOR – Electron Nuclear Double Resonance

EPR – Electron Paramagnetic Resonance

ER – Endoplasmic Reticulum

FAD - Flavin Adenine Dinucleotide

FDH – Formate Dehydrogenase

FdR – Ferredoxin Reductase

FdX – Ferredoxin

FMN – Flavin Mononucleotide

FTIR – Fourier Transform Infrared Spectroscopy

GC/MS – Gas Chromotography Mass Spectrometry

GC/Q-TOF – Gas Chromotography Quadrapole Time of Flight

GDH – Glucose Dehydrogenase

HS – High Spin (S = 5/2)

Int2 – Second Intermediate

IPTG – Isopropyl 1-thio-b-D-galactopyranoside

Kd – Dissociation Constant

KIE – Kinetic Isotope Effect

LS – Low Spin (S = 1/2)

μM – Micromolar

mM – Millimolar

M – Molar

mV – Millivolt

MWCO – Molecular Weight Cutoff

NAD(P)H – Nicotinamide Adenine Dinucleotide (phosphate)

NHE – Normal Hydrogen Electrode

Ni-NTA – Nickel Nitrilotriacetic Acid

nM – nanomolar

Ole-I – $OleT_{JE}$ Compound I

$OleT_{JE}$ – Cytochrome P450 OleTJE CYP152L1 from *Jeogalicoccus* sp. 8456

P450 BM3 – Cytochrome P450 BM3 (CYP102A1) from *Bacillus megaterium*

P450 BSβ - P450 BSβ (CYP152A1) from *Bacillus subtilis*

P450 CAM – Cytochrome P450 CAM (CYP101A1) from *Pseudomonas putida*

P450 KR – Cytochrome P450 from *Kocuria rhizophila*

P450 SPα - P450 SPα (CYP152B1) from *Sphingomonas paucimobilis*

PDA – Photon Diode Array

PDH – Phosphite Dehydrogenase

PDOR – Phthalate Dioxygenase Reductase

PdR – Putidaredoxin reductase

PdX – Putidaredoxin

pKa – Isoelectric Point

PMT – Photon Multiplier Tube

ROS – Reactive Oxygen Species

TAG – Triacylglycerol

V – Volt

Declaration

No portion of the work referred to in the thesis has been submitted in support of an application for another degree or qualification of this or any other university or other institute of learning.

Copyright statement

i. The author of this thesis (including any appendices and/or schedules to this thesis) owns certain copyright or related rights in it (the "Copyright") and s/he has given The University of Manchester certain rights to use such Copyright, including for administrative purposes.

ii. ii. Copies of this thesis, either in full or in extracts and whether in hard or electronic copy, may be made only in accordance with the Copyright, Designs and Patents Act 1988 (as amended) and regulations issued under it or, where appropriate, in accordance with licensing agreements which the University has from time to time. This page must form part of any such copies made.

iii. iii. The ownership of certain Copyright, patents, designs, trade marks and other intellectual property (the "Intellectual Property") and any reproductions of copyright works in the thesis, for example graphs and tables ("Reproductions"), which may be described in this thesis, may not be owned by the author and may be owned by third parties. Such Intellectual Property and Reproductions cannot and must not be made available for use without the prior written permission of the owner(s) of the relevant Intellectual Property and/or Reproductions. iv. Further information on the conditions under which disclosure, publication and commercialisation of this thesis, the Copyright and any Intellectual Property University IP Policy (see http://documents.manchester.ac.uk/display.aspx?DocID=24420), in any relevant Thesis restriction declarations deposited in the University Library, The University Library's regulations (see http://www.library.manchester.ac.uk/about/regulations/) and in The University's policy on Presentation of Theses

Acknowledgements

Firstly I would like to thank my supervisor Andrew Munro for giving me the opportunity to carry out my PhD, and for the guidance I have received throughout the process. I would also like to thank him for the amazing experiences that have come with this PhD including travelling to Tokyo and Vancouver to present my work at the 19th International Conference on Cytochrome P450 and the 13th International Symposium on Cytochrome P450 Biodiversity and Biotechnology

I would like to acknowledge the BBSRC and Agilent, who provided funding. Without them this work would not have been possible.

I am hugely grateful to everyone that has helped me over the course of my PhD, especially Kirsty Mclean, Jim Belcher, Lang Lan Tee, Nik Rattray, Hazel Girvan, Marina Golovanova, Derren Heyes, Colin Levy and David Leys. I feel so lucky to have been part of the Munro group, who are all such amazing people, and I believe that I have made friends for life.

I would also like to thank all those at Agilent that have provided me with assistance, including Richard Blankley, John Doel, Alan Lewis , Michael Baynham, Donna Potts and Bernhard Rottweiler.

Lastly I would like to thank all of my family for all their support. Especially my Mum for all her love and everything she has done for me, Max for always being so supportive and understanding, and my Grandma and Grandpa for encouraging me to get 10/10 on my spelling and maths tests.

Preface to the alternative format thesis

This thesis has been presented in the format of a University of Manchester's alternative style PhD thesis. This allows data to be included in the format of papers that have already been published, or have been prepared for publication. Each results chapter has been prepared in the format required for journal submission. This gives an overall structure of: abstract, introduction, four results chapters and summary/further work. Each section has a self-contained set of references. For consistency, text formatting, figure/table numbering and page numbering have been altered to incorporate the whole thesis.

The alternative format thesis reduces conflict between publishing scientific papers and writing a conventional format thesis. In addition, the alternative style PhD thesis also promotes a collaborative approach to scientific research, which ultimately is beneficial for research as a whole. As part of the alternative format, the individual contributions of each co-author has been detailed below.

Papers Included as Results Chapters

Chapter Two

Belcher, J., McLean, K. J., Matthews, S., Woodward, L. S., Fisher, K., Rigby, S. E., Nelson, D. R., Potts, D., Baynham, M. T., Parker, D. A., Leys, D., and Munro, A. W. (2014) Structure and biochemical properties of the alkene producing cytochrome P450 OleTJE (CYP152L1) from the Jeotgalicoccus sp. 8456 bacterium. *J Biol Chem* **289**, 6535-6550

Chapter Three

Matthews S, Belcher JD, Tee KL, Girvan HM, McLean KJ, Rigby SE, Levy CW, Leys D, Parker DA, Blankley RT, Munro AW. (2017) Catalytic Determinants of Alkene Production by the Cytochrome P450 Peroxygenase $OleT_{JE}$. Journal of Biological Chemistry jbc-M116

Chapter Four

Matthews S, Tee KL, Rattray NJ, McLean KJ, Leys D, Parker DA, Blankley RT, Munro AW. (2017) Production of alkenes and novel secondary products by P450 OleTJE using novel H2O2-generating fusion protein systems. *FEBS letters*. 591: 737-750.

Chapter Five

Tee, K.L., Matthews, S., McLean, K.J., Girvan, H.M., Rigby, S.E., Matak-Vinkovic, D., Leys, D., Blankley, R.T., Munro, A.W. (2016) Catalytic and structural properties of the peroxygenase cytochrome P450 KR from *Kocuria rhizophila. Awaiting further data before publishing*

Contributions from Authors

As a supervisor, Andrew W. Munro contributed to data analysis and manuscript preparation for all papers

Chapter Two

Belcher, J. performed cloning; enzyme purification; fatty acid binding titrations; stopped-flow kinetic analysis; *in vitro* turnover reactions with arachidic acid (C20:0); prepared crystals for X-Ray crystallography

McLean, K.J. and Woodward, L. S. performed enzyme purification; inhibitor binding (CO and cyanide binding); redox poteniometry

Matthews, S performed enzyme purification; inhibitor binding with dithiothreitol (DTT); prepared samples for electron paramagnetic resonance (EPR); prepared, ran and analysed *in vitro* lauric acid (C12:0) samples by GC/MS

Fisher, K. and Rigby, S. E. performed EPR experiments and data analysis

Leys, D. collected X-ray diffraction data and solved the molecular structures of $OleT_{JE}$ (arachidic acid bound and substrate free) by molecular replacement

Nelson, D.R. performed bioinformatics and assignment of $OleT_{JE}$ as CYP152L1

Parker, D. A. performed GC/MS experiment and analysis of arachidic acid turnover by $OleT_{JE}$

Chapter Three

Belcher, J.D. and Tee, K.L. aided in cloning of WT $OleT_{JE}$

Matthews, S. performed mutagenesis of $OleT_{JE}$ to form H85Q, F79A, F79W, F79Y, R245L and R245E mutants; purification of enzymes; fatty acid binding studies; stopped-flow kinetic analysis; prepared *in vitro* reaction samples; performed GC/MS experiments and analysis of data; prepared samples for EPR; prepared crystals for X-Ray crystallography

Girvan, H. and McLean, K.J. performed EPR experiments and analysis

Tee, K.L purified WT $OleT_{JE}$ protein and prepared formate bound crystals for X-Ray crystallography

Levy, C.W. and Leys, D. collected X-Ray diffraction data

Leys, D. solved the structures of formate bound WT $OleT_{JE}$ and $OleT_{JE}$ H85Q by molecular replacement

Matthews, S. solved the structure of $OleT_{JE}$ F79A by molecular replacement under the guidance of Leys, D.

Chapter four

Tee, K.L. performed cloning and purification of $OleT_{JE}$-HRV3C-AldO; prepared *in vitro* turnover samples for GC/MS with different AldO substrates

Matthews, S. performed enzyme purification; hydrogen peroxide tolerance studies; prepared *in* vitro reactions for kinetic analysis, optimizing glycerol concentration and secondary product formation.

Rattray, N.J. performed GC/Q-TOF experiments

Matthews, S.J. analysed GC/Q-TOF data

Chapter five

Tee, K.L. performed cloning; purification; binding studies; redox potentiometry; prepared samples for EPR and for *in vitro* substrate conversion samples using GC/MS

Matthews, S. performed GC/MS experiments and analysis

McLean, K.J., Girvan, H.M., and Rigby, S.E. performed EPR experiments and analysis

Abstract

$OleT_{JE}$ (CYP152L1) is a P450 peroxygenase that was first isolated from *Jeotgalicoccus* sp. 8456 in 2011. $OleT_{JE}$ is primarily a fatty acid decarboxylase, converting mid-chain fatty acids (C10:0 to C22:0) to terminal alkenes, which are industrially useful petrochemicals. Terminal alkenes are hydrophobic with high energy density, and are compatible with existing transportation infrastructure. Thus $OleT_{JE}$ has attracted considerable interest due to potential applications for generating "drop-in" biofuels. As a P450 peroxygenase, $OleT_{JE}$ is able to utilise H_2O_2 as a sole oxygen and hydrogen donor. This is atypical of P450s, which usually require electron transfer from redox partners to perform substrate oxidation. Other P450 peroxygenases have previously been characterised, including fatty acid hydroxylases P450 Spα (CYP152B1) from *Sphingomonas paucimobilis* and P450 BSβ (CYP152A1) from *Bacillus subtilis*. In addition to decarboxylation, $OleT_{JE}$ also hydroxylates fatty acids, generating 2-OH and 3-OH fatty acids as minor products. P450 BSβ has also been reported to perform low levels of decarboxylation. However, $OleT_{JE}$ has superior decarboxylase activity, posing questions about the mechanism of $OleT_{JE}$.

This thesis describes initial structural and biochemical characterisation of $OleT_{JE}$. These data highlighted three amino acid residues thought to be key for effective catalysis: His85, Phe79 and Arg245. We hypothesised that the active site His85 could act as a proton donor to the reactive ferryl-oxo species compound I, allowing homolytic scission of the substrate C-Cα bond to form the alkene product. Phe79 sandwiches His85 between the heme, and Arg245 co-ordinates the fatty acid carboxylate moiety. I performed mutagenesis studies to probe the roles of these residues, creating H85Q, F79A, F79W, F79Y, R245L and R245E $OleT_{JE}$ mutants, and characterised them by a combination of spectroscopic, analytical and structural methods. I also developed a novel system, where $OleT_{JE}$ was fused to alditol oxidase (AldO) from *Streptomyces coelicolor*, creating a fusion protein where addition of glycerol drives hydrogen peroxide production and the decarboxylation of fatty acids. Finally, studies showed that $OleT_{JE}$ is capable of performing secondary oxidation of hydroxylated products, which has expanded our knowledge of $OleT_{JE}$'s catalytic repertoire. This thesis also describes the initial characterisation of the $OleT_{JE}$ orthologue P450 KR from *Kocuria rhizophila*, which is also a terminal alkene-forming fatty acid decarboxylase. The crystal structure of P450 KR revealed an unusual dimeric state, with structural interactions unprecedented for a P450 enzyme. These data thus provide characterisation of two P450 peroxygenases involved in the production of terminal alkenes and which are of great interest as tools for the development of alternative sources of advanced biofuels.

1 Introduction

1.1. The Biofuels Industry

Due to rapidly increasing petroleum consumption and diminishing supplies, the production of advanced biofuels from microorganisms has become attractive. First generation biofuels generally form two groups: bioethanol and biodiesel. Bioethanol is be made by fermentation of crops including maize, wheat, barley, rye, sugar cane, sweet sorghum and sugar beet, and tends to be mixed with gasoline. First generation biodiesel is generally derived from vegetable oils including soybean oil, rapeseed oil and palm oil (1). However, the production of first generation biofuels does pose ethical issues such as land use change and deforestation, and can have negative effects on the environment. In addition, production of these biofuels requires resources that could be used for the production of food. This is particularly questionable due to recent food crises and spikes in food prices. It has been estimated that biofuels rely on 2-3% of global water and land used for agriculture, and these resources could be used to feed around 30% of the malnourished population (1). Another option is to produce advanced biofuels, which are derived from the cellulose in biomass, which cannot be used as a food source This means that they do not pose the same issues as first generation biofuels (2).

Microbial engineering offers a valuable approach to producing fuel sources including butanol, alkanes, and alkenes (2). Alkanes and alkenes (C8 to C21) have high energy density and hydrophobicity, which would be compatible with existing fuel infrastructures, i.e. fuel engines, refinery equipment and transportation pipelines (3). Longer chain alkenes can also be used in plastics, lubricants and synthetic lubricants. Alkenes can also serve as a feedstock for other compounds including plasticisers, surfactants, enhanced oil recovery agents, fuel additives and drag reducing agents (4).

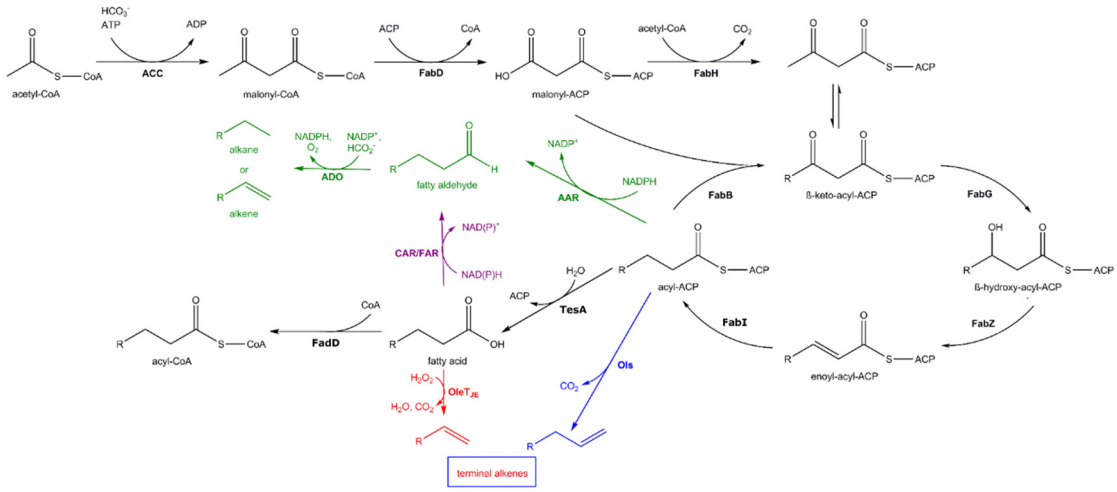

Figure 1.1. Pathways for fatty acid-based alkene production. The native *E. coli* fatty acid pathway is coloured in black. Components of this native pathway include acetyl-CoA carboxylase (ACC), malonyl-CoA:ACP transacylase (FabD), β-keto-acyl ACP synthase III (FabH), β-keto-acyl-ACP synthase I (FabB), β-keto-acyl-ACP reductase (FabG), β-hydroxyacyl-ACP dehydratase (FabZ), enoyl-acyl-ACP-reductase (FabI), acyl-ACP thioesterase (TesA), acyl-CoA synthase (FadD), and acyl-ACP thioesterase (TesA). The green/purple pathways represent acyl-ACP reductase (AAR)/aldehyde deformylating oxygenase (ADO) and carboxylic acid reductase (CAR)/fatty acid reductase (FAR)/ADO systems, respectively, which produce alkenes and alkanes depending on the nature of the fatty aldehyde substrate. Red and blue pathways show terminal alkene production by the cytochrome P450 fatty acid decarboxylase $OleT_{JE}$ and the type I polyketide synthase Ols, respectively. This figure is based on pathways published by Zhang et al and Wang et al (2,3).

1.2. Hydrocarbon Biosynthesis in Microorganisms

Hydrocarbon biosynthesis in sulfate-reducing bacteria (5) and marine bacteria (6) was first reported in the 1940s and 1950s. Specifically, alkene-producing microorganisms have been identified in *Kocuria rhizophila* (formerly known as *Sarcina lutea*), a gram-positive bacterium belonging to the *Micrococcaceae* family (7) (1), *which* was found to produce *iso-* and *anteiso-* branched chain long chain alkenes (8). Alkene biosynthesis was studied in *Micrococcus luteus* ATTC 4698 (a close relative of *Kocuria rhizophila*) (9). Here it was identified that heterologous expression of a three-gene cluster (Mlut_1320-13250) (known as *ole)* in a fatty acid overproducing strain of *Escherichia coli* yielded 40 µg/L alkenes composed of 27:2, 27:3, 29:2 and 29:3 (carbon chain length: double bond position). Similarly, deletion of this gene cluster in *Shewanella oneidensis* led to the absence of the polyunsaturated hydrocarbon 3,6,9,12,15,19,22,25,28-hentriacontanonaene that was previously identified in cell extracts (10). These alkenes are thought to be the product of head-to-head condensation of fatty acid derivatives, and produced by the OleABCD proteins. In a bioinformatic genome analysis of

3558 bacterial, eukaryotic and archaic strains, 69 of the bacterial genomes (corresponding to 5.2 % of bacterial genomes and 1.9% of total genomes) were shown to contain putative *ole* genes (11). The first step in the pathway involves condensation of fatty acid derivatives to form β-ketoacids (12). This reaction is carried out by OleA, which was first crystalised from *Xanthomonas campestris* in 2012 (13). OleA alsobelongs to the thiolase superfamily, which are a group of enzymes that typically carry out similar condensation reactions (14) . . The β-ketoacid intermediate is then converted to the alkene product by OleC and OleD, and studies have shown that this reaction cannot be completed by OleC alone (12).

Medium chain length terminal alkene production has also been reported in the marine cyanobacterium *Synechococcus* sp. PCC 7002. The gene responsible for this activity was identified and termed *ols* (the name derived from olefin synthase). The *ols* gene encodes a large multidomain protein that shows homology to type I polyketide synthases (15), which also tend to be large with multiple domains that are capable of solely producing the polyketide product (16) (3). This enzyme was hypothesised to use an elongation-decarboxylation mechanism, converting fatty acyl-acyl carrier proteins (fatty acyl-ACPs) to terminal alkenes. In this mechanism, the fatty acyl-ACP is loaded onto the ACP-1 domain by the loading domain (LD). The central extension module is comprised of ketosynthase (KS), acyltransferase (AT), ketoreductase (KR) and ACP protein domains. This central extension module transfers two carbons from malonyl-coenzyme A (CoA) to the substrate, reducing the β-keto moiety to a β-hydroxyl group. It has been suggested that a sulfotransferase (ST) domain then activates the β-hydroxyl group, driving dehydration and decarboxylation mechanisms performed by the C-terminal thioesterase (TE) domain (15). Subsequent bioinformatic analyses have identified at least twelve strains that possess the OLS pathway (17).

In 2011, an enzyme capable of decarboxylating fatty acids to produce terminal alkenes was isolated via a reverse genetic approach from *Jeotgalicoccus* sp. 8456(18). This reverse genetic approach involved purifying the protein responsible for decarboxylation activity from *Jeotgalicoccus* sp. 8456, and determining its amino acid sequence by mass spectrometry; this was then be used to identify the gene that encoded the decarboxylase enzyme (18). This enzyme was named $OleT_{JE}$. $OleT_{JE}$ shares a high sequence similarity with P450 BSβ and

P450 SPα (18), which were previously characterized as fatty acid hydroxylases (19,20). P450 BSβ and P450 SPα are members of the family of P450 peroxygenases, which will be discussed further in section 1.8. $OleT_{JE}$ also produces 2-hydroxy and 3-hydroxy fatty acids as minor products. Biochemical and structural characterization of $OleT_{JE}$ was reported in 2014, where the enzyme was classified as CYP152L1, belonging to the CYP152 family of P450 peroxygenases (21). $OleT_{JE}$, and further studies related to the enzyme, will be discussed in later sections.

Other pathways have been identified that synthesize alkanes and, when unsaturated substrates are precursors, can also lead to the formation of alkenes (alk(a/e)ne production). Examples of these pathways include the AAR-ADO and CAR/FAR-ADO pathways (shown in figure 1.1). Alk(a/e)ne production is widespread in cyanobacteria, and subtractive genome analysis (where the genomes of alkene and non-alkene producing organisms are compared to identify the genes responsible for producing alkene products) followed by gene knockout studies have indicated two genes were capable of forming alk(a/e)nes (22). These enzymes have been identified as an acyl-ACP reductase (AAR) that converts acyl-ACP to fatty aldehyde (23), and an aldehyde deformylating oxygenase (ADO) that catalyses oxygenative aldehyde cleavage to generate formate (HCO_2^-) and the alk(a/e)ne (24). These cyanobacterial ADOs were previously thought to be aldehyde decarbonylase (AD) enzymes that released carbon monoxide (CO) as a co-product with alkanes (25). However, experimental evidence has indicated that formate is stoichiometrically released as the co-product rather than CO (26). Subsequent studies also demonstrated that dioxygen (O_2) is required for activity, and that O^- is incorporated into formate (27). Thus, it was suggested that these cyanobacterial enzymes should be reclassified as ADOs (24). Overexpression of AAR and ADO in *Synechocystis* has been shown to increase alk(a/e)ne production from 300 µg/L/OD in the parent strain, to 700 µg/L/OD (3).

Other groups have engineered biosynthetic pathways in *E. coli* that produce alk(a/e)nes. These include the artificial CAR-ADO and FAR-ADO pathways (shown in figure 1.1). These pathways focus on the conversion of free fatty acids to alk(a/e)nes. These pathways are believed to be superior for several reasons: the introduction of thioesterases would give

greater control over alk(a/e)ne chain length by specifically determining fatty acid chain length (25,28,29), fatty acids are more abundant than fatty acyl-ACP in the cell (25), and genetic manipulation can be used to alter the fatty acid pool (30). Expression of the Fatty Acid Reductase (FAR) complex (encoded by *luxC, luxE and luxD* from *Photorhabdus luminescens*) in conjunction with an ADO (from *Nostoc punctiforme*) resulted in the production of mg/L concentrations of alkanes/alkenes of carbon lengths C13-C17 (25). Similarly, another study has shown that *in vitro* turnover reactions with a carboxylic acid reductase (CAR) from *Mycobacterium marinum* and an ADO from *Prochlorococcus marinus* leads to the production of alkanes C7-C15 (31).

1.3. Cytochromes P450: An Overview

The cytochromes P450 (P450s, CYPs) are a superfamily of heme *b* containing enzymes, where the heme iron is proximally coordinated by a cysteine thiolate bond (32). These enzymes are widespread in nature and present in all three phylogenetic domains (33). P450s are defined as monooxygenases or mixed-function oxidases, and catalyse the reductive activation and scission of heme iron-bound dioxygen. Commonly this results in the insertion of an oxygen atom into the substrate, and the production of water. This reaction requires the delivery of two electrons and two protons to the heme iron as shown in equation (i) (34).

$$RH + O_2 + 2e^- + 2H^+ \rightarrow ROH + H_2O \qquad \text{equation. (i)}$$

P450s are capable of performing an array of reactions, including desaturation, C-C bond cleavage, aryl ring coupling, heteroatom dealkylation, heteroatom oxygenation, ring formation and rearrangement of oxygenated chemicals (35). Across the enzyme superfamily, P450s are also capable of accepting a vast range of substrates, exceeding those of other enzymes, and their oxidative reactions are usually highly regio- and stereoselective. This makes these enzymes ideal targets for synthetic biology applications (36).

1.4. History of Cytochromes P450

P450s were first recognized in rat liver microsomes when, upon addition of CO to a diphosphopyridine nucleotide (DPNH, now known as NADH) reduced or a dithionite (DT) reduced microsomal sample, a broad absorption band with a maximum at 450 nm appeared (37). In 1962, this pigment was reported to behave as a typical hemoprotein when liberated from the microsomal structure by anaerobic solubilisation (38,39). The monooxygenase activity of P450s in adrenal cortex microsomes was first identified in 1963 (40). Purification of P450s from microsomes and mitochondria in the mid-1970s allowed the characterization of many P450 forms (39). In 2016, there were 812 entries of P450 enzymes in the Protein Data Bank (PDB). These were comprised of 590 microbial P450s, 218 mammalian P450s and 163 structures of 22 separate human P450 enzymes (35).

A system of P450 nomenclature was first devised in 1987 (41). This system reflects the evolutionary relationships between P450 enzymes and classifies them accordingly (33). Using CYP102A1 (P450 BM3) as an example, 102 refers to the family in which the P450 is classified, and A1 refers to the subfamily. Membership of a particular CYP gene family requires at least 40% amino acid sequence identity to other family members, and membership of a subfamily requires at least 55% amino acid sequence identity with other subfamily members (42). As the numbers of P450s increases (with new genome sequences), the decisions on the classifications for a P450 into a particular family or subfamily can also depend on how a particular P450 sequence clusters with other P450s on a phylogenetic tree rather than (or as well as) its absolute percentage sequence identity with other P450s (42). P450 sequences are classified by David Nelson and published on the Cytochrome P450 Homepage at http://drnelson.uthsc.edu/CytochromeP450.html (43).

1.5. Cytochrome P450 Structure

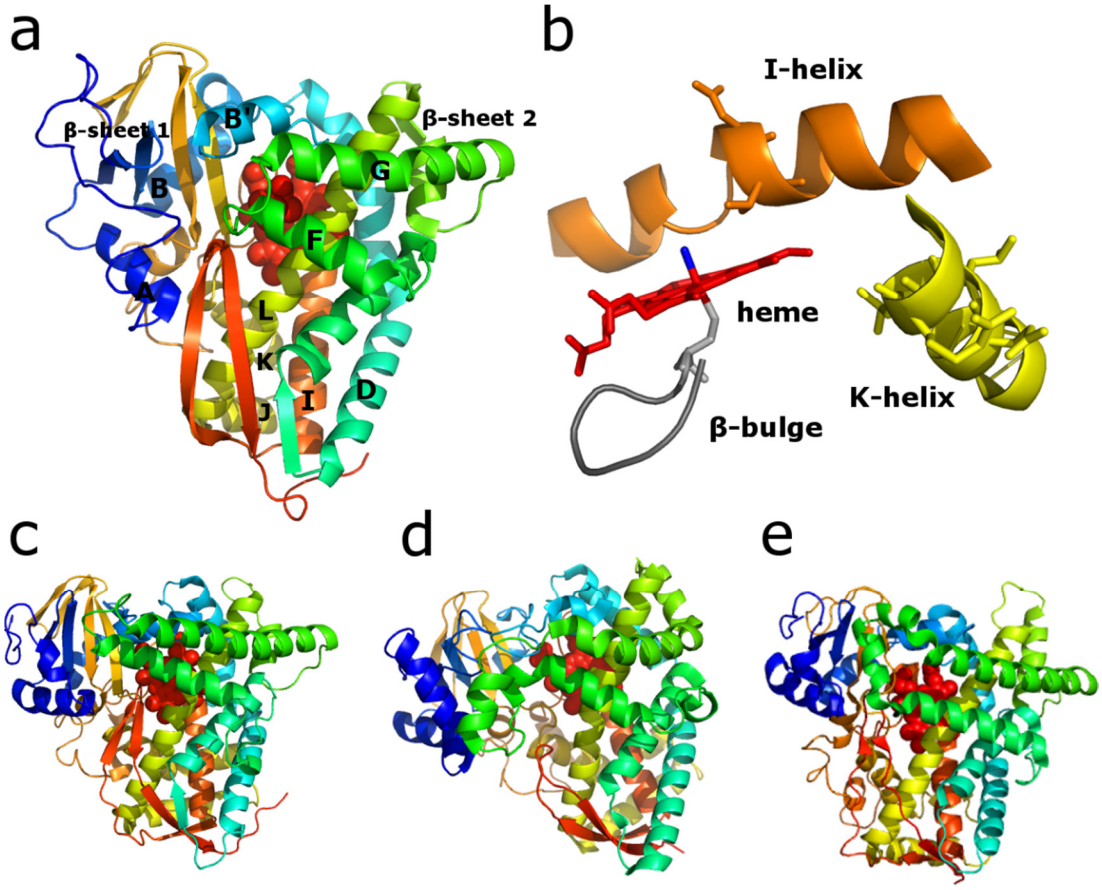

Figure 1.2 Structural similarity of cytochrome P450 enzymes. a) P450cam (CYP101A1), a camphor hydroxylase from *Pseudomonas putida* with annotated features including: A, B, B', D, F, G, I, J, K and L helices, as well as β-sheet 1 and 2. b) Substrate-free P450cam active site c) P450 BM3 (CYP102A1) heme (P450) domain from *Bacillus megaterium* e) Allene oxide synthase (CYP74A2) from *Parthenium argentatum*. e) CYP2C9 from *Homo sapiens.* The similarity in the P450 fold between enzymes from microbes through to man is evident.

The first solved crystal structure of a P450 was that of the camphor hydroxylase P450cam (CYP101A1) from *Pseudomonas putida*, obtained in 1985 (44). This was followed by the crystal structure of the P450 (heme) domain of the *Bacillus megaterium* fatty acid hydroxylase P450 BM3 in 1993 (45). Since then, the number of P450 structures in the PDB has grown rapidly. This has provided information that allows us to better understand the structural organization of these enzymes, and thus be able to engineer them for specific catalytic functions. Despite the fact that sequence identities between P450 families are often low, at between 10-30% for P450s with distinct functions (46), these enzymes share a common overall fold and topology. This is comprised of a conserved core, formed by a four-helix bundle of three parallel helices (D, L and I) and an anti-parallel helix (E) (47), which is associated with

helices K and J. Helix I contains a conserved alcohol side chain-bearing amino acid (Thr or Ser) together with an acidic residue immediately preceding the Thr/Ser and that is positioned over pyrrole ring B. This is thought to be important for protonation of the ferric-superoxo and ferric-hydroperoxo intermediates during the process of oxygen activation for substrate oxidation Mutagenesis of the conserved threonine residue was shown to disrupt the proton delivery pathways of Lys/178/Arg186, Asp251 and Thr252 in P450cam (48,49).

Helix K also contains the conserved EXXR amino acid sequence on the proximal side of the heme (i.e. the face of the heme on which a cysteine thiolate coordinates the heme iron). This motif is thought to be important in stabilising the β-meander loop, which preceeds helix K, and the overall tertiary structure of the P450 (50). However, there are exceptions, and the CYP157 family does not contain the EXXR motif. For example, this sequence is EQSLW in CYP157C1 from *Streptomyces coelicolor* A3(2) (51). Another conserved region is the β-bulge, which contains the heme ligating Cys residue, located prior to the L helix (52). This region is also associated with the strongly conserved FXXGXXXCXG motif (53). This is a rigid architecture that constrains the Cys residue and that is important for maintaining correct H-bonding geometry around the proximal ligand. This geometry is crucial for regulation of the heme iron redox potential in P450s (54) and related heme-thiolate enzymes such as nitric oxide synthase (NOS) (55,56) and chloroperoxidase (CPO) (57), as well as in other Cys-Fe ligating proteins such as ferredoxins (58). This structural arrangement helps to poise the redox potential of the heme iron, a property which is also affected by substrate binding and its associated displacement of the 6th distal (water) ligand to the ferric heme iron. In absence of the structural and H-bonding organization around the Fe-Cys bond, the redox potential of the heme iron would be too low, and reduction by the cognate redox partners may be inefficient or impossible (52).

There are also two structurally conserved sets of β-sheets in the P450s. These sheets form part of the hydrophobic substrate access channel and consist of β-sheet 1 (containing five strands) and β-sheet 2 (containing two strands) (59). There are also more variable structural regions. These allow the large range of substrates utilized by P450 enzymes to be accommodated, and enable interactions with different redox partners to occur. Comparing

P450s of the CYP2 family with P450cam, several sites were identified that are involved in substrate recognition (substrate recognition sites or SRSs) (60). These regions are associated with helices A, B, B',F and G along with their adjacent loops (61).

1.6. Redox Partners

Most P450 enzymes require the transfer of electrons from NAD(P)H in order for catalysis to occur. Initially, electron transfer by redox partners was classified into two types - either class I or class II systems. However, the discovery of new, distinct redox partner systems in recent years has highlighted that this classification is outdated and that P450 redox partner specificity is more complex than originally envisaged (62).

Class I P450 systems contain two separate redox partners: an FAD-containing ferredoxin reductase (FdR) which transfers two electrons from NAD(P)H to an iron sulfur protein (ferredoxin or Fdx) one at a time. The ferredoxin then passes the electrons to the P450 one at a time (63). Class I systems have been observed in bacterial and eukaryotic mitochondrial P450 systems, though the two systems were found not to be phylogenetically related (64). In bacterial systems, all three proteins are soluble, whereas in eukaryotes the ferredoxin reductase and P450 are membrane associated. In higher eukaryotes the class I system is found in adrenal gland mitochondria and supports function of the steroidogenic P450s (65).

Class II systems are typically located in the endoplasmic reticulum (ER) of eukaryotic organisms. This system utilizes an NADPH-cytochrome P450 reductase (CPR), which binds FAD and FMN cofactors (66). In these systems, NADPH transfer two electrons (as hydride ion, H^-) to the FAD cofactor reducing it to the hydroquinone form. Electrons are then shuttled one at a time to the FMN-binding domain, which delivers two single electrons to the P450 after docking to its recognition site on the proximal face of the heme. In eukaryotic P450s, it is likely that the resting form of the CPR is one that has a stable FMN neutral semiquinone. This means that the CPR passes through a 1-3-2-1 cycle during catalysis, in which the CPR accepts 2 electrons (from NADPH) to convert to the 3-electron reduced form which has a single electron (semiquinone) on the FAD and two electrons (hydroquinone) on the FMN. The FMN

hydroquinone passes the first electron to the P450 (reducing ferric to ferrous heme iron and allowing oxygen binding) and its hydroquinone form is restored by electron transfer from the FAD. The FMN hydroquinone then passes a second electron to the ferrous-oxy heme iron, producing the ferric-peroxo form and enabling the progression of the P450 catalytic cycle. The CPR is then restored to the resting FMN semiquinone state. The eukaryotic P450s have N-terminal transmembrane spanning helices that tether them to the ER. However, bacterial CPRs are also recognized, with the best known being the P450 BM3 P450-CPR fusion enzyme (67). In this case, the resting state of the CPR is fully oxidised, and the enzyme passes through a 0-2-1-0 cycle in which the FMN semiquinone is the electron donor to the fused P450 domain (67).

1.7. The Cytochrome P450 Catalytic Cycle

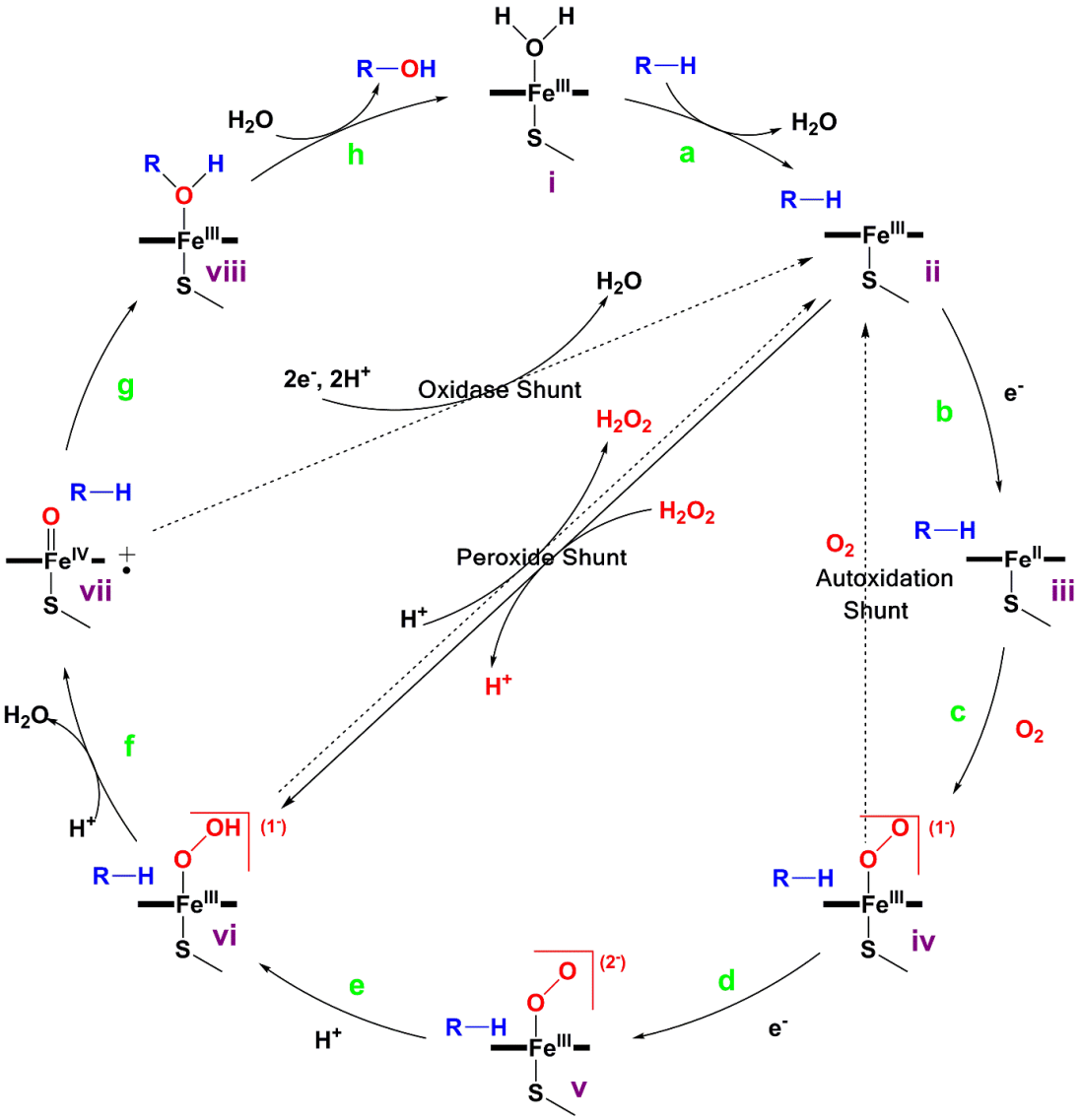

Figure 1.3 P450 catalytic cycle. This cycle depicts the process of substrate hydroxylation by a typical P450. In its resting state, ferric (Fe^{III}) heme (i) is axially ligated by a proximal cysteine thiolate and a distal water molecule. Substrate binding displaces the ligated water molecule, causing a HS (S = 5/2) heme iron shift, which in turn increases the heme redox potential (a). This increase in redox potential facilitates the transfer of an electron (b) from a redox partner to form ferrous (Fe^{II}) heme (ii) (66). Dioxygen binding (c) then produces the ferric superoxy complex (iv), and further reduction (d) by a redox partner gives rise to the ferric peroxy state (v). Protonation of this species by a proton derived from the bulk solvent and delivered from the acid/alcohol amino acid pair in the I-helix (e.g. Asp251/Thr252 in P450 cam) (e) forms compound 0 (ferric-hydroperoxy intermediate) (vi). A further protonation event (f) then results in O-O bond scission to give Compound I (a ferryl-oxo intermediate with a porphyrin π radical cation) (vii) (45). Typically, Compound I then attacks the substrate, to give rise to the hydroxylated product using the radical (oxygen) rebound mechanism (g) (88). The hydroxylated product then dissociates and water rebinds to the heme (h), reforming the ferric resting state (i). This cycle also highlights non-productive pathways that lead to the collapse of reaction cycle intermediates. These include the autoxidation shunt, peroxide shunt and oxidase shunt, which describe the collapse of the ferric superoxy, Compound 0 and Compound I intermediates (30).

1.7a. Substrate Binding

Most reactions catalysed by P450 enzymes can be described by the well-characterized P450 cycle shown in Figure 1.2. In the resting state, ferric (Fe^{III}) heme is present in a hexa-coordinated state, with four in-plane pyrrole nitrogens, an axial cysteine and a distally ligated water iron in the sixth position. In both the substrate-bound and substrate-free forms, the heme iron is present as a mixture of S=1/2 low spin (LS) and S=5/2 high spin (HS) states. The crystal field in the hexa-coordinated heme causes energetics to favour spin-pairing of electrons, as opposed to population of upper levels, thus pushing the equilibrium towards the S=1/2 LS state (68). Substrate binding perturbs the water molecule, and the heme iron becomes penta-coordinate, weakening the crystal field. This favours population of all orbitals with a minimum of spin-pairing, and so the equilibrium is pushed towards a rearrangement of the d-orbitals to a 5/2 high spin (HS) state (68,69). This, in turn, increases the reduction potential, allowing the transfer of an electron from a redox partner. For example, camphor binding to P450cam has been shown to increase the reduction potential for the ferric Fe^{III}/Fe^{II} pair by around 125 mV (70).

1.7b. Reduction of Ferric (Fe^{III}) to Ferrous (Fe^{II}) Heme Iron

Electron transfer from a redox partner reduces the heme iron from Fe^{III} to Fe^{II}, which is necessary for binding of dioxygen. In this way, substrate binding provides a regulatory role, by initiating reduction, and minimising the production of reactive oxygen species and any wastage of reducing equivalents in the form of reduced nicotinamide adenine dinucleotide (NADH) and reduced nicotinamide adenine dinucleotide phosphate (NADPH) (71). This has been documented in P450 BM3 from *Bacillus megaterium*: a 119 kDa polypeptide with fused heme (P450) and diflavin (CPR) domains, where redox potentiometry was used to determine the redox potentials of the heme, FAD and FMN cofactors, and to rationalise the route of transfer of electrons from NADPH to FAD, then to FMN and subsequently onto the heme iron. In this case, it was shown that fatty acid substrate binding increased the redox potential by over 100 mV. The particular substrate used also had a specific effect, with arachidonate

inducing a greater potential shift than did palmitic acid (129 mV increase compared to a 103 mV increase, respectively), apparently related to the extent of HS heme developed induced by the different substrates (72).

1.7c. Binding of Dioxygen to Fe^{II} Heme Iron

Dioxygen binding to the ferrous (Fe^{II}) heme iron leads to the formation of a ferrous-oxy intermediate that is isoelectronic with the ferric-superoxy form (32). Here, there is partial transfer of electron density from the iron to the dioxygen moiety that is coordinated head on with the heme iron. This oxy-complex has been reported by X-ray crystallographic studies in P450cam. Cryogenic trapping techniques and rapid data collection were successful in generating a 0.91 Å structure, showing the dioxygen molecule bound end-on to the heme iron. In this complex, the Fe-O bond has a distance of 1.81 Å and the Fe-O-O has an angle of 132.0° (73,74). Another ferrous dioxygen complex of P450cam showed Fe-O distances of 1.85 and 1.70 Å, and Fe-O-O angles of 129° and 133° for each molecule in the asymmetric unit. In this study, dioxygen binding was accompanied by the introduction of two new water molecules into the active site. It was postulated that these water molecules form part of the proton relay system, and are crucial for proton delivery to the distal oxygen atom of the heme iron-bound dioxygen complex (75). A similar study was conducted with the *Saccharopolyspora erythraea* 6-deoxyerythronolide B hydroxylating (erythromycin forming) P450eryF, which was reported to have a Fe-O distance of 1.81 Å and a Fe-O-O angle of 131°(76).

Temperature-dependent Mössbauer spectroscopy has been useful in providing geometric parameters for the Fe-oxy intermediate (71) using “Picket Fence Porphyrins”, which are synthetic porphyrin models. In one study a 2-methylimidazole derivative of the picket fence porphyrin [Fe9(TpivPP)(Rim)(O_2)] was used to resolve the oxygen atom positions and to provide geometric descriptions of the Fe-O_2 unit. These values were recorded as an Fe-O distance of 1.811 Å, an Fe-O-O angle of 118.2° and an O-O distance of 1.281 Å (77). These values correlate to a high level of superoxide anion character, as O-O bond length has been determined as 1.21 Å in dioxygen and 1.33 Å in the superoxide anion form (71,78). X-ray

absorption spectra (XAS) data have also revealed that there is strong σ donation and strong π interaction of the dioxygen moiety with the heme iron. This indicates that the Fe-O bond is highly covalent (71).

1.7d. Second Electron Transfer to the Ferric-Superoxy Complex

The next step in the process involves a second electron transfer to the heme iron, reducing it to a ferric-peroxy state. In this reduced form, one electron is on the oxygen, and another is delocalized over the cysteine ligand (79). This intermediate has been studied in the D251N mutant of P450cam, which shows hindered proton delivery, allowing the capture of the unprotonated peroxy-ferric intermediate (80). This study used resonance Raman spectroscopy to determine vibrational data for the superoxy, peroxy and hydroperoxy states. Upon reduction of the ferric superoxy state, there is a shift in the ν(O-O) from the characteristic ~1135 cm^{-1} to ~800 cm^{-1}, which is indicative of a bound peroxo species, along with a shift in the ν(Fe-O) mode from 537 to 553 cm^{-1} (80).

Evidence was provided to show that, in some P450s, the ferric-peroxy intermediate is able to act as the active species. In these cases, the ferric-peroxy intermediate is able to act as a nucleophile with some electrophilic moieties. One example of this phenomenon is seen in lanosterol 14α-demethylase, which catalyses the oxidative deformylation of lanosterol in its conversion to form other sterols (81).

1.7e. Protonation of the Ferric-Peroxy Species

Protonation of the ferric-peroxy species from the bulk solvent occurs by the proton relay pathway described earlier, and gives rise to a ferric-hydroperoxy intermediate, also known as compound 0. In the P450cam D251N mutant, this protonation event caused the ν(O-O) signal to decrease by 18 cm^{-1} and the ν(Fe-O) to increase by 11 cm^{-1}, which indicates a weakening of the O-O bond (80). Theoretical calculations using Density Functional Theory (DFT) have also suggested that this protonation event strengthens the Fe-S bond (with respect to a

reduced oxyferrous porphine), with distal oxygen atom protonation reducing the Fe-S bond length by 0.14 Å, and proximal oxygen protonation causing a decrease in bond length of 0.19 Å (82). Distal oxygen atom protonation was found to be more energetically favourable, and was 18.4 kcal/mol more favourable over the proximally protonated form. These calculations showed a weakening of the O-O bond by 0.13 Å and a decrease in bond order from 0.87 to 0.48 upon distal oxygen atom protonation (82).

1.7f. Protonation of the Ferric-Hydroperoxy Intermediate Resulting in the Formation of the Ferryl-Oxo Intermediate (Compound I)

Protonation of Compound 0 results in scission of the O-O bond, and in the release of a water molecule. This gives rise to Compound I (Cpd I), which is a ferryl-oxo intermediate with a π-cation radical delocalised on the porphyrin ring system (71). This species was first observed in CYP119A1 from *Sulfolobus acidocaldarius*. Here, mixing of ferric CYP119A1 with *meta*-chloroperoxybenzoic acid (*m*-CPBA) yielded 70% compound I after 35 ms. In terms of the UV-visible spectrum, Cpd I was characterised by a blue shift of the Soret peak, in conjunction with disappearance of the heme α and β bands, and the appearance of a feature at 690 nm (83). These data are similar to those reported for the multifunctional heme enzyme chloroperoxidase (CPO) (84,85). In CYP119A1, Mössbauer measurements and electron paramagnetic resonance (EPR) spectroscopy also confirmed the presence of Cpd I. Collectively, these data described the electronic structure of compound I as an S=1 iron(IV)oxo unit exchange coupled with an S=1/2 ligand-based radical (83).

Compound I has also been observed in CYP119A2 from *Sulfolobus tokodaii*, and reports on this system have detailed the importance of pure and endogenous substrate-free sample preparations for the spectroscopic capture of the transient Cpd I intermediate (86).

P450 Cpd I appears to be more reactive than CPO Cpd I, as P450s are able to hydroxylate unactivated hydrocarbons while CPO is only capable of hydroxylating activated hydrocarbons such as benzylic or propargylic compounds (87). Comparing these two Cpd I forms is important for characterising the increased reactivity of Cpd I in P450s. Extended X-ray

Absorption Fine Structure (EXAFS) measurements have indicated that the Fe-S bond distance is ~0.1 Å shorter in CYP119A1-I than for CPO-I (88). This shorter Fe-S distance in P450-I allows greater electron donation from the axial-thiolate ligand into the ferryl π* orbitals. These differences are thought to be as a result of variations in hydrogen bonding patterns in the "cys pocket" on the proximal face of the heme (88).

The formation of Cpd I has also been observed in the P450 peroxygenase $OleT_{JE}$ by mixing hydrogen peroxide with a deuterated substrate-enzyme complex. This resulted in the transient formation of Cpd I and, within 15 ms, the Soret maximum had blue-shifted from 392 to 370 nm, together with the formation of an additional absorption band at 690 nm (89).

Substrate oxidation is generally thought to occur by the "Radical Oxygen Rebound Mechanism" first postulated by Groves in 1978 (90). Here, Cpd I abstracts a hydrogen atom from the substrate, yielding the rebound intermediate iron(IV) hydroxide species (compound II, Cpd II) and a substrate radical. The substrate radical and Cpd II then combine, forming and releasing the hydroxylated product and leaving the heme in the ferric (Fe^{III}) state (91).

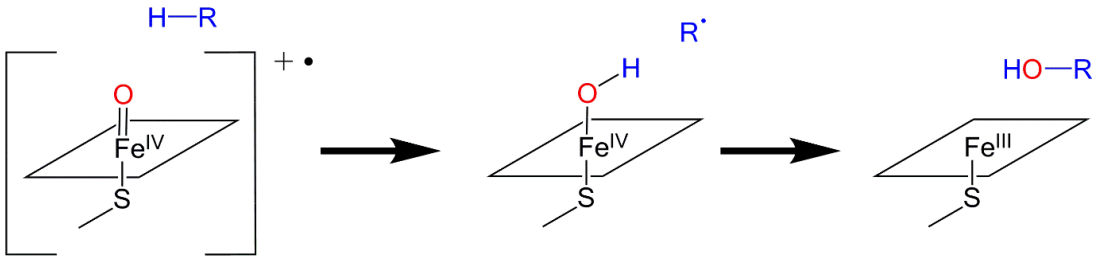

Figure 1.4. Oxygen rebound mechanism of substrate hydroxylation by cytochromes P450. In this mechanism, the ferryl-oxo intermediate (compound I) abstracts a hydrogen from the substrate to form a substrate carbon radical intermediate (R•). The radical intermediate then recombines with the ferryl-hydroxide species (Compound II) to form the hydroxylated product. The hydroxylated product (ROH) is subsequently released, leaving the heme in a ferric (Fe^{III}) state to which water can bind to restore the resting state of the P450 (90).

1.7g. Spectroscopic Properties of the Ferryl-Hydroxo Compound II

Cpd II was characterised in CYP119A1 by EXAFS studies. These studies identified a relatively short iron-sulfur bond length of 2.23 Å and a quite short iron-oxygen bond length of 1.81 Å which, based on computational models, indicates a single bond and thus a ferryl-hydroxide moiety (92). The pK_a of the ferryl-hydroxide species is very basic at almost 12, and is therefore protonated at neutral pH. This strong basicity is a function of the electron donating character

of the cysteine-thiolate bond (93). Recent studies by Makris' group have also described the UV-visible spectrum of Cpd II in the $OleT_{JE}$ enzyme, observed as a species with a heme absorbance maximum at 426 nm, and formed transiently as a product from the decay of $OleT_{JE}$ Cpd I (94).

1.7h. Inefficiency in the P450 Catalytic Cycle and the Peroxide Shunt

It was observed in the 1980s that microsomal P450 enzymes show significant production of activated oxygen species such as superoxide ($O^{\cdot-}$) and hydrogen peroxide (H_2O_2) without modification of the substrate (95,96). There are two points in the catalytic cycle at which reactive oxygen species (ROS) can be released. The first leads to the production of superoxide due to decay of the ferric-superoxy intermediate. This can occur if the second electron transfer event is inefficient or not fast enough. The second involves the collapse of compound 0 to produce hydrogen peroxide by dissociation of the hydroperoxy-anion. This happens if the second protonation does not occur efficiently. It is also possible for Cpd I to collapse if substrate is absent or improperly positioned, and this results in the production of a water molecule (97).

It has been demonstrated that oxidising agents such as cumene hydroperoxide, *m*-CPBA and hydrogen peroxide can be used in the absence of cofactors and redox partners in order to drive hydroxylation and other P450 reactions (98). This essentially acts in an opposite manner to the non-productive collapse of compound 0, with the hydroperoxo species converting the substrate-bound ferric heme iron directly to compound 0. However, this process is inefficient in many P450s, resulting in oxidative damage to the heme (99). Protein engineering efforts have been made in efforts to increase the efficiency of this "peroxide shunt" in P450cam and BM3 (99,100).

However, there are P450s that have evolved to use the peroxide shunt efficiently. These enzymes typically belong to the CYP152 family of P450 peroxygenases and include the well-characterised fatty acid hydroxylases P450 BSβ and P450 SPα (19,20).

1.8. P450 peroxygenases

P450 peroxygenases typically follow the reaction shown in equation (ii), where the ferric heme iron abstracts an oxygen atom and two oxidising equivalents from the peroxy compound (XOOH), and delivers them to the substrate (A) which acts as an electron donor. This generates the oxygenated product (AO) and reduced peroxy compound (XOH), which may be H_2O if the peroxy compound is H_2O_2 (101).

$$A + XOOH \rightarrow AO + XOH \qquad \text{eqn (ii)}$$

P450 peroxygenases have been found to carry out reactions including hydroxylations (102-105), decarboxylations (18), N-demethylations (106) and O-deethylation (107), using H_2O_2 (18,19), tert-Butyl hydroperoxide (*t*-BuOOH) (106), cumene hydroperoxide (CuOOH) (103) and *p*-menthyl hydroperoxide (*p*-menthylOOH) (98).

1.9. P450 Peroxygenases and P450 Evolution

The early atmosphere of Earth is believed to have been anaerobic and reducing (H_2 rich) or neutral (CO_2N_2). There is evidence to suggest that the ancestral P450 gene arose 3.5 billion years ago during this time (109), when typical P450 monooxygenases could not have functioned, due to a lack of oxygen in the environment. It is possible, however, that the atmosphere was rich in H_2O_2 and peroxygenated organic molecules (110), and this has led many to believe that ancient prokaryotic P450s that utilise H_2O_2 and organic peroxides are ancestors to modern P450 enzymes (111). An example of these ancient P450s is the archaeal CYP119A1 from *Sulfolobus acidocaldarius*, which is able to hydroxylate laurate and to epoxidise styrene and *cis*-stilbene in the presence of H_2O_2, *t*-BuOOH and *m*-CPBA (83,112,113).

The evolution of anaerobic photosynthetic cyanobacteria is thought to have led to an increase in oxygen levels around 2 billion years ago (109). However, this caused an increase in levels of reactive oxygen species (ROS), such as the superoxide radical ($O_2^{\bullet-}$), H_2O_2 and the hydroxyl radical ($^{\bullet}OH$). P450s were able to partially reduce levels of ROS by utilizing H_2O_2 and removing unwanted O_2. However, they were not completely effective as O_2 levels began to rise (111).

Further increases in oxygen levels allowed the evolution of unicellular eukaryotic organisms. The evolution of enzymes such as superoxide dismutase, catalase and peroxidase, that could efficiently remove peroxide and ROS, allowed the diversification of P450s so that they could perform other functions (109).

1.10. Homolytic and Heterolytic Cleavage of the Peroxy O-O bond

During P450 peroxygenase reactions, oxidising equivalents for the monooxygenase reaction are derived from the scission of the peroxy O-O bond of the peroxide or peracid. Scission of the peroxy O-O bond can occur by a homolytic (one-electron) or a heterolytic (two-electron) mechanism, depending on the peroxy compound and the substrate (111,113).

It has been postulated that heterolytic scission generates a reduced hydroperoxide and Cpd I. Hydroxylation reactions then proceed by the "Radical Oxygen Rebound Mechanism" that was postulated by Groves and colleagues (described in section 1.6f). These reactions are described in equations (iii and iv):

$$Fe^{III} + XOOH \rightarrow Por^{\bullet+}Fe^{IV}=O + XOH \qquad \text{equation. (iii)}$$

$$Por^{\bullet+}Fe^{IV}=O + AH \rightarrow Fe^{VI}\text{-}OH + A^{\bullet} \rightarrow A^{\bullet}\text{-}Fe^{IV}\text{-}OH \rightarrow AOH\text{-}Fe^{III} \rightarrow AOH + Fe^{III} \qquad \text{equation. (iv)}$$

In this mechanism, ferric (Fe^{III}) heme reacts with the hydroperoxide (XOOH, where X can either be an organic substituent or, in the case of H_2O_2, a hydrogen atom). This reaction generates Cpd I (shown in equations (iii) and (iv) as $Por^{\bullet+}Fe^{IV}=O$) and the reduced peroxide, which can be either XOH or H_2O. Cpd I then abstracts a hydrogen atom from the substrate (AH), resulting in the formation of Cpd II (Fe^{VI}-OH), and a carbon-centred substrate radical ($A^{\bullet}$). The radical then rebounds onto the Cpd II ferryl-hydroxy moiety giving rise to the substrate radical-bound protonated Cpd II complex ($A^{\bullet}$-Fe^{IV}-OH). The substrate radical is then hydroxylated by the ferryl-hydroxy moiety to generate a ferric-product complex, which dissociates to produce the resting ferric (Fe^{III}) heme and hydroxylated product (111,115).

Although less common, scission of the peroxy O-O bond can also occur by homolytic reduction. This reaction proceeds as shown in equations (v, vi and vii):

$Fe^{III} + XOOH \rightarrow Fe^{VI}\text{-}OH + XO^{\bullet}$ equation (v)

$XO^{\bullet} + AH \rightarrow XOH + A^{\bullet}$ equation (vi)

$A^{\bullet} + Fe^{VI}\text{-}OH \rightarrow A^{\bullet}\text{-}\ Fe^{VI}\text{-}OH \rightarrow AOH\text{-}Fe^{III} \rightarrow AOH + Fe^{III}$ equation (vii)

During this reaction, homolytic reduction of the O-O bond results in the formation of an alkoxy radical ($XO^{\bullet}$) and Cpd II. The alkoxy radical then reacts with the substrate to form a reduced hydroperoxide (XOH) and a carbon centred substrate radical. This gives rise to the radical-bound protonated Cpd II complex, and results in the hydroxylation of the substrate by the ferryl-hydroxy moiety in the same way as in heterolytic scission (101,116).

1.11. P450 Peroxygenase Structure

In the protein data bank (PDB), there are currently a total of 12 crystal structures of CYP152 family P450 peroxygenases. This number will increase with the pending submission of the three further $OleT_{JE}$ crystal structures described later in this thesis. These structures are made up of various mutants and ligand-bound complexes of 3 enzymes: CYP152A1 (P450 BSβ), CYP152B1 (P450 SPα) and CYP152L1 ($OleT_{JE}$). The crystal structures of $OleT_{JE}$ will be discussed further in chapters 2 and 3.

P450 SPα from *Sphingomonas paucimobilis* was first purified in 1996, and was found to specifically catalyse the α-hydroxylation of fatty acids (117,118). P450 BSβ from *Bacillus subtilis* has 44% amino acid sequence identity to P450 SPα, and was first isolated in 1999 (119). Unlike P450 SPα, P450 BSβ has also been shown to hydroxylate fatty acids in the β position, with an α-hydroxylase:β-hydroxylase ratio of 40:60 (19). Other studies have shown that P450 BSβ is also capable of carrying out decarboxylation of fatty acids, with a hydroxylase:decarboxylase activity ratio of around 80:20 (18).

The structure of P450 SPα was solved to 1.65 Å in 2011 (102), and the structure of P450 BSβ was solved to 2.1 Å in 2003 (19). Both proteins show a typical P450 trigonal prism-shaped

structure, with a buried heme. The I helix is positioned on the interior of both proteins, and lies on the distal side of the heme. Both proteins appear to have two channels: channel I and channel II. Channel I is involved in substrate binding, and is lined with hydrophobic residues which allow the binding of hydrocarbon substrates. In P450 SPα these residues include Ile^{73}, Leu^{78}, Phe^{169}, Ala^{172}, Ala^{245}, Phe^{287}, Phe^{288}, Pro^{289}, Leu^{398} and Pro^{399} (102). In P450 BSβ these residues include Leu^{17}, Leu^{70}, Val^{74}, Leu^{78}, Phe^{79}, Val^{170}, Phe^{173}, Ala^{246}, Phe^{289} and Phe^{292} (19). Channel II is thought to allow the ingress of H_2O_2, and the egress of H_2O during the reaction (19,102).

Typical P450 monooxygenases show a positive surface potential on the proximal side of the protein, a region which is important for recognition of redox partners and the transfer of electrons to the heme iron (46). There is also a negative surface potential on the distal side of the protein that helps facilitate the delivery of protons to the heme through a specific hydrogen bonding network (74). In P450 SPα and P450 BSβ these trends are not observed. In P450 BSβ the proximal face contains negatively charged (acidic) residues including Glu^{113}, Glu^{216}, Glu^{275}, Glu^{341}, Glu^{343}, Glu^{358}, Glu^{366} and Glu^{371}, while the distal surface contains a positively charged (basic) cluster comprised of Lys^{17}, Arg^{40}, Lys^{44}, Lys^{72}, Arg^{73}, Lys^{76}, Arg^{179}, Arg^{184} and Arg^{399} (19). These variations characterise the peroxygenase nature of the enzymes, which do not require any interaction with redox partners, or a proton delivery network to the heme.

Differences between typical P450 monooxygenases and P450 peroxygenases have also been observed in the length of the “proximal cys ligand loop”. This loop typically contains the conserved sequence FXXGXXXCXGA, which is important for regulating heme iron potential and for interactions with the flavin or iron-sulfur binding portion of the redox partner to enable transfer of electrons to the heme (120). The proximal cys ligand loops in P450 SPα and P450 BSβ are longer than those in typical P450 monooxygenases. For example, P450cam has the loop structure ^{350}FGHGSHLC^{357}, whereas P450 SPα and P450 BSβ have the longer structures of ^{349}QGGGDHYLGHRC^{361} and ^{352}QGGGHAEKGHRC^{363}, respectively (19). This difference has also been observed in other non-redox partner utilising P450s, including allene oxide synthase (AOS) from *Arabidopsis thaliana*, which has the long loop structure ^{455}WSNGPETETPTVGNKQC^{472} (121). For optimal electron transfer, it is important for the

proximal cys ligand loop to be conserved in sequence and length. It is believed that its structural conservation is not necessary in P450s that do not depend on electron transfer from redox partners and, in fact, proteins with longer loop structures may have evolved to avoid potential interactions with diflavin reductases (i.e. CPRs) or other flavin-containing reductases or ferredoxins (121).

It has been noted that the conserved acid/alcohol pair of residues (e.g. Asp^{251}/Thr^{252} in P450cam), typically found on the distal side of the heme, are absent in the peroxygenases (19,102). These residues are important for protonation of the ferric-superoxo and ferric-hydroperoxo species in typical P450s, by forming a hydrogen bonding network that facilitates proton transfer relay (48,49). Instead, these residues are conserved as Arg/Pro in CYP152 P450 peroxygenases, with an Arg residue (Arg^{241} in P450 SPα and Arg^{242} in P450 BSβ). In comparison with typical P450 monooxygenases, the differences in these residues appear to alter the environment of the active site, leading to an absence of water molecules that would typically act as a hydrogen bonding network (19). Mutagenesis studies in P450 BSβ have shown these Arg and Pro residues (Arg^{242} and Pro^{243} in P450 BSβ) are important for catalysis. The R242K and R242A P450 BSβ mutants showed increased K_m values for H_2O_2 (0.21 mM and 4.4 mM for R242K and R242A mutants, respectively, compared to 0.021 mM for WT P450 BSβ) and decreased V_{max} values (22 min^{-1} and 0.17 min^{-1} for R242K and R242A mutants, respectively, compared to 240 min^{-1} for WT P450 BSβ), giving much lower V_{max}/K_m values of 105 min^{-1} mM^{-1} for R242K and 0.04 min^{-1} mM^{-1} for R242A mutants, compared to a WT P450 BSβ value of 11429 min^{-1} mM^{-1} (122).

In both P450 SPα and P450 BSβ, Arg^{241}/Arg^{242}, respectively, are located above the heme, The guanidinium group of these arginine residues interacts with the carboxylate group of the fatty acid substrate, forming a salt bridge (19,102). In P450 SPα, the distances between the two oxygen atoms of the fatty acid carboxylate group and the guanidinium moiety of Arg^{241} are 2.9 Å and 3.0 Å for $N_{\eta 2}$ and N_{ε}, respectively (19). This is similar for P450 BSβ, where the $N_{\eta 2}$ and N_{ε} distances are both 2.8 Å (102).

For both P450 SPα and P450 BSβ, the terminal carboxylate of the fatty acid substrate is positioned in close proximity to the heme, with P450 SPα showing heme iron-carboxylate oxygen distances of 5.2 Å in oxygen position A, and 5.5 Å in oxygen position B (102). The carboxylate moiety of the fatty acid is thought to act as an acid-base catalyst, with P450 SPα Arg^{241} and P450 BSβ Arg^{242} being important for modulating the basicity of the carboxylate. This is crucial for achieving heterolytic cleavage of the H_2O_2 O-O bond (19). The configuration of Arg^{241}/Arg^{242} with the fatty acid carboxylate in relation to the heme in P450 SPα and P450 BSβ is very similar to the orientations of His^{105} and Glu^{183} carboxylate in CPO (57,123) and Arg^{189} and Glu^{196} carboxylate in ascorbate peroxidase (APO) (124).

Studies have shown that the carboxylate groups of short chain fatty acids (C4:0-C10:0) can act as an acid-base catalyst and promote the oxidation of non-natural substrates by P450 BSβ. These reactions include one-electron oxidation of guaiacol, epoxidation of styrene, and hydroxylation of ethylbenzene (125). A crystal structure was obtained for heptanoic acid (C7:0)-bound P450 BSβ (126), showing that the carboxylate group is fixed by electrostatic interactions with Arg^{242}, occupying a similar position to that of palmitic acid-bound P450 BSβ (19). This indicates that the carboxylate of heptanoic acid is able to act as a general acid-base catalyst. In addition, there are no structural changes to the active site observed upon binding of heptanoic acid (compared to the substrate-free P450 BSβ), indicating that it is the formation of the electrostatic interaction between Arg^{242} and the substrate carboxylate that switches the enzyme to a catalytically active state (126). In addition, high concentrations of acetate anion can assist in the oxidation of non-native substrates, including styrene epoxidation and 1-methoxynaphthalene hydroxylation in P450 SPα and BS BSβ (127). In this case it appears that decoy molecules as small as acetate can bind to the Arg^{241}/Arg^{242} and serve as general acid-base catalysts (127).

A similar system was also reported for P450 SPα, where an A245E mutation was designed so that Glu^{245} could mimic binding of the substrate carboxylate(128). The crystal structure of this mutant showed an Arg^{241}/Glu^{245} distance of 3.2 Å and Glu^{245}/ heme iron distance of 4.9 Å. The structure shows that a water molecule occupies a position between Arg^{241} and Glu^{245}, at a distance of 4.9 Å from the heme iron, which is an almost identical position to that of the

carboxylate oxygen atom of palmitic acid in the wild type structure, and at a suitable distance to act as a general acid-base catalyst (128). This P450 SPα A245E was shown to oxidise styrene with a k_{cat} of 280 min^{-1}, an activity not seen in the WT P450 SPα (128).

In addition, there are other hydrophilic residues positioned distally to the heme, and in P450 SPα these include Gln^{84}, Asp^{238} and Arg^{241} (102). These residues provide a polar environment that is thought to facilitate the heterolytic cleavage of the O-O bond of H_2O_2.

Addition of fatty acid substrates to $OleT_{JE}$ causes high-spin shifts, but similar substrates do not induce any high-spin shift in P450 SPα and only small high-spin shifts in P450 BSβ. Similarly, addition of H_2O_2 to substrate-free enzyme did not change the UV-visible spectrum of P450 BSβ. These results indicate that H_2O_2 is only effective in displacing the distal water when a substrate is bound to P450 BSβ (25). The acid-base functionality of the salt bridge formed between fatty acid carboxylate and $Arg^{241/242}$ then allows the generation of Cpd I, leading to the stereospecific hydroxylation of the fatty acid (19).

1.12. The Discovery of $OleT_{JE}$, a Fatty Acid Decarboxylase

$OleT_{JE}$ was first discovered in *Jeotgalicoccus* sp. 8456 by Rude et al in 2011(18). The *Jeotgalicoccus* genus was first isolated from jeotgal (a traditional Korean fermented seafood), and has been described as Gram-positive cocci (129,130). Rude and colleagues identified that *Jeotgalicoccus* sp. 8456 could produce terminal alkenes naturally, as shown *in vivo* after addition of fatty acids to bacterial cell cultures, as well as *in vitro* with cell extracts, leading to increased levels of formation of terminal alkenes. This group used a reverse genetics approach to isolate the fatty acid decarboxylase, and to assign the sequence of the protein. This 48,367 Da protein is a member of the CYP152 family of P450 peroxygenases based on its amino acid sequence. Recombinant expression in *E. coli* and its purification confirmed that $OleT_{JE}$ was able to decarboxylate fatty acids to form terminal alkenes, and to hydroxylate fatty acids in the α- and β- positions in the presence of H_2O_2 (18).

Rude and colleagues identified that P450 BSβ has 41% protein sequence identity to $OleT_{JE}$. They performed homology modelling of $OleT_{JE}$ based on the structure of P450 BSβ using

Swiss-Model (131). The model showed that the most notable difference between $OleT_{JE}$ and P450 BSβ is at His85 in $OleT_{JE}$, which appeared to be a conserved Gln85 in other selected P450 peroxygenases (although a number of CYP152 enzymes are now known also to have a histidine in this position). They then created a P450 BSβ Q85H mutant, and found that, during *in vitro* reaction with palmitic acid, the mutant showed a decreased rate of 2-hydroxy palmitic acid production, and an increased rate of 1-pentadecene production when compared to WT P450 BSβ. The ratio of decarboxylation to hydroxylation was increased from 0.19 in WT P450 BSβ to 0.30 in P450 BSβ Q85H. However, this ratio is still much lower than for WT $OleT_{JE}$, which has a decarboxylation/hydroxylation ratio of 3.32 (18).

$OleT_{JE}$ was shown to catalyse the turnover of fatty acids of chain length C12-C20 when incubated with 500 μM H_2O_2 for 2 hours (130). $OleT_{JE}$ also proved active as a P450 monooxygenase, forming hydroxylated fatty acid products (132,133). Other studies have shown that high levels of turnover can be achieved with $OleT_{JE}$ by using electron transfer proteins from spinach (ferredoxin and ferredoxin reductase) and *Pseudomonas putida* (putidaredoxin and putidaredoxin reductase, CamAB) in conjunction with a NAD(P)H regeneration system (133). Regeneration systems based on phosphite dehydrogenase (PDH; NADPH-dependent) and formate dehydrogenase (FDH; NADH-dependent) gave 1-heptadecene yields of 2.6 mM and 3.1 mM, respectively, from 5 mM stearic acid (C18), which corresponds to conversion rates of 52% and 62%, respectively (133). A glucose dehydrogenase (GDH) system was also tested, but 1-heptadecene was produced to only 36% yield with 1 mM stearic acid. Activity is thought to be decreased in this system as generation of gluconic acid as a by-product may competitively bind to the Arg245 residue, giving an inhibitory effect (133). By using an $OleT_{JE}$/CamAB/FDH system, the decarboxylation of fatty acids from C4:0 to C20:0 has also been observed (133).

A fusion of the P450 phthalate dioxygenase reductase (PDOR) domain (RhFRED from the *Rhodococcus* sp. 9784 CYP116B2 P450-PDOR fusion protein) to $OleT_{JE}$ has also been reported to catalyse 83% conversion of 200 μM myristic acid (C14) in the presence of NADPH (28). *In vivo* studies showed that expression of the $OleT_{JE}$-RhFRED fusion in *E. coli* gave decreased alkene production compared to the expression of $OleT_{JE}$ in isolation. It was

reported that H_2O_2 levels in growing *E. coli* cells are less than 20 nM, and that H_2O_2 levels of 2 µM are enough to cause growth inhibition of *E. coli* cells (134). It therefore seems likely that $OleT_{JE}$ successfully utilises a native redox system of *E. coli*, a behaviour that was also shown in P450 CLA (CYP152B1), a fatty acid α-hydroxylase from *Clostridium acetobutylicum* (103). This finding was confirmed by *in vitro* studies that showed 63% conversion of 200 µM myristic acid in the presence of *E. coli* flavodoxin, flavodoxin reductase and NADPH (133).

Light has also been demonstrated to drive catalysis in $OleT_{JE}$ when the P450 is incubated with ethylenediaminetetraacetate (EDTA) and FMN (135). In this system, light-excited FMN is reduced by electrons from EDTA. The reduced FMN then reacts with O_2 to produce H_2O_2. This system was also reported to drive reactions of P450 BSβ and P450 CLA (136). When crude cell extracts of recombinantly expressed $OleT_{JE}$ were used in conjunction with this light-driven system, conversion of stearic acid was low, at around 5%. However, when the light-driven system was used *in vitro* with purified $OleT_{JE}$, a much higher substrate conversion level of 99% was achieved. Shorter chain length fatty acids showed low levels of conversion, with reactions using lauric acid and myristic acid showing conversions of less than 10% (135). This study also used naturally derived fatty acids from vegetable fats and hardened palm oil in this photo-enzymatic system. In hardened palm oil, which is comprised mainly of stearic acid and palmitic acid, reaction mixtures showed 15% conversion of stearic acid to 1-heptadecene and 8% conversion of palmitic acid to 1-pentadecene when ~1 mM of the fatty acid mixture was incubated with 100 µg/ml $OleT_{JE}$, 50 mM EDTA and 10 µM FMN. When the same reactions were performed with hardened palm oil (made up of ~72% saturated fatty acids and ~28% unsaturated fatty acids), only traces of alkenes were detected. It was hypothesised that oleic acid present in the hardened palm oil may be responsible for inhibiting $OleT_{JE}$, which was confirmed by experiments that showed that $OleT_{JE}$ was unable to decarboxylate stearic acid in the presence of oleic acid. This inhibitory effect may pose a problem if $OleT_{JE}$ was to be used industrially, as certain endogenous fatty acids of host organisms could cause an inhibitory effect.

Rude et al. also investigated the activity of four other previously uncharacterised P450 peroxygenases that share high sequence similarity to $OleT_{JE}$. These studies highlighted three

other CYP152 family enzymes from the organisms *Corynebacterium efficiens*, *Kocuria rhizophila* and *Methylobacterium populi* (18). From these enzymes, the orthologue from *M. populi* was recently expressed and characterised by Amaya et al., and was named P450 MP (137).

In order to achieve successful expression and purification, P450 MP was expressed with a cleavable glutathione-S-transferase (GST) solubility tag. When purified, this P450 showed an atypically long wavelength Soret peak at 422 nm (137). P450s usually have a Soret peak at around 416-420 nm (138), along with α/β bands at around 570 and 545 nm, respectively. The formation of a ferrous-CO complex resulted in a characteristic Soret peak shift to a wavelength of 448 nm, indicative of cysteine thiolate coordination of the heme iron, with only ~15% P420, resulting from cysteine thiol ligation. Interestingly, addition of fatty acid substrates (C12-C18) to P450 MP resulted in no significant spectroscopic changes, unlike in $OleT_{JE}$ where several fatty acids produce extensive spin-state equilibrium shifts towards high-spin (137).

EPR spectroscopy indicated a single low-spin species in the substrate-free form of P450 MP, with g-values of g_z= 2.49, g_y= 2.26 and g_x= 1.87 (2.49/2.26/1.87) (137). In agreement with EPR data from P450 SPα (102), the g_z value of P450 MP is quite high for a P450 monooxygenase, with the value generally falling in the range of g ≤ 2.45. For example a g_z = 2.45 was reported for the substrate-free form of P450cam (139), and a g_z = 2.42 was reported for P450 BM3 (140). High g_z values were also reported in other P450 enzymes, including the P450-flavodoxin fusion enzyme XplA (CYP177A1) from *Rhodococcus rhodochrous*, which catalyses the reduction of the explosive hexahydro-1,3,5-trinitro-1,3,5-triazene (Royal Demolition Explosive, RDX). For this enzyme, two low-spin populations were reported with g-values of 2.56/2.26/1.84 and 2.49/2.26/1.86, and it was postulated that these g-values reflected unusual hydrogen bonding or other interactions of the distal ligand with active site residues of XplA (141).

Addition of fatty acids to P450 MP did not result in any HS signal formation. However, addition of stearic acid (C18:0) resulted in a new set of LS ferric heme EPR g-values of 2.52/2.26/1.87, deriving from changes in the hydrogen bonding network in the distal pocket. Shorter fatty acid chain lengths did not produce any further changes in the EPR spectra from that of the

substrate-free enzyme (137). Makris et al also performed *in vitro* turnover studies with P450 MP using fatty acid chain lengths from C12-C20. Unlike $OleT_{JE}$, arachidic acid was shown to be a poor substrate for P450 MP, and only small levels of β-OH arachidic acid product were detected. However, substrate conversion levels increased for shorter chain fatty acids. Alkene products were not detected for reactions carried out with lauric acid and myristic acid, with only hydroxylation of these fatty acids substrates observed. However, for longer chain fatty acids, substrate decarboxylation does take place. Alkenes contributed 24 and 38% of the products formed for palmitic and stearic acid, respectively. Despite this, hydroxylation was still the major reaction catalysed by P450 MP, with β-OH fatty acids being the most prevalent product, even at higher fatty acid substrate chain lengths. Interestingly, however, Makris et al reported an increased diversity of hydroxylated products when reactions were carried out with fatty acids of chain lengths ≤ C16, and the formation of α, β, γ, δ, and even ε-OH fatty acids were reported in the cases of myristic and lauric acid (137). This finding suggests multiple binding modes for the fatty acid substrate in P450 MP, with product profiles becoming more diverse as the chain length of the substrate decreases. Homology models suggest that this decreased regioselectivity with respect to $OleT_{JE}$ may be due to the lack of phenylalanine residues at positions 79 and 172, which are present as the smaller and more hydrophilic residues Thr183 and Gln90, respectively, in P450 MP. It was proposed that the Phe residues played a role in anchoring the fatty acid in $OleT_{JE}$, altering the propensity for its decarboxylation (137).

Another residue hypothesised to be key in explaining the differences in catalytic activity between P450 MP and $OleT_{JE}$ is His85 in $OleT_{JE}$, which is present as Met96 in P450 MP. In order to explore this difference, a P450 MP M96H mutant was created. However this mutant converted less than 1% of fatty acid substrates into products. In addition, CO binding to ferrous P450 MP gave a reduced level of P450 formation (compared to $OleT_{JE}$), with ~40% P420 formed (137).

1.13. Mechanistic Analysis of $OleT_{JE}$

In 2015, Grant et al. definitively showed that CO_2 is released upon C-C bond scission in $OleT_{JE}$-dependent fatty acid decarboxylation. Headspace FTIR measurements of reaction mixtures showed the formation of a doublet at 2340^{-1} and 2360 cm^{-1} which derives from the asymmetric stretch of CO_2. Additionally, single turnover reactions were carried out where the carboxylate group of the fatty acid substrate (arachidic acid) was isotopically labelled (using $CH_3(CH_2)_{18}{}^{13}COOH$), and headspace GC/MS was used to confirm the presence of isotopically labelled CO_2(94).

Grant et al also observed Cpd I in $OleT_{JE}$, referred to as Ole-I, by using deuterated arachidic acid as a substrate, and by monitoring turnover using stopped-flow absorption spectroscopy following rapid mixing of H_2O_2 with the $OleT_{JE}$-substrate complex. It was reported that, within 15 ms of addition of H_2O_2 to the high-spin E-S complex, the Soret peak at 392 nm decayed and a new species with a Soret maximum at 370 nm and an additional absorption band at 690 nm had appeared. These characteristics are almost identical to those of Cpd I in CYP119A1 (described in section 1.7f). Ole-I was reported to accumulate to over 70% at 15 ms, and then to decay completely within 1 s back to the LS ferric resting state. The decay rate constant of Ole-I was determined as 80 s^{-1}, and this rate constant was unaffected by changes in H_2O_2 concentration, indicating irreversible heterolysis of the O-O bond. Rapid mixing of a protiated fatty acid substrate with $OleT_{JE}$ led to the decay of the HS species to the LS ferric resting state within 15 ms. Although initial attempts to observe Ole-I using protiated substrate were unsuccessful, this was later achieved using a photomultiplier tube (PMT), which provided greater sensitivity (94). Absorbance at 370 nm was recorded for both D_{39}-arachidic acid- and H_{39}-arachidic acid-bound $OleT_{JE}$ reactions and data were fitted using two-summed exponential functions. Isotopic sensitivity was only observed for the fast relaxation time in the first phase where $1/\tau_1 = 630 \pm 60$ s^{-1} for H_{39}-arachidic acid and $1/\tau_1 = 77 \pm 2$ s^{-1} for D_{39}-arachidic acid. This gave a ^2H KIE ≤ 8.1 ±1.1 (94), which is similar to values reported by Rittle and Green, in which kinetic characterisation of CYP119A1 Compound I was carried out by rapid mixing of CYP119A1 and m-CPBA incubated with various concentrations of protiated and deuterated hexanoic acid (KIE_{obs} = 12.5), octanoic acid (KIE_{obs} = 5.3) and lauric acid (KIE_{obs} = 1.0) (140).

The ^{2}H KIE for Ole-I decay was also similar to that obtained by steady-state studies of norbornane oxidation by a purified liver microsomal P450 system, which showed a KIE of 11.5 ± 1 (90). This observed KIE indicates that C-Cα bond cleavage involves hydrogen abstraction from the substrate, in a similar mechanism to that generally accepted to occur by typical P450 hydroxylases. The observed slower phase ($1/\tau_2$ = 6.9 ± 0.4 s^{-1} for H_{39}-arachidic acid and $1/\tau_2$ = 8.1± 0.4 s^{-1} for D_{39}-arachidic acid) is indicative of decay of a second intermediate (Int2), and similar reciprocal relaxation time (RRT) rates between protiated and perdeuterated substrates indicate that this intermediate does not directly abstract an H atom (94). Int2 was spectroscopically observed as having a red-shifted Soret maximum at 426 nm with a lower molar extinction coefficient than that observed in the water-ligated, LS ferric heme. Int2 also shows a split Soret band with an additional absorption maximum at 370 nm (94). These features are similar to those observed in Fe^{VI}-OH Compound II that has been isolated in CYP158, which exhibits a split Soret band with maxima at 370 and 426 nm at pH 9 (93). Int2 is also similar to compound II observed in APO (APO-II), which is a heme-thiolate peroxygenase from *Agrocybe aegerita*. Here the UV-visible spectrum of APO-II features a split Soret with maxima at 370 and 428 nm (143).

A mechanism was proposed (shown in figure 1.5) in which Ole-I abstracts a hydrogen atom to form Ole-II, resulting in the formation of a substrate radical. Competition between two separate pathways could then occur. Hydroxylated product formation would involve •OH rebound. Alternatively, abstraction of another substrate electron by Ole-II could take place, which, when coupled to recruitment of a proton, would restore the water-ligated ferric LS heme. This would also generate a carbocation or substrate diradical, resulting in C-Cα cleavage to produce terminal alkene and CO_2 (89,94).

The generation of substrate carbocations was also proposed to play a role in the desaturation of α/β alkylbenzenes by P450 BM3, and (more effectively) by the P450 BM3 KT5 mutant (F87A/A330P/E377A/D425N). For this reaction, Whitehouse et al. postulated that α/β-desaturation is initiated by abstraction of a proton from the α or β position of the alkylbenzene by Cpd I. At this point, radical rebound is able to occur, leading to the formation of hydroxylated product. However, a further proton abstraction is also possible, leading to the formation of a

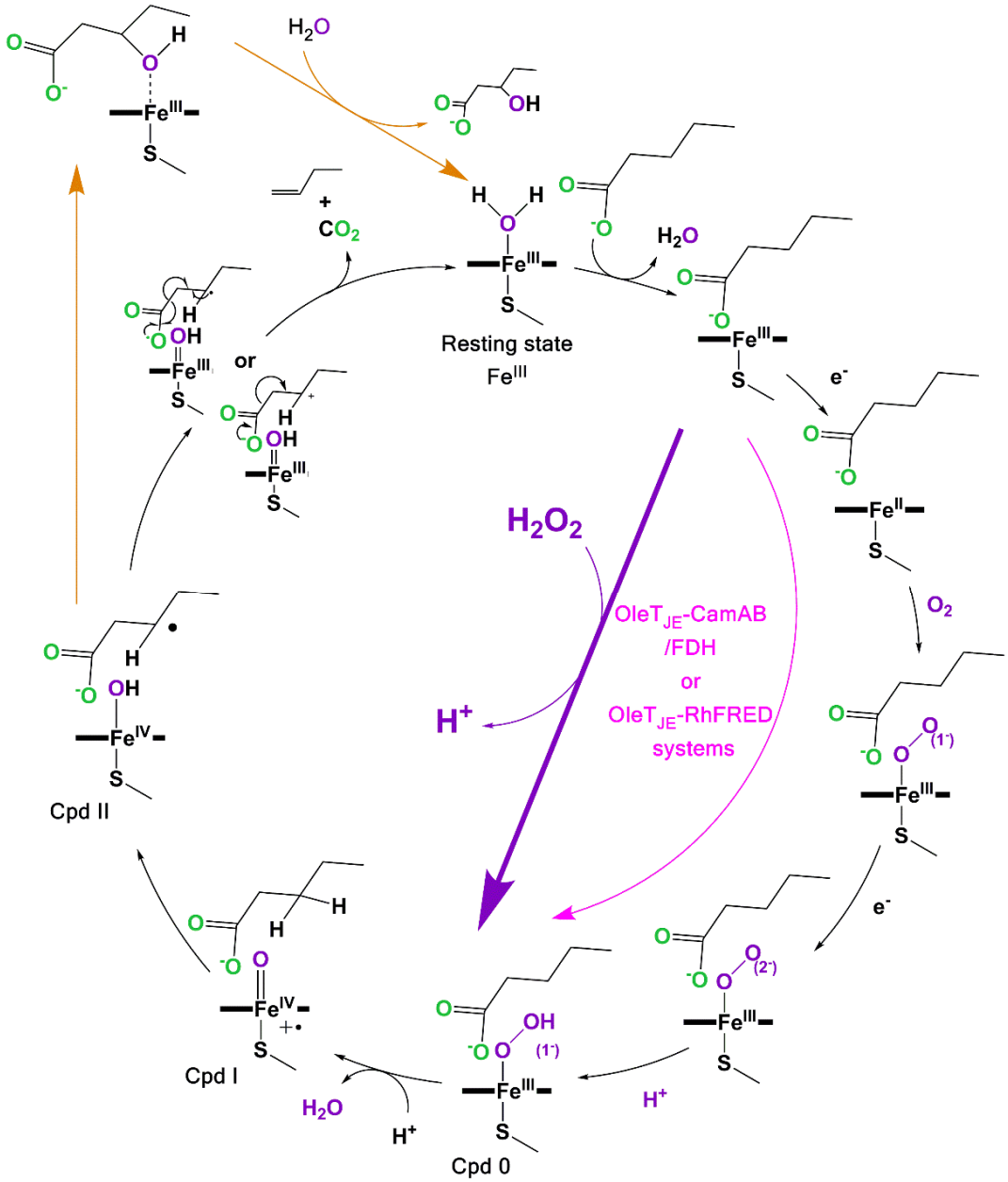

Figure 1.5. Catalytic pathways of $OleT_{JE}$. The ferric (Fe^{III}) resting state of $OleT_{JE}$ is co-ordinated by a distal water molecule and a proximal cysteine thiolate. Fatty acid binding displaces this distal water, shifting the heme iron to a HS state. At this point, $OleT_{JE}$ can either bind H_2O_2 (purple arrow), or can be reduced by two single electrons using heterologous redox partners such as the CamAB (putidaredoxin reductase/putidaredoxin) or FDH (flavoprotein dehydrogenase) enzymes, or using a *Rhodococcus* sp. phthalate dioxygenase reductase (RhFRED) system (131) (pink arrow). Both pathways lead to the formation of Ole-0 (the Cpd 0 state), which undergoes protonation and dehydration to give rise to Ole-I (the Cpd I state). Ole-I then abstracts a substrate proton, forming Ole-II (Cpd II) which gives rise to a substrate carbon radical. At this point $OleT_{JE}$ can perform "radical oxygen rebound" to produce hydroxylated fatty acid product (orange arrows) (88). The hydroxylated product is subsequently released, allowing water to rebind and reinstate the ferric resting form. Alternatively, another electron can be abstracted from the substrate radical by Ole-II, forming either a carbocation or substrate diradical intermediate. These intermediates would then undergo C-C_α cleavage to release a terminal alkene and CO_2. Recruitment of a proton would then restore the water ligated ferric (Fe^{III}) resting state (92,87).

Cα-Cβ double bond. Alternatively, α- or β-hydrogen abstraction followed by single electron oxidation could give rise to an α- or a β-cation, which is subsequently deprotonated to form the α/β desaturated product (144).

Cationic intermediates are also involved in the oxidative rearrangement of pentalenolactone F to pentalenolactone catalysed by CYP161C3 and CYP161C2 from *Streptomyces exfoliates* UC5319 and *Streptomyces arenae* TU469. In this case, a C1 cation is generated by transfer of the H-1 *si* hydride to Cpd I. This neopentyl cation intermediate then goes through *syn* migration of the C-12 methyl group and deprotonation of H-3 in order to generate pentalenolactone (145).

Cationic rearrangement products have also been observed in studies utilising radical clock substrates. In these studies, oxidation of norcarane by P450cam, P450 BM3 and CYP2B1 gave rise to trace amounts of cationic rearrangement products (146). Additionally, carbocation chemistry is believed to be important for the conversion of androgens to oestrogens. In this case, CYP19A1 is thought to catalyse the conversion of androstenedione to estrone. The reaction is thought to be initiated by abstraction of the 1β-hydrogen, with further electron transfer giving rise to a C-1 carbocation. Proton extraction by Fe^{IV}-OH and rearrangement of the molecule then forms the estrone product and formic acid (147,148).

1.14 Engineering of $OleT_{JE}$

$OleT_{JE}$ has been engineered to catalyse the hydroxylation and epoxidation of non-natural hydrocarbon substrates (149). An acidic residue was introduced into the protein framework of OleTJE, providing the necessary carboxylate for H_2O_2 heterolysis that is usually provided by the fatty acid substrate carboxylate (149). This P246D mutant no longer showed any decarboxylation or hydroxylation activity for arachidic acid and palmitic acid, perhaps due to restrictions imposed in the active site. However, this mutant was shown to epoxidise styrene with a yield of 96%, to hydroxylate nonane forming 2-, 3- and 4-nonanols, and to hydroxylate cyclohexane (149).

$OleT_{JE}$ is a promising candidate for a synthetic biology approach to producing "drop-in" biofuels, that are compatible with our existing transportation infrastructure. An artificial pathway has been reported whereby renewable low-cost triacylglycerols (TAGs) could be used as a feedstock to generate terminal alkenes (150). In this system, TAGs are cleaved by *Thermomyces lanuginosus* lipase (TII) to form fatty acids and glycerol. The fatty acids produced from this step could then be used by $OleT_{JE}$ to form terminal alkenes. Using this pathway, terminal alkene yields of 6.7-46% of the starting material were achieved, with trimyristin (a TAG containing three C14 fatty acyl chains) (150).

This thesis describes the structural and biochemical charaterisation of $OleT_{JE}$. The properties of this enzyme were investigated by evaluating the wild type enzyme, in addition to key mutants: $OleT_{JE}$ H85Q, F79A, F79W, F79Y, R245L and R245E. Engineering of an $OleT_{JE}$ fusion with alditol oxidase (AldO) from *Streptomyces Coelicolor* is also reported. In this system, H_2O_2 was slowly produced from the oxidation of glycerol by AldO; this H_2O_2 was then used to drive the decarboxylation of fatty acids by $OleT_{JE}$. The biochemical properties of an $OleT_{JE}$ homologue, named P450KR from *Kocuria rhizophilia*, is also discussed.

1.15. References

1. Rulli, M. C., Bellomi, D., Cazzoli, A., De Carolis, G., and D'Odorico, P. (2016) The water-land-food nexus of first-generation biofuels. *Scientific reports* **6**, 22521-22531
2. Zhang, F., Rodriguez, S., and Keasling, J. D. (2011) Metabolic engineering of microbial pathways for advanced biofuels production. in *Curr Opin Biotechnol*, 2011 Elsevier Ltd, England. pp 775-783
3. Wang, W., and Lu, X. (2013) Microbial Synthesis of Alka(e)nes. *Front Bioeng Biotechnol* **1**, 10
4. Schirmer, A., Rue, M., and Brubaker, S. (2009) Methods and compositions for producing hydrocarbons. Google Patents
5. Zobell, C. E. (1945) The Role of Bacteria in the Formation and Transformation of Petroleum Hydrocarbons. *Science* **102**, 364-369

6. Stone, R. W., and ZoBell, C. E. (1952) Bacterial Aspects of the Origin of Petroleum. *Ind Eng Chem Res* **44**, 2564-2567

7. Takarada, H., Sekine, M., Kosugi, H., Matsuo, Y., Fujisawa, T., Omata, S., Kishi, E., Shimizu, A., Tsukatani, N., Tanikawa, S., Fujita, N., and Harayama, S. (2008) Complete Genome Sequence of the Soil Actinomycete Kocuria rhizophila. in *J Bacteriol*. 4139-4146

8. Albro, P. W., and Dittmer, J. C. (1969) The biochemistry of long-chain, nonisoprenoid hydrocarbons. 3. The metabolic relationship of long-chain fatty acids and hydrocarbons and other aspects of hydrocarbon metabolism in Sarcina lutea. *Biochemistry* **8**, 1913-1918

9. Beller, H. R., Goh, E. B., and Keasling, J. D. (2010) Genes involved in long-chain alkene biosynthesis in Micrococcus luteus. *Appl Environ Microbiol* **76**, 1212-1223

10. Sukovich, D. J., Seffernick, J. L., Richman, J. E., Hunt, K. A., Gralnick, J. A., and Wackett, L. P. (2010) Structure, Function, and Insights into the Biosynthesis of a Head-to-Head Hydrocarbon in Shewanella oneidensis Strain MR-1. *Appl Environ Microbiol* **76**, 3842-3849

11. Sukovich, D. J., Seffernick, J. L., Richman, J. E., Gralnick, J. A., and Wackett, L. P. (2010) Widespread head-to-head hydrocarbon biosynthesis in bacteria and role of OleA. *Appl Environ Microbiol* **76**, 3850-3862

12. Frias, J. A., Richman, J. E., Erickson, J. S., and Wackett, L. P. (2011) Purification and characterization of OleA from Xanthomonas campestris and demonstration of a non-decarboxylative Claisen condensation reaction. *J Biol Chem* **286**, 10930-10938

13. Goblirsch, B. R., Frias, J. A., Wackett, L. P., and Wilmot, C. M. (2012) Crystal structures of Xanthomonas campestris OleA reveal features that promote head-to-head condensation of two long-chain fatty acids. *Biochemistry* **51**, 4138-414614.

Haapalainen, A. M., Merilainen, G., and Wierenga, R. K. (2006) The thiolase superfamily: condensing enzymes with diverse reaction specificities. *Trends Biochem Sci* **31**, 64-71

15. Mendez-Perez, D., Begemann, M. B., and Pfleger, B. F. (2011) Modular synthase-encoding gene involved in alpha-olefin biosynthesis in Synechococcus sp. strain PCC 7002. *Appl Environ Microbiol* **77**, 4264-4267

16. Khosla, C., Gokhale, R. S., Jacobsen, J. R., and Cane, D. E. (1999) Tolerance and specificity of polyketide synthases. *Annual review of biochemistry* **68**, 219-253

17. Coates, R. C., Podell, S., Korobeynikov, A., Lapidus, A., Pevzner, P., Sherman, D. H., Allen, E. E., Gerwick, L., and Gerwick, W. H. (2014) Characterization of cyanobacterial hydrocarbon composition and distribution of biosynthetic pathways. *PLoS One* **9**, 85140-85152

18. Rude, M. A., Baron, T. S., Brubaker, S., Alibhai, M., Del Cardayre, S. B., and Schirmer, A. (2011) Terminal olefin (1-alkene) biosynthesis by a novel p450 fatty acid decarboxylase. *Appl Environ Microbiol* **77**, 1718-1727

19. Lee, D. S., Yamada, A., Sugimoto, H., Matsunaga, I., Ogura, H., Ichihara, K., Adachi, S., Park, S. Y., and Shiro, Y. (2003) Substrate recognition and molecular mechanism of fatty acid hydroxylation by. *J Biol Chem* **278**, 9761-9767

20. Imai, Y., Matsunaga, I., Kusunose, E., and Ichihara, K. (2000) Unique heme environment at the putative distal region of hydrogen peroxide-dependent fatty acid alpha-hydroxylase from Sphingomonas paucimobilis (peroxygenase P450(SPalpha). *J Biochem* **128**, 189-194

21. Belcher, J., McLean, K. J., Matthews, S., Woodward, L. S., Fisher, K., Rigby, S. E., Nelson, D. R., Potts, D., Baynham, M. T., Parker, D. A., Leys, D., and Munro, A. W. (2014) Structure and biochemical properties of the alkene producing cytochrome P450 OleTJE (CYP152L1) from the Jeotgalicoccus sp. 8456 bacterium. *J Biol Chem* **289**, 6535-6550

22. Schirmer, A., Rude, M. A., Li, X., Popova, E., and del Cardayre, S. B. (2010) Microbial Biosynthesis of Alkanes. *Science* **329**, 559-562

23. Schirmer, A., Rude, M. A., Li, X., Popova, E., and del Cardayre, S. B. (2010) Microbial biosynthesis of alkanes. *Science* **329**, 559-562

24. Li, N., Chang, W. C., Warui, D. M., Booker, S. J., Krebs, C., and Bollinger, J. M., Jr. (2012) Evidence for only oxygenative cleavage of aldehydes to alk(a/e)nes and formate by cyanobacterial aldehyde decarbonylases. *Biochemistry* **51**, 7908-7916

25. Howard, T. P., Middelhaufe, S., Moore, K., Edner, C., Kolak, D. M., Taylor, G. N., Parker, D. A., Lee, R., Smirnoff, N., Aves, S. J., and Love, J. (2013) Synthesis of customized petroleum-replica fuel molecules by targeted modification of free fatty acid pools in Escherichia coli. *Proc Natl Acad Sci USA* **110**, 7636-7641

26. Warui, D. M., Li, N., Norgaard, H., Krebs, C., Bollinger, J. M., Jr., and Booker, S. J. (2011) Detection of formate, rather than carbon monoxide, as the stoichiometric coproduct in conversion of fatty aldehydes to alkanes by a cyanobacterial aldehyde decarbonylase. *J Am Chem Soc* **133**, 3316-3319

27. Li, N., Norgaard, H., Warui, D. M., Booker, S. J., Krebs, C., and Bollinger, J. M., Jr. (2011) Conversion of fatty aldehydes to alka(e)nes and formate by a cyanobacterial aldehyde decarbonylase: cryptic redox by an unusual dimetal oxygenase. *J Am Chem Soc* **133**, 6158-6161

28. Yuan, L., Voelker, T. A., and Hawkins, D. J. (1995) Modification of the substrate specificity of an acyl-acyl carrier protein thioesterase by protein engineering. *Proc Natl Acad Sci USA* **92**, 10639-10643

29. Voelker, T. A., Worrell, A. C., Anderson, L., Bleibaum, J., Fan, C., Hawkins, D. J., Radke, S. E., and Davies, H. M. (1992) Fatty acid biosynthesis redirected to medium chains in transgenic oilseed plants. *Science* **257**, 72-74

30. Liu, T., Vora, H., and Khosla, C. (2010) Quantitative analysis and engineering of fatty acid biosynthesis in E. coli. *Metab Eng* **12**, 378-386

31. Akhtar, M. K., Turner, N. J., and Jones, P. R. (2013) Carboxylic acid reductase is a versatile enzyme for the conversion of fatty acids into fuels and chemical commodities. *Proc Natl Acad Sci USA* **110**, 87-92

32. Munro, A. W., Girvan, H. M., and McLean, K. J. (2007) Variations on a (t)heme--novel mechanisms, redox partners and catalytic functions. *Nat Prod Rep* **24**, 585-609

33. Nelson, D. R., Koymans, L., Kamataki, T., Stegeman, J. J., Feyereisen, R., Waxman, D. J., Waterman, M. R., Gotoh, O., Coon, M. J., Estabrook, R. W., Gunsalus, I. C.,

and Nebert, D. W. (1996) P450 superfamily: update on new sequences, gene mapping, accession numbers and nomenclature. *Pharmacogenetics* **6**, 1-42

33. Munro, A. W., Girvan, H. M., Mason, A. E., Dunford, A. J., and McLean, K. J. (2013) What makes a P450 tick? *Trends Biochem Sci* **38**, 140-150

35. Guengerich, F. P., Waterman, M. R., and Egli, M. Recent Structural Insights into Cytochrome P450 Function. *Trends Pharmacol Sci*

36. Girvan, H. M., and Munro, A. W. (2016) Applications of microbial cytochrome P450 enzymes in biotechnology and synthetic biology. *Curr Opin Chem Biol* **31**, 136-145

37. Klingenberg, M. (1958) Pigments of rat liver microsomes. *Arch Biochem Biophys* **75**, 376-386

38. Omura, T., and Sato, R. (1962) A new cytochrome in liver microsomes. *J Biol Chem* **237**, 1375-1376

39. Omura, T. (2011) Recollection of the early years of the research on cytochrome P450. *Proc Jpn Acad Ser B Phys Biol Sci* **87**, 617-640

40. Cooper, D. Y., Estabrook, R. W., and Rosenthal, O. (1963) The stoichiometry of C21 hydroxylation of steroids by adrenocortical microsomes. *J Biol Chem* **238**, 1320-1323

41. Nebert, D. W., Adesnik, M., Coon, M. J., Estabrook, R. W., Gonzalez, F. J., Guengerich, F. P., Gunsalus, I. C., Johnson, E. F., Kemper, B., Levin, W., and et al. (1987) The P450 gene superfamily: recommended nomenclature. *Dna* **6**, 1-11

42. Nelson, D. R. (2006) Cytochrome P450 nomenclature, 2004. *Methods Mol Biol* **320**, 1-10

43. Nelson, D. R. (2009) The Cytochrome P450 Homepage. *Human Genomics* **4**, 59-65

44. Poulos, T. L., Finzel, B. C., and Howard, A. J. (1986) Crystal structure of substrate-free Pseudomonas putida cytochrome P-450. *Biochemistry* **25**, 5314-5322

45. Ravichandran, K. G., Boddupalli, S. S., Hasermann, C. A., Peterson, J. A., and Deisenhofer, J. (1993) Crystal structure of hemoprotein domain of P450BM-3, a prototype for microsomal P450's. *Science* **261**, 731-736

46. Hasemann, C. A., Kurumbail, R. G., Boddupalli, S. S., Peterson, J. A., and Deisenhofer, J. (1995) Structure and function of cytochromes P450:a comparative analysis of three crystal structures. *Structure* **3**, 41-62

47. Denisov, I. G., Makris, T. M., Sligar, S. G., and Schlichting, I. (2005) Structure and chemistry of cytochrome P450. *Chem Rev* **105**, 2253-2277

48. Hishiki, T., Shimada, H., Nagano, S., Egawa, T., Kanamori, Y., Makino, R., Park, S. Y., Adachi, S., Shiro, Y., and Ishimura, Y. (2000) X-ray crystal structure and catalytic properties of Thr252Ile mutant of cytochrome P450cam: roles of Thr252 and water in the active center. *J Biochem* **128**, 965-974

49. Raag, R., Martinis, S. A., Sligar, S. G., and Poulos, T. L. (1991) Crystal structure of the cytochrome P-450CAM active site mutant Thr252Ala. *Biochemistry* **30**, 11420-11429

50. Syed, K., and Mashele, S. S. (2014) Comparative Analysis of P450 Signature Motifs EXXR and CXG in the Large and Diverse Kingdom of Fungi: Identification of Evolutionarily Conserved Amino Acid Patterns Characteristic of P450 Family. *PLoS ONE* **9**, e95616

51. Rupasinghe, S., Schuler, M. A., Kagawa, N., Yuan, H., Lei, L., Zhao, B., Kelly, S. L., Waterman, M. R., and Lamb, D. C. (2006) The cytochrome P450 gene family CYP157 does not contain EXXR in the K-helix reducing the absolute conserved P450 residues to a single cysteine. *FEBS Lett* **580**, 6338-6342

52. Poulos, T. L., and Johnson, E. F. (2015) Structure of Cytochrome P450 Enzyme. in *Cytochrome P450: Structure, Mechanism and Biochemsitry* (Ortiz de Montellano, P. R. ed.), 4 Ed., Springer International Publishing, Switzerland. pp 3-32

53. McLean, K. J., Leys, D., and Munro, A. W. (2015) Microbial Cytochromes P450. in *Cytochrome P450: Structure, Mechanism and Biochemistry* (Ortiz de Montellano, P. R. ed.), 4 Ed., Springer International Publishing, Switzerland. pp 261-408

54. Ost, T. W., Miles, C. S., Munro, A. W., Murdoch, J., Reid, G. A., and Chapman, S. K. (2001) Phenylalanine 393 exerts thermodynamic control over the heme of flavocytochrome P450 BM3. *Biochemistry* **40**, 13421-13429

55. Crane, B. R., Arvai, A. S., Ghosh, D. K., Wu, C., Getzoff, E. D., Stuehr, D. J., and Tainer, J. A. (1998) Structure of Nitric Oxide Synthase Oxygenase Dimer with Pterin and Substrate. *Science* **279**, 2121-2126

56. Raman, C. S., Li, H., Martasek, P., Kral, V., Masters, B. S., and Poulos, T. L. (1998) Crystal structure of constitutive endothelial nitric oxide synthase: a paradigm for pterin function involving a novel metal center. *Cell* **95**, 939-950

57. Sundaramoorthy, M., Terner, J., and Poulos, T. L. (1995) The crystal structure of chloroperoxidase: a heme peroxidase--cytochrome P450 functional hybrid. *Structure* **3**, 1367-1377

58. Adman, E., Watenpaugh, K. D., and Jensen, L. H. (1975) NH---S hydrogen bonds in Peptococcus aerogenes ferredoxin, Clostridium pasteurianum rubredoxin, and Chromatium high potential iron protein. *Proc Natl Acad Sci USA* **72**, 4854-4858

59. Graham, S. E., and Peterson, J. A. (1999) How Similar Are P450s and What Can Their Differences Teach Us? *Arch Biochem Biophys* **369**, 24-29

60. Gotoh, O. (1992) Substrate recognition sites in cytochrome P450 family 2 (CYP2) proteins inferred from comparative analyses of amino acid and coding nucleotide sequences. *J Biol Chem* **267**, 83-90

61. Peterson, J. A., and Graham, S. E. (1998) A close family resemblance: the importance of structure in understanding cytochromes P450. *Structure* **6**, 1079-1085

62. Munro, A. W., Girvan, H. M., and McLean, K. J. (2007) Cytochrome P450--redox partner fusion enzymes. *Biochim Biophys Acta* **1770**, 345-359

63. Hannemann, F., Bichet, A., Ewen, K. M., and Bernhardt, R. (2007) Cytochrome P450 systems—biological variations of electron transport chains. *Biochimica et Biophysica Acta (BBA) - General Subjects* **1770**, 330-344

64. Werck-Reichhart, D., and Feyereisen, R. (2000) Cytochromes P450: a success story. *Genome Biology* **1**, 1-9

65. Ewen, K. M., Ringle, M., and Bernhardt, R. (2012) Adrenodoxin--a versatile ferredoxin. *IUBMB Life* **64**, 506-512

66. Wang, M., Roberts, D. L., Paschke, R., Shea, T. M., Masters, B. S., and Kim, J. J. (1997) Three-dimensional structure of NADPH-cytochrome P450 reductase: prototype for FMN- and FAD-containing enzymes. *Proc Natl Acad Sci U S A* **94**, 8411-8416

67. Munro, A. W., Leys, D. G., McLean, K. J., Marshall, K. R., Ost, T. W., Daff, S., Miles, C. S., Chapman, S. K., Lysek, D. A., Moser, C. C., Page, C. C., and Dutton, P. L. (2002) P450 BM3: the very model of a modern flavocytochrome. *Trends Biochem Sci* **27**, 250-257

68. Sligar, S. G., and Gunsalus, I. C. (1979) Proton coupling in the cytochrome P-450 spin and redox equilibria. *Biochemistry* **18**, 2290-2295

69. Collman, J. P., Sorrell, T. N., Hodgson, K. O., Kulshrestha, A. K., and Strouse, C. E. (1977) Molecular dynamics in the solid state. A dynamic model of the low-spin iron(III) to high-spin iron(III) transformation in P450 enzymes. *J Am Chem Soc* **99**, 5180-5181

70. Fisher, M. T., and Sligar, S. G. (1985) Control of heme protein redox potential and reduction rate: linear free energy relation between potential and ferric spin state equilibrium. *J Am Chem Soc* **107**, 5018-5019

71. Denisov, I. G., and Sligar, S. G. (2015) Activation of Molecular Oxygen in Cytochromes P450. in *Cytochrome P450: Structure, Mechanism and Biochemistry* (Ortiz de Montellano, P. R. ed.), 4 Ed., Springer Publishing International, Switzerland. pp 69-110

72. Daff, S. N., Chapman, S. K., Turner, K. L., Holt, R. A., Govindaraj, S., Poulos, T. L., and Munro, A. W. (1997) Redox control of the catalytic cycle of flavocytochrome P-450 BM3. *Biochemistry* **36**, 13816-13823

73. Carrondo, M. A., Bento, I., Matias, P. M., and Lindley, P. F. (2007) Crystallographic evidence for dioxygen interactions with iron proteins. *J Biol Inorg Chem* **12**, 429-442

74. Schlichting, I., Berendzen, J., Chu, K., Stock, A. M., Maves, S. A., Benson, D. E., Sweet, R. M., Ringe, D., Petsko, G. A., and Sligar, S. G. (2000) The catalytic pathway of cytochrome p450cam at atomic resolution. *Science* **287**, 1615-1622

75. Nagano, S., and Poulos, T. L. (2005) Crystallographic study on the dioxygen complex of wild-type and mutant cytochrome P450cam. Implications for the dioxygen activation mechanism. *J Biol Chem* **280**, 31659-31663

76. Nagano, S., Cupp-Vickery, J. R., and Poulos, T. L. (2005) Crystal structures of the ferrous dioxygen complex of wild-type cytochrome P450eryF and its mutants, A245S

and A245T: investigation of the proton transfer system in P450eryF. *J Biol Chem* **280**, 22102-22107

77. Li, J., Noll, B. C., Oliver, A. G., Schulz, C. E., and Scheidt, W. R. (2013) Correlated Ligand Dynamics in Oxyiron Picket Fence Porphyrins: Structural and Mössbauer Investigations. *J Am Chem Soc* **135**

78. Dietzel, P. D. C., Kremer, R. K., and Jansen, M. (2004) Tetraorganylammonium Superoxide Compounds: Close to Unperturbed Superoxide Ions in the Solid State. *J Am Chem Soc* **126**, 4689-4696

79. Butler, C. (2013) *Production of high value drug metabolites using engineered cytochromes P450.* PhD, University of Manchester

80. Denisov, I. G., Mak, P. J., Makris, T. M., Sligar, S. G., and Kincaid, J. R. (2008) Resonance Raman Characterization of the Peroxo and Hydroperoxo Intermediates in Cytochrome P450. *The Journal of Physical Chemistry A* **112**, 13172-13179

81. Akhtar, M., Corina, D., Miller, S., Shyadehi, A. Z., and Wright, J. N. (1994) Mechanism of the Acyl-Carbon Cleavage and Related Reactions Catalyzed by Multifunctional P-450s: Studies on Cytochrome P-45017.alpha. *Biochemistry* **33**, 4410-4418

82. Harris, D. L., and Loew, G. H. (1998) Theoretical Investigation of the Proton Assisted Pathway to Formation of Cytochrome P450 Compound I. *J Am Chem Soc* **120**, 8941-8948

83. Rittle, J., and Green, M. T. (2010) Cytochrome P450 Compound I: Capture, Characterization, and C-H Bond Activation Kinetics. *Science* **330**, 933-937

84. Zhang, R., Nagraj, N., Lansakara-P, D. S. P., Hager, L. P., and Newcomb, M. (2006) Kinetics of Two-Electron Oxidations by the Compound I Derivative of Chloroperoxidase, a Model for Cytochrome P450 Oxidants. *Organic letters* **8**, 2731-2734

85. Rutter, R., Hager, L. P., Dhonau, H., Hendrich, M., Valentine, M., and Debrunner, P. (1984) Chloroperoxidase compound I: Electron paramagnetic resonance and Mossbauer studies. *Biochemistry* **23**, 6809-6816

86. Krest, C. M., Onderko, E. L., Yosca, T. H., Calixto, J. C., Karp, R. F., Livada, J., Rittle, J., and Green, M. T. (2013) Reactive Intermediates in Cytochrome P450 Catalysis. *J Biol Chem* **288**, 17074-17081

87. van Rantwijk, F., and Sheldon, R. A. (2000) Selective oxygen transfer catalysed by heme peroxidases: synthetic and mechanistic aspects. *Curr Opin Biotechnol* **11**, 554-564

88. Krest, C. M., Silakov, A., Rittle, J., Yosca, T. H., Onderko, E. L., Calixto, J. C., and Green, M. T. (2015) Significantly shorter Fe-S bond in cytochrome P450-I is consistent with greater reactivity relative to chloroperoxidase. *Nature chemistry* **7**, 696-702

89. Grant, J. L., Hsieh, C. H., and Makris, T. M. (2015) Decarboxylation of fatty acids to terminal alkenes by cytochrome P450 compound I. *J Am Chem Soc* **137**, 4940-4943

90. Groves, J. T., McClusky, G. A., White, R. E., and Coon, M. J. (1978) Aliphatic hydroxylation by highly purified liver microsomal cytochrome P-450. Evidence for a carbon radical intermediate. *Biochem Biophys Res Commun* **81**, 154-160

91. Green, M. T. (2009) CH bond activation in heme proteins: the role of thiolate ligation in cytochrome P450. *Curr Opin Chem Biol* **13**, 84-88

92. Newcomb, M., Halgrimson, J. A., Horner, J. H., Wasinger, E. C., Chen, L. X., and Sligar, S. G. (2008) X-ray absorption spectroscopic characterization of a cytochrome P450 compound II derivative. *Proc Natl Acad Sci USA* **105**, 8179-8184

93. Yosca, T. H., Rittle, J., Krest, C. M., Onderko, E. L., Silakov, A., Calixto, J. C., Behan, R. K., and Green, M. T. (2013) Iron(IV)hydroxide pKa and the Role of Thiolate Ligation in C–H Bond Activation by Cytochrome P450. *Science* **342**, 825-829

94. Grant, J. L., Mitchell, M. E., and Makris, T. M. (2016) Catalytic strategy for carbon-carbon bond scission by the cytochrome P450 OleT. *Proc Natl Acad Sci U S A* **113**, 10049-10054

95. Kuthan, H., and Ullrich, V. (1982) Oxidase and oxygenase function of the microsomal cytochrome P450 monooxygenase system. *Eur J Biochem* **126**, 583-588

96. Gorsky, L. D., Koop, D. R., and Coon, M. J. (1984) On the stoichiometry of the oxidase and monooxygenase reactions catalyzed by liver microsomal cytochrome P-450. Products of oxygen reduction. *J Biol Chem* **259**, 6812-6817

97. Zangar, R. C., Davydov, D. R., and Verma, S. (2004) Mechanisms that regulate production of reactive oxygen species by cytochrome P450. *Toxicol Appl Pharmacol* **199**, 316-331

98. Nordblom, G. D., White, R. E., and Coon, M. J. (1976) Studies on hydroperoxide-dependent substrate hydroxylation by purified liver microsomal cytochrome P-450. *Arch Biochem Biophys* **175**, 524-533

99. Li, Q., Ogawa, J., and Shimizu, S. (2001) Critical Role of the Residue Size at Position 87 in H2O2-Dependent Substrate Hydroxylation Activity and H2O2 Inactivation of Cytochrome P450BM-3. *Biochem Biophys Res Commun* **280**, 1258-1261

100. Joo, H., Lin, Z., and Arnold, F. H. (1999) Laboratory evolution of peroxide-mediated cytochrome P450 hydroxylation. *Nature* **399**, 670-673

101. Hrycay, E. G., and Bandiera, S. M. (2012) The monooxygenase, peroxidase, and peroxygenase properties of cytochrome P450. *Arch Biochem Biophys* **522**, 71-89

102. Fujishiro, T., Shoji, O., Nagano, S., Sugimoto, H., Shiro, Y., and Watanabe, Y. (2011) Crystal structure of H2O2-dependent cytochrome P450SPalpha with its bound fatty. *J Biol Chem* **286**, 29941-29950

103. Girhard, M., Schuster, S., Dietrich, M., Durre, P., and Urlacher, V. B. (2007) Cytochrome P450 monooxygenase from Clostridium acetobutylicum: a new alpha-fatty acid hydroxylase. *Biochem Biophys Res Commun* **362**, 114-119

104. Matsunaga, I., Yamada, A., Lee, D. S., Obayashi, E., Fujiwara, N., Kobayashi, K., Ogura, H., and Shiro, Y. (2002) Enzymatic reaction of hydrogen peroxide-dependent peroxygenase cytochrome P450s. *Biochemistry* **41**, 1886-1892

105. Otton, S. V., Gillam, E. M., Lennard, M. S., Tucker, G. T., and Woods, H. F. (1990) Propranolol oxidation by human liver microsomes--the use of cumene hydroperoxide to probe isoenzyme specificity and regio- and stereoselectivity. *Br J Clin Pharmacol* **30**, 751-760

106. Kadlubar, F. F., Morton, K. C., and Ziegler, D. M. (1973) Microsomal-catalyzed hydroperoxide-dependent C-oxidation of amines. *Biochem Biophys Res Commun* **54**, 1255-1261

107. Reed, C. J., and De Matteis, F. (1989) Cumene hydroperoxide-dependent oxidation of NNN'N'-tetramethyl-p-phenylenediamine and 7-ethoxycoumarin by cytochrome P-450. Comparison between the haemoproteins from liver and olfactory tissue. *Biochem J* **261**, 793-800

108. Cederbaum, A. I. (1983) Organic hydroperoxide-dependent oxidation of ethanol by microsomes: lack of a role for free hydroxyl radicals. *Arch Biochem Biophys* **227**, 329-338

109. Lewis, D. F., and Sheridan, G. (2001) Cytochromes P450, oxygen, and evolution. *ScientificWorldJournal* **1**, 151-167

110. McKay, C. P., and Hartman, H. (1991) Hydrogen peroxide and the evolution of oxygenic photosynthesis. *Orig Life Evol Biosph* **21**, 157-163

111. Hrycay, E. G., and Bandiera, S. M. (2015) Monoxygenase, Peroxidase and Peroxygenase Properties and Reaction Mechanisms of Cytochrome P450 Enzymes. in *Monoxygenase, Peroxidase and Peroxygenase Properties and Reaction Mechanisms of Cytochrome P450 Enzymes* (Hrycay, E. G., and Bandiera, S. M. eds.), Springer International Publishing, Switzerland. pp 1-48

112. Koo, L. S., Tschirret-Guth, R. A., Straub, W. E., Moenne-Loccoz, P., Loehr, T. M., and Ortiz de Montellano, P. R. (2000) The active site of the thermophilic CYP119 from Sulfolobus solfataricus. *J Biol Chem* **275**, 14112-14123

113. Rabe, K. S., Kiko, K., and Niemeyer, C. M. (2008) Characterization of the peroxidase activity of CYP119, a thermostable P450 from Sulfolobus acidocaldarius. *Chembiochem* **9**, 420-425

114. Shimizu, T., Murakami, Y., and Hatano, M. (1994) Glu318 and Thr319 mutations of cytochrome P450 1A2 remarkably enhance homolytic O-O cleavage of alkyl hydroperoxides. An optical absorption spectral study. *J Biol Chem* **269**, 13296-13304

115. Groves, J. T. (2006) High-valent iron in chemical and biological oxidations. *J Inorg Biochem* **100**, 434-447

116. Barr, D. P., Martin, M. V., Guengerich, F. P., and Mason, R. P. (1996) Reaction of cytochrome P450 with cumene hydroperoxide: ESR spin-trapping evidence for the homolytic scission of the peroxide O-O bond by ferric cytochrome P450 1A2. *Chem Res Toxicol* **9**, 318-325

117. Matsunaga, I., Yamada, M., Kusunose, E., Nishiuchi, Y., Yano, I., and Ichihara, K. (1996) Direct involvement of hydrogen peroxide in bacterial alpha-hydroxylation of fatty acid. *FEBS Lett* **386**, 252-254

118. Matsunaga, I., Yokotani, N., Gotoh, O., Kusunose, E., Yamada, M., and Ichihara, K. (1997) Molecular cloning and expression of fatty acid alpha-hydroxylase from Sphingomonas paucimobilis. *J Biol Chem* **272**, 23592-23596

119. Matsunaga, I., Ueda, A., Fujiwara, N., Sumimoto, T., and Ichihara, K. (1999) Characterization of the ybdT gene product of Bacillus subtilis: novel fatty acid beta-hydroxylating cytochrome P450. *Lipids* **34**, 841-846

120. Sevrioukova, I. F., Li, H., Zhang, H., Peterson, J. A., and Poulos, T. L. (1999) Structure of a cytochrome P450–redox partner electron-transfer complex. *Proc Natl Acad Sci USA* **96**, 1863-1868

121. Lee, D. S., Nioche, P., Hamberg, M., and Raman, C. S. (2008) Structural insights into the evolutionary paths of oxylipin biosynthetic enzymes. *Nature* **455**, 363-368

122. Matsunaga, I., Ueda, A., Sumimoto, T., Ichihara, K., Ayata, M., and Ogura, H. (2001) Site-Directed Mutagenesis of the Putative Distal Helix of Peroxygenase Cytochrome P450. *Arch Biochem Biophys* **394**, 45-53

122. Sundaramoorthy, M., Terner, J., and Poulos, T. L. (1998) Stereochemistry of the chloroperoxidase active site: crystallographic and molecular-modeling studies. *Chem Biol* **5**, 461-473

124. Piontek, K., Strittmatter, E., Ullrich, R., Grobe, G., Pecyna, M. J., Kluge, M., Scheibner, K., Hofrichter, M., and Plattner, D. A. (2013) Structural basis of substrate conversion in a new aromatic peroxygenase: cytochrome P450 functionality with benefits. *J Biol Chem* **288**, 34767-34776

125. Shoji, O., Fujishiro, T., Nakajima, H., Kim, M., Nagano, S., Shiro, Y., and Watanabe, Y. (2007) Hydrogen peroxide dependent monooxygenations by tricking the substrate recognition of cytochrome P450BSbeta. *Angew Chem Int Ed Engl* **46**, 3656-3659

126. Shoji, O., Fujishiro, T., Nagano, S., Tanaka, S., Hirose, T., Shiro, Y., and Watanabe, Y. (2010) Understanding substrate misrecognition of hydrogen peroxide dependent cytochrome P450 from Bacillus subtilis. *J Biol Inorg Chem* **15**, 1331-1339

127. Onoda, H., Shoji, O., and Watanabe, Y. (2015) Acetate anion-triggered peroxygenation of non-native substrates by wild-type cytochrome P450s. *Dalton Trans* **44**, 15316-15323

128. Shoji, O., Fujishiro, T., Nishio, K., Kano, Y., Kimoto, H., Chien, S.-C., Onoda, H., Muramatsu, A., Tanaka, S., Hori, A., Sugimoto, H., Shiro, Y., and Watanabe, Y. (2016) A substrate-binding-state mimic of H2O2-dependent cytochrome P450 produced by one-point mutagenesis and peroxygenation of non-native substrates. *Catal Sci Tech* **6**, 5806-5811

129. Yoon, J. H., Lee, K. C., Weiss, N., Kang, K. H., and Park, Y. H. (2003) Jeotgalicoccus halotolerans gen. nov., sp. nov. and Jeotgalicoccus psychrophilus sp. nov., isolated from the traditional Korean fermented seafood jeotgal. *Int J Syst Evol Microbiol* **53**, 595-602

130. Schwaiger, K., Holzel, C., Mayer, M., and Bauer, J. (2010) Notes on the almost unknown genus Jeotgalicoccus. *Lett Appl Microbiol* **50**, 441-444

131. Arnold, K., Bordoli, L., Kopp, J., and Schwede, T. (2006) The SWISS-MODEL workspace: a web-based environment for protein structure homology modelling. *Bioinformatics* **22**, 195-201

132. Liu, Y., Wang, C., Yan, J., Zhang, W., Guan, W., Lu, X., and Li, S. (2014) Hydrogen peroxide-independent production of alpha-alkenes by OleTJE P450 fatty acid decarboxylase. *Biotechnol Biofuels* **7**, 28

133. Dennig, A., Kuhn, M., Tassoti, S., Thiessenhusen, A., Gilch, S., Bulter, T., Haas, T., Hall, M., and Faber, K. (2015) Oxidative Decarboxylation of Short-Chain Fatty Acids to 1-Alkenes. *Angew Chem Int Ed Engl* **54**, 8819-8822

134. Seaver, L. C., and Imlay, J. A. (2001) Hydrogen peroxide fluxes and compartmentalization inside growing Escherichia coli. *J Bacteriol* **183**, 7182-7189

135. Zachos, I., Gassmeyer, S. K., Bauer, D., Sieber, V., Hollmann, F., and Kourist, R. (2015) Photobiocatalytic decarboxylation for olefin synthesis. *Chem Commun (Camb)* **51**, 1918-1921

136. Girhard, M., Kunigk, E., Tihovsky, S., Shumyantseva, V. V., and Urlacher, V. B. (2013) Light-driven biocatalysis with cytochrome P450 peroxygenases. *Biotechnol Appl Biochem* **60**, 111-118

137. Amaya, J. A., Rutland, C. D., and Makris, T. M. (2016) Mixed regiospecificity compromises alkene synthesis by a cytochrome P450 peroxygenase from Methylobacterium populi. *J Inorg Biochem* **158**, 11-16

138. Luthra, A., Denisov, I. G., and Sligar, S. G. (2011) Spectroscopic features of cytochrome P450 reaction intermediates. *Arch Biochem Biophys* **507**, 26-35

139. Lipscomb, J. D. (1980) Electron paramagnetic resonance detectable states of cytochrome P-450cam. *Biochemistry* **19**, 3590-3599

140. Miles, J. S., Munro, A. W., Rospendowski, B. N., Smith, W. E., McKnight, J., and Thomson, A. J. (1992) Domains of the catalytically self-sufficient cytochrome P-450 BM-3. Genetic construction, overexpression, purification and spectroscopic characterization. *J Biochem* **288**, 503-509

141. Bui, S. H., McLean, K. J., Cheesman, M. R., Bradley, J. M., Rigby, S. E., Levy, C. W., Leys, D., and Munro, A. W. (2012) Unusual spectroscopic and ligand binding properties of the cytochrome P450-flavodoxin fusion enzyme XplA. in *J Biol Chem*. pp 19699-19714

142. Rittle, J., and Green, M. T. (2010) Cytochrome P450 compound I: capture, characterization, and C-H bond activation kinetics. *Science* **330**, 933-937

143. Wang, X., Ullrich, R., Hofrichter, M., and Groves, J. T. (2015) Heme-thiolate ferryl of aromatic peroxygenase is basic and reactive. *Proceedings of the National Academy of Sciences* **112**, 3686-3691

144. Whitehouse, C. J., Bell, S. G., and Wong, L. L. (2008) Desaturation of alkylbenzenes by cytochrome P450(BM3) (CYP102A1). *Chemistry* **14**, 10905-10908

145. Zhu, D., Seo, M. J., Ikeda, H., and Cane, D. E. (2011) Genome mining in streptomyces. Discovery of an unprecedented P450-catalyzed oxidative rearrangement that is the final step in the biosynthesis of pentalenolactone. *J Am Chem Soc* **133**, 2128-2131

146. Auclair, K., Hu, Z., Little, D. M., Ortiz De Montellano, P. R., and Groves, J. T. (2002) Revisiting the mechanism of P450 enzymes with the radical clocks norcarane and spiro[2,5]octane. *J Am Chem Soc* **124**, 6020-6027

147. Yoshimoto, F. K., and Guengerich, F. P. (2014) Mechanism of the third oxidative step in the conversion of androgens to estrogens by cytochrome P450 19A1 steroid aromatase. *J Am Chem Soc* **136**, 15016-15025

148. Hackett, J. C., Brueggemeier, R. W., and Hadad, C. M. (2005) The final catalytic step of cytochrome p450 aromatase: a density functional theory study. *J Am Chem Soc* **127**, 5224-5237

149. Hsieh, C. H., and Makris, T. M. (2016) Expanding the substrate scope and reactivity of cytochrome P450 OleT. *Biochem Biophys Res Commun* **476**, 462-466

150. Yan, J., Liu, Y., Wang, C., Han, B., and Li, S. (2015) Assembly of lipase and P450 fatty acid decarboxylase to constitute a novel biosynthetic pathway for production of 1-alkenes from renewable triacylglycerols and oils. *Biotechnol Biofuels* **8**, 34

Chapter Two

Structure and biochemical properties of the alkene producing $OleT_{JE}$ (CYP152L1) from *Jeotgalicoccus* sp. 8456

[1]James Belcher, [1]Kirsty J. McLean, [1]Sarah Matthews, [1]Laura S. Woodward, [1]Karl Fisher [1]Stephen E. J. Rigby, [2]David R. Nelson, [3]Donna Potts, [3]Michael T. Baynham, [4]David A. Parker, [1]David Leys and [1]Andrew W. Munro*

[1]Manchester Institute of Biotechnology, Faculty of Life Sciences, University of Manchester, 131 Princess Street, Manchester M1 7DN, UK. [2]Department of Microbiology, Immunology and Biochemistry, University of Tennessee Health Science Center, 858 Madison Avenue Suite G01, Memphis, TN 38163, USA. [3]Agilent Technologies UK Ltd, Lakeside, Cheadle Royal Business Park, Stockport, Cheshire SK8 3GR, UK. [4]Westhollow Technology Center, 3333 Highway 6 South, Houston, TX 77028-3101, USA.

Background: $OleT_{JE}$ oxidatively decarboxylates fatty acids to produce terminal alkenes.

Results: $OleT_{JE}$ is an efficient peroxide-dependent lipid decarboxylase, with high affinity substrate-binding and the capacity to be resolubilized from precipitate in an active form.

Conclusion: $OleT_{JE}$ has key differences in active site structure and substrate binding/mechanistic properties to related CYP152 hydroxylases.

Significance: $OleT_{JE}$ is an efficient and robust biocatalyst with applications in biofuel production.

2.1. Abstract

The production of hydrocarbons in Nature has been documented for only a limited set of organisms, with many of the molecular components underpinning these processes only recently identified. There is an obvious scope for application of these catalysts, and engineered variants thereof, in future production of drop-in biofuels. Here we present biochemical characterization and crystal structures of a biotechnologically important cytochrome P450 peroxygenase: the terminal alkene forming $OleT_{JE}$ (CYP152L1) from *Jeotgalicoccus* sp. 8456. $OleT_{JE}$ is stabilized at high ionic strength, but aggregation and precipitation of $OleT_{JE}$ in low salt buffer can be turned to advantage for purification, since resolubilized $OleT_{JE}$ is fully active and extensively dissociated from lipids. $OleT_{JE}$ binds avidly to a range of long chain fatty acids and structures of both ligand-free and arachidic acid-bound $OleT_{JE}$ reveal that the P450 active site is preformed for fatty acid binding. $OleT_{JE}$ heme iron has an unusually positive redox potential (-103 mV vs. NHE) which is not significantly affected by substrate binding, despite extensive conversion of the heme iron to a high-spin ferric state. Terminal alkenes are produced from a range of saturated fatty acids (C12-C20), and stopped-flow spectroscopy indicates a rapid reaction between peroxide and fatty acid-bound $OleT_{JE}$ (167 s^{-1} at 200 μM H_2O_2). Surprisingly, the active site is highly similar in structure to the related $P450_{BS\beta}$, which catalyzes hydroxylation of fatty acids as opposed to decarboxylation. Our data provide new insights into structural and mechanistic properties of a robust P450 with potential industrial applications.

2.1. Introduction

The cytochromes P450 (P450s or CYPs) are oxidases that catalyze a vast array of oxidative reactions in nature (1). These hemoproteins are found in virtually all organisms from bacteria and archaea through to man, and are responsible for several chemical transformations that are essential, for instance, in the microbial biosynthesis of antibiotics (e.g. erythromycin in *Saccharopolyspora erythraea*, and vancomycin in *Amycolatopsis orientalis*) (2,3), and in the mammalian formation of estrogens (estrone and 17β-estradiol) through the action of the aromatase P450 (CYP19A1) on androgen substrates (androstanedione and testosterone,

respectively) (4,5). The majority of characterized P450s are

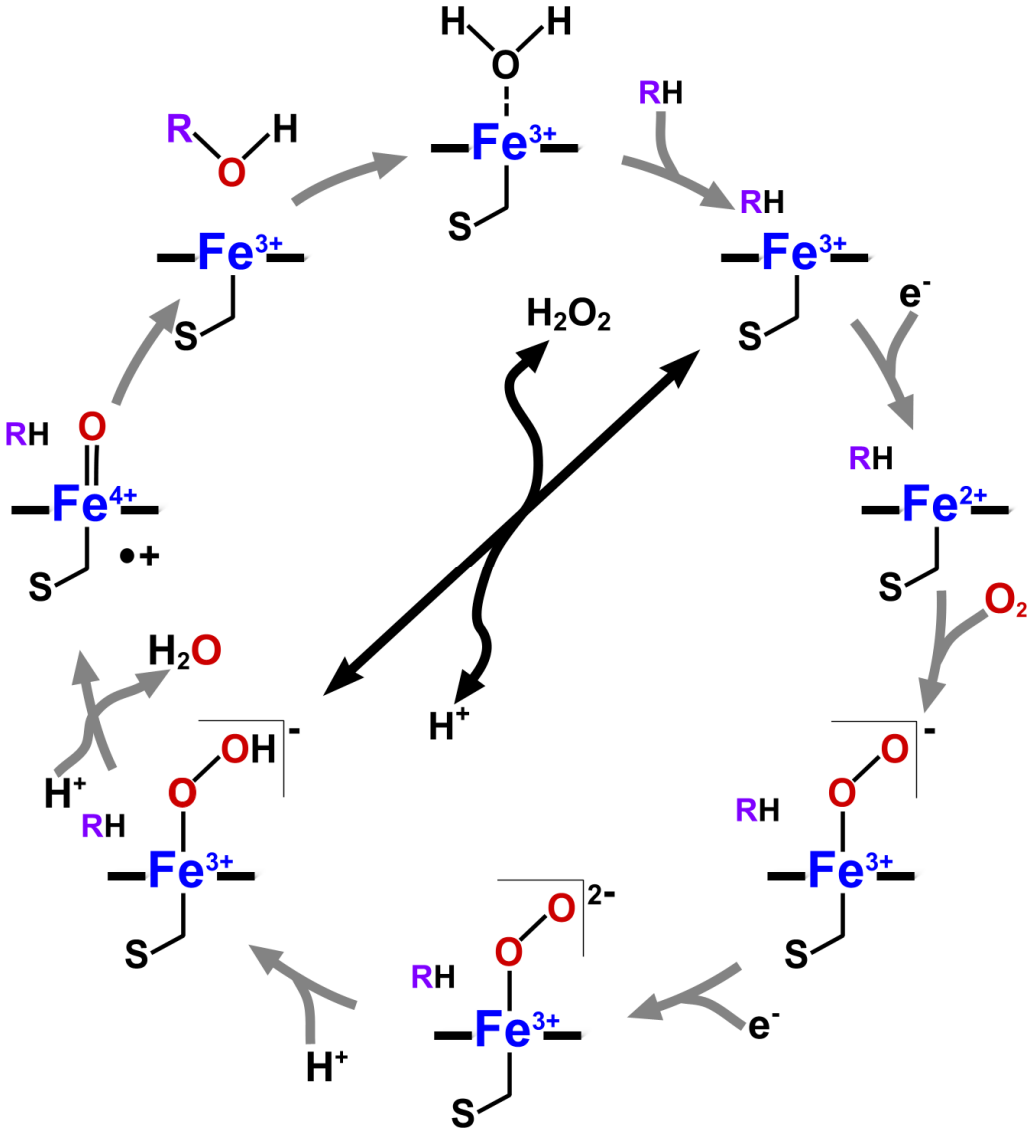

monooxygenases that interact with one or more redox partners to provide them with the two

Figure 2.1. The cytochrome P450 catalytic cycle. The reaction sequence starts at the top, with the P450 "resting" state having a ferric (Fe^3) 6-coordinate low spin heme iron axially coordinated by cysteine thiolate (S) and a weakly bound water molecule (H_2O). Binding of substrate (RH) displaces the water ligand to leave a 5-coordinate high spin heme iron. This is reduced by a redox partner, and the ferrous iron then binds dioxygen to form a ferricsuperoxo complex. A further single electron reduction by the redox partner generates the ferric-peroxo intermediate, which is protonated to form the transient ferric-hydroperoxo (compound 0) species. Compound 0 is further protonated and dehydrated to form the ferryl-oxo porphyrin radical cation species compound I. The compound I is considered to be the major oxidant in P450 reactions and abstracts a hydrogen from RH to produce a substrate radical, prior to "rebounding" the hydroxyl to the substrate to form hydroxylated product (ROH) and to restore the resting state of the P450 (8, 55). The double-headed arrow crossing the cycle between the substrate-bound ferric P450 and compound 0 describes the catalytic mechanism for $OleT_{JE}$ and related peroxygenase P450s (e.g. P450BSβ and P450SPα) (16 –18). Direct interaction of $OleT_{JE}$ with H_2O_2 produces a reactive iron-oxo species (compound 0) that is further protonated and dehydrated to form compound I, leading to either fatty acid substrate decarboxylation (major route) or fatty acid hydroxylation (minor route), as described under "Discussion" section and in the legend to Fig. 3.13.

electrons (typically derived from NAD(P)H) required for oxidative catalysis (6). The first electron reduces the P450 cysteine thiolate-coordinated heme iron from ferric to ferrous, enabling dioxygen binding to the ferrous iron. The second electron reduces the resulting ferric-superoxo complex to the ferric-peroxo state. Two successive protonations produce first the ferric-hydroperoxo species (compound 0) and then (following the loss of a water molecule) the ferryl-oxo compound I (7) (Figure 2.1). The transient and highly reactive nature of compound I prevented its definitive characterization for many years, until Rittle and Green produced compound I in large yield following rapid mixing of CYP119 (from the thermoacidophilic crenarchaeon *Sulfolobus acidocaldarius*) with the oxidant *m*-chloroperbenzoic acid, and confirmed its identity using Mössbauer, EPR and UV-visible spectroscopy (8). Compound I is considered to be the major oxidizing species in the P450 catalytic cycle, and to be responsible for the bulk of oxidative reactions (e.g. hydroxylation, epoxidation, oxidative demethylation *etc*) observed throughout the P450 superfamily (9, 10).

The vast majority of P450s use NAD(P)H-dependent redox systems consisting of either (i) an FAD-binding reductase that shuttles electrons to the P450 via a ferredoxin (or a flavodoxin in a small number of cases), or (ii) an FAD- and FMN-binding cytochrome P450 reductase (CPR), the individual flavin-binding domains of which are evolutionarily related to NAD(P)H-binding ferredoxin oxidoreductases and flavodoxins (5,11). However, other types of P450 redox partner systems exist (e.g. P450-redox partner fusion enzymes, such as the CYP116B family of P450:phthalate dioxygenase reductase fusions) (12). In addition, other P450s catalyze isomerization (e.g. mammalian thromboxane synthase, CYP5A1) and dehydration (e.g. flax allene oxide synthase, CYP74A1) reactions that do not require an external source of electrons and which are completed entirely within the P450 active site (13,14). Further, through exploration of *in vitro* routes to driving P450 catalysis, it is now well established that the addition of hydrogen peroxide (H_2O_2) or organic peroxides (e.g. cumene hydroperoxide) to P450s can facilitate substrate oxidation by directly producing compound 0, which is then protonated to generate compound I (15). This “peroxide shunt” procedure is rarely an efficient means of driving P450s, since the peroxides oxidize heme and protein. However, a small number of P450s that have evolved to exploit the peroxide shunt are now known. Notably, the

Bacillus subtilis CYP152A1 ($P450_{BS\beta}$) and the *Sphingomonas paucimobilis* CYP152B1 ($P450_{SP\alpha}$) naturally use H_2O_2 to catalyze long chain fatty acid hydroxylation, and are thus referred to as peroxygenases (16,17). $P450_{SP\alpha}$ catalyzes near-exclusively hydroxylation at the alpha position, whereas $P450_{BS\beta}$ catalyzes hydroxylation at alpha and beta positions, but with the majority at the beta position (~60:40 ratio) (16).

In recent studies, Rude *et al*. characterized a novel enzyme from the bacterium *Jeotgalicoccus* sp. ATCC 8456 ($OleT_{JE}$) that is 41% identical in amino sequence to $P450_{BS\beta}$, and 37% identical to $P450_{SP\alpha}$. $OleT_{JE}$ was identified as a P450 based on this sequence similarity, and designated by the authors as a CYP152 P450 family member (18). The *Jeotgalicoccus* ATCC 8456 host strain was shown to produce a number of C18-C20 linear and branched chain terminal alkenes, and other *Jeotgalicoccus* strains were shown to generate a similar spectrum of terminal alkenes in the C18-C21 range. A His-tagged version of $OleT_{JE}$ was expressed in *E. coli* and purified using Ni-NTA column chromatography, and shown to catalyze formation of n-1 alkenes through H_2O_2-dependent decarboxylation of C14, C16, C18 and C20 saturated fatty acids (18).

In view of the potential importance of the $OleT_{JE}$ enzyme as a producer of terminal alkenes for exploitation in areas such as biofuels and fine chemical production, we have undertaken a study of the biochemical and biophysical properties of the isolated $OleT_{JE}$ (CYP152L1) enzyme, and have determined its crystal structure in complex with arachidic acid. These data reveal novel properties of this biotechnologically important P450 peroxygenase.

2.3. Materials and Methods

2.3.1 Bioinformatics

The $OleT_{JE}$ sequence and additional members of the CYP152 family, including all known subfamilies, were BLAST searched against a set of all the prokaryotic P450 sequences. Members of the highest scoring CYP families from these searches were used to build a tree. Sequence alignments were computed using ClustalW and checked manually for consistent

alignment of known CYP motifs. Neighbor-joining trees were generated with the Phylip package (Felsenstein, J. [2005], PHYLIP – Phylogeny Inference Package version 3.6, distributed by the author, Department of Genome Sciences, University of Washington, Seattle) using ProtDist (a program in Phylip) to compute difference matrices. Trees were drawn and colored with FigTree version 1.3.1 (http://tree.bio.ed.ac.uk/software/figtree/) and labeled in Adobe Illustrator CS version 11.0.0 (Adobe Systems Incorporated). Sequences producing long branches on the tree were removed and the tree was recomputed.

2.3.2. Expression and purification of OleT

The gene encoding $OleT_{JE}$ from *Jeotgalicoccus* sp. ATCC 8456 was codon optimized (for expression in *E. coli*), synthesised and cloned into the pET47b (Merck Millipore, Madison USA) vector by GenScript (New Jersey, USA). The *E. coli* strain C41 (DE3) (Lucigen, Middleton USA) was used as the expression host. Cells transformed with the pET47b-$OleT_{JE}$ plasmid were grown at 37°C with shaking at 200 rpm in total volumes of 500 mL to 3 L of 2YT broth containing kanamycin (30 µg/mL) supplemented with 500 µM δ-aminolevulinic acid. Expression of $OleT_{JE}$ was induced by addition of 100 µM IPTG when an optical density of 0.5 (at 600 nm) was reached, at which point the incubation temperature was lowered to 25°C and the cells grown for a further 16 h. Cells were harvested by centrifugation at 6000 rpm, 4°C using a JLA-8.1000 rotor in an Avanti J-26 XP centrifuge. Pellets were resuspended in a minimal volume of ice cold buffer A (100 mM potassium phosphate [KPi], pH 8.0), combined and centrifuged as before. The cell pellet was then frozen at -80°C until required.

Cells were thawed at 4°C and resuspended in 3 volumes of extraction buffer per gram of cell pellet. The extraction buffer consisted of buffer A containing 1 M NaCl, 20% glycerol, with a Complete™ EDTA-free protease inhibitor cocktail tablet (Roche, Mannheim Germany) per 50 mL of cell suspension, DNase I (100 µg/mL, bovine pancreas, Sigma-Aldrich, Poole UK) and lysozyme (100 µg/mL, hen egg white, Sigma-Aldrich). The cells were disrupted by two passes through a French Press (Thermo Scientific, Hemel Hempstead UK), and the homogenate centrifuged at 20,000 rpm, 4°C for 90 min using a JA-25.50 rotor. Alternatively, cells were

lysed by sonication using a Bandelin Sonopuls sonicator set to 45% amplitude with 30 x 30 s pulses, at 60 s intervals, with the cell suspension kept on ice throughout. The homogenate was then centrifuged as previously. The supernatant was removed and the pH re-set to 8.0 as necessary. The sample was then incubated overnight with 10 mL (per 100 g cell pellet) of Ni-IDA chromatographic medium (Generon, Maidenhead UK) on a rolling table at 4°C. The mixture was then poured into a column and the collected bed of $OleT_{JE}$-bound medium was washed with 10 column volumes (CV) of 100 mM KPi (pH 8.0) containing 750 mM NaCl, 20% glycerol (buffer B) and 50 mM imidazole to remove weakly bound contaminants. The column was then washed with 2 CV of the buffer B containing 125 mM imidazole, followed by 5 CV of buffer B plus 150 mM imidazole, which eluted the bulk of the $OleT_{JE}$ protein. The partially purified $OleT_{JE}$ sample was dialyzed overnight against 15 L of buffer A at 4°C, which caused $OleT_{JE}$ to precipitate. Post-dialysis, precipitated protein was isolated by centrifugation at 4000 rpm, 4°C using an A-4-62 rotor in an Eppendorf 5810 R centrifuge. The pellet was washed gently with 50 mL of buffer A and centrifugation repeated. $OleT_{JE}$ was resuspended in 5 mL of buffer A containing 1 M NaCl and 10% glycerol, which produced $OleT_{JE}$ at high purity (Method 1). For $OleT_{JE}$ destined for crystallographic studies, HRV 3C protease (Merck Millipore, Darmstadt Germany) was incubated with $OleT_{JE}$ for ~16 h at 4°C (50:1 µg protein/U protease) to remove the N-terminal poly-histidine tag. The proteolysed protein was applied to 5 mL of pre-equilibrated Ni-Sepharose resin (GE Healthcare, Little Chalfont UK) to bind the cleaved His-tag and the tagged HRV 3C. The cleaved $OleT_{JE}$ was eluted from the column by washing with 100 mM KPi (pH 8.0) plus 750 mM NaCl and 10% glycerol (buffer C).

In separate preparations (avoiding the $OleT_{JE}$ precipitation step, Method 2) the dialysis step post Ni-NDA chromatography was removed and the $OleT_{JE}$ eluate was instead diluted (5x) in buffer C and concentrated in an Amicon ultrafiltration device. The $OleT_{JE}$ sample was then centrifuged to clarify the sample (16000 rpm, 4°C using the JA-25.50 rotor) and the supernatant was then applied again to a 5 mL Ni-IDA column. The column was washed with 5 CV of buffer C containing 50 mM imidazole and then 10 CV of buffer C plus 100 mM imidazole. The His-tagged $OleT_{JE}$ was then eluted with 150 mM imidazole in the same buffer. All procedures generated highly purified $OleT_{JE}$ protein. In both cases, the pure $OleT_{JE}$ protein

was concentrated to >20 mg/ml using a Vivaspin centrifugal concentrator (Generon), snap frozen in liquid nitrogen and stored at -80°C.

2.3.3. UV-visible spectroscopy

Analysis of the UV-visible spectroscopic properties of $OleT_{JE}$ was done on a Cary 60 UV-visible spectrophotometer (Varian UK). Spectra were recorded using ~4-10 μM $OleT_{JE}$ in 100 mM KPi (pH 8.0) plus 750 mM NaCl (buffer D). Reduction of $OleT_{JE}$ was achieved by addition of sodium dithionite to enzyme in buffer D made anerobic by extensive bubbling with oxygen-free nitrogen. The ferrous-CO complex of $OleT_{JE}$ was formed by slow bubbling of gas into anerobically reduced enzyme until no further absorbance change occurred. The NO complex was formed by addition of 5-8 bubbles of NO into a sample of ferric $OleT_{JE}$ in anerobic buffer.

2.3.4. Fatty acid and inhibitor binding titrations with $OleT_{JE}$

Spectral binding titrations of $OleT_{JE}$ with saturated fatty acids (C12, C14, C16, C18 and C20) were performed at 25°C in buffer D. Fatty acids were from Sigma-Aldrich. Substrates (typically 0.25 mg/ml) were dissolved in 70% (v/v) EtOH (for C18, C20) or 70% MeOH (with the sodium salts of C12, C14 and C16 fatty acids) and 30% (v/v) Triton X-100 (Sigma-Aldrich). A parallel set of binding titrations was also performed using fatty acids (1 mg/ml) dissolved in 100% EtOH or MeOH without Triton X-100. Prior to titrations, $OleT_{JE}$ samples were passed through a Lipidex column (Perkin Elmer, Cambridge UK) in order to remove any residual lipid retained during purification of the protein from *E. coli*. Titrations were performed by stepwise additions of aliquots (0.1-1 μL) of the fatty acids to the $OleT_{JE}$ sample (substrate additions to < 1% of total volume). Spectra (800-300 nm) were recorded for the ligand-free $OleT_{JE}$ and following each addition of substrate using a Cary 60 UV-visible spectrophotometer. Difference spectra at each stage in the titration were computed by subtracting the spectrum of ligand-free $OleT_{JE}$ from each successive fatty acid-bound spectrum collected during the titration. A pair of wavelengths were identified that defined the absorbance maximum (A_{peak}) and minimum

(A_{trough}) in the difference spectra from each titration set. The overall absorbance change (A_{max}) at each substrate concentration point was calculated as A_{peak} minus A_{trough}, and A_{max} was plotted versus [substrate]. These data were fitted using either a hyperbolic (Michaelis-Menten) function, the Morrison equation for tight binding ligands, or the Hill function (where sigmoidal behaviour was observed) in order to determine dissociation constants (K_d values), as described previously (19,20). Titrations and data fitting for $OleT_{JE}$ with dithiothreitol (DTT), imidazole and cyanide (sodium salt) inhibitors were done in the same way as for the fatty acids, with ligands dissolved in buffer D.

2.3.5. Stopped-flow analysis of substrate turnover

Stopped-flow absorption measurements were made using an Applied Photophysics SX18 MR stopped-flow spectrophotometer (Leatherhead, UK). Stopped-flow spectral accumulation was done using a photodiode array (PDA) detector on the same instrument. Fatty acid substrate-bound $OleT_{JE}$ was mixed *versus* different concentrations of H_2O_2 in 100 mM KPi (pH 8.0) containing 750 mM NaCl at 25°C. $OleT_{JE}$ (9.2 μM) was converted to an extensively high-spin heme iron form by mixing with arachidic acid (12 μM) from a concentrated stock prepared in 80% EtOH/20% Triton X-100. Reactions were initiated by mixing the arachidic acid bound $OleT_{JE}$ (4.6 μM final concentration) with H_2O_2 (3.29 – 200 μM final concentration). Stopped-flow traces at single wavelengths reporting on the conversion of high-spin $OleT_{JE}$ heme iron from high-spin towards low-spin (418 and 390 nm) were collected over periods of up to 30 s. Data were analyzed and fitted using a single exponential function with the Pro-Data SX software suite (Applied Photophysics). The observed reaction rate constants (k_{obs} values) were plotted *versus* the relevant H_2O_2 concentrations, and the resultant data plot fitted using a linear function to obtain the 2nd order rate constant reporting on H_2O_2-dependent decarboxylation of substrate and the consequent heme iron spin-state conversion. Entire spectral acquisition (750-280 nm) was also done using the PDA detector for the same set of stopped-flow reactions analyzed in single wavelength mode.

2.3.6. Redox potentiometry

To determine the midpoint potential for the $OleT_{JE}$ Fe^{3+}/Fe^{2+} couple, redox titrations were performed at 25°C in an anerobic glove-box (Belle Technology, Weymouth UK) under a nitrogen atmosphere with O_2 levels maintained at less than 2 ppm. All solutions were deoxygenated by sparging with nitrogen gas. For substrate-free $OleT_{JE}$, the titration was done using 9.3 μM $OleT_{JE}$ in 100 mM KPi (pH 7.0) plus 10% glycerol. For substrate-bound $OleT_{JE}$, the titration was done under the same conditions, following addition of arachidic acid (from a 32 mM stock in 80% EtOH, 20% Triton X-100) until no further conversion of the heme iron to the high-spin heme state was observed (*ca* 12 μM arachidic acid). Mediators were added to expedite electronic equilibration in the system, and data fitting (using the Nernst equation) and analysis was done as described in previous publications (21-23).

2.3.7. EPR/ENDOR analysis of $OleT_{JE}$

Continuous wave X-band electron paramagnetic resonance EPR spectra of $OleT_{JE}$ were obtained at 10 K using a Bruker ELEXSYS E500 EPR spectrometer equipped with an ER 4122SHQ Super High Q cavity. Temperature control was effected using an Oxford Instruments ESR900 cryostat connected to an ITC 503 temperature controller. Microwave power was 0.5 mW, modulation frequency was 100 KHz and the modulation amplitude was 5 G. EPR spectra were collected for $OleT_{JE}$ (305 μM) in the substrate-free form, and for $OleT_{JE}$ (205 μM) bound to arachidic (C20:0) acid (at a saturating concentration).

2.3.8. Crystallography of $OleT_{JE}$

Crystallization trials for $OleT_{JE}$ were performed using 400 nL (200 nL protein plus 200 nL precipitant) sitting drops in Art Robbins 96-well plates, using Molecular Dimensions 96-deep well crystallisation screens [Clear Strategy Screen I (CSS1), Clear Strategy Screen II, PACT premier, JCSG-*plus* and Morpheus] and a Mosquito nanoliter pipetting robot (TTP Labtech, Melbourn UK). Crystals formed between 2 days and 1 month at 4°C in several conditions. The

crystals giving best diffraction were formed under the following conditions: 35 mg/ml $OleT_{JE}$ in 0.1 M Tris (pH 8.5) containing 0.2 M $MgCl_2$ and 25% (w/v) polyethylene glycol 2K monomethyl ether (substrate-free $OleT_{JE}$); and 43 mg/ml $OleT_{JE}$ incubated with 235 µM arachidic acid in 0.1 M Tris (pH 8.5) containing 0.2 M $MgCl_2$, 10% (w/v) polyethylene glycol 8K and 10% (w/v) polyethylene glycol 1K (substrate-bound $OleT_{JE}$).

For preparation of substrate-bound $OleT_{JE}$, P450 samples were concentrated by ultrafiltration and a stock solution of arachidic acid (32 mM) dissolved in 100% EtOH was added to a final concentration of 235 µM. The concentration of EtOH did not exceed 1% of the total volume. The mother liquor was supplemented with 10% PEG 200 where an additional cryo-protectant was required and crystals were flash-cooled in liquid nitrogen prior to data collection. Data were collected at Diamond synchrotron beamlines and reduced and scaled using XDS (24). Structures were solved by molecular replacement with the previously solved P450 BS_β crystal structure (PDB 2ZQJ) using PHASER (25). Structures were refined using Refmac5 (25) and Coot (26). Final refinement statistics are given in Table 1.

	$OleT_{JE}$ (4L40)	***$OleT_{JE}$:C20 (4L54)***
Space group	$P4_32_12$	$P4_32_12$
Cell parameters	a=59.7Å, c=245.5Å	a=59.3Å b=151.7Å c=60.8Å beta=95.9˚
Resolution (Å)	41-2.30 (2.36-2.3)	33.6-2.50 (2.56-2.50)
Rmerge (%)	9.2 (56.5)	8.8 (49.1)
I/sigI	9.2 (1.9)	8.4 (2.2)
R/Rfree (%)	20.0/25.6 (17.5/26.8)	19.8/26.9 (27.6/31.3)
Average B ($Å^2$)	20.5	15.4
Rmsd bonds/angles	0.018Å/1.56˚	0.015Å/1.47˚
Crystallization conditions	25% PEG2000MME, 0.2 M $MgCl_2$, pH 6.5 (0.1 M sodium cacodylate)	15% PEG20K, 15% PEG550MME 0.06 M $MgCl_2$, pH 6.5 (0.1 M imidazole/MES)

Table 2.1. Data reduction and final structural refinement statistics for the substrate-free $OleT_{JE}$ P450 and for its arachidic acid substrate complex. Substrate-free $OleT_{JE}$ has PDB code 4L54, and arachidic acid-bound $OleT_{JE}$has PDB code 4L40

2.3.9. Analysis of products formed by $OleT_{JE}$ in reactions with H_2O_2 and fatty acids

$OleT_{JE}$ reactions with long chain saturated fatty acids (C12 to C20) were set up as follows. 5 mL reactions were done in buffer D, with 250 µM dodecanoic acid (sodium salt), palmitic acid or arachidic acid, 500 µM hydrogen peroxide and 0.6 µM $OleT_{JE}$. The final reaction mixtures were incubated for periods up to 30 minutes at room temperature. 1 mL of the reaction mixture was then extracted (at different reaction times) with an equal volume of HPLC-grade heptane, and the sample centrifuged at 14000 rpm for 20 minutes. The top layer was then analyzed by GC/MS. Analysis was done using a Thermo Fisher DSQ II GC/MS instrument with a 30 m x 0.25 mm x 0.25 µm ZB5MS GC column (Phenomenex). Injection was cold on-column. The oven program was set so that an initial temperature of 50°C was ramped at 10°C/min to 300°C post-injection. Electronic ionization was used, and ions in the range of 40-640 m/z scanned at two scans per second.

2.4. Results

2.4.1. Classification of $OleT_{JE}$ as CYP152L1

There are currently 21,039 named cytochrome P450 sequences (drnelson.uthsc.edu/P450.stats.Aug2013.png). Approximately 6% are bacterial (1254 sequences) and an additional 48 are from archaea. Initial BLAST searches with $OleT_{JE}$ showed that it was less than 40% identical to most known CYP152 sequences and barely over the 40% recommended cutoff for CYP family membership to two CYP152 sequences (41% to CYP152A1 from *Bacillus subtilis* and 40% to CYP152A2 from *Clostridium acetobutylicum*). The location of the $OleT_{JE}$ sequence in a phylogenetic tree (as CYP152L1) strongly argues for inclusion in the distinct CYP152 clade. The same logic applies to the renamed CYP152M1 from *Enterococcus faecium* that has a long branch in the tree. This sequence was previously named CYP241A1, but that nomenclature has been changed based on its inclusion within the CYP152 clade. A second sequence, CYP152L2 from *Staphylococcus massiliensis* S46, is 64% identical to CYP152L1 (Figure 2.2).

2.4.2. Expression and purification of $OleT_{JE}$

The $OleT_{JE}$ gene was codon optimized for expression in *E. coli*, and preliminary studies revealed that the enzyme was expressed well in a number of *E. coli* strains. The C41 (DE3) strain (Lucigen) was selected for protein production with the gene cloned into pET47b via the BamHI and EcoRI restriction sites with a 6-His N-terminal tag, and transcribed using the T7-lac RNA polymerase/promoter system. Expression cell extracts were red in colour, indicative of the production of a heme protein. However, our initial studies revealed that the $OleT_{JE}$

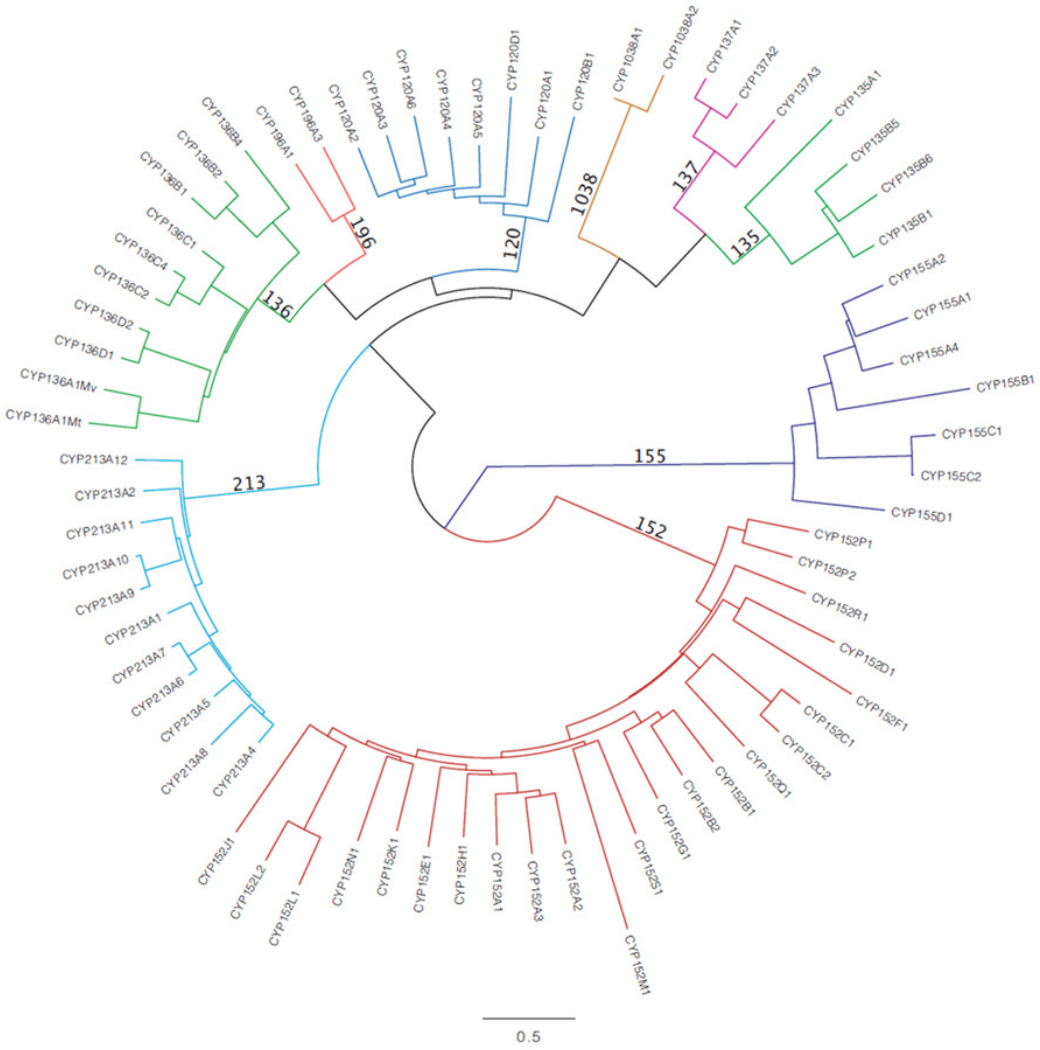

Figure 2.2. Phylogenetic tree for $OleT_{JE}$ and other members of the CYP152 P450 family. The tree shows the relationship between members of the bacterial CYP152 family, and between the CYP152s and other bacterial cytochrome P450 families. CYP152L1 ($OleT_{JE}$) is most closely related to CYP152L2 from *Staphylococcus massiliensis* S46 (64% amino acid identity).

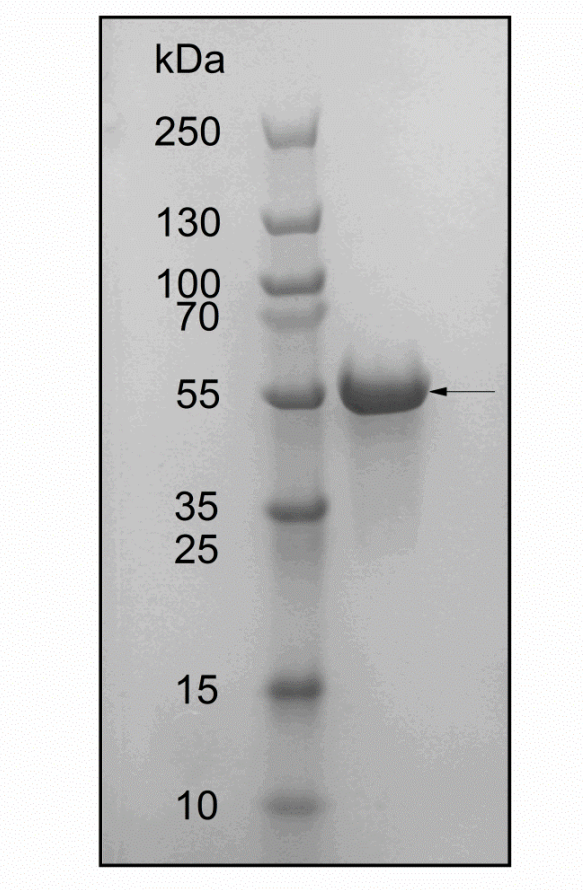

Figure 2.3. Purification of $OleT_{JE}$. Proteins are resolved on a 12% SDS PAGE gel. The first lane shows markers of indicated sizes (Fermentas PageRuler Plus pre-stained protein marker, Thermo Scientific). Purified non-tagged $OleT_{JE}$ (~1.5 µg) is in lane 2, and shows protein isolated from *E. coli* following steps of Ni-IDA chromatography, protein precipitation and resolubilization, His-tag removal by proteolysis using HRV 3C, and passage through a Ni-Sepharose column.

protein precipitated on dialysis following elution from a Ni-IDA protein in the first chromatographic purification step. Previous studies by Rude et al. used high salt (NaCl) concentration in several purification buffers (18), and in view of this and the halophilic nature of the host bacterium (*Jeotgalicoccus* sp. ATCC 8456) we considered that the protein might be stabilized in solution at high ionic strength. This proved to be the case, and it was found that the precipitation of $OleT_{JE}$ could be used to advantage, since resolubilization of the centrifuged protein pellet in buffer A containing 1 M NaCl and 10% glycerol produced an $OleT_{JE}$ sample with a P450-like heme spectrum (A_{max} at ~418 nm). SDS-PAGE at this stage also indicated the protein to be extensively purified (purification Method 1). Specifically for crystallization, the $OleT_{JE}$ His-tag was removed by incubation with HRV 3C protease, and the mixture loaded onto a Ni-Sepharose column. Washing the column in buffer C (100 mM KPi (pH 8.0) plus 750 mM NaCl and 10% glycerol) resulted in elution of a highly purified tag-free OleT protein (Figure 2.3), and the retention of the cleaved His-tag and the tagged protease on the column.

Having identified the issues with propensity of $OleT_{JE}$ to aggregate at low ionic strength, an alternative strategy was developed to avoid its precipitation – by eluting $OleT_{JE}$ from Ni-IDA in the high salt buffer C, centrifuging the sample and then re-applying to Ni-IDA resin equilibrated in buffer C. By washing the column with increasing concentrations of imidazole in buffer C,

His-tagged $OleT_{JE}$ was eluted at 150 mM imidazole in a highly pure form (purification Method 2).

2.4.3. UV-visible absorption properties of $OleT_{JE}$

Rude et al. inferred the cytochrome P450 nature of $OleT_{JE}$ from amino acid sequence similarities to peroxygenase members of the CYP152 family of P450s, and demonstrated in vitro that cell extracts of *Jeogalicoccus* sp. ATCC 8456 could decarboxylate the saturated fatty acids arachidic acid (C20) and stearic acid (C18) to their respective n-1 terminal alkenes (1-nonadecene and 1-heptadecene, respectively). A His-tagged $OleT_{JE}$ isolated from *E. coli* was also shown to catalyze stearic acid decarboxylation in a H_2O_2-dependent

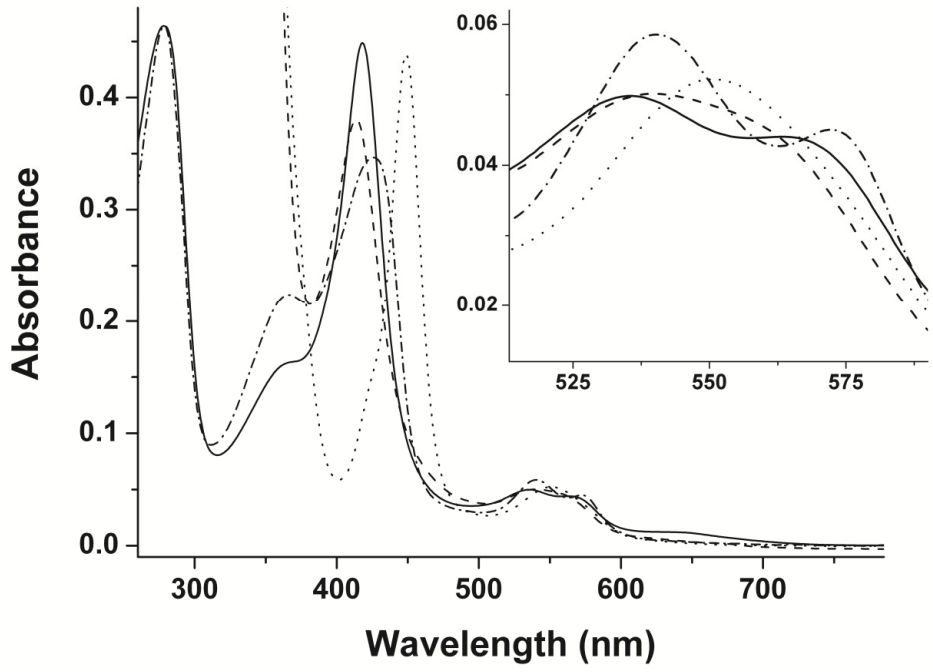

Figure 2.4. UV-visible spectroscopic features of $OleT_{JE}$. UV-Visible absorption spectra of OleT (4.9 μM) are shown for (i) the oxidized (ferric), substrate-free form (solid back line) with Soret maximum at 418 nm; (ii) the sodium dithionite-reduced (ferrous) form (dashed line) with Soret maximum at 414 nm; (iii) the ferrous-CO complex (dotted line) with the Soret band shifted to 449 nm (the P450 form); and for (iv) the ferric-NO complex (dash-dot-dash line), with Soret maximum at ~427 nm. The inset shows magnification of the Q-band region for the same $OleT_{JE}$ spectra, highlighting changes observed on $OleT_{JE}$ reduction and on formation of its CO and NO complexes. Lines are identified in the same way as in the main panel.

reaction (18). However, UV-visible absorption features typical of a P450 enzyme were not presented in this earlier study.

Figure 2.4 shows characteristic absorption spectra for pure $OleT_{JE}$ in its oxidized (ferric, Fe^{3+}) and sodium dithionite-reduced (ferrous, Fe^{2+}) forms; and for the ferrous-carbon monoxide (Fe^{2+}-CO) and ferric-nitric oxide (Fe^{3+}-NO) species. The resting (ferric) form of $OleT_{JE}$ shows a heme spectrum typical of a P450 enzyme with its ferric heme iron in a low-spin (LS) state. The major absorption feature (the Soret band) is at 418 nm, with the smaller alpha and beta bands in the visible region at ~566 nm and 535 nm, respectively. These values are similar to those of other LS bacterial P450s (e.g. the *Bacillus megaterium* P450 BM3 [CYP102A1] heme domain with maxima at 418, 534 and 568 nm; and the *Mycobacterium tuberculosis* CYP121A1 at 416.5, 538 and 568 nm) (27,28). The two methods of preparing $OleT_{JE}$ (i.e. with or without a protein precipitation step) produced identical oxidized $OleT_{JE}$ spectra. Any residual imidazole ligand from nickel column chromatography (in both cases) was completely removed by ultrafiltration used to concentrate the proteins and thus did not produce any imidazole-ligated $OleT_{JE}$ heme iron.

Reduction of $OleT_{JE}$ with sodium dithionite produced a ferrous hemoprotein with the Soret band diminished in intensity and shifted to 414 nm. In the visible (heme Q-band) region, a single, slightly asymmetric feature is seen at ~540 nm. The blue shift of the Soret spectrum on reduction indicates substantial retention of cysteine thiolate proximal coordination in the $OleT_{JE}$ ferrous state, and the spectral maxima are similar to those features seen for e.g. the well characterized *Pseudomonas putida* camphor hydroxylase P450cam (CYP101A1, 411 and 540 nm) and for the explosive degrading P450 XplA from *Rhodococcus rhodochrous* strain 11Y (CYP177A1, 408 and 542 nm) (23,29). Addition of carbon monoxide to anerobically reduced $OleT_{JE}$ produced a characteristic P450 heme spectrum with the Soret band red-shifted to 449 nm and a Q-band feature at 551 nm. A small shoulder on the Soret feature at ~423 nm likely indicates a minor proportion (~5%) of the P420 (likely cysteine thiol-coordinated) form of the $OleT_{JE}$ Fe^{2+}-CO complex. The NO-bound ferric $OleT_{JE}$ spectrum is also typical of other P450-NO adducts, with an asymmetric Soret feature (~427 nm) and distinctive, enhanced intensity alpha and beta bands at ~573 and 540 nm (30). Using the

method of Berry and Trumpower, an extinction coefficient of ε_{418} = 91.5 mM^{-1} cm^{-1} was established for the LS ferric form of $OleT_{JE}$ (31,32).

Fatty Acid	K_d (μM)[A]	High-spin heme (%)[A]	K_d (μM)[B]	High-spin heme (%)[B]	K_d (μM)[C]	High-spin heme (%)[C]
C20:0 (arachidic acid)	0.29 ± 0.05	95	2.32 ± 0.17	84	1.54 ± 0.19	59
C18:0 (stearic acid)	0.20 ± 0.02	67	7.43 ± 0.44	51	3.95 ± 0.76	36
C16:0 (palmitic acid)	0.67 ± 0.03	27	6.20 ± 0.26	27	4.29 ± 0.89	23
C14:0 (myristic acid)	0.66 ± 0.03	39	37.7 ± 1.9	41	11.4 ± 0.5	29
C12:0 (lauric acid)	0.77 ± 0.02	45	59.2 ± 7.7	27	12.7 ± 0.3	30

Table 2.2. Determination of the affinity of $OleT_{JE}$ for long chain fatty acids. Dissociation constants (K_d values) for the binding of fatty acids to $OleT_{JE}$ were determined by optical titration, as described in the *Fatty acid and inhibitor binding titrations with $OleT_{JE}$* section of the *Experimental Procedures*. The K_d values stated are for titrations done using $OleT_{JE}$ prepared using Method 1 and using fatty acid stocks made up in alcohol containing 30% v/v Triton X-100 (A), or in alcohol without the addition of the detergent (B). The final set of K_d data (C) are for $OleT_{JE}$ prepared using Method 2 and using fatty acid stocks in alcohol with 30% v/v Triton X-100. For protein prepared using Method 1, the K_d values are lower and the extent of spectral shift towards the ferric HS state is improved in the presence of Triton X-100, which in itself does not induce any significant HS heme development. In the case of $OleT_{JE}$ prepared using Method 2, the fatty acid K_d values are consistently higher than those for enzyme produced using Method 1 from comparable titrations with Triton X-100 in the fatty acid stocks. The percentage of high-spin heme is estimated with reference to the near-complete conversion to HS of the $OleT_{JE}$ sample titrated with arachidic acid including 30% Triton X-100 (estimated at 95% HS at apparent saturation with arachidic acid).

2.4.4. Analysis of substrate and inhibitor binding to $OleT_{JE}$

The binding of substrates to P450s is often associated with alteration of the spin-state of their ferric heme iron, usually through displacing its weakly bound 6th ligand water molecule and inducing a shift towards the high-spin (HS) form (e.g. 33,34). For $OleT_{JE}$, we investigated the binding of a series of saturated fatty acids (C12-C20), and found that in all cases the lipids induced a LS to HS transition, with the Soret band shifting from 418 nm towards 394 nm. Table 2 shows fatty acid binding K_d data for $OleT_{JE}$ (purified using Method 1) and using fatty acid stocks dissolved in alcohol, or in alcohol containing 30% v/v Triton X-100 (see Experimental Procedures). The K_d values and the extent of HS heme iron developed were improved in all

cases in presence of the detergent, although Triton X-100 alone induces no spin-state change (e.g. 0.67 ± 0.03 μM versus 6.20 ± 0.26 μM for palmitic acid). The extent of spin-state change induced varied according to chain length, with the longer chain fatty acids (C18:0 and C20:0) inducing a more complete conversion to the HS ferric state than observed for the C12:0 to C16:0 fatty acids). For a titration using an arachidic acid (C20:0) stock including Triton X-100,

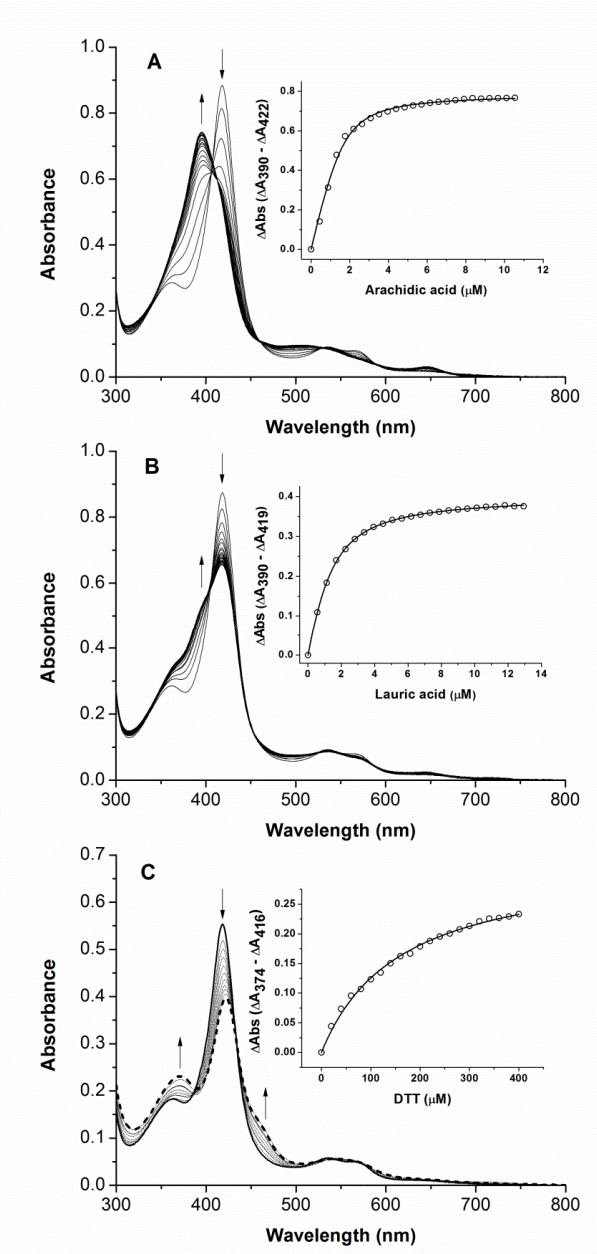

Figure 2.5. Analysis of fatty acid and dithiothreitol binding to OleT$_{JE}$. Panel A shows a spectral titration for OleT$_{JE}$ (9.8 μM) with arachidic acid (C20:0). Arrows indicate the progressive decrease in the ferric low-spin Soret band (at 418 nm) and the concomitant increase in the ferric high-spin feature at 394 nm. The development of a small thiolate-to-high spin ferric charge transfer band is seen at ~650 nm as the titration progresses. The inset shows a fit (using the Morrison equation) of arachidic acid-induced Soret absorbance change *versus* fatty acid concentration, yielding a K_d value of 0.29 ± 0.05 μM for arachidic acid. Panel B shows spectra for an OleT$_{JE}$ (9.8 μM) titration with lauric acid (C12:0). In this case, high-spin heme development is less extensive than for arachidic acid, and the K_d value (inset) is 0.77 ± 0.02 μM. Panel C show titration of OleT$_{JE}$ (6.1 μM) with dithiothreitol (DTT). The binding of DTT is associated with the splitting of the heme signal into two distinct features – a hyperporphyrin (split Soret) spectrum with maxima at 372 and ~460 nm, and a distinct Soret feature at 423 nm. The former results from distal coordination of the OleT$_{JE}$ by DTT thiolate (*trans* to cysteine thiolate), while the latter has DTT thiol as the distal ligand (23). The inset shows a plot of DTT-induced Soret absorbance shift *versus* DTT concentration, fitted using a hyperbolic equation to yield a K_d value of 159 ± 7 μM. Data were collected, processed and fitted as described in the *Experimental Procedures*.

the HS conversion was almost complete (estimated at ≥95%), as shown in Figure 2.5A. In contrast, lauric acid (C12:0) produced 52% HS at saturation (Figure 2.5B). For studies with non-precipitated OleT$_{JE}$ (prepared using Method 2) in the presence of Triton X-100, tight

binding of fatty acids was again observed (e.g. K_d values of 1.54 ± 0.19 μM for arachidic acid and 12.7 ± 0.3 μM for lauric acid).

However, the K_d values increase by approximately an order of magnitude for all fatty acids tested compared to those for $OleT_{JE}$ prepared by Method 1 (Table 2.2). Thus, contrary to what may have been expected, the resolubilized $OleT_{JE}$ shows higher affinity than the non-precipitated form for the panel of fatty acid substrates tested.

Binding of cyanide and imidazole to $OleT_{JE}$ produced typical type II P450 heme absorption shifts to longer wavelength. Soret shifts to 433 nm (K_d >10 mM) and 424 nm (K_d = 193 ± 11 μM) were observed for cyanide and imidazole, respectively. The binding of DTT to $OleT_{JE}$ was also analyzed in view of the report from Rude et al., which indicated that DTT could support $OleT_{JE}$ fatty acid decarboxylase activity by producing H_2O_2 under aerobic conditions in the presence of the P450 heme iron (18,35). However, in previous studies we showed that DTT coordinated the heme iron in the explosive degrading XplA P450 (23). DTT is known to bind P450 heme iron and ligation is feasible in both DTT thiol and thiolate forms (36,37). Figure 2.5C shows data from a spectral titration of $OleT_{JE}$ with DTT in buffer D. The DTT-bound form has three distinct absorption features in the Soret region, with peaks at 372 nm and 423 nm, and a strong absorbance shoulder at ~460 nm. The central band is the most intense. The 423 nm peak arises from distal ligation of DTT thiol to $OleT_{JE}$ heme iron, whereas the outer peaks result from a split (hyperporphyrin) Soret spectrum in which DTT thiolate ligates the iron (36,37). Comparable spectral maxima are at 374, 423.5 and 453.5 nm for XplA (23). In XplA, the intensities of the three absorbance bands are quite similar, but in $OleT_{JE}$ the outer bands are much weaker than the 423 nm feature, suggesting that DTT favors heme ligation in the thiol state under the conditions used. The Figure 2.5C inset shows fitting of DTT-induced heme absorption change for $OleT_{JE}$, leading to a K_d of 159 ± 7 μM. In the Rude et al. study, DTT at 200 μM was used to support $OleT_{JE}$ catalysis (18). However, our data indicate that substantial inhibition of $OleT_{JE}$ likely occurs under such conditions.

2.4.5. Determination of the heme iron redox potentials of substrate-free and substrate-bound OleT$_{JE}$

Fatty acid binding to OleT$_{JE}$ induces substantial shifts in heme iron spin-state equilibrium towards HS (e.g. Figure 2.5A), and such shifts in spin-state equilibrium are often associated with the heme iron developing a more positive potential and becoming easier to reduce (e.g. 22,33). Spectroelectrochemical titrations were done for both substrate-free and arachidic acid-bound forms of OleT$_{JE}$ to determine the midpoint potentials for the heme iron Fe^{3+}/Fe^{2+} couples (versus the normal hydrogen electrode, NHE). Despite the extensive HS heme content in the arachidic acid-bound OleT$_{JE}$, its heme potential (-105 ± 6 mV) is not significantly different from

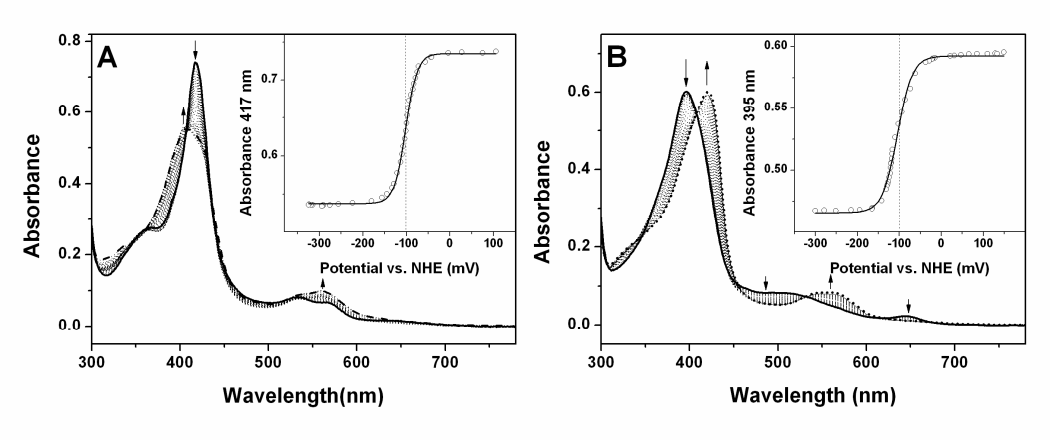

Figure 2.6. Determination of the OleT$_{JE}$ heme iron reduction potential in its substrate-free and arachidic acid-bound forms. Panel A shows data from a spectroelectrochemical redox titration of ligand-free OleT$_{JE}$ (8.1 μM). The spectrum for the oxidized enzyme (solid line) shows the Soret maximum at 419 nm, while that for the fully dithionite-reduced P450 (dashed line) has its Soret maximum at 406 nm, and show a single feature in Q-band region at ~560 nm. Intermediate spectra are shown in dotted lines. Arrows indicate the direction of absorption changes observed during the reductive part of the titration. The inset shows a plot of absorbance at the Soret peak (417 nm) versus the applied potential corrected for the normal hydrogen electrode (NHE). Data are fitted using the Nernst equation to give a midpoint potential of $E^{0'}$ = -103 ± 6 mV. Panel B shows a redox titration for arachidic acid-bound OleT$_{JE}$ (8.1 μM, thick solid line). The oxidized substrate-bound species has its Soret maximum at 395 nm, and the fully reduced form (thick dotted line) has a maximum at ~420 nm. Intermediate spectra in the titration are shown in dotted lines. Arrows again indicate absorption changes observed during the reductive part of the titration. The inset shows a plot of absorbance at the substrate-bound Soret peak (395 nm) versus the applied potential corrected for the NHE, with data fitted using the Nernst equation to yield $E^{0'}$ = -105 ± 6 mV.

that of the substrate-free form (-103 ± 6 mV) (Figure 2.6). In both cases, the heme iron potentials are quite positive compared to many bacterial P450s which rely on NAD(P)H-dependent electron transfer from protein redox partner systems. Examples include the camphor binding-induced shift in heme iron potential from -300 mV to -170 mV (vs. NHE) in

P450cam (enabling electron transfer from the ferredoxin partner at -240 mV) (33,38); and the arachidonic acid-induced shift in potential from -429 mV to -289 mV (vs. NHE) in P450 BM3 (22). However, unlike the aforementioned P450s, $OleT_{JE}$ is evolutionarily adapted to interact directly with H_2O_2 in order to form reactive iron-oxo species (initially the ferric-hydroperoxo compound 0, which is likely transformed to the ferryl-oxo compound I), and its positive potential is likely a consequence of the environment of the heme and its cysteine thiolate ligand. The fact that the $OleT_{JE}$ heme potential is effectively unchanged in the HS substrate-bound form may be a consequence of the proximity of a negatively charged substrate carboxylate group to the heme iron in the arachidic acid bound form.

Another notable feature in the spectra for the reduced forms of substrate-free and arachidic acid-bound $OleT_{JE}$ is that neither form a unique spectral species that could be assigned to a cysteine thiolate-coordinated ferrous P450 heme iron. As shown in Figure 2.4, the UV-visible spectrum for $OleT_{JE}$ immediately following reduction has its Soret feature at 414 nm, with a small shoulder at ~423 nm – indicative of a mixture of Cys thiolate-coordinated (major species) and thiol-coordinated (minor species) forms. In the redox titration for substrate-free $OleT_{JE}$ (Figure 2.6A) the Soret peak for the reduced P450 is split into two components, with a peak at 406 nm and a shoulder at ~425 nm. The former likely represents thiolate-coordinated ferrous $OleT_{JE}$, and the latter the thiol-coordinated form (39). A similar phenomenon is seen for the arachidic acid-bound $OleT_{JE}$ (Figure 2.6B), although in this case the main peak is at 420 nm with a shoulder at ~400 nm, suggesting a higher proportion of the thiol-coordinated ferrous form in the substrate-bound $OleT_{JE}$. For both substrate-free and arachidic acid-bound $OleT_{JE}$ redox titrations, it is evident that there is a single set of isosbestic points throughout the titrations, indicating that the equilibrium between thiol- and thiolate-coordinated ferrous forms remains constant as the concentration of ferrous $OleT_{JE}$ accumulates. The Soret isosbestic point is at 408 nm for the arachidic acid-bound form, and at 410 nm for substrate-free $OleT_{JE}$. Thus, under the same redox titration conditions, arachidic acid substrate binding seems to push the ferrous heme cysteine thiolate/thiol equilibrium slightly further towards the thiol-coordinated state.

2.4.6. Stopped-flow analysis of $OleT_{JE}$ turnover kinetics

In order to determine the kinetics of H_2O_2-dependent fatty acid oxidation, we exploited the fact that turnover of bound substrate is accompanied by a reconversion of $OleT_{JE}$ heme iron spin-state from HS to LS as the substrate is decarboxylated. The two states of the P450 have considerably different heme spectra, and thus we used stopped-flow absorbance spectroscopy to measure the rate constants for LS $OleT_{JE}$ heme formation at 417 nm across a range of H_2O_2 concentrations up to 200 μM. Reaction kinetics are 2nd order with respect to [H_2O_2], with observed rate constants (k_{obs}) for arachidic acid oxidation and concomitant LS heme recovery up to 167 s^{-1} at the highest [H_2O_2] tested (200 μM) (Figure 2.7A). The k_{obs}

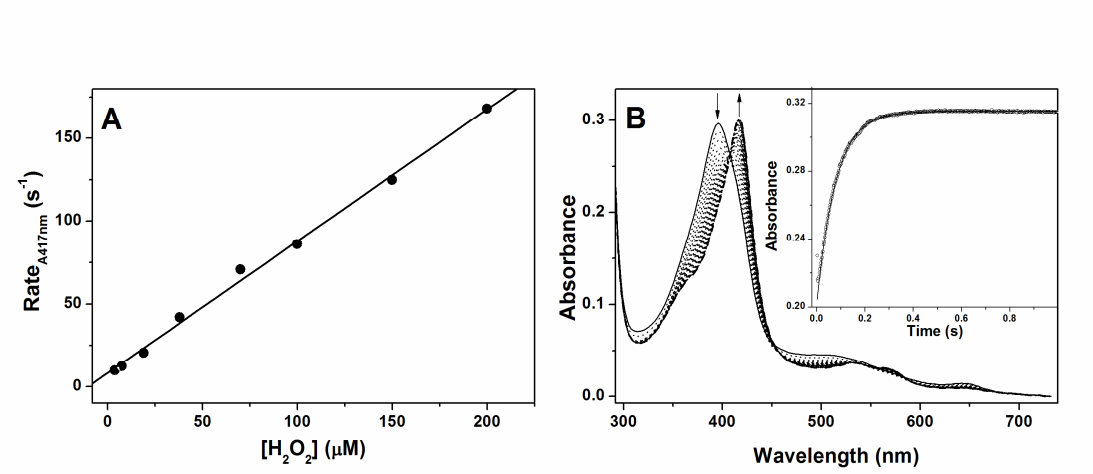

Figure 2.7.Stopped-flow kinetics of H_2O_2-dependent oxidation of substrate-bound $OleT_{JE}$. Panel A: Plot of the observed rate constants (k_{obs}) for H_2O_2 binding to $OleT_{JE}$ (and concomitant substrate oxidation) *versus* the H_2O_2 concentration. Data were measured at 417 nm, reflecting recovery of the LS $OleT_{JE}$ form. The k_{obs} versus [H_2O_2] data were fitted to a linear function to yield the 2nd order rate constant of H_2O_2 binding/substrate (arichidic acid) oxidation of k_{on} = 0.80 ± 0.02 μM^{-1} s^{-1}, k_{off} = 8.32 ± 1.96 s^{-1} and an apparent K_d value of 10.40 ± 2.71 μM for H_2O_2 binding, derived from k_{off}/k_{on}. Panel B shows stopped-flow photodiode array (PDA) data observed at 7.58 μM H_2O_2, demonstrating the $OleT_{JE}$ spectral conversion from the HS, substrate-bound form (Soret maximum at 394 nm) to the LS reoxidized state (Soret maximum at ~417 nm) upon mixing with H_2O_2. The inset shows the corresponding plot of the absorbance data at 417 nm (open circles) against time. The data were fitted using a single exponential function to yield an apparent rate constant of 12.50 ± 1.16 s^{-1}.

versus [H_2O_2] data were fitted using a linear equation – giving a 2nd order rate constant (k_{on}) of (8.0 ± 0.2) x 10^5 M^{-1} s^{-1} to describe the catalytic process. The apparent k_{obs} value at the y-axis intercept (zero [H_2O_2]) is 8.32 ± 1.96 s^{-1}, giving an estimate for the H_2O_2 k_{off} rate constant. The k_{off}/k_{on} ratio thus gives an estimate of the apparent K_d for H_2O_2 as 10.40 ± 2.71 μM. Figure 2.7B shows overlaid spectra captured during the reaction of arachidic acid-bound $OleT_{JE}$ with

H_2O_2 at a final concentration of 7.58 μM. The spectral overlay describes a smooth transition from the substrate-bound, extensively HS form of $OleT_{JE}$ at 394 nm towards the substrate-free LS form at 418 nm as the oxidation reaction occurs and the product leaves the heme environment and a water ligand binds to the heme iron. A series of isosbestic points are observed in the overlaid spectra (notably in the Soret region at 410 nm) that indicate no significant accumulation of any intermediate species in the reaction. The Figure 2.7B inset shows the accompanying stopped-flow data for this reaction at 417 nm and 7.58 μM H_2O_2, with data fitted accurately using a single exponential function to give a k_{obs} of 12.50 ± 1.16 s^{-1}.

2.4.7. EPR analysis of $OleT_{JE}$

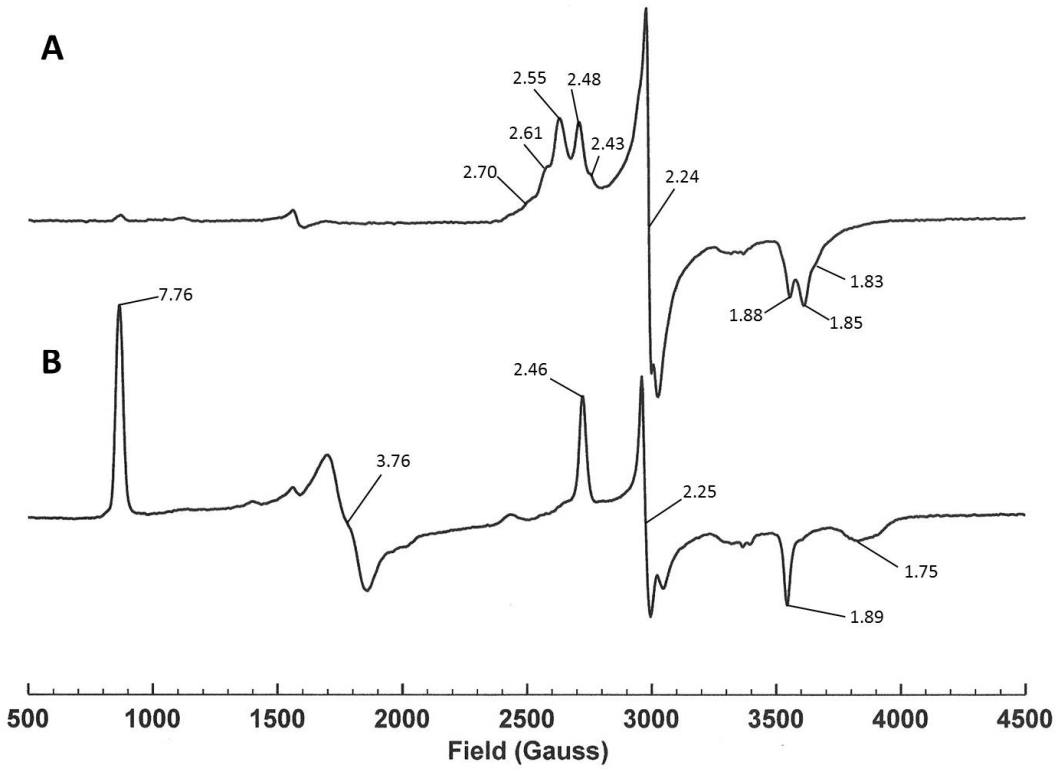

Figure 2.8. EPR spectroscopic analysis of $OleT_{JE}$. X-band continuous wave EPR spectra (see *Experimental Procedures* for acquisition parameters) are shown for A) purified $OleT_{JE}$; and B) $OleT_{JE}$ plus arachidic acid, with both enzymes purified using Method 1 (see *Experimental Procedures*). The g-values are marked in each case. The $OleT_{JE}$ concentration is 305 μM for substrate-free enzyme and 205 μM for arachidic acid-bound $OleT_{JE}$, with arachidic acid added to a saturating concentration.

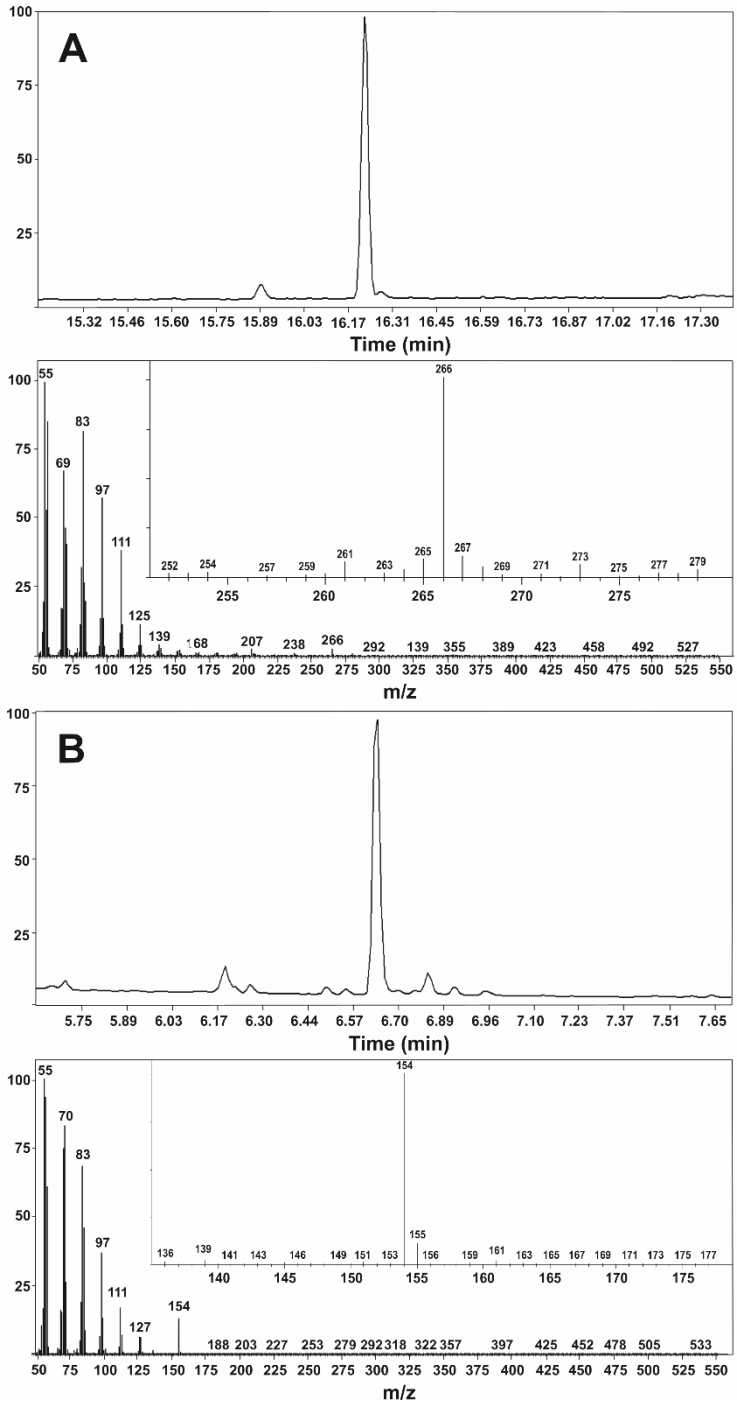

Figure 2.9. Oxidative decarboxylation of arachidic acid and lauric acid by OleT$_{JE}$. Figure 8A shows the total ion count from GC separation of the C19 terminal alkene 1-nonadecene in the reaction of OleT$_{JE}$ with arachidic acid (C20:0) (upper panel), with mass spectrometric analysis of the major peak at 16.21 minutes confirming its identity (lower panel, with inset highlighting the region of the 1-nonadecene mass ion with m/z = 266). Figure 8B shows the total ion count from GC separation of the C11 terminal alkene 1-undecene following reaction of OleT$_{JE}$ with lauric acid (C12:0) (upper panel), with mass spectrometric analysis of the major peak at 6.63 minutes confirming its identity (lower panel, with inset highlighting the region of the 1-undecene mass ion with m/z = 154).

Th

e continuous wave X-band EPR spectrum of substrate-free $OleT_{JE}$ (prepared using Method 1) displays features attributable to the S = ½ low spin ferric heme with a thiolate proximal ligand to the iron and a distal ligating water molecule (Figure 2.8A). Several such low spin forms with rhombic anisotropy are evident from the multiplicity of lines observed and the resolvable contributions at g_z show g-values ranging from those typical for LS ferric P450s (2.43, 2.48) (e.g. 39-42) to those associated with chloroperoxidases and the fatty acid hydroxylase $P450_{SP\alpha}$ (CYP152B1) (2.55, 2.61 and possibly 2.70) (17,43). Overall the EPR spectrum suggests a large, water filled site with multiple coordination geometries and hydrogen bonding partners available to the distal water ligand. The addition of substrate, arachidic acid, produces a very different EPR spectrum dominated by a S = 5/2 rhombic HS ferric thiolate-ligated heme signal having five-coordinate iron and g-values $g_z = 7.76$, $g_y = 3.76$ and $g_x = 1.75$ (Figure 2.8B). This is in contrast to $P450_{SP\alpha}$ that shows no spin state change on substrate binding (17), and where x-ray crystallography has shown that the heme retains the water sixth ligand when substrate is bound. Approximately 15% of the protein is converted to a new low spin species having $g_z = 2.46$, $g_y = 2.25$ and $g_x = 1.89$ which is not present in the substrate free enzyme. It is likely that this minor LS species is in equilibrium with the HS form.

2.4.8. $OleT_{JE}$-catalyzed substrate turnover

$OleT_{JE}$ turnover assays were done using H_2O_2 and with a range of saturated fatty acids (C12-C20), as described in the Experimental Procedures. As reported, by Rude et al. (18), products were identified and characterized as terminal alkenes. Figure 2.9 shows formation of 1-alkene products from arachidic acid (forming 1-nonadecene) and from lauric acid (forming 1-undecene). Rude et al. reported (from in vivo and/or in vitro analyses) data consistent with the oxidative decarboxylation of fatty acids in the chain length range 14-22, forming the n-1 terminal alkenes (18). Here we demonstrate that the chain length selectivity of $OleT_{JE}$ extends to the C12:0 saturated fatty acid lauric acid.

2.4.9. Crystal structure of $OleT_{JE}$

The structure of the $OleT_{JE}$ P450 was determined to a resolution of 2.3 Å for the substrate-free form, and to 2.5 Å for the arachidic acid fatty acid-bound form. Despite the fact that both forms were obtained from different crystallization conditions, the crystal packing is identical, with little difference in structure noted between the C20-bound and ligand-free $OleT_{JE}$ P450s (r.m.s.d of 0.125 for 410 C_α atoms). The overall $OleT_{JE}$ P450 structure closely resembles the related peroxygenase $P450_{BS\beta}$ with an r.m.s.d of 0.99 Å for 379 C_α atoms (Figure 2.10). Areas where significant deviations occur are located at the FG-loop and the adjacent C-terminal loop regions. Both these regions line the fatty acid binding pocket, more specifically the area involved in binding the fatty acid tail. In $OleT_{JE}$, residue Leu177 from the FG-loop closes the The $OleT_{JE}$ fatty acid binding pocket is elongated in comparison to $P450_{BS\beta}$, due to three point mutations in the N-terminal β-sheet region (from $P450_{BS\beta}$ Ile25, Leu41 and Leu315 to the corresponding $OleT_{JE}$ Thr24, Ala40 and Ala317) (Figure 2.11). This provides additional space

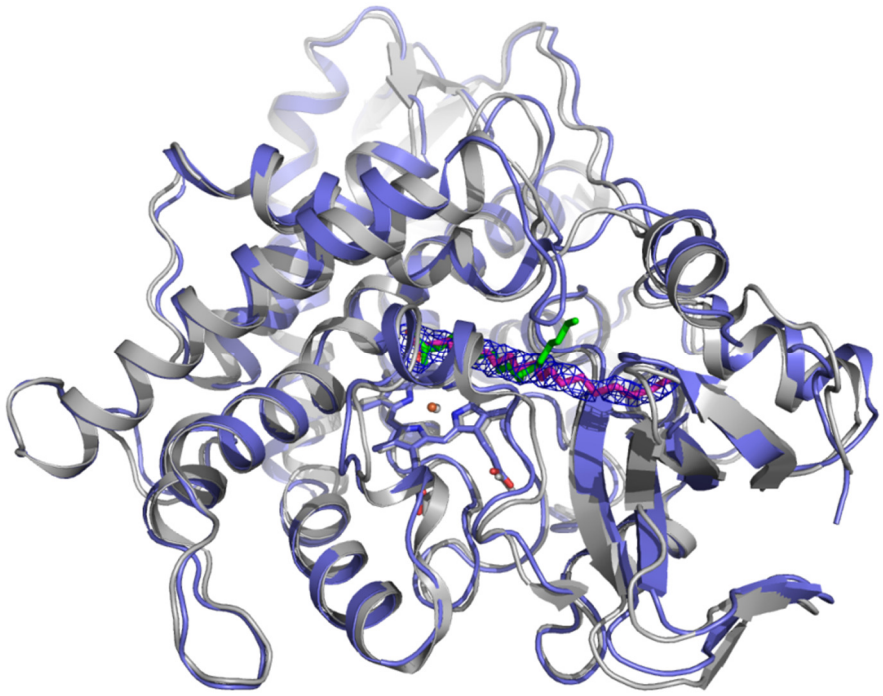

Figure 2.10. Comparison between the $OleT_{JE}$ and $P450_{BS\beta}$ P450 structures An overlay is shown for the substrate-bound forms of $OleT_{JE}$ (in blue, PDB code 4L40) and $P450_{BS\beta}$ (in grey, PDB code 1IZO) in cartoon representation. The bound substrates and heme groups are represented in sticks, colored in magenta for the $OleT_{JE}$ arachidic acid-bound form, and in green for the palmitic acid-bound form of $P450_{BS\beta}$.

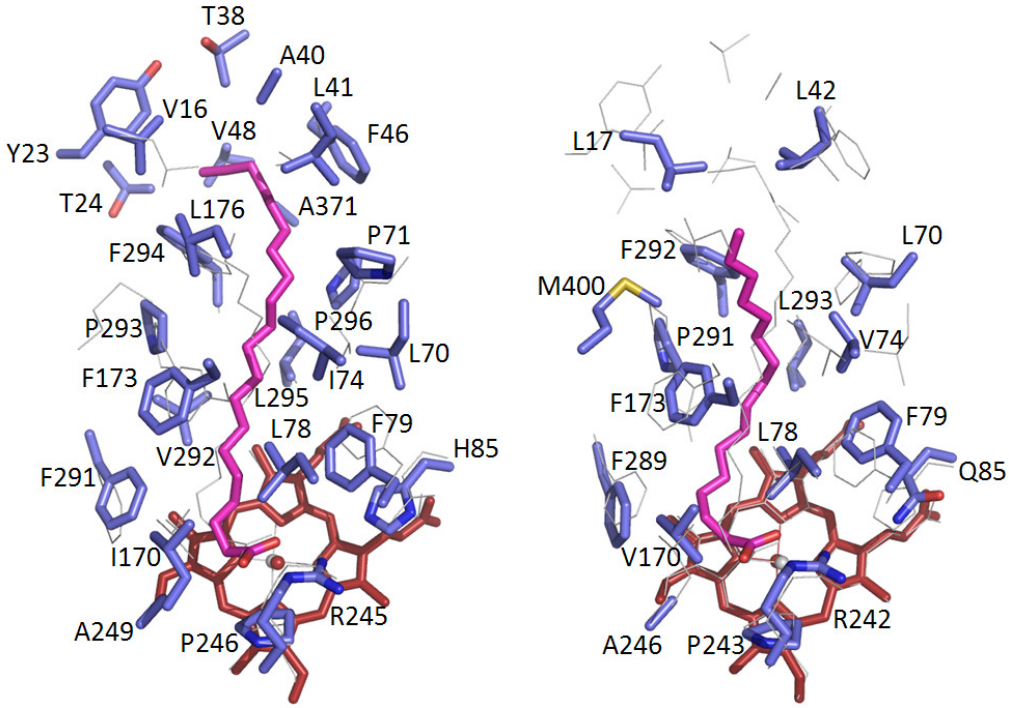

Figure 2.11. Comparison of the OleT$_{JE}$ and P450$_{BS\beta}$ fatty acid binding modes. The image shows a side by side overlay of the OleT$_{JE}$ and P450$_{BS\beta}$ fatty acid-bound active sites, with key residues contacting the substrates shown. For clarity, main chain atoms have been removed. The left panel depicts OleT$_{JE}$ in atom colored sticks, with the corresponding P450$_{BS\beta}$ residues shown in grey lines. The right panel shows the same view, but with the P450$_{BS\beta}$ residues in atom colored sticks, and OleT$_{JE}$ shown in grey lines. Substrates are arachidic acid (C20:0) for OleT$_{JE}$ and palmitic acid (C16:0) for P450$_{BS\beta}$.

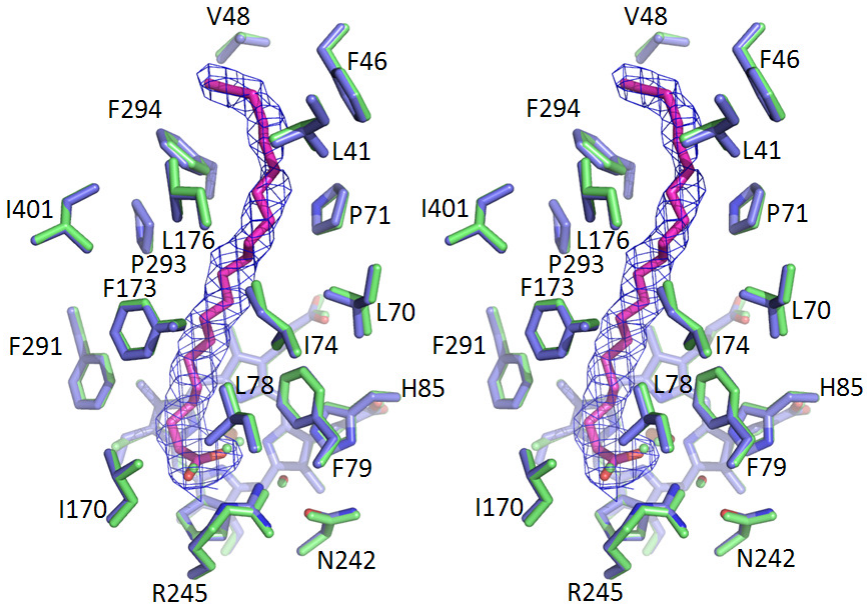

Figure 2.12. Detailed view of the OleT$_{JE}$ active site. A stereoview of the OleT$_{JE}$ active site region is shown, with both arachidic acid substrate-bound (in blue) and substrate-free (in green) key residues shown. The 2FoFc density corresponding to the bound fatty acid substrate is shown as a blue mesh.

to accommodate fatty acids with a chain length up to C20.

The active site of $OleT_{JE}$ is remarkably similar to $P450_{BS\beta}$, despite the fact both enzymes favor distinct catalytic reactions (decarboxylation versus hydroxylation, respectively). The fatty acid carboxylate group is bound by the conserved Arg245 and placed approximately perpendicular to the heme plane in $OleT_{JE}$, with the C_α and C_β carbons closest to the heme narrow access channel to the solvent that is present in both $P450_{BS\beta}$ and the related $P450_{SP\alpha}$ iron (at 5.1 and 5.7 Å, respectively; Figure 2.12). No other direct polar contacts are made between the carboxylate head group and the protein. A water molecule is seen to occupy a position in between His85 and the C20 carboxylate, in close proximity to both moieties (at distances of 3.3 and 2.7 Å, respectively). This water molecule is too distant from the heme iron (3.3 Å) to act as a direct ligand, and the heme is pentacoordinate in the substrate-bound $OleT_{JE}$ P450 structure. In comparison, the substrate-free $OleT_{JE}$ active site contains several water molecules with ill defined density above the heme plane, likely corresponding to a range of distinct water structures in the absence of the substrate, consistent with conclusions from EPR data.

One of the few key differences between the $OleT_{JE}$ and $P450_{BS\beta}$ active sites is the switch from His85 ($OleT_{JE}$) to Gln85 ($P450_{BS\beta}$). In $OleT_{JE}$ the His85 imidazole side chain points into the active site, directly towards the heme iron (at a distance of 5.8 Å). The imidazole moiety is sandwiched in between the heme edge and Phe79, and makes no polar contacts with other amino acids. In addition, the A and B pyrrole groups of the $OleT_{JE}$ P450 heme are distorted, with the effect of moving these closer to the substrate by approximately 0.8 Å when compared to $P450_{BS\beta}$. This is independent of substrate binding, as the same deviation from planarity can be observed for the substrate-free $OleT_{JE}$ P450 heme group. The difference in heme conformation between $OleT_{JE}$ and $P450_{BS\beta}$ cannot be attributed directly to mutations in the heme vicinity, as most heme binding residues are identical, but appears instead to be linked to small changes in the position of secondary elements containing heme binding residues.

2.5. Discussion

In this paper we present the first structural and detailed kinetic and biochemical characterization of the *Jeotgalicoccus* $OleT_{JE}$ enzyme, which catalyzes the production of terminal alkenes from long chain fatty acids – an industrially relevant reaction. The enzyme is one of a growing number of P450 enzymes that has evolved to use hydrogen peroxide (rather than NAD(P)H-dependent redox partners) in order to form reactive iron-oxo species for substrate oxidation (5,16). Its closest bacterial relatives are the *S. paucimobilis* $P450_{SP}$ and the *B. subtilis* $P450_{BS\beta}$, which catalyze predominantly the alpha- and beta-hydroxylation of long chain fatty acids (44,45). $OleT_{JE}$ was classified as CYP152L1, in the same family as the peroxygenases $P450_{SP\alpha}$ (CYP152B1), $P450_{BS\beta}$ (CYP152A1) and the *Clostridium acetobutylicum* CYP152A2 – a further fatty acid alpha hydroxylase (46). $OleT_{JE}$ is assigned as the first member of a new CYP152 subfamily (CYP152L1).

Crystal structure data are confirmatory of the typical P450 fold in $OleT_{JE}$, and also of a close evolutionary relationship with the other structurally resolved peroxygenases $P450_{SP\alpha}$ and $P450_{BS\beta}$. $OleT_{JE}$ does not undergo any major structural change on binding the C20:0 lipid arachidic acid, which near-completely occupies the entire P450 active site cavity. The $OleT_{JE}$ fatty acid binding mode is very similar to that seen in $P450_{SP\alpha}$ and $P450_{BS\beta}$. The major differences seen in $OleT_{JE}$ relate to the active site His85 residue (which is replaced by a glutamine residue in both the hydroxylases $P450_{SP\alpha}$ and $P450_{BS\beta}$) and the distortion of its heme cofactor (as compared to these hydroxylases). Despite extensive structural identity between $OleT_{JE}$, $P450_{SP\alpha}$ and $P450_{BS\beta}$ and the similarities in their specificity for long chain fatty acids, there is a major difference in reaction mechanism and product formation. $OleT_{JE}$ catalyzes mainly oxidative decarboxylation to form terminal alkenes from fatty acids, while $P450_{SP\alpha}$ and $P450_{BS\beta}$ favour hydroxylation at the alpha- and beta-carbons, respectively (16-18). The initial reaction with H_2O_2 in each of these P450s should form the reactive iron-oxo species compound 0 (the ferric hydroperoxo intermediate in the P450 catalytic cycle) using the peroxide “shunt” mechanism (7). However, a fundamental difference in the $OleT_{JE}$ reaction

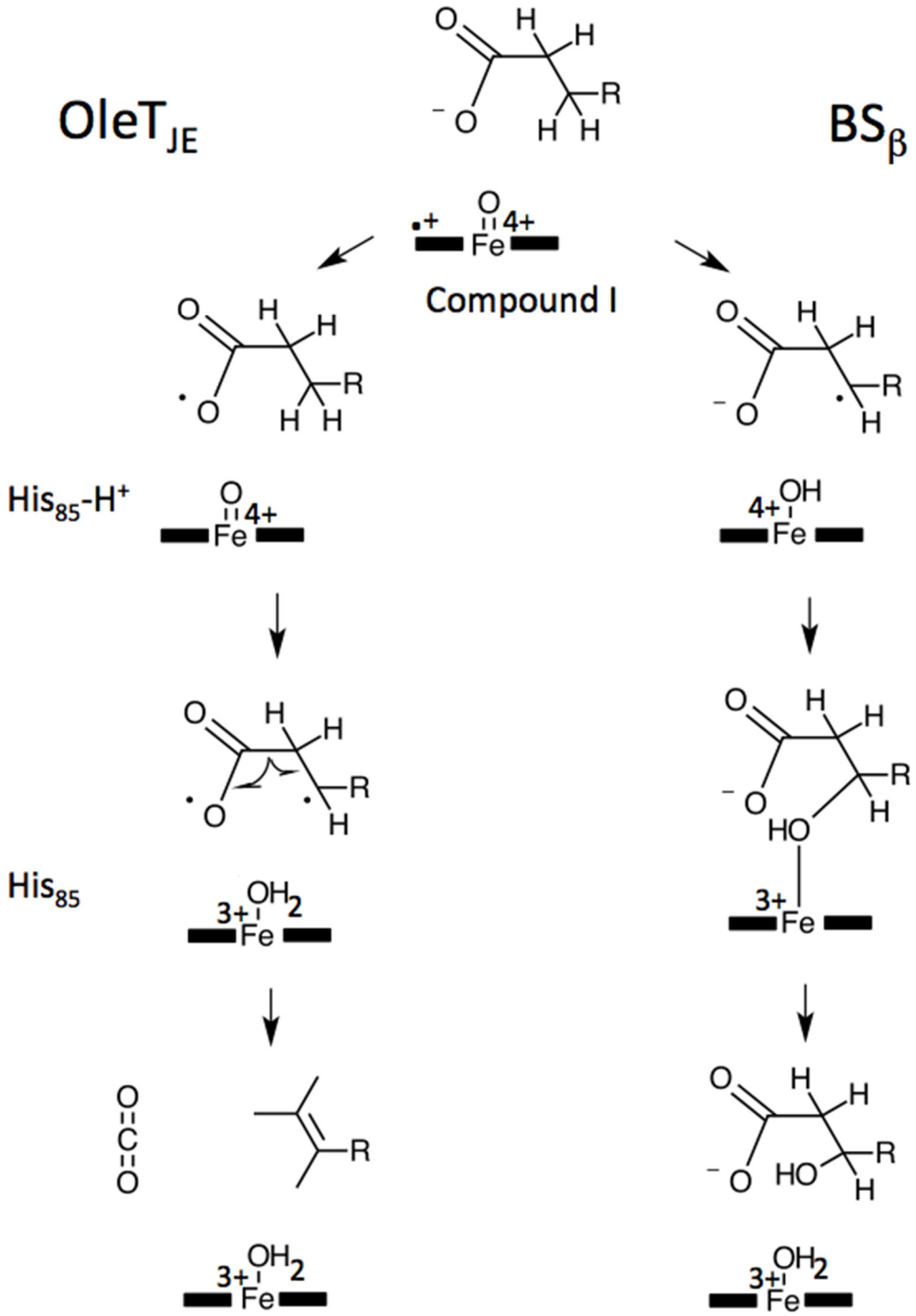

Figure 2.13. Proposed mechanism for OleT$_{JE}$. The cytochrome P450 OleT$_{JE}$ catalyzes oxidative decarboxylation of long chain fatty acids as its major reaction, while the highly related P450$_{BS\beta}$ produces predominantly *beta*-hydroxylated fatty acids from the same substrates (16,17). OleT$_{JE}$ His85 (replaced by Gln85 in P450$_{BS\beta}$) is proposed to act as a proton donor to the ferryl-oxo porphyrin radical cation (compound I) intermediate in this P450, concomitant with its reduction to compound II by an electron abstracted from the fatty acid carboxylate. Homolytic scission of the C-C$_\alpha$ bond, concomitant with hydrogen abstraction from C$_\alpha$ to compound II leads to production of the terminal alkene and CO_2. For the hydroxylase P450$_{BS\beta}$, this reaction cannot occur in absence of an appropriate proton donor to compound II, with the catalytic outcome instead being a typical P450 hydroxylation at the C$_\beta$ position.

mechanism leads to formation of the terminal alkene as the major product (rather than hydroxylated fatty acids).

To explain this phenomenon, we are drawn to the role of the active site histidine (His85) in $OleT_{JE}$. It has been postulated that the high pK_a of compound II in P450s generally ensures that compound I in these enzymes effectively abstracts a hydrogen atom from the substrate (as opposed to a single electron). However, in $OleT_{JE}$, His85 could function to donate a proton to compound I, concomitant with its reduction to compound II by abstraction of an electron from the fatty acid carboxylate moiety. The formation of the carboxylate radical would lead to homolytic scission of the substrate C-C_α bond, following hydrogen atom abstraction from the C_α position by compound II. In the hydroxylases, such a reaction is unlikely to occur in the absence of a proton donor to form protonated compound II, and these enzymes are thus likely to use compound I to abstract hydrogen from either the C_α or the C_β position, ultimately leading to mono-hydroxylation of substrate (Figure 2.13) (47).

In early studies of $OleT_{JE}$ we noted the propensity of the enzyme to aggregate and precipitate in typical (low salt) buffer conditions. However, we were able to turn this to our advantage through demonstrating that precipitation of $OleT_{JE}$ P450 (induced through dialysis into low salt buffer) could readily be resolubilized (in high salt buffer) in a form that retained thiolate-coordinated heme and ability to bind fatty acids. Moreover, $OleT_{JE}$ purified using this route (Method 1) had a higher proportion of LS ferric heme iron (likely due to displacement of lipid retained in its active site during isolation from *E. coli*) than did the enzyme isolated without the precipitation step (Method 2). $OleT_{JE}$ prepared using Method 1 was readily crystallized to produce the structural data shown in Figures 2.10-2.12 for substrate-free and arachidic acid-bound forms.

The binding of fatty acids displaces the axial water ligand from the heme iron of $OleT_{JE}$, leading to a shift of the ferric heme iron towards the HS state and to accompanying large changes in the heme absorption spectrum. This provides the basis for determination of fatty acid K_d values by optical titration. Many of the fatty acids tested for binding to $OleT_{JE}$ have very limited solubility in water. For this reason we investigated their suspension in detergent solutions, and

found that while there was no evidence for binding of Triton X-100 to $OleT_{JE}$, The K_d values for fatty acids suspended in 30% Triton X-100 were markedly improved over those suspended in alcohol alone for $OleT_{JE}$ prepared by Method 1. By comparison, the K_d values for Triton X-100-suspended lipids with $OleT_{JE}$ prepared by Method 2 were ~5-20 fold greater, possibly due to the P450 prepared without the precipitation step retaining contaminant short lipids that hinder the binding of the C12 to C20 fatty acids tested (Table 2.2). The robust nature of $OleT_{JE}$ and its stability to low salt precipitation and resolubilization in high salt is unusual in the P450 superfamily, but perhaps not surprising given the halotolerant nature of the *Jeotgalicoccus* bacterial genus. The cysteine thiolate ligand to the $OleT_{JE}$ heme iron is clearly retained following its resolubilization – as evidenced by retention of catalytic activity, and the production of a Fe(II)CO (P450) complex with Soret maximum at 449 nm (Figure 2.4.). $OleT_{JE}$'s stability to precipitation and resolubilization thus provides a convenient route to its purification, and also bodes well for its application in synthesis of terminal alkenes.

Stopped-flow kinetic analysis of $OleT_{JE}$ indicated that the extensively HS fatty acid-bound form is rapidly reconverted back to the LS ferric form on mixing with H_2O_2, with a 2nd order rate constant of 0.80 ± 0.02 μM^{-1} s^{-1} with respect to H_2O_2 concentration. Previous studies of $P450_{SP\alpha}$ reported a specific activity of 838 min^{-1} for the alpha-hydroxylation of myristic acid using 200 μM H_2O_2, while $P450_{BS\beta}$, catalyzed the alpha/beta-hydroxylation of myristic acid with a specific activity of 209 min^{-1} at 100 μM H_2O_2 (16,44,48). The $OleT_{JE}$ rate constants determined here are substantially faster than those for $P450_{SP\alpha}$ and $P450_{BS\beta}$, although report only on the catalytic steps of substrate decarboxylation, alkene displacement from the active site and restoration of the water ligand to the $OleT_{JE}$ heme iron. However, in turnover studies with different fatty acids, considerable amounts of alkene products were observed, consistent with efficient decarboxylase activity of $OleT_{JE}$. Another notable difference between these peroxygenases lies in their optical response to binding fatty acid substrates. For $P450_{SP\alpha}$, there is negligible heme iron spin-state and associated Soret absorption change on binding fatty acids, whereas with $P450_{BS\beta}$, some HS shift does occur, but to a much smaller extent than is observed for $OleT_{JE}$ with its best substrates (49). Since binding of H_2O_2 requires displacement of the 6th ligand water on the P450 heme iron, this process may be much more

efficient for $OleT_{JE}$ compared to $P450_{SP\alpha}$ and $P450_{BS\beta}$. While Rude *et al*. suggested the use of DTT as a peroxide generating agent to drive catalysis by $OleT_{JE}$, our data here indicate that DTT coordinates the ferric heme iron to inhibit the enzyme with a K_d of 159 μM, and thus is unlikely to be as effective as H_2O_2 in driving $OleT_{JE}$ activity (Figure 2.5C).

In its evolution towards peroxygenase activity, $OleT_{JE}$ has undergone mutations that reinforce its divergence from the typical class I and II P450 enzymes that interact with NAD(P)H-dependent redox partner enzymes and reductively activate oxygen bound to the heme iron to facilitate substrate oxidation (50). Most notably, it is evident that the acid-alcohol amino acid pair in the P450 I helix that is common to oxidase P450s (e.g. Asp251 and Thr252 in P450cam; or Glu267 and Thr268 in P450 BM3) is not conserved in $OleT_{JE}$, or in either $P450_{BS\beta}$ or $P450_{SP\alpha}$ (44,45,51,52). Since protonation reactions on heme iron-bound dioxygen do not feature in the catalytic cycle of the peroxygenases, this motif is dispensed with in these enzymes. Instead, the acid-alcohol pair is replaced in $OleT_{JE}$ by Arg245 (which binds the substrate carboxylate) and Pro246 in a highly conserved I-helix region of the CYP152 family enzymes (7). A conserved phenylalanine residue (Phe393 in P450 BM3; Phe350 in P450cam) in the P450 heme binding region is also absent from the bacterial peroxygenases. Phe393 interacts with the heme thiolate bond in CYP102A1 and was shown to be important in maximizing P450 catalytic efficiency through regulating heme iron potential, and thus heme iron reduction rate and ferrous-oxy complex stability in studies of various Phe393 variants (53,54). In $OleT_{JE}$ and the other bacterial peroxygenases, the absence of this extensively conserved phenylalanine and amino acid insertions into this “heme binding loop” consensus region indicate that heme thermodynamic properties are regulated differently (45). Our potentiometric data show that $OleT_{JE}$ has a very positive heme iron Fe(III)/Fe(II) redox potential (-103 mV versus NHE), which is not significantly altered in the HS form when bound to arachidic acid (-105 mV) (Figure 2.6). Thus, the absence of key residues in $OleT_{JE}$, BS_β and SP_α is a clear indicator of their distinct evolutionary pathway, such that protonation of iron-oxo intermediates, or substrate-dependent regulation of electron transfer from redox partners has been bypassed through direct use of H_2O_2.

In conclusion, we have determined novel structural and biochemical properties of an unusual P450 peroxygenase enzyme (CYP152L1, $OleT_{JE}$) that catalyzes oxidative decarboxylation of fatty acids to produce terminal alkenes. $OleT_{JE}$ is a catalytically efficient and structurally robust P450 with great potential in synthesis of a variety of alkenes as drop-in biofuels or chemical reagents. Ongoing research is directed at engineering altered fatty acid chain length selectivity into $OleT_{JE}$ in order to enable production of short chain, volatile alkenes.

2.6.0. References

1. Guengerich, F. P. (2005) *Human cytochrome P450 enzymes*. Pp. 377-530 in *Cytochrome P450: Structure, Mechanism and Biochemistry* (3rd edition). Ed. Ortiz de Montellano, P. R., Kluwer Academic/Plenum Press, New York

2. Cupp-Vickery, J. R., and Poulos, T. L. (1997) Structure of cytochrome P450eryF: substrate, inhibitors, and model compounds bound in the active site. *Steroids* **62**, 112-116

3. Pylypenko, O., Vitali, F., Zerbe, K., Robinson, J. A., and Schlichting, I. (2003) Crystal structure of OxyC, a cytochrome P450 implicated in an oxidative C-C coupling reaction during vancomycin biosynthesis. *J. Biol. Chem*. **278**, 46727-46733

4. Ghosh, D., Griswold, J., Erman, M., and Pangborn, W. (2009) Structural basis for androgen specificity and oestrogen synthesis in human aromatase. *Nature* **457**, 219-223

5. Munro, A. W., Girvan, H. M., and McLean, K. J. (2007) Variations on a (t)heme – novel mechanisms, redox partners and catalytic functions in the cytochrome P450 superfamily. *Nat. Prod. Rep*. **24**, 585-609

6. Munro, A. W., Girvan, H. M., and McLean, K. J. (2007) Cytochrome P450-redox partner fusion enzymes. *Biochim. Biophys. Acta* **1770**, 345-349

7. Denisov, I. G., Makris, T. M., Sligar, S. G., and Schlichting, I. (2005) Structure and chemistry of cytochrome P450. *Chem. Rev.* **105**, 2253-2277

8. Rittle, J., and Green, M. T. (2010) Cytochrome P450 compound I: capture, characterization, and C-H bond activation kinetics. *Science* **330**, 933-937

9. Guengerich, F. P. and Munro, A. W. (2013) Unusual cytochrome enzymes and reactions. *J. Biol. Chem*. **288**, 17065-17073.

10. Isin, E. M. and Guengerich, F. P. (2007) Complex reactions catalyzed by cytochrome P450 enzymes. *Biochim. Biophys. Acta* **1770**, 314-329

11. Porter, T. D. (1991) An unusual yet strongly conserved flavoprotein reductase in bacteria and mammals. *Trends Biochem. Sci*. **16**, 154-158

12. Ortiz de Montellano, P. R. (1995) *Oxygen activation and reactivity*. Pp. 245-303 in *Cytochrome P450: Structure, Mechanism, and Biochemistry* (2nd edition). Ed. Ortiz de Montellano, P. R., Plenum Press, New York.

13. Warman, A. J., Robinson, J. W., Luciakova, D., Lawrence, A. D., Marshall, K. R., Warren, M. J., Cheesman, M. R., Rigby, S.E., Munro, A. W., and McLean, K. J. (2012) Characterization of *Cupriavidus metallidurans* CYP116B1 – a thiocarbamate herbicide oxygenating P450-phthalate dioxygenase reductase fusion protein. *FEBS J*. **279**, 1675-1693

14. Hecker, M., and Ullrich, V. (1989) On the mechanism of prostacyclin and thromboxane A2 biosynthesis. *J. Biol. Chem*. **264**, 141-150

15. Song, W. C. and Brash, A. R. (1991) Purification of an allene oxide synthase and identification of the enzyme as a cytochrome P-450. *Science* **233**, 781-784

16. Lee, D.-S., Yamada, A., Sugimoto, H., Matsunaga, I., Ogura, H., Ichihara, K., Adachi, S.-I., Park, S.-Y., and Shiro, Y. (2003) Substrate recognition and molecular mechanism of fatty acid hydroxylation by cytochrome P450 from *Bacillus subtilis*. *J. Biol. Chem*. **278**, 9761-9767

17. Fujishiro, T., Shoji, O., Nagano, S., Sugimoto, H., Shiro, Y., and Watanabe, Y. (2011) Crystal structure of H_2O_2-dependent cytochrome P450$_{SP\alpha}$ with its bound fatty acid substrate. Insight into the regioselective hydroxylation of fatty acids at the α position. *J. Biol. Chem*. **286**, 29941-29950

18. Rude, M. A., Baron, T. S., Brubaker, S., Alibhai, M., Del Cadayre, S. B., and Schirmer, A. (2011) Terminal olefin (1-alkene) biosynthesis by a novel P450 fatty acid decarboxylase from *Jeotgalicoccus* species. *Appl. Environ. Microbiol*. **77**, 1718-1727

19. McLean, K. J., Carroll, P., Lewis, D. G., Dunford, A. J., Seward, H. E., Neeli, R., Cheesman, M. R., Marsollier, L., Douglas, P., Smith, W. E., Rosenkrands, I., Cole, S. T., Leys, D., Parish, T. and Munro. A. W. (2008) Characterization of active site structure in CYP121. A cytochrome P450 essential for viability of *Mycobacterium tuberculosis* H37Rv. *J. Biol. Chem*. **283**, 33406-16

20. Morrison, J. F. (1969) Kinetics of the reversible inhibition of enzyme-catalysed reactions by tight-binding inhibitors. *Biochim. Biophys. Acta* **185**, 269-286

21. Dutton, P. L. (1978) Redox potentiometry: determination of midpoint potentials of oxidation-reduction components of biological electron-transfer systems. *Methods Enzymol*. **54**, 411-435

22. Daff, S. N., Chapman, S. K., Turner, K. L., Holt, R. A., Govindaraj, S., Poulos, T. L., and Munro, A. W. (1997) Redox control of the catalytic cycle of flavocytochrome P450 BM3. *Biochemistry* **36**, 13816-13823

23. Bui, S. H., McLean, K. J., Cheesman, M. R., Bradley, J. M., Rigby, S. E., Levy, C. W., Leys, D., and Munro, A. W. (2012) Unusual spectroscopic and ligand binding properties of the cytochrome P450-favodoxin fusion enzyme XplA. *J. Biol. Chem*. **287**, 19699-19714

24. Kabsch, W. J. (1993) Automatic processing of rotation diffraction data from crystals of initially unknown symmetry and cell constants. *J. Appl. Crystallogr*. **26**, 795-800.

25. Collaborative Computation Project No. 4. (1994) *Acta Crystallogr. D Biol. Crystallogr*. **50**, 760-763.

26. Emsley, P., and Cowtan, K. (2004) Coot: model-building tools for molecular graphics. *Acta Crystallogr. D Biol. Crystallogr*. **60**, 2126-2132.

27. Girvan, H. M., Marshall, K. R., Lawson, R. J., Leys, D., Joyce, M. G., Clarkson, J., Smith, W. E., Cheesman, M. R., and Munro, A. W. (2004) Flavocytochrome P450 BM3 undergoes

substrate-dependent formation of a novel heme iron ligand set. *J. Biol. Chem*. **279**, 23274-23286.

28. McLean, K. J., Cheesman, M. R., Rivers, S. L., Richmond, A., Leys, D., Chapman, S. K., Reid, G. A., Price, N. C., Kelly, S. M., Clarkson. J., Smith, W. E., and Munro, A. W. (2002) Expression, purification and spectroscopic characterization of the cytochrome P450 CYP121 from *Mycobacterium tuberculosis*. *J. Inorg. Biochem*. **91**, 527-541.

29. Tyson, C. A., Lipscomb, J. D., and Gunsalus, I. C. (1972) The roles of putidaredoxin and P450cam in methylene hydroxylation. *J. Biol. Chem*. **247**, 5777-5784.

30. Quaroni, L. G., Seward, H. E., McLean, K. J., Girvan, H. M., Ost, T. W. B., Noble, M. A., Kelly, S. M., Price, N. C., Cheesman, M. R., Smith, W. E., and Munro, A. W. (2004) Interaction of nitric oxide with cytochrome P450 BM3. *Biochemistry* **43**, 16416-16431.

31. Berry, E. A., and Trumpower, B. L. (1987) Simultaneous determination of hemes *a*, *b* and *c* from pyridine hemochrome spectra. *Anal. Biochem.* **161**, 1-15.

32. Omura, T., and Sato, R. (1964) The carbon monoxide-binding pigment of liver microsomes. II. Solubilization, purification, and properties. *J. Biol. Chem.* **239**, 2379-2385.

33. Sligar, S. G., and Gunsalus, I. C. (1976) A thermodynamic model of regulation: modulation of redox equilibria in camphor monoxygenase. *Proc. Natl. Acad. Sci. U. S. A*. **73**, 1078-1082.

34. Miles, J. S., Munro, A. W., Rospendowski, B. N., Smith, W. E., McKnight, J., and Thomson, A. J. (1992) Domains of the catalytically self-sufficient cytochrome P-450 BM-3. Genetic construction, overexpression, purification and spectroscopic characterization. *Biochem. J*. **288**, 503-509.

35. Netto, L. E., and Stadtman, E. R. (1996) The iron-catalyzed oxidation of dithiothreitol is a biphasic process:hydrogen peroxide is involved in the initiation of a free radical chain of reactions. *Arch. Biochem. Biophys*. **333**, 233-242.

36. Sono, M., Andersson, L. A., and Dawson, J. H. (1982) Sulfur donor ligand binding to ferric cytochrome P450-CAM and myoglobin. Ultraviolet-visible absorption, magnetic circular

dichroism, and electron paramagnetic resonance spectroscopic investigation of the complexes. *J. Biol. Chem.* **257**, 8308-8320.

37. Ullrich, V., Nastainczyk, W., and Ruf, H. H. (1975) Ligand reactions of cytochrome P-450. *Biochem. Soc. Trans*. **3**, 803-807.

38. Harford-Cross, C. F., Carmichael, A. B., Allan, F. K., England, P. A., Rouch, D. A., and Wong, L.-L. (2000) Protein engineering of cytochrome $P450_{cam}$ (CYP101) for the oxidation of polycyclic aromatic hydrocarbons. *Protein Eng*. **13**, 121-128.

39. McLean, K. J., Warman, A. J., Seward, H. E., Marshall, K. R., Girvan, H. M., Cheesman, M. R., Waterman, M. R., and Munro, A. W. (2006) Biophysical characterization of the sterol demethylase P450 from *Mycobacterium tuberculosis*, its cognate ferredoxin, and their interactions. *Biochemistry* **45**, 8427-8443.

40. Driscoll, M. D., McLean, K. J., Levy, C., Mast, N., Pikuleva, I. A., Lafite, P., Rigby, S. E., Leys, D., and Munro, A.W. (2010) Structural and biochemical characterization of *Mycobacterium tuberculosis* CYP142: evidence for multiple cholesterol 27-hydroxylase activities in a human pathogen. *J. Biol. Chem*. **285**, 38270-38282.

41. Dawson, J. H., Anderson, L. A., and Sono, M. (1982) Spectroscopic investigations of ferric cytochrome P-450-CAM ligand complexes. Identification of the ligand trans to the cysteinate in the native enzyme. *J. Biol. Chem*. **257**, 3606-3617.

42. Lipscomb, J. D. (1980) Electron paramagnetic resonance detectable states of cytochrome P450CAM. *Biochemistry* **19**, 3590-3599.

43. Hollenberg, P. F., Hager, L. P., Blumberg, W. E., and Peisach, J. (1980) An electron-paramagnetic resonance study of the high and low-spin forms of chloroperoxidase. *J. Biol. Chem*. **255**, 4801-4807.

44. Matsunaga, I., Yokotani, N., Gotoh, O., Kusunonse, E., Yamada, M., and Ichihara, K. 1997) Molecular cloning and expression of fatty acid alpha-hydroxylase from *Sphingomonas paucimobilis*. *J. Biol. Chem*. **272**, 23592-23596.

45. Matsunaga, I., Ueda, A., Fujiwara, N., Sumimoto, T., and Ichihara, K. (1999) Characterization of the ybdT gene product of *Bacillus subtilis*: Novel fatty acid β-hydroxylating cytochrome P450. *Lipids* **34**, 841-846.

46. Girhard, M., Schuster, S., Dietrich, M., Dürre, P., and Urlacher, V. B. (2007) Cytochrome P450 monooxygenase from *Clostridium acetobutylicum*: a new alpha-fatty acid hydroxylase. *Biochem. Biophys. Res. Commun.* **362**, 114-119.

47. Krest, C. M., Onderko, E. L., Yosca, T. H., Calixto, J. C., Karp, R. F., Livada, J., Rittle, J., and Green, M. T. (2013) Reactive intermediates in cytochrome P450 catalysis. *J. Biol. Chem*. **288**, 17074-17081.

48. Matsunaga, I., Ueda, A., Sumimoto, T., Ichihara, K., Ayata, M., and Ogura, H. (2001) Site-directed mutagenesis of the putative distal helix of peroxygenase cytochrome P450. *Arch. Biochem. Biophys*. **394**, 45-53.

49. Matsunaga, I., Yamada, A., Lee, D.-S., Obayashi. E., Fujiwara, N., Kobayashi, K., Ogura, H., and Shiro, Y. (2002) Enzymatic reaction of hydrogen peroxide-dependent peroxygenase cytochrome P450s: Kinetic deuterium isotope effects and analyses by resonance Raman spectroscopy. *Biochemistry* **41**, 1886-1892.

50. Munro, A. W., Girvan, H. M., Mason, A. E., Dunford, A. J., and McLean, K. J. (2013) What makes a P450 tick? *Trends Biochem. Sci*. **38**, 140-150.

51.Yeom, H., Sligar, S. G., Li, H., Poulos, T. L., and Fulco, A. J. (1995) The role of Thr268 in oxygen activation of cytochrome P450BM-3. *Biochemistry* **34**, 14733-14730.

521. Raag, R., Martinis, S. A., Sligar, S. G., and Poulos, T. L. (1991) Crystal structure of the cytochrome P-450CAM active site mutant Thr252Ala. *Biochemistry* **30**, 11420-11429.

53. Ost, T. W., Clark, J., Mowat, C. G., Miles, C. S., Walkinshaw, M. D., Reid, G. A., Chapman, S. K., and Daff, S. (2003) Oxygen activation and electron transfer in flavocytochrome P450 BM3. *J. Am. Chem. Soc*. **125**, 15010-15020.

54. Ost, T. W., Miles, C. S., Munro, A. W., Murdoch, J., Reid, G. A., and Chapman, S. K. (2001) Phenylalanine exerts thermodynamic control over the heme of flavocytochrome P450 BM3. *Biochemistry* **40**, 13421-13429.

Chapter 3

Interrogation of the fatty acid carboxylate-binding site in the alkene producing cytochrome P450 peroxygenase $OleT_{JE}$

[1]Sarah Matthews, [1]James D. Belcher, [1]Kang Lan Tee, [1]Hazel M. Girvan, [1]Kirsty J. McLean, [1]Stephen E.J. Rigby, [1]Colin W. Levy, [1]David Leys, [2]David A. Parker, [3]Richard T. Blankley and [1]Andrew W. Munro*

[1]Manchester Institute of Biotechnology, School of Chemistry, University of Manchester, 131 Princess Street, Manchester M1 7DN, UK. [2]The Westhollow Technology Center, Houston, Texas 77028-3101, USA. [3]Agilent Technologies UK Ltd., Lakeside, Cheadle Royal Business Park, Stockport, Cheshire SK8 3GR, United Kingdom.[3]Agilent Technologies UK Ltd., 5500 Lakeside, Cheadle SK8 3GR, UK.

Keywords: $OleT_{JE}$, cytochrome P450, CYP152L1, oxidative decarboxylation, substrate binding, alkenes, enzyme mechanism, biofuels

3.1. Abstract

The *Jeotgalicoccus* sp. ATCC 8456 peroxygenase cytochrome P450 $OleT_{JE}$ (CYP152L1) is a hydrogen peroxide-driven oxidase that catalyzes oxidative decarboxylation of fatty acid substrates to generate terminal alkenes with applications in fine chemical and biofuel production. $OleT_{JE}$ active site residues Phe79, His85 and Arg245 were mutated to interrogate their roles in substrate binding and catalytic activity. His85 is a potential proton donor to reactive iron-oxo species during $OleT_{JE}$-dependent substrate decarboxylation. The H85Q mutant substitutes a glutamine that is found in several peroxygenases that favour fatty acid hydroxylation. H85Q $OleT_{JE}$ favours alkene production, pointing to alternative protonation mechanisms. However, the mutant undergoes only minor substrate binding-induced heme iron spin-state shift towards high-spin by comparison with WT $OleT_{JE}$, indicating an important role for His85 in this process. Phe79 interacts with His85 and F79A/W/Y mutants show diminished affinity for shorter chain (C10-C16) fatty acids, as well as weak high-spin conversion in titrations. The F79A variant is least affected in substrate oxidation, but the F79W/Y mutants show lower stability and evidence of cysteine thiolate protonation on reduction. Arg245 is crucial for binding the substrate carboxylate, and R245E/L mutants severely compromise activity and heme content, although alkene products are formed from some substrates, most notably from stearic acid (C18:0). EPR spectroscopy demonstrates multiple and distinctive heme coordination environments in the wild-type and mutant $OleT_{JE}$. The results identify crucial roles for the active site amino acid trio in determining $OleT_{JE}$ catalytic efficiency in alkene production, in addition to their regulating protein stability, heme iron coordination and spin-state.

3.2. Introduction

The cytochromes P450 (P450s or CYPs) are a superfamily of heme *b*-containing monooxygenase enzymes widespread in nature and spanning all three domains of life: archaea, bacteria and eukaryota (1). Most P450s catalyze reductive scission of dioxygen bound to their heme iron, relying on the delivery of two electrons acquired from pyridine nucleotide coenzymes (NADPH or NADH). In the canonical P450 catalytic cycle, two electrons

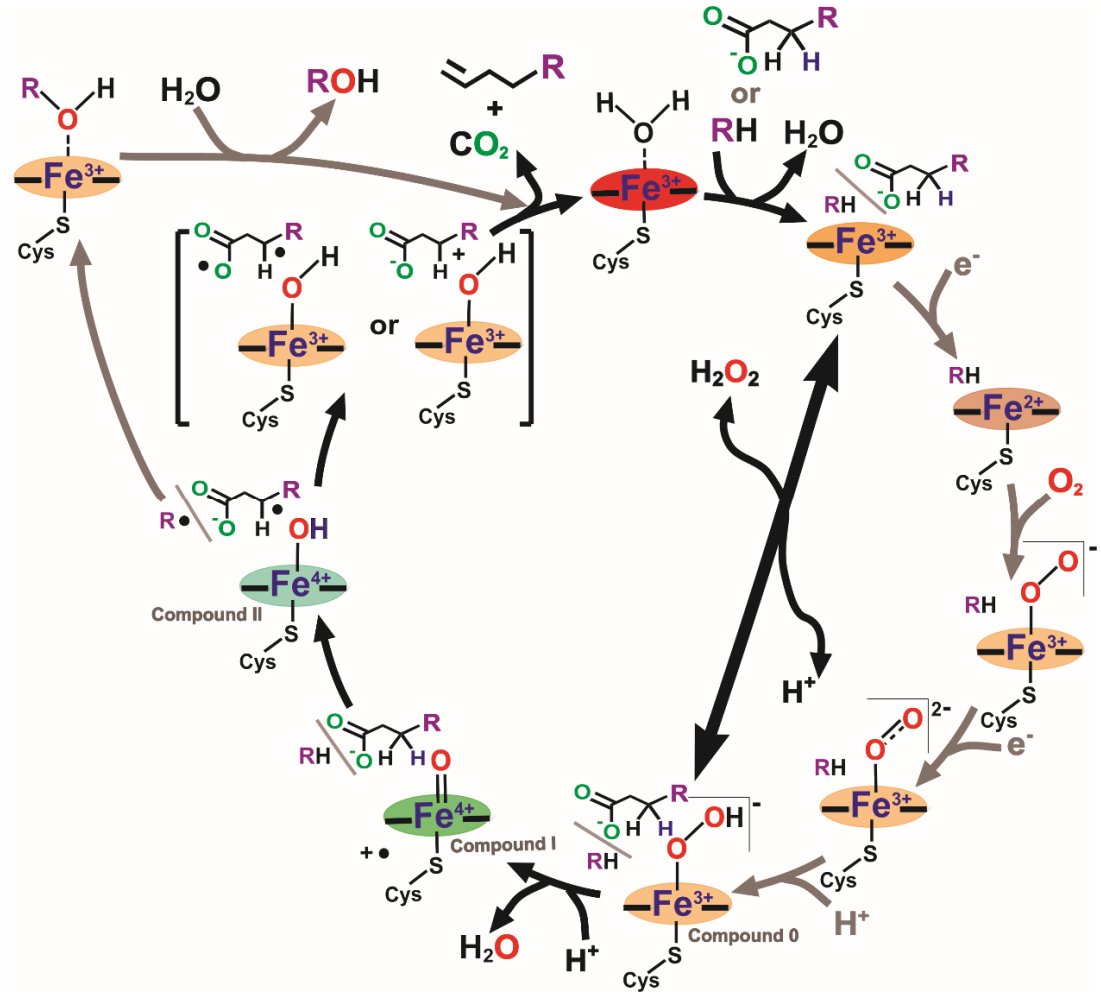

Figure 3.1. The OleT$_{JE}$ catalytic cycle. OleT$_{JE}$ catalyzes the oxidative decarboxylation of fatty acids (major reaction), and can also hydroxylate fatty acids at the α- and β-positions (minor reaction). The canonical P450 catalytic cycle is shown in circular representation, initiating with the binding of fatty acid substrate (shown as RH, and also as a chemical structure) that converts the LS OleT$_{JE}$ P450 to a HS form. Shown in grey arrows from this point onwards are reduction (x2) and protonation (x1) steps that follow the canonical path and require one or more redox partners. The thick black arrow traversing the cycle illustrates the "peroxide shunt" pathway by which ferric, fatty acid-bound OleT$_{JE}$ can be converted directly to the transient ferric-hydroperoxo (compound 0) form using H_2O_2. At this point, the canonical and peroxide shunt pathways converge with a protonation step that results in dehydration of a transient intermediate to form the ferryl-oxo compound I. Compound I deprotonates the substrate, producing a substrate radical and the ferryl-hydroxo compound II. At this stage, the catalytic pathways for substrate hydroxylation and decarboxylation diverge. Hydroxylated fatty acids are formed by the "radical rebound" mechanism (5), as shown in the outer loop to the left of the main cycle (grey arrows). However, recent studies have indicated that that fatty acid decarboxylation to form terminal alkenes likely involves an unusually stable compound II, and that reduction of compound II (or another oxidant) by the substrate radical could form a substrate diradical or carbocation species that decomposes with CO_2 release to form the terminal alkene product (15,39). The P450 heme (illustrated by the iron in the relevant oxidation state and equatorial/axial bonds) is shaded to approximate the colour of the relevant heme intermediate species.

are donated at discrete points in the cycle via a redox partner protein (2). The first electron is delivered to the substrate-bound, cysteine thiolate-coordinated ferric heme iron, reducing it to the ferrous form, allowing dioxygen to bind. The second electron reduces the ferric-superoxo

complex to form the ferric-peroxo state. As shown in **Figure 3.1**, two successive protonations of iron-oxo species then occur. Protons are typically relayed from a conserved acid-alcohol amino acid pair (e.g. Asp251/Thr252 in the camphor hydroxylase P450cam, CYP101A1) to form first the ferric-hydroperoxo species (compound 0) and then the highly reactive ferryl-oxo radical cation species compound I (with loss of a water molecule) (3,4). The P450 compound I abstracts a hydrogen from the substrate to form the ferryl-hydroxo (compound II) form, prior to oxidizing the substrate to complete the catalytic process (5).

While most P450s operate in this way, several are also known to catalyze substrate oxidation using the "peroxide shunt" mechanism, in which hydrogen peroxide (H_2O_2) or an organic hydroperoxide (e.g. *meta*-chloroperoxybenzoic acid, m-CPBA) convert a substrate-bound resting state of the P450 directly to compound 0, as shown in **Figure 3.1** (4,6). As in the canonical cycle, a further protonation of compound 0 then leads to formation of compound I and to oxidative catalysis. In many P450s, this reaction is inefficient, and oxidative damage to the protein and/or heme occurs alongside any productive turnover (7). However, there are examples of P450s that have evolved to use the peroxide shunt efficiently for substrate oxidation. The best characterized of these P450s are in the CYP152 family of P450 peroxygenases. These enzymes may have evolved in ancient prokaryotes at a time when the environment was devoid of oxygen, but relatively rich in hydrogen peroxide and peroxygenated organic compounds. While peroxygenase activity is likely to have evolved in archaea, it has been conserved in P450s from bacteria and eukaryotes, including humans (8).

Among the best characterized of the CYP152 family peroxygenases is the industrially relevant $OleT_{JE}$ (CYP52L1) that was first isolated from *Jeotgalicoccus* sp. ATCC 8456 in 2011 by Schirmer and coworkers (9). $OleT_{JE}$ acts primarily as a H_2O_2-dependent fatty acid decarboxylase to form terminal alkenes, but also hydroxylates a proportion these substrates to generate a α- and β-hydroxylated fatty acids. Lipid substrates with chain lengths ~C12-C20 were shown to be good substrates (9,10). Later studies showed that the P450cam redox partner system (NADH-putidaredoxin reductase [PdR] and putidaredoxin [Pdx], along with a NADH recycling system) could also be used effectively with $OleT_{JE}$ to decarboxylate alkanoic acids as short as C4 (11). $OleT_{JE}$ was also shown to function as a typical P450

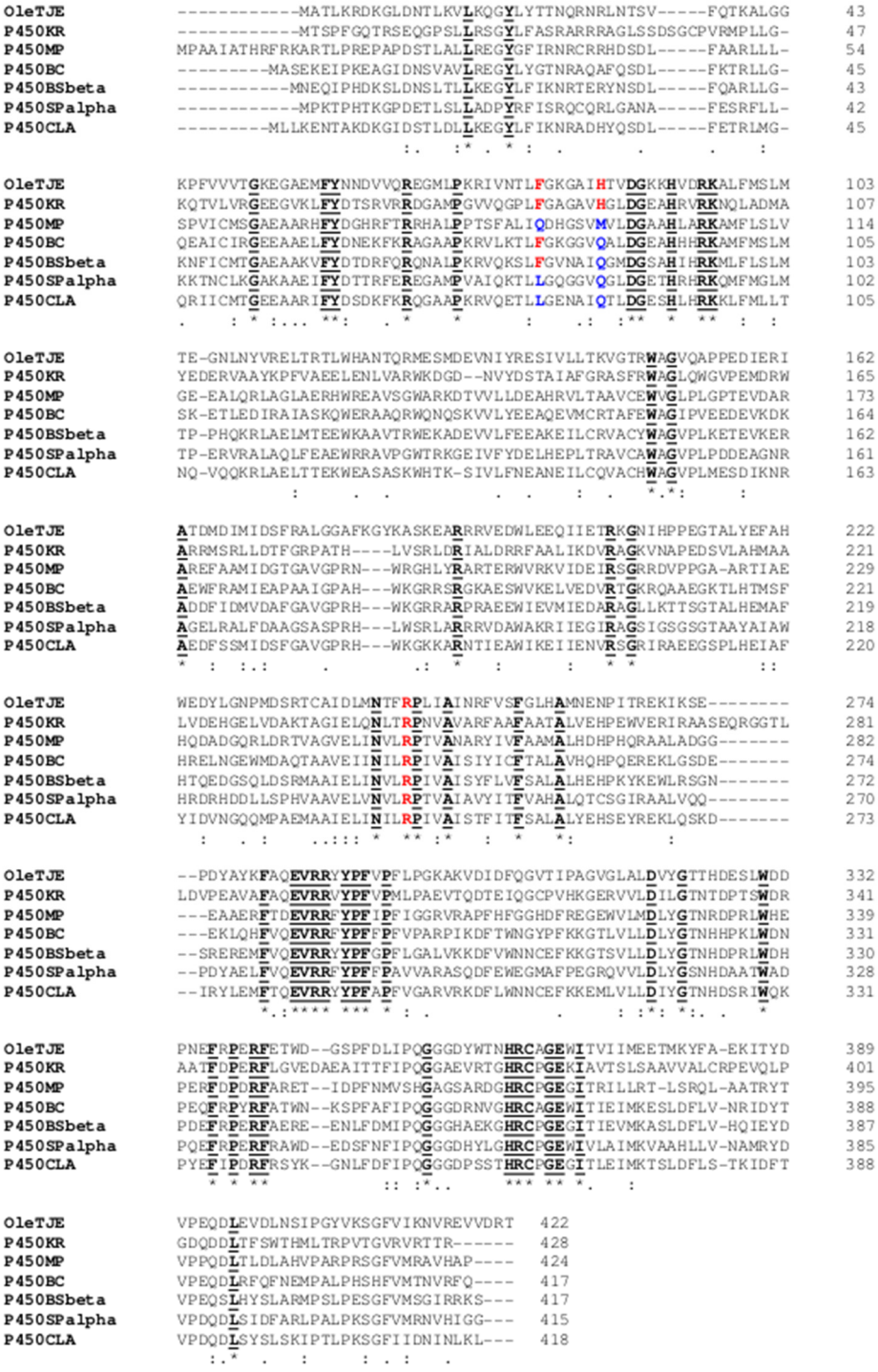

Figure 3.2. Alignment of OleT$_{JE}$ with other bacterial peroxygenase P450s. OleT$_{JE}$ (CYP152L1) is aligned with the peroxygenases P450 KR from *Kocuria rhizophila*, CYP-MP (P450MP) from *Methylobacterium populi* (30), a peroxygenase from *Bacillus clausii* (P450BC) (9), *Bacillus subtilis* P450 BS$_{\beta}$ (CYP152A1) (27), *Sphingomonas paucimobilis* P450 SP$_{\alpha}$ (CYP152B1) (28) and *Clostridium acetobutylicum* P450 CLA (CYP152A2) (33). The OleT$_{JE}$ active site residues Phe79, His85 and Arg245 are in bold, red font. Non-conserved residues at these positions are shown in bold, blue font. Arg245 and the adjacent Pro246 are conserved in all the peroxygenases. Other completely conserved residues are indicated in bold, underlined black font.

monooxygenase when fused to the phthalate dioxygenase reductase (PDOR)-like domain of CYP116B2 (RhFRED) from *Rhodococcus* sp. NCIMB9784 (12), or by utilizing the flavodoxin/flavodoxin reductase system of *E. coli in vivo* (12,13). $OleT_{JE}$ is also active when used in conjunction with a light-driven, *in situ* H_2O_2-generating system (14).

Transient formation of P450 compound I in $OleT_{JE}$ was reported by Makris *et al*. on addition of H_2O_2 to $OleT_{JE}$ in complex with perdeuterated arachidic acid, and identified by the appearance of a characteristic 370 nm Soret maximum and an additional absorption band at 690 nm (15). These spectral data are similar to those reported by Green and co-workers in studies with *Sulfolobus acidocaldarius* CYP119A1 (4). The transient capture of compound I in the perdeuterated substrate-bound form of $OleT_{JE}$ likely results from a ^{2}H-kinetic isotope effect on compound I decay. Compound I formation is considered to initiate fatty acid decarboxylation by abstracting a substrate hydrogen atom (15).

As an alkene-producing enzyme, $OleT_{JE}$ has attracted interest for industrial applications, including in the production of biofuels and petrochemicals (16). *In vivo* production of alkenes has been reported in *E. coli* strains transformed with $OleT_{JE}$ (12). Yan *et al*. also reported systems in which the tandem activities of a lipase and $OleT_{JE}$ were used to produce 1-alkenes from low-cost triacylglycerol feedstocks (17).

Other prominent members of the P450 peroxygenase family include P450 BS_β from *Bacillus subtilis* (CYP152A1, 41% sequence identity to $OleT_{JE}$) and P450 SP_α from *Sphingomonas paucimobilis* (CYP152B1, 37% sequence identity to $OleT_{JE}$) (10). Both enzymes are primarily fatty acid hydroxylases, with P450 SP_α hydroxylating 100% at the C_α position, and P450 BS_β initially reported to hydroxylate at ~43% in the C_α position and ~57% in the C_β position (18). However, studies by Rude *et al*. indicated that P450 BS_β could produce 1-pentadecene at ~15% of total product alongside α- and β-hydroxylated palmitic acid products (7). Crystal structure data show that the active sites of $OleT_{JE}$ and P450 BS_β are very similar, with the carboxylate group of fatty acid substrates being coordinated by a conserved arginine residue (Arg245 in $OleT_{JE}$, Arg242 in P450 BS_β and Arg241 in P450 SP_α) (10,18). An R242A mutant

of P450 BS_β abolished fatty acid hydroxylase activity, while an R242K mutation substantially reduced substrate hydroxylation (19).

A key difference in the active sites of $OleT_{JE}$ and P450 BS_β is at position 85 (His85 in $OleT_{JE}$ and Gln85 in P450 BS_β) (10). In $OleT_{JE}$, the His85 imidazole side chain points into the active site towards the heme iron. This orientation sandwiches the imidazole sidechain between the heme and Phe79. It was postulated that the difference in the nature of the residue at position 85 may underlie the strong decarboxylase activity of $OleT_{JE}$. His85 could act as a proton donor to the compound I intermediate, together with its reduction to compound II with an electron from the fatty acid substrate carboxylate group. Homolytic scission of the C-C_α bond of the fatty acid, concomitant with abstraction of a hydrogen from C_α to form compound II, could then produce the terminal alkene and CO_2 products (10). Rude et al. investigated the role of the residue at position 85 in P450 BS_β by creating the mutant P450 BS_β Q85H. During *in vitro* turnover experiments with hexadecanoic acid, the P450 BS_β Q85H mutation resulted in decreased α-hydroxy-hexadecanoic acid formation, and in increased 1-pentadecene and β-hydroxy hexadecanoic acid formation. Despite this, the ratio of decarboxylation to hydroxylation only increased from 0.19 in WT P450 BS_β to 0.30 in the P450 BS_β Q85H mutant, compared with a ratio of 3.32 in $OleT_{JE}$ (9).

Through its interactions with His85 in $OleT_{JE}$, Phe79 is also likely to be important for catalytic activity in $OleT_{JE}$. A phenylalanine (Phe79) is retained at this position in P450 BS_β. However, the exclusive fatty acid α-hydroxylase P450 SP_α has a leucine at the corresponding position (Leu79). In P450 BS_β, the F79L mutation resulted in increased α-hydroxylation, with levels of β-hydroxylation falling from 58% to 17% of the overall product (20).

In this study, we explore further the structure and mechanism of $OleT_{JE}$ by mutating the key active site residues His85, Phe79 and Arg245, and by analyzing their effects on the catalytic properties of this biotechnologically important alkene-producing enzyme. The H85Q mutant was characterized to establish whether this residue is crucial to $OleT_{JE}$'s decarboxylase activity, and also since its replacement by Glu85 in P450 BS_β results mainly in fatty acid hydroxylation (**Figure 3.2**). The importance of Phe79 in its interactions with His85, and in

regulating active site structure and catalytic activity were explored by characterization of F79A, F79W and F79Y variants. Finally, the fatty acid carboxylate coordinating Arg245 was mutated to neutral (R245L) and charge reversal (R245E) variants to assess influence on activity and regioselectivity of substrate oxidation. Mutants were characterized by a combination of kinetic, spectroscopic, structural and analytical methods to provide new insights into $OleT_{JE}$ structure/function.

3.3. Experimental Procedures

3.3.1. Expression and purification of $OleT_{JE}$ and $OleT_{JE}$ mutants

The gene encoding $OleT_{JE}$ from *Jeotgalicoccus* sp. ATCC 8456 was codon-optimized for expression in *E. coli*, and cloned into a modified pET15b (GenScript, Cherwell UK), incorporating a TEV cleavage site with an N-terminal polyhistidine tag. Rationally designed mutants (H85Q, F79A, F79W, F79Y, R245L and R245E) were created by site-directed mutagenesis, using a QuikChange Lightning Kit (Agilent Technologies LDA UK Ltd, Cheadle UK). Oligonucleotide primers used were: H85Q Forward (F): 5'-ttttaccatcaaccgtctg gattgcgcctttaccaaac-3', H85Q Reverse (R): 5'-gtttggtaaaggcgcaatccagacggttgatggtaaaa-3'; F79AF: 5'-gtatggattgcgcctttaccagccagggtattcacaatacgttt-3', F79AR: 5'-aaacgtattgtgaataccctggctggtaaaggcg caatccatac-3'; F79WF: 5'-attgcgcctttaccc cacagggtattcacaatacgtttcggc-3', F79WR: 5'-gccgaaacgtattgtgaataccctgtggggtaaaggcgcatt-3'; F79YF: 5' tgcgcctttaccatacagggtattcacaatacgtttcg-3', F79YR: 5'-cgaaacgtattgtgaataccctgtatggtaa aggcgca-3'; R245LF: 5'-gatgaacacgttcctg ccgctgattgcgatc-3', R245LR: 5'-gatcgcaatcagcggcaggaacgtgttcatc-3'; R245EF: 5'-ttgatctgatgaacacgttcgagccgctgattgcgatcaatcg-3', R245ER: 5'-cgattgatcgcaatcagcggctcgaacgtgttcatcagatcaa-3'. *E. coli* strain C41 (DE3) (Lucigen, Middleton UK) was used as the expression host for WT $OleT_{JE}$ and all mutants. Cells transformed with the plasmids were grown at 37°C with shaking at 200 rpm in total volumes of 500 ml 2YT broth containing 50 μg/ml ampicillin. Expression of WT/mutant $OleT_{JE}$ genes was induced with 100 μM isopropyl 1-thio-ß-D-galactopyranoside (IPTG) when an OD_{600} of

0.5 was reached. At point of induction, 500 μM δ-aminolevulinic acid (ΔALA) was added to all mutants, and 4 μg/ml hemin was also added to the R245L and R245E expression cultures in order to aid heme incorporation. At this point, the incubation temperature was lowered to 25°C, and the cells were grown for a further 16 hours. Cells were harvested by centrifugation at 6000 rpm, at 4°C using a JLA-8.1000 rotor in an Avanti J-26 XP centrifuge. Cells were resuspended in 100 mM potassium phosphate (pH 8.0), combined and centrifuged as before. The cell pellet was then frozen at -80°C until required for purification.

Cells were thawed and resuspended in 200 g/l extraction buffer (100 mM potassium phosphate, 1 M NaCl, 10% glycerol, pH 8.0) along with SigmaFAST Protease Inhibitor Cocktail Tablets, EDTA-Free (Sigma-Aldrich, Poole UK) using 1 tablet per 100 ml, and 100 μg/ml DNase I (bovine pancreas, Sigma-Aldrich). Cells were lysed using a cell disruptor (Constant Cell Disruption Systems, Daventry UK) at a pressure of 15,000 psi. The homogenate was then centrifuged at 20,000 rpm at 4°C for 90 minutes using a JA-25.50 rotor (Beckman-Coulter Ltd., High Wycombe UK). The supernatant was removed, and incubated overnight at 4°C with (10 ml per 100 g cell pellet) nickel-iminodiacetic acid (Ni-IDA) chromatographic medium (Generon, Maidenhead UK). The mixture was then transferred to a column, and the resin bed washed with 20 column volumes of buffer A (100 mM KPi, 750 mM NaCl, 10% glycerol, pH 8.0) containing 50 mM imidazole. The resin was then washed with 2 column volumes of buffer A with 150 mM imidazole, and the protein was eluted in buffer A with 175 mM imidazole. For $OleT_{JE}$ samples not destined for protein crystallization, the protein was extensively dialyzed into buffer A in order to remove any imidazole and bound fatty acids retained from expression in *E. coli*, and then concentrated by ultrafiltration in a Vivaspin (30,000 MWCO, GE Healthcare, Little Chalfont UK) and transferred to buffer B (100 mM KPi, 750 mM NaCl, 20% glycerol, pH 8.0) using a PD 10 Desalting Column (GE Healthcare). The protein was then snap frozen in liquid nitrogen, and stored at -80°C until required. Protein destined for crystallography was not frozen at this point, and instead TEV protease (*ca* 500 U) was added to the eluted protein to remove the His-tag, and the sample incubated at 4°C overnight. The S219V variant of TEV protease was expressed using plasmid pRK793 (Addgene plasmid no. 8827) (37). The protein was then exchanged into buffer A using a PD10

Desalting column, and added to a bed of Ni-IDA resin. Cleaved protein was eluted with buffer A including 20 mM imidazole. This was then dialysed extensively in order to remove imidazole and bound lipids. The protein was concentrated using a Vivaspin, and then gel filtered using a Superdex 200 16/600 (GE Healthcare) column pre-equilibrated with buffer C (100 mM KPi, 750 mM NaCl, pH 8.0).

3.3.2. UV-visible spectroscopy of WT and mutant $OleT_{JE}$ hemoproteins

The UV-visible spectra of WT and mutant forms $OleT_{JE}$ were collected using a Cary 60 UV-visible spectrophotometer (Agilent, Cheadle UK). Spectra were recorded at ambient temperature for the proteins in buffer A, typically at a concentration of ~4-6 µM. The ferrous and Fe^{II}-CO forms of the hemoproteins were produced under anaerobic conditions using degassed buffer A. Reduced enzymes were formed by the addition of a few grains of solid sodium dithionite to ferric enzymes. The Fe^{II}-CO complexes were then formed by slowly bubbling CO gas into reduced $OleT_{JE}$ proteins until no further spectral shift was observed.

3.3.3. Fatty acid binding titrations with $OleT_{JE}$ mutants

Binding of saturated fatty acids (C12:0, C14:0, C16:0, C18:0 and C20:0) to the $OleT_{JE}$ mutants was performed at 25°C in buffer A. Substrates were dissolved in 100% ethanol, and additions of 0.5 µl aliquots of substrate stocks (of concentration from 1-100 mM, according to the particular substrate and its affinity for the P450s) were made until no further spectral shift was observed. Spectra (800-300 nm) were recorded using a Cary 60 UV-visible spectrophotometer. Difference spectra were obtained by subtracting the ligand-free spectrum of the P450 from the ligand-bound spectra at each substrate concentration. The absorbance difference maximum (ΔA_{peak}) and minimum (ΔA_{trough}) were then identified from the individual data sets, and the maximal absorbance change (ΔA_{max}) was calculated by subtracting ΔA_{trough} from ΔA_{peak} in each case, using the same wavelength pair throughout each individual titration. ΔA_{max} was then plotted against substrate concentration, and the data fitted using either a

hyperbolic (Michaelis-Menten or Morrison equations) (40), or a sigmoidal (Hill) function in order to determine the dissociation constants (K_d values) for fatty acid substrate binding.

3.3.4. Stopped-flow kinetic analysis of substrate oxidation by $OleT_{JE}$ WT and mutant enzymes

An Applied Photophysics SX18 MR stopped-flow spectrophotometer with a photodiode array (PDA) detector (Leatherhead, UK) was used to collect stopped-flow absorption data. For the WT, H85Q, F79A and F79W $OleT_{JE}$ mutants, proteins were saturated with arachidic acid (C20:0); while the F79Y mutant was saturated with lauric acid (C12:0). Enzymes were then passed through a 0.2 µm syringe filter (Sartorius UK Ltd., Epsom, UK) to remove excess lipids from the P450 protein solution. The substrate-bound $OleT_{JE}$ proteins were then mixed with different concentrations of H_2O_2 (6.25-200 µM) in the stopped-flow instrument at 25°C.

Conversion of the fatty acid-bound, HS ferric forms of the $OleT_{JE}$ enzymes to their LS forms was monitored at 421 nm for the $OleT_{JE}$ WT and $OleT_{JE}$ H85Q mutant enzymes, and at 423 nm for the $OleT_{JE}$ F79A enzyme. Data were fitted using a single exponential function and using the Pro-Data SX software suite (Applied Photophysics). The observed reaction rate constants (k_{obs} values) were plotted against the relevant H_2O_2 concentration, and the data were fitted using a hyperbolic (Michaelis-Menten) function (for the WT, F79Y and H85Q $OleT_{JE}$ enzymes) or using a linear function in the case of the other $OleT_{JE}$ mutants.

3.3.5. EPR analysis of $OleT_{JE}$ mutants

Continuous wave (CW) X-band electron paramagnetic resonance (EPR) spectra for the $OleT_{JE}$ WT and mutant P450s were obtained at 10 K using a Bruker ELEXSYS E500 EPR spectrometer with an ER 4122SHQ Super High Q cavity. Temperature was controlled with an ESR900 cryostat (Oxford Instruments, Abingdon UK). EPR spectra were collected for WT and $OleT_{JE}$ mutants at concentrations of 100 to 200 µM for ligand-free, arachidic acid-bound and imidazole-bound forms. Arachidic acid was added to dilute $OleT_{JE}$ protein until the UV-visible

spectrum showed no further optical change towards high-spin. The enzyme was then concentrated to an appropriate concentration (200 µM for WT, H85Q and F79A $OleT_{JE}$, 150 µM for R245L $OleT_{JE}$, and 100 µM for the F79W, F79Y and R245E mutants [the latter in its substrate-free form], taking into consideration that some of the mutants are prone to precipitation at high concentrations) using a Vivaspin (30,000 MWCO).

3.3.6. Crystallography of the $OleT_{JE}$ H85Q and $OleT_{JE}$ F79A mutants

Crystallization trials for the $OleT_{JE}$ H85Q and $OleT_{JE}$ F79A mutant enzymes were carried out with 400 nl (200 nl protein and 200 nl precipitant) sitting drops in MRC 96-well plates (Molecular Dimensions, Newmarket UK). Molecular Dimensions screens Clear Strategy Screen I (CSS1), Clear Strategy Screen II (CSSII), PACT premier, JCSG-plus and Morpheus were used for $OleT_{JE}$ H85Q. Diffracting crystals were taken from well H10 of JCSG-plus (0.2 M ammonium acetate, 0.1 M Bis Tris, 25% w/v PEG 3350, pH 5.5). For $OleT_{JE}$ F79A, C3 Shotgun Screen (SG1) and JCSG-plus screens were used. Crystals formed were used to make a seed stock, and further plates were set up using an optimized screen. Diffracting crystals were grown in 0.2 M $MgCl_2$, 0.1 M HEPES, 20% PEG 6000, pH 7.5. Plates were set up using a Mosquito nanolitre pipetting robot (TTP Labtech, Melbourn UK). For $OleT_{JE}$ H85Q, ligand-free and arachidic acid-bound proteins were used for crystal trials at a concentration of 11.5 mg/ml. For the $OleT_{JE}$ F79A mutant, arachidic acid-bound enzyme was used at a protein concentration of 13.5 mg/ml. Arachidic acid was bound to the proteins in the same way as described for the EPR studies.

3.3.7. Fatty acid substrate conversion reactions with WT and mutant $OleT_{JE}$ enzymes

Fatty acid substrate conversion reactions were set up using 1 µM of wild-type, H85Q, F79A, F79W, F79Y, R245L and R245E $OleT_{JE}$ enzymes. The proteins were incubated with 200 µM fatty acid (capric acid, lauric acid, myristic acid, palmitic acid, stearic acid or arachidic acid), and the reactions were started by the addition of 400 µM H_2O_2 in a total volume of 500 µl

buffer A. Reactions were incubated at 32 ºC with shaking for 30 minutes. Thereafter, reactions were stopped by acidifying with 20 µl of 37% HCl. For the C10:0, C12:0 and C16:0 reactions,

	$OleT_{JE}$ WT (Formic acid)	**$OleT_{JE}$ H85Q (C20:0)**	**$OleT_{JE}$ F79A (C20:0)**
Data collection			
Space group	$P4_32_12$	$P2_12_12_1$	$P2_12_12_1$
Cell dimensions			
a,b,c (Å)	60.170, 60.170, 241.70	48.928, 115.494, 163.247	51.88, 110.120, 164.850
α,β,γ (º)	90, 90, 90	90, 90, 90	90, 90, 90
R_{merge} (%)	0.035 (0.625)	0.051 (0.681)	0.057 (0.842)
$I/\sigma I$	25.8 (2.9)	11.4 (2.6)	8.6 (1.8)
Completeness (%)	99.9 (100.0)	99.7 (99.6)	99.6 (99.8)
Redundancy	12.8 (6.5)	6.1 (5.2)	6.5 (6.6)
Refinement			
Resolution (Å)	48.21-1.44 (1.47-1.44)	25.50-1.80 (1.83-1.80)	55.06-1.95 (2.00-1.95)
No. reflections	77736 (5628)	81942 (5951)	66360 (4861)
R_{work}/R_{free}	13.46/17.27 (21.4/28.0)	18.27/21.99 (25.7/29.3)	15.72/20.12 (27.1/33.1)
No. non-hydrogen atoms	3798	7482	7704
Mean B factor (A^2)	19.79	27.35	29.706
R.m.s. deviations			
Bond lengths (Å)	0.020	0.019	0.013
Bond angles (º)	2.020	1.875	1.270

Table 3.1. Data reduction and final structural refinement statistics for $OleT_{JE}$ WT and mutant crystal structures. Data are presented for WT $OleT_{JE}$ bound to formate, and for the arachidic acid-bound forms of the H85Q and F79A $OleT_{JE}$ mutants. **PDB codes pending**.

the internal standards 1-undecene, myristic acid (C14:0), α-OH myristic acid and β-OH myristic acid were added. For the C14:0, C18:0 and C20:0 reactions, internal standards 1-pentadecene, palmitic acid (C16:0), β-OH palmitic acid and α-OH palmitic acid were added. After completion of the reactions, the mixtures were extracted with an equal volume of dichloromethane. The dichloromethane extract was then dried with anhydrous magnesium sulfate before the product sample was subjected to GC/MS analysis.

3.3.8. Characterization of fatty acid oxidation products using GC/MS

Analysis of products formed by fatty acid oxidation using WT and mutant $OleT_{JE}$ enzymes was done using an Agilent 6977A series GC/MSD installed with an Agilent HP-5MS UI 30 m x 0.250 mm x 0.25 µM column (helium flow rate 1.2 ml/min) (Agilent). A 1 µl sample was injected via sandwich injection with 1 µl N,O-*bis*(trimethylsilyl)trifluoroacetamide containing 1% trimethylchlorosilane in order to derivatize fatty acids and hydroxylated fatty acids. The split ratio was 10:1, and the inlet was set to a temperature of 280°C. The oven temperature was held at 40 °C for 1 minute, then ramped at 10°C/minute to 290 °C, where it was held for 1 minute. Electronic ionization was used, scanning ions in the range of 40-550 m/z at a temperature of 250°C. For quantitation, external standard calibrations were generated, and selected ion monitoring (SIM) mode was used to identify appropriate m/z ion fragments for substrate and product analysis.

3.4. Results

3.4.1. Expression and purification of $OleT_{JE}$ and $OleT_{JE}$ mutants

The expression, purification and structural characterization of the wild-type (WT) OleT P450 were reported by Belcher *et al*. (10). The structural data for the substrate-bound and substrate-free forms of $OleT_{JE}$ were used to design mutations to explore the fatty acid carboxylate binding site of the P450. The codon-optimized $OleT_{JE}$ (*CYP152L1*) gene was cloned into pET15b, and site-directed mutagenesis was done to create the H85Q, F79A, F79W, F79Y, R245E and R245L mutants. All mutants were found to express reasonably well in the *E. coli* C41 (DE3) strain. Typical $OleT_{JE}$ mutant recovery was approximately 15 mg/l for H85Q and F79W, 8 mg/l for F79Y and R245L, 2 mg/l for F79A, and 1.5 mg/l for the R245E $OleT_{JE}$ mutant, compared to ~20 mg/l for WT $OleT_{JE}$. The heme precursor δ-aminolevulinic acid (500 µM) was added at the point of induction of $OleT_{JE}$ mutant gene expression with IPTG in order to aid heme incorporation. However, heme insertion levels were diminished in the R245E and R245L mutants (~25-35% heme incorporation). The simultaneous addition of hemin (4 µg/ml) at the point of induction increased heme incorporation by ~5-10% in these mutants.

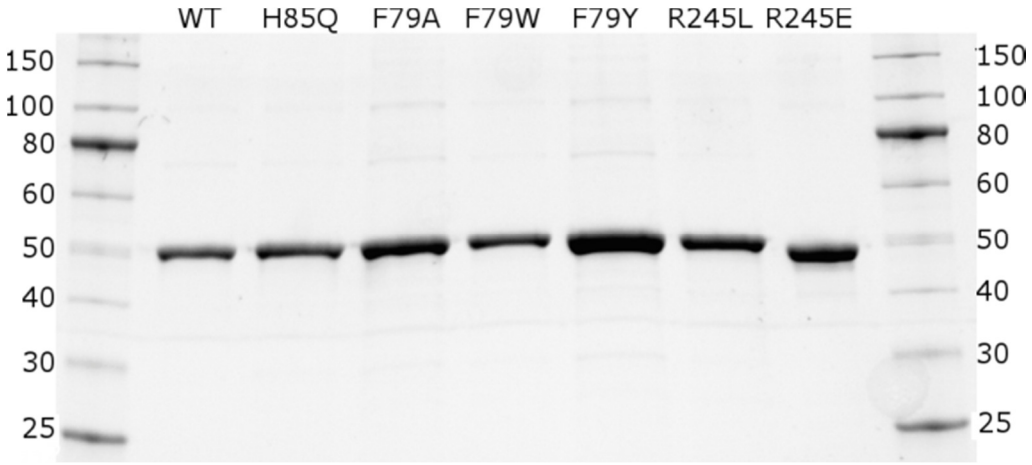

Figure 3.3. Purification of WT and active site mutants of OleT$_{JE}$. The gel image shows the purified forms (from left to right) of WT OleT$_{JE}$ and its active site mutants H85Q, F79A, F79W, F79Y, R245L and R245E. The outside lanes show protein markers with their associated molecular weights (kDa) indicated (NEB Broad Range Protein Ladder).

All OleT$_{JE}$ mutants were purified in the same way, using Ni-IDA chromatography. Samples for enzymatic/spectroscopic assays were frozen after ensuring a high level of purity by SDS-PAGE. Samples destined for crystallography were treated with TEV protease to cleave the N-terminal His-tag, and then passed through a Ni-IDA column to separate the untagged form from column-retained tagged OleT$_{JE}$. Gel filtration chromatography was used to further purify untagged OleT$_{JE}$ proteins, and samples were then used directly in crystallographic trials. **Figure 3.3.** shows an SDS-PAGE gel containing samples of purified WT and mutant OleT$_{JE}$ proteins. The F79W, F79Y, R245E and R245L OleT$_{JE}$ mutants proved less stable than the WT and the H85Q and F79A mutants in that they were prone to aggregation and precipitation on refrigeration, or during crystallization trials. However, the H85Q and F79A OleT$_{JE}$ P450s were successfully crystallized for structural analysis (see *Structural properties of OleT$_{JE}$ mutant enzymes* section below). UV-visible spectral data also showed reduced heme incorporation for OleT$_{JE}$ R245L and R245E mutants; this was further supported by SDS-PAGE which indicated a lower apparent molecular weight for OleT$_{JE}$ R245E (Figure 3.3).

3.4.2. UV-visible absorbance properties of $OleT_{JE}$ mutants

When purified from *E. coli*, the WT, ferric $OleT_{JE}$ exhibits a mixed low-spin (LS)/high-spin (HS) heme iron state that can be converted essentially completely to a LS form by the addition of H_2O_2. This likely indicates that fatty acids from *E. coli* are bound and retained by the enzyme during the purification process. The WT $OleT_{JE}$ was extensively dialyzed in order to remove bound fatty acids. However, this mixed spin character was absent in all $OleT_{JE}$ mutants generated, suggesting that the mutations may compromise affinity for mid- to long-chain fatty acids through structural perturbation of the P450 active site.

In WT $OleT_{JE}$ the ferric heme Soret peak is at 418.5 nm, with the alpha and beta bands at ~567 and 535 nm, respectively. The H85Q mutant has a similar spectrum with a Soret peak at 418.5 nm, while the F79A/W/Y mutants have Soret maxima at 419/419/419.5 nm. In the R245E mutant, there is a substantial spectral change, with the Soret peak at ~423 nm and a major Q-band feature at ~538 nm. This phenomenon is not observed in the R245L $OleT_{JE}$ (Soret maximum at 417.5 nm, with alpha/beta bands at ~566/535 nm), indicating that the

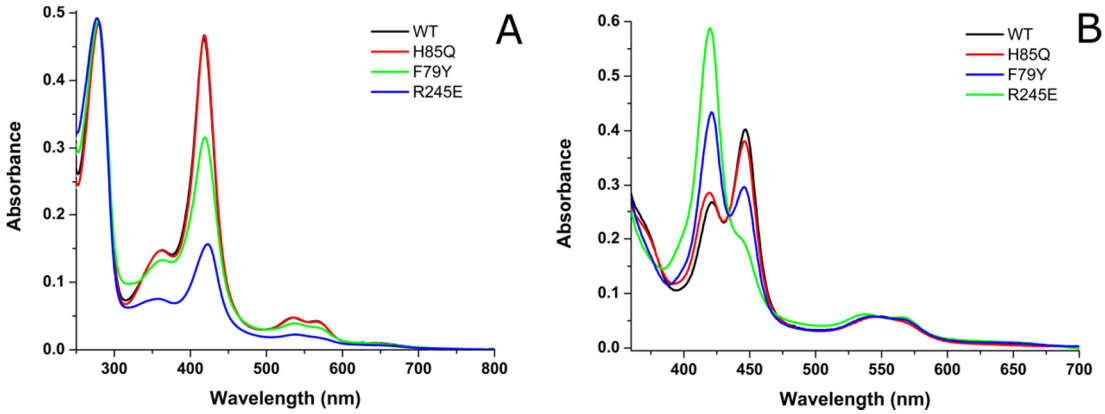

Figure 3.4. UV-visible spectroscopy of $OleT_{JE}$ and key active site mutants. **Panel A** shows typical UV-visible absorption spectra for the ferric, substrate-free forms of WT (black), H85Q (red), F79Y (green) and R245E (blue) $OleT_{JE}$. The spectra are near-identical at the heme Soret and protein (~280 nm) peaks for the WT and H85Q forms (both at 5 µM) and reflect essentially complete heme incorporation into these proteins. However, the heme/protein (Reinheitszahl, Rz) ratio is much lower in the F79Y and R245E $OleT_{JE}$ mutants, indicating lower heme incorporation in these variants. **Panel B** shows the Fe^{II}-CO complexes of the same proteins (corrected to 5 µM by heme content in all cases), showing that the WT and H85Q mutants form predominantly the cysteine thiolate-coordinated P450 form, with a proportion of the thiol-coordinated P420 state. There is a considerably greater proportion of the P420 species in the F79Y mutant, while the R245E mutant forms almost completely the P420 form. The P450 species have a Soret maximum at 446 ± 1 nm and the P420 species a Soret maximum at 420 ± 1 nm in all cases.

R245E mutation alters the heme environment in the distal pocket (**Figure 3.4A**). A likely model is that Glu245 coordinates the R245E mutant heme iron, as was demonstrated previously in the A264E mutant of *Bacillus megaterium* P450 BM3 (CYP102A1) (21).

Spectral differences are observed between the dithionite-reduced WT and mutant forms of $OleT_{JE}$. For WT $OleT_{JE}$, reduction is associated with a decreased Soret peak intensity and a shift in absorption maximum to 415 nm, with merging of the alpha and beta bands into a broad feature peaking at ~540 nm (10). Similar spectral shifts occur on the reduction of $OleT_{JE}$ mutants H85Q and F79A (Soret shifts to 416.5 nm and 418. However, for F79W and F79Y $OleT_{JE}$, the Soret band is red shifted to ~422 nm with peak intensity less diminished than in the WT and the H85Q/F79A variants. The red shift suggests that cysteine thiolate protonation occurs in the F79Y/W variants (22). In reduced R245E $OleT_{JE}$, the Soret peak shifts to 417.5 nm, with a Q-band peak at ~547.5 nm, while in reduced R245L the Soret is at 420 nm with alpha/beta bands at 559/536 nm.

Further comparative studies of the heme environments in WT and mutant $OleT_{JE}$ proteins were done using the Fe^{II}-CO complexes of these P450s. The WT $OleT_{JE}$ formed predominantly the P450 state with a Soret band at 449 nm, and a smaller P420 feature at ~423 nm. These bands originate from $OleT_{JE}$ Fe^{II}-CO complexes in which the proximal ligand is either a cysteine thiolate (P450) or a cysteine thiol (P420) (23,24). The P450:P420 ratio differs considerably between WT $OleT_{JE}$ and the various mutants. Under the conditions used, the highest P450:P420 ratio occurs for the WT $OleT_{JE}$ with a P450 component of ~75%. H85Q has a similar proportion of P450 (~70%), but P450 content decreases in the F79Y mutant (~45%, similar to the F79A/W mutants) and the R245E mutant forms almost completely the P420 form (~10% P450) (**Figure 3.4B**). These data show that active site mutations influence the $OleT_{JE}$ variant heme environments, including perturbation of the proximal ligand protonation state in the ferrous and/or Fe^{II}-CO forms. While the heme iron of R245E $OleT_{JE}$ is likely coordinated by Glu245 carboxylate in the ferric state, CO can clearly displace this distal ligand in the ferrous state of the enzyme. The ferrous R245L/E mutant Soret spectral peaks are similarly positioned at 416.5/417 nm, suggesting displacement of a Glu245 distal ligand in

the ferrous state for the R245E mutant. The R245L mutant also forms a much higher proportion of the P450 Fe^{II}-CO complex, at ~35% (not shown).

3.4.3. Interactions of WT and mutant $OleT_{JE}$ proteins with fatty acid substrates

In order to examine the influence of lipid substrates on $OleT_{JE}$ ferric heme iron spin-state equilibrium and to determine K_d values for substrate binding, fatty acids of different chain lengths were titrated with WT and mutant $OleT_{JE}$ P450s. For WT $OleT_{JE}$, binding of arachidic acid (C20:0) gives an extensive shift towards HS ferric heme iron, with decreased Soret band intensity at ~418 nm, and increased HS band intensity at 389 nm. Development of HS character is further confirmed by the appearance of a thiolate-to-HS ferric heme iron charge transfer (CT) band at ~650 nm. For WT $OleT_{JE}$, the amount of HS heme formed decreases as the fatty acid chain length decreases. The K_d values remain low for saturated fatty acids tested in the chain length range from C20 to C14, but affinity decreases considerably for C12 and C10 substrates; e.g. K_d = 1.73 ± 0.08 μM for palmitic acid (C16:0) compared to 47.1 ± 2.1 μM for capric acid (C10:0) (**Table 3.2**).

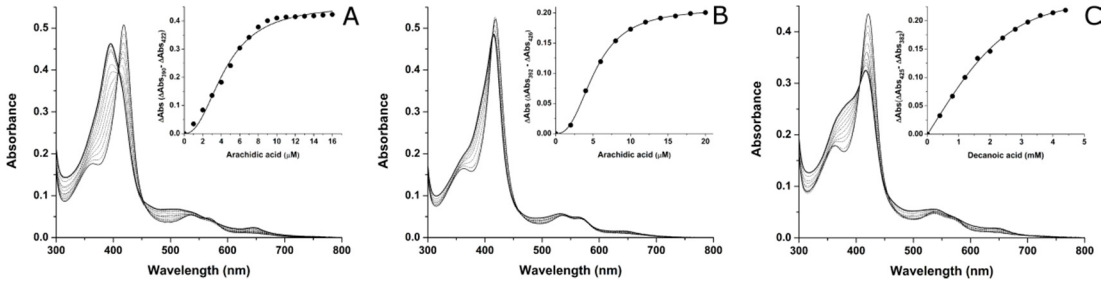

Figure 3.5. Fatty acid binding titrations with WT and mutant $OleT_{JE}$ proteins. **Panel A** shows a UV-visible spectral binding titration for WT $OleT_{JE}$ (5.5 μM) with arachidic acid (C20:0). There is extensive conversion of the LS heme iron (at 418.5 nm) towards HS (at 395 nm). HS heme iron development is also evident from the development of a cysteine thiolate-to-HS ferric heme iron charge transfer (CT) species at ~650 nm. Inset shows the fitting of absorbance change *versus* [arachidic acid] using the Hill function, producing an apparent K_d of 4.43 ± 0.19 μM. **Panel B** shows a titration of the $OleT_{JE}$ H85Q mutant (5.6 μM) with arachidic acid, in this case producing a much smaller spectral conversion towards HS. Inset shows the fit of induced absorption change (418.5 to 415 nm) *versus* [arachidic acid], fitted as above to give a K_d of 5.27 ± 0.05 μM. **Panel C** shows a titration of the $OleT_{JE}$ R245E mutant (4.7 μM) with capric acid (C10:0), with absorption change (~422.5 to 384 nm) *versus* [capric acid] data fitted using a hyperbolic function to give a K_d of 1260 ± 160 μM.

Binding of arachidic acid also induces HS heme formation in H85Q and F79A $OleT_{JE}$ mutants, but with a much less extensive HS shift than seen in WT $OleT_{JE}$. At apparent saturation with arachidic acid, the Soret band shifts to ~415 nm for H85Q and to ~414 nm for F79A $OleT_{JE}$. Arachidic acid spectral binding data for WT and the H85Q $OleT_{JE}$ mutant are compared in (**Figure 3.5**). Despite incomplete HS shifts in these mutants, substrate turnover data confirm that both the H85Q and F79A mutant P450s can oxidize fatty acids in the C10-C20 range (see *Products formed by novel $OleT_{JE}$ mutants* section below). Thus, productive substrate binding occurs for these fatty acids in both mutants. These mutations may influence the binding mode of the fatty acid and its carboxylate group, which in turn affects the efficiency with which the substrate can displace the distal water ligand to convert the P450s to a HS state. The reaction of H_2O_2 with substrate-bound $OleT_{JE}$ generates reactive heme species (ferryl-oxo and ferryl-hydroxo compounds I and II, see **Figure 3.1**) that oxidize the substrate, and the retention of catalytic activity in the H85Q/F79A mutants indicates that fatty acid binding modes remain close to this reactive iron-oxo species such that hydroxylation (at substrate α- and β-carbons) and decarboxylation remain feasible.

It should be noted that for P450 BS_β, and P450 SP_α (where residue 85 is a glutamine), the HS shift upon substrate binding is very small (BS_β), or not observed at all (SP_α) (25). The H85Q $OleT_{JE}$ mutant thus mimics the spectral properties of these other bacterial peroxygenases on binding fatty acid substrates. For both the H85Q and F79A $OleT_{JE}$ mutants, there is a pattern of increasing substrate K_d values as the fatty acid chain length decreases, consistent with the properties of WT $OleT_{JE}$, and likely reflecting the fewer hydrophobic interactions made by shorter chain substrates in the active site channel (**Table 3.2**).

The F79W and F79Y $OleT_{JE}$ proteins show modest spin-state shifts with most fatty acids tested, suggesting again that the binding modes of these substrates are perturbed. However, in the F79Y $OleT_{JE}$ there is a notable increase in HS content on saturation with lauric acid (C12:0, ~25% high spin) and myristic acid (C14:0, ~20% high spin) compared with longer chain fatty acids (<10% for arachidic acid, stearic acid [C18:0] and palmitic acid). This suggests that these shorter chain fatty acids can adopt binding modes in F79Y $OleT_{JE}$ that are compatible with more efficient displacement of the distal water molecule than can occur with

longer chain substrates, probably in part due to their greater solubility. With the exception of the R245E $OleT_{JE}$ variant, K_d values for the longest substrates (C20:0 and C18:0) are similar for the WT and mutant $OleT_{JE}$ enzymes (**Table 3.2**). As fatty acid chain length decreases from C16:0, there are wider variations in the substrate K_d values, with all mutants apart from R245E (see below) showing weaker binding of fatty acids from C16:0 to C10:0 by

comparison with the WT $OleT_{JE}$.

$OleT_{JE}$ variant	**Fatty Acid K_d (μM) [HS (%)]**					
	C20:0	**C18:0**	**C16:0**	**C14:0**	**C12:0**	**C10:0**
WT	4.43 ± 0.19 [95]	4.09 ± 0.16 [70]	1.73 ± 0.08 [25]	1.45 ± 0.05 [45]	11.7 ± 0.43 [40]	47.1 ± 2.1 [35]
H85Q	5.27 ± 0.05 [25]	5.92 ± 0.08 [<10]	5.36 ± 0.18 [<10]	10.5 ± 0.1 [<10]	37.3 ± 2.5 [<10]	NB [NB]
F79A	3.4 ± 0.3 [<10]	8.7 ± 0.5 [<10]	22.6 ± 1.9 [<10]	39.1 ± 2.5 [<10]	55.0 ± 4.8 [<10]	465 ± 11 [<10]
F79W	4.41 ± 0.27 [20]	4.52 ± 0.20 [15]	12.7 ± 0.7 [<10]	24.1 ± 0.9 [15]	106 ± 9 [<10]	NB [NB]
F79Y	4.25 ± 0.21 [<10]	8.91 ± 0.33 [<10]	18.2 ± 0.7 [<10]	30.7 ± 1.0 [20]	196 ± 5 [25]	NB [NB]
R245E	NB [NB]	NB [NB]	NB [NB]	NB [NB]	NB [NB]	1260 ± 160 [40]

Table 3.2. Binding affinity of saturated fatty acids for WT and mutant forms of $OleT_{JE}$. The dissociation constants (K_d values) for the binding of the saturated fatty acids decanoic acid (capric acid, C10:0), dodecanoic acid (lauric acid, C12:0), tetradecanoic acid (myristic acid, C14:0), hexadecanoic acid (palmitic acid, C16:0), octadecanoic acid (stearic acid, C18:0) and arachidic acid (eicosanoic acid, C20:0) were determined by UV-visible titration with WT $OleT_{JE}$ and with the H85Q, R245E, and F79A/W/Y mutants. NB indicates that no significant binding (indicated by lack of HS heme iron development) was detected for the indicated mutants. In the case of the R245L $OleT_{JE}$ mutant, no optical binding could be detected for any fatty acid.

In the case of the R245L mutant, addition of the solvents ethanol, methanol and dimethyl sulfoxide (DMSO) resulted in the development of up to ~10% HS heme iron. This phenomenon was not observed with the R245E mutant, likely due to the Glu245 carboxylate occupying the distal ligand position on the heme iron. This issue prevented any accurate assessment of the role of fatty acids in perturbing the R245L heme iron spin-state equilibrium, since spectral changes induced by fatty acids dissolved in these solvents were of similar magnitude to those induced using solvents alone. However, addition of 1 mM lauric acid prepared in aqueous buffer A produced no significant change in the R245L UV-visible spectrum. Similarly, addition

of a saturating amount of arachidic acid (in ethanol) did not induce any further R245L HS heme iron development over that caused by solvent alone. Thus, fatty acid substrate binding modes in this mutant may be particularly inefficient in displacement of the axial water ligand in ferric R245L $OleT_{JE}$.

The R245E $OleT_{JE}$ mutant exhibits unusual behaviour in that there is no apparent shift in Soret maximum from 423 nm or development of HS heme iron observed in optical titrations with any of the fatty acids from C20:0 to C12:0. However, titration with capric acid (C10:0), resulted in ~40% HS heme iron accumulation at apparent saturation (**Figure 3.5C**). These observations suggest that the longer chain fatty acids do not bind R245E $OleT_{JE}$ in a mode that enables HS development/displacement of a Glu245 axial ligand. However, the substantial HS heme accumulation in R245E $OleT_{JE}$ on binding capric acid suggests that this short chain substrate can displace the axial ligand, albeit with a very high K_d (1260 ± 160 μM). Coordination of heme iron by glutamate oxygen was also observed in the P450 BM3 A264E mutant, with arachidonic acid substrate binding causing near-complete distal coordination by the Glu264 carboxylate (21,26). However, the situation may be reversed for the $OleT_{JE}$ R245E mutant, with capric acid partially displacing a glutamate ligand at high concentrations.

3.4.4. Stopped-flow kinetic analysis of fatty acid oxidation by WT and mutant $OleT_{JE}$ P450s

Stopped-flow absorption spectroscopy was used to probe the effects of mutations to His85 (H85Q) and Phe79 (F79A/W/Y) on the kinetics of $OleT_{JE}$ single turnover substrate oxidation reactions. WT, H85Q and F79A/W variants were incubated with arachidic acid, while F79Y $OleT_{JE}$ was incubated with near-saturating lauric acid to achieve the maximal heme iron spin-state conversion for this mutant. The H_2O_2-dependent oxidation of substrates was observed by the rapid HS-to-LS conversion of the $OleT_{JE}$ heme iron in each case. Reaction progress was monitored at wavelengths close to the ferric, LS Soret maximum for WT $OleT_{JE}$ and the four mutants. Rate constants for the single turnover reactions (k_{obs}) were determined using H_2O_2 concentrations up to 200 μM. Under the conditions used, plots of k_{obs} *vs.* [H_2O_2] were hyperbolic for WT $OleT_{JE}$ and for the H85Q and F79Y variants. Data were fitted using a

hyperbolic function to derive the limiting rate constant (k_{lim}) and the apparent K_d for H_2O_2. The WT $OleT_{JE}$ had values of k_{lim} = 115 ± 8 s^{-1}, K_d = 107 ± 16 μM, compared to 101 ± 16 s^{-1}, 749 ± 141 μM for F79Y, and 286 ± 18 s^{-1}, 327 ± 29 μM for H85Q. The dependence of k_{obs} vs. [H_2O_2] was linear for the F79A and F79W mutants, with 2nd order rate constants of 0.188 ± 0.004 μM^{-1} s^{-1} and 0.107 ± 0.005 μM^{-1} s^{-1}, respectively. The comparable 2nd order rate constants (k_{lim}/K_d) for the other proteins are 1.075 ± 0.236 μM^{-1} s^{-1} (WT); 0.875 ± 0.133 μM^{-1} s^{-1} (H85Q); and 0.838 ± 0.507 μM^{-1} s^{-1} (F79Y).

Stopped-flow kinetic data for the reactions of WT and mutant forms of fatty acid-bound $OleT_{JE}$ with H_2O_2 indicate that the WT, H85Q and F79Y enzyme single turnovers are more efficient than are those of the other two Phe79 mutants. While this is consistent with the superior catalytic properties of the WT and H85Q mutants in product formation (**Table 3.4**), the F79A $OleT_{JE}$ is a more productive enzyme for C10-C16 substrates than are F79Y/W, with more similar levels of product formation for the F79A/Y/W mutants with C18 and C20 substrates. However, in view of only minor development of HS heme iron in arachidic acid-bound F79Y $OleT_{JE}$, lauric acid was used instead with the F79Y variant to enhance HS formation and to improve experimental data quality. In this case it appears that single turnover efficiency (i.e. the apparent 2nd order rate constant for F79Y $OleT_{JE}$-dependent substrate oxidation by H_2O_2) is at a level similar to that of the WT and H85Q $OleT_{JE}$ enzymes with arachidic acid. Despite this finding, percentage product formation for lauric acid with the F79Y mutant is much lower than observed for the WT/H85Q/F79A $OleT_{JE}$ enzymes with the same substrate, and similar to that for the F79A $OleT_{JE}$ with arachidic acid. These data suggest that other factors (e.g. the rate constants for substrate association/product dissociation and/or efficiency of substrate oxidation with different chain substrates) have a strong influence on overall product formation.

3.4.5.Characterization of $OleT_{JE}$ WT and mutant P450 heme coordination by EPR

Continuous wave X-band EPR spectra were recorded for WT and all mutant forms of $OleT_{JE}$ in their substrate-free and arachidic acid-bound states in order to characterize the heme coordination state and the influence of mutations to the key residues in the heme distal pocket. As reported previously, the substrate-free form of WT $OleT_{JE}$ has a complex EPR spectrum

with at least four LS (S = 1/2) ferric species with rhombic anisotropy; the most prominent of which have g-values of g_z = 2.49, g_y = 2.24, g_x = 1.89 (2.49/2.24/1/89) and 2.55/2.24/1.85 (**Figure 3.6**) (10). The g-values for these species and those for all other mutants and their substrate-bound forms are presented in **Table 3.4**. These LS species are consistent with ferric heme iron coordinated by cysteine thiolate and a distal water ligand in a large water-filled active site, and with there being a variety of coordination geometries and hydrogen bonding interactions/networks with the distal water ligand. There is no major contribution from a HS (S = 5/2) species in the WT substrate-free form, but a substantial HS component appears on the addition of arachidic acid to WT $OleT_{JE}$. This is split into two major species with g-values of 7.76/3.84/1.71 and 7.76/3.67/1.75. As discussed previously, this heterogeneity likely results from e.g. changes in conformation of the heme and thiolate ligand geometry, rather than from any axial ligand switch in the HS, pentacoordinate state (10). The binding of arachidic acid also results in a dominant LS form with g-values of 2.47/2.25/1.89, suggesting a much more ordered active site organization in the substrate-bound state.

For the H85Q $OleT_{JE}$ mutant, the substrate-free LS spectrum is less complex than that for WT $OleT_{JE}$. There are two major LS species at 2.59/2.25/1.85 and 2.49/2/25/1.89. The signal for the former is broad, and may encompass two LS species. Addition of arachidic acid produces a much smaller HS signal than in WT $OleT_{JE}$ (with features at g_z = 7.8 and g_y = 3.75) and alters the LS spectrum, with two major species at 2.50/2.25/1.88 and 2.48/2.25/1.89. The LS heme iron signals for the H85Q mutant are quite distinct from those for WT $OleT_{JE}$ in both the substrate-free and arachidic acid-bound forms, indicating that the H85Q mutation alters the environment of the distal pocket around the heme iron, e.g. through altering the hydrogen bonding network to the distal water ligand in the LS substrate-free form (**Figure 3.6**).

In F79A $OleT_{JE}$ the major LS species is at 2.48/2.25/1.89, similar to that of the main LS species in the WT enzyme. Minor species are at 2.65/2.25/1.84 and 2.58/2.25/1.86. The F79Y and F79W mutants have similar spectra to F79A $OleT_{JE}$, although the central set of g-values is predominant in these mutants (2.55/2.26/1.87 and 2.54/2.25/1.86, respectively). Binding of arachidic acid does not produce any significant HS signal in the F79A/W mutants, although a small HS signal is observed for substrate-bound F79Y $OleT_{JE}$ (g_z = 7.79). However, substrate does cause some perturbations to the Phe79 mutants LS g-values, particularly in the case of

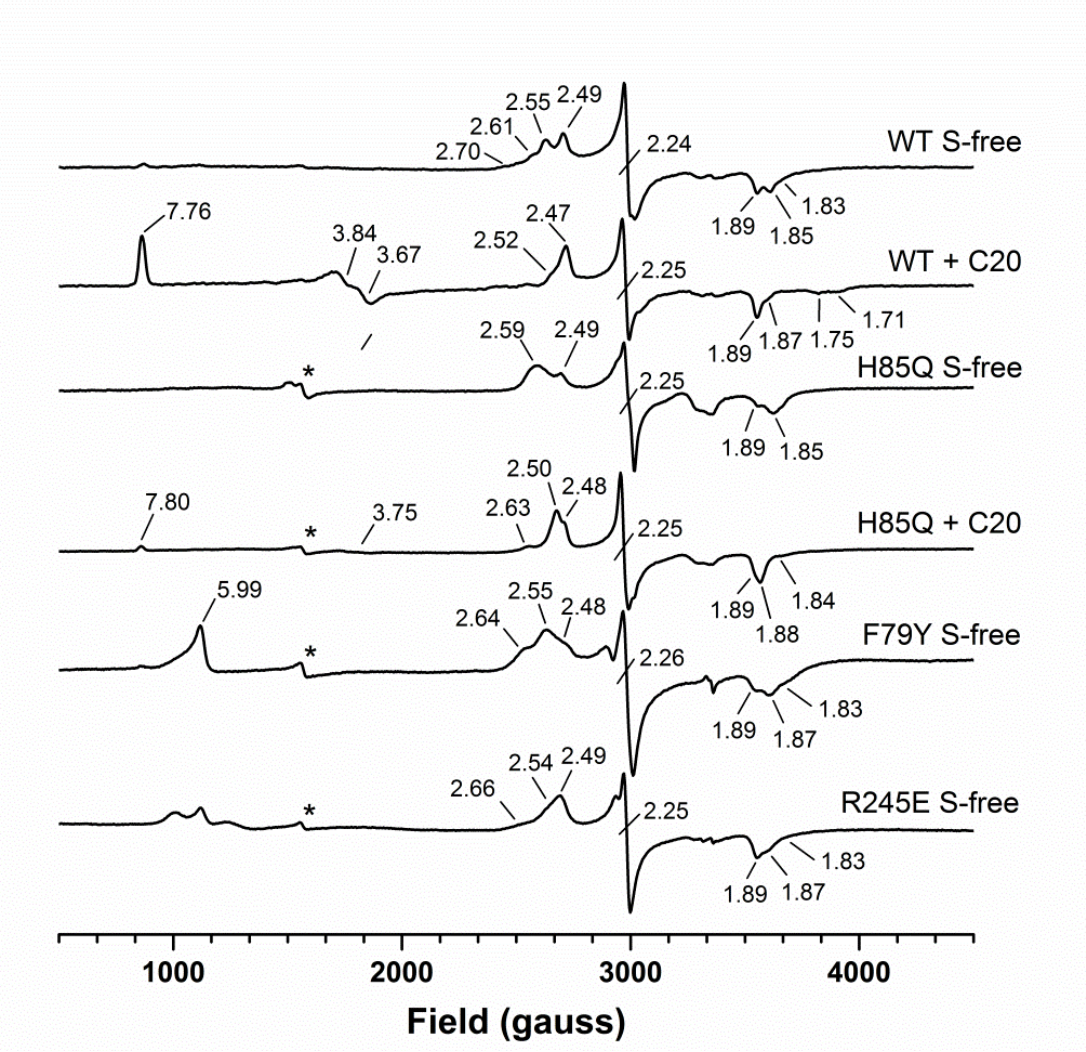

Figure 3.6. EPR spectroscopic properties of WT and mutant forms of $OleT_{JE}$. X-band EPR spectra are shown for WT and H85Q $OleT_{JE}$ mutants in both ligand-free and arachidic acid substrate-bound (C20:0) forms, and for the F79Y and R245E $OleT_{JE}$ mutants in their ligand-free forms. The WT and mutant forms of $OleT_{JE}$ have complex LS EPR spectra with several distinct species (see **Table 3.3** for sets of g-values). HS heme iron accumulation is seen following addition of arachidic acid to WT $OleT_{JE}$ (g = 7.76/3.84/1.71 and 7.76/3.67/1.75), but only a very small HS signal is seen for the arachidic acid-bound H85Q mutant (g = 7.80/3.75). The asterisks show signals for a proportion of a HS penta-coordinated, thiol-ligated, ferric heme species in the H85Q, F79Y and R245E mutants.

the F79A variant (**Table 3.3**). Notably, there is a large axial HS signal at g = 5.99 in both the F79W and F79Y $OleT_{JE}$ mutants that likely relates to HS penta-coordinated, thiol-ligated, ferric heme species in these mutants. This observation is consistent with some loss of heme in these variants, and UV-vis studies of these mutants also revealed a propensity for cysteine thiolate protonation of their heme iron to form the P420 state.

The R245E/L mutants result in less complex substrate-free EPR spectra than in WT $OleT_{JE}$, with two major, similar sets of g-values for both R245E (2.54/2.25/1.87 and 2.49/2.25/1.89)

OleT$_{JE}$ variant	Rhombic HS signals	Rhombic LS signals ($g_z/g_y/g_x$)	
		Major species	Minor species
WT	ND	2.49/2.24/1.89	2.70/2.24/1.83; 2.61/2.24/1.85; 2.55/2.24/1.85
H85Q	ND	2.59/2.25/1.85	2.49/2.25/1.89
F79A	ND	2.48/2.25/1.89	2.65/2.25/1.84; 2.58/2.25/1.86
F79W	ND	2.54/2.25/1.86	2.65/2.25/1.84; 2.47/2.25/1.89
F79Y	ND	2.55/2.26/1.87	2.64/2.26/1.83; 2.48/2.26/1.89
R245L	ND	2.54/2.25/1.87	2.65/2.25/1.85; 2.46/2.25/1.90
R245E	ND	2.49/2.25/1.89	2.66/2.25/1.83; 2.54/2.25/1.87
WT+C20:0	7.76/3.84/1.71; 7.76/3.67/1.75	2.47/2.25/1.89	2.52/2.25/1.87
H85Q+C20:0	7.80/3.75	2.50/2.25/1.88	2.63/2.25/1.84; 2.48/2.25/1.89
F79A+C20:0	ND	2.49/2.26/1.89	2.60/2.26/1.84; 2.54/2.26/1.86
F79W+C20:0	ND	2.54/2.25/1.86	2.67/2.25/1.83; 2.46/2.25/1.89
F79Y+C20:0	7.79	2.56/2.26/1.86	2.65/2.26/1.83; 2.49/2.26/1.89
R245L+C20:0	7.70, 3.74	2.53/2.25/1.87	2.65/2.25/1.85; 2.46/2.25/1.90
R245E+C20:0	ND	2.53/2.25/1.87	2.67/2.25/1.85; 2.47/2.25/1.90

Table 3.3. EPR g-values for substrate-free and fatty acid-bound forms of WT and mutant OleT$_{JE}$ proteins. X-band EPR data were collected at 10 K for the substrate-free and arachidic acid-bound forms of OleT$_{JE}$. The g-values for the LS species and for HS species (where evident) are presented. In the case of fatty acid-bound forms giving weak HS signals, only those component g-values that can be accurately identified are shown. For each of the OleT$_{JE}$ LS forms, 2-4 different rhombic species are identified in each case. The most prominent of these species is indicated in bold text for each of the OleT$_{JE}$ substrate-free and substrate-bound forms.

and R245L (2.54/2.25/1.87 and 2.46/2.25/1.90). Addition of arachidic acid has little effect on these LS g-values, but does produce a small rhombic HS signal (g_z = 7.70, g_y = 3.74) in the R245L mutant that mirrors the data from UV-vis titrations and results from effects of the solvent (**Figure 3.6, Table 3.4**). The R245E/capric acid complex proved unstable at the high protein concentration required for EPR analysis, aggregating and precipitating at ~50 μM.

3.4.6. Products formed by novel OleT$_{JE}$ mutants

Fatty acid substrate conversion reactions were set up using 1 μM WT, H85Q, F79A/W/Y and R245L/E OleT$_{JE}$ enzymes, and using 200 μM fatty acids (capric acid, lauric acid, myristic acid, palmitic acid, stearic acid or arachidic acid), as described in the *Experimental Procedures*.

For WT OleT$_{JE}$, activity was highest for shorter chain length substrates (C10:0 to C14:0), with essentially complete oxidation of myristic acid observed. These data are consistent with studies by Liu *et al* (12). Activity decreased with longer chain lengths, possibly due to the lower

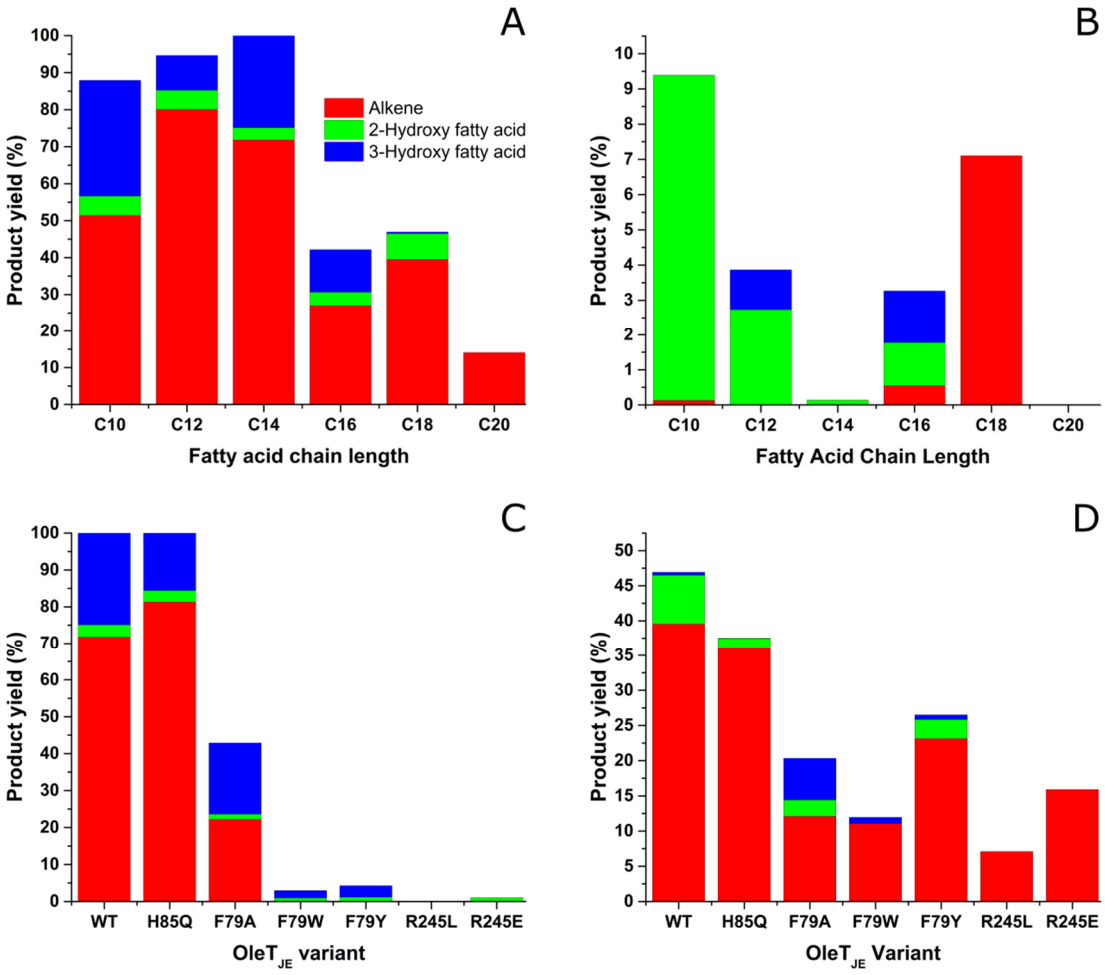

Figure 3.7. Products of fatty acid turnover from WT and mutant OleT$_{JE}$ enzymes. The bar charts show yields of different alkenes (red), 2-hydroxy fatty acids (green) and 3-hydroxy fatty acids (blue) resulting from catalytic turnover by WT and mutant forms of OleT$_{JE}$, as described in the *Experimental Procedures* section. Data shown are averages from two sets of experiments, with values varying by <10% in all cases. **Panel A** shows proportions of the different products formed in turnover of C10:0, C12:0, C14:0, C16:0, C18:0 and C20:0 substrates by WT OleT$_{JE}$. **Panel B** shows the products formed by the R245L OleT$_{JE}$ mutant with the same substrates, illustrating a switch from fatty acid hydroxylation towards fatty acid decarboxylation (terminal alkene formation) at longer substrate chain lengths. **Panel C** shows products formed from the C14:0 substrate (myristic acid) by WT and all OleT$_{JE}$ mutants. **Panel D** shows products formed from the C18:0 substrate (stearic acid) by WT and all OleT$_{JE}$ mutants.

solubility of the substrates and/or the higher affinity of the terminal alkenes/hydroxylated products formed for the OleT$_{JE}$ active site (15). For all the fatty acids tested with WT OleT$_{JE}$ (C10:0 to C20:0), the major reaction was decarboxylation of the fatty acids to form terminal alkenes. For most substrates, 3-hydroxy fatty acid products were more prevalent than 2-hydroxy fatty acids. However, the reverse was the case for stearic acid (C18:0). When arachidic acid was used as a substrate, only 1-nonadecene was detected, with negligible amounts of 2-/3-hydroxy arachidic acid produced (**Figure 3.7A, Table 3.4**).

$OleT_{JE}$ His85 was postulated as a proton donor to iron-oxo species in the WT $OleT_{JE}$ reaction (10). The P450 BS_{β} and SP_{α} enzymes have a glutamine at this position, and catalyze predominantly (BS_{β}) or exclusively (SP_{α}) fatty acid hydroxylation. The H85Q mutant was found

Substrate	Products	$OleT_{JE}$ variant and % products formed						
		WT	H85Q	F79A	F79W	F79Y	R254L	R245E
C10:0	1-nonene	51	65	37	1.5	0.3	0.1	0.2
	2-OH capric acid	5.2	8	1.4	2.1	0	9.3	0
	3-OH capric acid	31	25	15	2.1	0	0	0
	total conversion	87	98	53	5.7	0.3	9.4	0.2
C12:0	1-undecene	80	79	64	1.3	1.3	0	0
	2-OH lauric acid	5.2	7.8	7.4	3.6	3.4	2.7	2.6
	3-OH lauric acid	9.0	9.2	8.5	1.6	1.4	1.1	1.1
	total conversion	94	96	80	6.5	6.1	3.8	3.7
C14:0	1-tridecene	72	81	22	0	0	0	0
	2-OH myristic acid	3.3	3.1	1.4	1.0	1.2	0.1	1.1
	3-OH myristic acid	25	16	19	2.0	3.1	0	0
	total conversion	100	100	42	3.0	4.3	0.1	1.1
C16:0	1-pentadecene	27	22	9.3	1.2	0.8	0.5	0.6
	2-OH palmitic acid	3.6	3.2	2	2	1.6	1.2	1.2
	3-OH palmitic acid	12	13	5.1	2.3	1.7	1.5	1.5
	total conversion	43	38	16	5.5	4.1	3.2	3.3
C18:0	1-heptadecene	40	36	12	11	23	7.1	16
	2-OH stearic acid	7	1.4	2.3	0	2.7	0	0
	3-OH stearic acid	0.4	0.1	5.9	0.9	0.7	0	0
	total conversion	47	38	20	12	27	7.1	16
C20:0	1-nonadecene	14	11	5	3.4	2.5	0	0.1
	2-OH arachidic acid	0	0	0	0	0	0	0
	3-OH arachidic acid	0	0	0	0	0	0	0
	total conversion	14	11	5	3.4	2.5	0	0.1

Table 3.4. Conversion of fatty acid substrates into alkene and hydroxylated fatty acid products by WT and mutant $OleT_{JE}$ enzymes. The WT and H85Q, R245E/L and F79A/W/Y $OleT_{JE}$ enzymes were used to catalyze H_2O_2-dependent decarboxylation/hydroxylation of saturated fatty acid substrates (C10:0-C20:0) as described in the *Experimental Procedures*. The percentage conversions of each fatty acid substrate into their respective (i) n-1 terminal alkene, (ii) 2-OH fatty acid and (iii) 3-OH fatty acid products are shown for each $OleT_{JE}$ variant. The percentage of the various products formed in each reaction is given to the nearest 1% where these products form 10% or more of the total, and to the nearest 0.1% where products form less than 10% of the overall yield. The total product formation for each $OleT_{JE}$ variant/substrate combination is presented in the same way. The data presented are average values from two sets of experiments differing by less than 10% in all cases.

to generate a product profile very similar to that for the wild type $OleT_{JE}$ for all substrates tested (**Figure 3.7B, Table 3.4**). The n-1 terminal alkenes are again the dominant products in all cases, with 3-hydroxy fatty acids formed to greater extents than 2-hydroxy fatty acids for substrates from C10:0-C16:0. As with WT $OleT_{JE}$, the 2-hydroxy stearic acid product is formed to higher levels than 3-hydroxy stearic acid, and 1-nonadecene is the only significant product from arachidic acid with H85Q $OleT_{JE}$.

The F79A $OleT_{JE}$ mutant exhibited decreased activity compared to the WT and H85Q enzymes for all fatty acids tested. F79A $OleT_{JE}$ mutant activity was highest with lauric acid, with 80% product conversion (compared to 94%/96% for WT/H85Q $OleT_{JE}$), but overall product formation was much lower with myristic acid (42% for F79A compared to 100% with WT/H85Q). The F79A $OleT_{JE}$ mutant produced 3-hydroxy fatty acids in excess over 2-hydroxy fatty acids for all substrate chain lengths from C10-C18. For arachidic acid, the only product formed was 1-nonadecene, albeit with only 5% conversion (compared to 14%/11% for WT/H85Q $OleT_{JE}$) (**Table 3.4**).

The F79W/Y mutants were generated to analyze effects of potentially more conservative mutations to Phe79. However it was found that, with one exception, both the F79W/Y $OleT_{JE}$ mutants had much lower activity than F79A $OleT_{JE}$. The only outlier was the F79Y mutant with stearic acid substrate, where overall product formation was 27% compared to 20% for F79A $OleT_{JE}$, due to a higher amount of 1-heptadecene produced by the F79Y mutant. While amounts of alkene products from the F79A/W/Y mutants are broadly comparable for the C18:0 and C20:0 substrates, alkenes are formed in much lower amounts in the F79W/Y mutants compared to the F79A $OleT_{JE}$ for the C10:0-C16:0 substrates (**Table 3.4**).

Crystallographic data indicated that $OleT_{JE}$ Arg245 plays a key role in catalysis by co-ordinating the carboxylate group of the fatty acid substrate (10). The R245L and R245E $OleT_{JE}$ mutants were generated and purified to investigate effects of side chain charge removal and reversal. The R245L/E $OleT_{JE}$ mutants generally have much lower levels of activity than WT $OleT_{JE}$ and the two most productive mutants (H85Q and F79A). However, the R245L/E mutants convert 7.1%/16% stearic acid to 1-heptadecene, with no detectable hydroxylated products. Almost no decarboxylated product (1-nonadecene) was observed for these mutants with arachidic acid, and alkene production was in the range from 0-0.6% for the R245L/E mutants and C10:0-C16:0 substrates (**Table 3.4**). The unusual “switch” from mainly substrate hydroxylase activity at shorter chain lengths towards decarboxylase activity for stearic acid is shown in **Figure 3.7C**, and **Figure 3.7D** shows the product profiles from WT and all $OleT_{JE}$ mutant enzymes with stearic acid (C18:0) substrate. Alkenes are the major products formed by WT and all $OleT_{JE}$ mutants with this substrate.

3.4.7. Structural properties of $OleT_{JE}$ mutant enzymes

Crystallization trials were undertaken for all $OleT_{JE}$ mutant enzymes. Crystals were obtained for both the H85Q and F79A mutant P450s in complex with arachidic acid substrate, as well as for the WT $OleT_{JE}$ in conditions containing formate. In the latter case, this produced a complex in which formate coordinates the WT $OleT_{JE}$ heme iron in the distal position. Structures for these mutant enzymes were determined to 1.44 Å (WT/formate), 1.80 Å (H85Q/arachidic acid) and 1.95 Å (F79A/arachidic acid) (**Table 3.1**). Attempts to crystallize other mutants were not successful, largely due to propensity of other $OleT_{JE}$ mutants to aggregate at high concentrations.

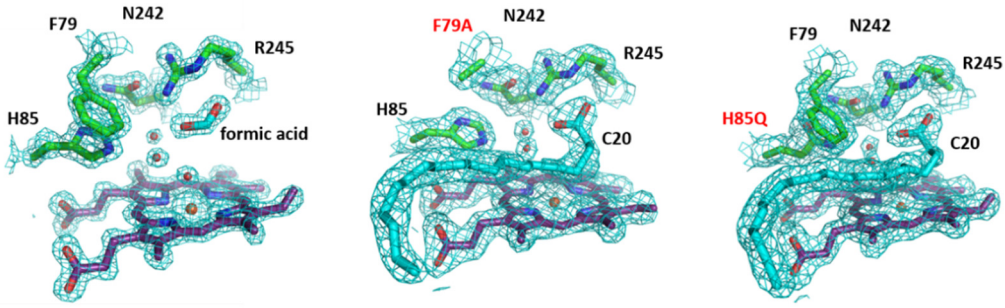

Figure 3.8. **Active site structures for WT and mutant $OleT_{JE}$ proteins**. The three panels show active site details from the crystal structures of WT $OleT_{JE}$ in complex with formic acid (**panel A**), and for the F79A (**panel B**) and H85Q (**panel C**) $OleT_{JE}$ mutants bound to arachidic acid. Selected residues in the active site are shown as atom coloured sticks (green carbons), while the heme group and associated ligands are shown with purple and cyan carbons, respectively. Positions of mutations are labelled in red. Electron density is shown as a blue mesh contoured at 2 sigma for the WT $OleT_{JE}$-formic acid complex, and at 1.5 sigma for the two mutant structures. Three water molecules are clearly defined in the active site of these three structures (oxygens shown as red spheres), one of which acts as the 6th ligand to the heme iron.

Few structural changes occur in the $OleT_{JE}$ structure due to the mutations. Arachidic acid substrate is bound similarly in both the H85Q and F79A mutants as was previously reported for the WT $OleT_{JE}$ (10). However, in the WT arachidic acid-bound structure a 6th ligand water molecule could not be distinguished, likely due to the HS state of the WT $OleT_{JE}$ substrate-ligand complex. In contrast, for both $OleT_{JE}$ H85Q/F79A mutant structures, a 6th ligand water molecule is clearly visible. A similar situation is observed for the higher resolution structure of the WT $OleT_{JE}$-formic acid complex, which remains LS in solution (**Figure 3.8**). UV-vis substrate binding data for the H85Q/F79A mutants indicate much smaller HS shifts than

observed for WT $OleT_{JE}$, consistent with retention of the aqua-ligated LS state in the major fraction of the mutant P450s in the crystal structures.

The lack of any large scale structural changes in the H85Q/F79A $OleT_{JE}$ mutants suggests that that differences in product profiles for the WT and various $OleT_{JE}$ mutants are linked to subtle changes in the active site, possibly related to mobility of active site residues and or substrate. Minor changes in the positioning and dynamic behaviour of the alpha and beta substrate hydrogens might have substantial effects on the product profile, but are unlikely to be distinguished using medium resolution crystallography.

3.5. Discussion

The peroxygenase enzyme P450 BS_β (CYP152A1) was discovered in the late 1990's by Matsunaga *et al*. and shown to catalyze the H_2O_2-dependent 1- (alpha) and 2- (beta) hydroxylation of myristic acid, with the 2-hydroxy myristic acid being the main product (27). Its counterpart P450 SP_α (CYP152B1) was also identified by Matsunaga *et al*. in the same period, and shown to catalyze the alpha-hydroxylation of lipids, producing 2-hydroxy myristic acid from the C14:0 substrate, as well as catalysing 2-hydroxylation of longer chain saturated fatty acids and mono-unsaturated fatty acids (28,29). However, only after studies by Rude *et al*. was the capacity revealed of the related $OleT_{JE}$ enzyme (CYP152L1) to oxidatively decarboxylate fatty acids to form terminal alkenes (9). They also demonstrated that 1-pentadecene was formed not only by H_2O_2-dependent oxidative decarboxylation of palmitic acid in $OleT_{JE}$, but also by P450 BS_β and related P450 enzymes from *Corynebacterium efficiens*, *Kocuria rhizophila* and *Methylobacterium populi* (9,30). $OleT_{JE}$ is the most productive of the fatty acid peroxygenase P450s characterized to date with respect to its generation of alkene products over hydroxylated fatty acids, and the enzyme was also shown to be functional in alkene production when driven by a redox partner system or using a photocatalytic system to generate H_2O_2 (11,14). $OleT_{JE}$ is currently the most studied of the

peroxygenase P450s, and the one with greatest potential for biotechnological applications in production of alkenes for use in e.g. biofuel production (31).

The determination of the crystal structure of $OleT_{JE}$ revealed a high level of similarity with P450 BS_{β} in overall fold and active site structure (10). The $OleT_{JE}$ binding pocket is more extended than that of P450 BS_{β}, explaining its ability to accommodate fatty acids as long as arachidic acid (C20:0). The $OleT_{JE}$ structure highlights structural features common to other P450 enzymes (including the heme binding motif surrounding the conserved cysteine thiolate) as well as key residues involved in interacting with the substrate carboxylate. Amino acid alignment of $OleT_{JE}$ with the sequences of other characterized P450 peroxygenase enzymes reveals that only 48 amino acids are in conserved positions in each of the seven P450 enzymes aligned, which vary in length from 415-428 amino acids (**Figure 3.2**). The substrate carboxylate coordinating $OleT_{JE}$ Arg245 and its adjacent Pro246 are conserved in all these peroxygenases, replacing the acid-alcohol pair (e.g. Asp251/Thr252 in P450cam) that is found in most monooxygenase P450s and involved in protonation of ferric-peroxo and ferric-hydroperoxo catalytic cycle intermediates (32). These key mutations illustrate how these peroxygenases have diverged from monooxygenase P450s, exchanging a dipeptide involved in iron-oxo species protonation for one that is essential for binding the substrate carboxylate. The R245E/L mutants are severely catalytically compromised, consistent with a crucial role of Arg245 in orientating fatty acid carboxylate into a position compatible with efficient decarboxylation/hydroxylation of the substrate. However, these mutants do form small amounts of products (**Table 3.4**). The R245L/E mutants produced most alkene from the C18:0 substrate stearic acid, but negligible amounts from the C20:0 substrate arachidic acid, potentially due to tighter product binding for the longer chain substrate. With one exception, the R245L/E mutants do not exhibit any significant substrate-induced HS ferric heme iron development. Only in the case of R245E with the C10:0 substrate capric acid is there any substantial HS accumulation (*ca* 40%), albeit achieved at high substrate concentration (K_d = 1260 ± 160 μM) (**Table 3.2**). The HS conversion suggest that capric acid does displace Glu245 from a distal position on the heme iron, although only a small proportion of the substrate is

converted to 1-nonene (0.2%) and no significant formation of hydroxylated forms of capric acid was observed (**Figure 3.5C, Table 3.4**).

The H85Q mutant was generated to explore the role of the $OleT_{JE}$ His85 residue, which is replaced by a glutamine in the well characterized P450 BS_{β}, P450 SP_{α} and *Clostridium acetobutylicum* P450 CLA (CYP152A2) enzymes, all of which catalyze predominantly or exclusively fatty acid hydroxylation (33) (**Figure 3.2**). The $OleT_{JE}$ H85Q mutant gives a very similar product profile to the WT enzyme with each substrate tested. However, UV-vis binding studies demonstrate that substrate-induced H85Q HS heme accumulation is considerably lower than in the WT $OleT_{JE}$ in all cases (**Tables 3.2 and 3.4**). EPR spectroscopy confirms much lower accumulation of HS heme iron in arachidic acid-bound H85Q $OleT_{JE}$ compared to the WT enzyme (**Figure 3.6**). However, heme spectral shifts are sufficient to determine K_d values for all substrates with H85Q $OleT_{JE}$, showing that affinity is similar to WT $OleT_{JE}$ for longer chain substrates, but significantly weaker for myristic acid and lauric acid substrates, with negligible heme spin-state change observed on titration of H85Q $OleT_{JE}$ with capric acid (**Table 3.2**). The substantially diminished (or completely absent) extents of substrate-dependent HS shift in the H85Q mutant are consistent with the properties of the SP_{α}, BS_{β} and CLA peroxygenases (18-20,33). The similarity in product profiles between WT and H85Q $OleT_{JE}$ suggests that His85 is not crucial for proton transfer to transient heme iron-oxo species to facilitate C-C bond scission and alkene production, or that alternative pathway(s) exist in the H85Q mutant. A similar conclusion regarding the non-essentiality of a histidine in this position was also reached by Amaya *et al*. in their studies of the *M. populi* $OleT_{JE}$ orthologue (CYP-MP), in which a methionine is located in the relevant position, although the CYP-MP enzyme is a less efficient decarboxylase than $OleT_{JE}$ (30).

$OleT_{JE}$ structural data demonstrated that the His85 imidazole moiety is “sandwiched” between Phe79 and the heme edge (10). The F79A/Y/W mutants were produced and characterized to explore the effects of both removing the aromatic side chain and extending its size and chemical character. All of these mutants showed reduced total activity by comparison with WT and H85Q $OleT_{JE}$, with F79A $OleT_{JE}$ being the most active, forming between 36-43% of the product amount from WT $OleT_{JE}$ in the same unit time for the C14:0-C20:0 substrates, but increasing to 61% and 85% of the amount for the shorter chain capric acid and lauric acid

substrates. The alkenes were the major products with F79A $OleT_{JE}$ and all substrates, with the 3-hydroxylated fatty acid formed in excess over 2-hydroxyated fatty acids for the C10-C18 substrates. For the C20:0 arachidic acid, only 1-nonadecene was formed to a detectable level at 5% of the starting material (**Table 3.4**).

Despite the more "conservative" nature of the F79W and (particularly) the F79Y mutations, the activities of these variants were much lower than observed for the F79A $OleT_{JE}$ mutant with the C10:0-C16:0 substrates. Within this group of substrates, hydroxylated fatty acids are formed in excess over alkenes in all cases except for the F79Y mutant with capric acid (where 1-nonene is the only product observed at 0.3% of the starting material), and total product formation does not exceed 6.5% for the F79Y/W mutants. However, with the C18:0 substrate stearic acid the major product is 1-heptadecene (23%/11% products, respectively), and 1-nonadecene is the only product from arachidic acid (2.5%/3.4% products, respectively).

As is also the case for the H85Q mutant, each of the F79A/Y/W mutants give less substantial HS heme conversions than is seen in WT $OleT_{JE}$ (**Table 3.2**). All the Phe79 mutants also show a similar pattern of decreasing affinity as fatty acid chain length decreases, with capric acid not inducing any significant heme spin-state change in the case of the F79Y/W $OleT_{JE}$ mutants.

Many bacterial P450s exploit a substrate binding-dependent LS-to-HS heme shift to regulate catalytic activity through development of a more positive potential in the substrate-bound form of the heme iron. For example, arachidonic acid binding to P450 BM3 causes an ~140 mV increase in the reduction potential of the ferric heme iron, facilitating electron transfer from the linked cytochrome P450 reductase domain to drive catalysis (34). However, $OleT_{JE}$ shows negligible change in the redox potential of the heme Fe^{III}/Fe^{II} couple on arachidic acid binding (-105 mV and -103 mV vs NHE, respectively, for substrate-free and substrate-bound forms), consistent with its dependence on H_2O_2 for generating reactive iron-oxo species (10). The relatively positive potential in $OleT_{JE}$ is likely related in part to the structural arrangement around the proximal cysteinate ligand. Here, it is notable that a phenylalanine residue (typically seven amino acids before the cysteinate) heavily conserved in monooxygenase P450s is absent in all of the peroxygenases aligned in **Figure 3.2**. Mutations to the relevant Phe393 residue in P450 BM3 result in substantial change in heme iron potential (35,36). Recent

studies have demonstrated that $OleT_{JE}$ turnover can be driven by heterologous redox partner systems, and this is likely facilitated by the large driving force (>230 mV) for electron transfer from NAD(P)H through redox partner proteins and onto the substrate-bound $OleT_{JE}$ heme iron (11,12).

In conclusion, we provide a detailed study of the properties of WT $OleT_{JE}$ and of important active site mutants of this terminal alkene producing enzyme. Our studies show that glutamine substitutes effectively for histidine in the $OleT_{JE}$ H85Q mutant, which has very similar product profiles to the WT enzyme. The major difference lies in the much weaker ability of fatty acid substrates to induce HS heme iron formation in the H85Q mutant (**Figure 3.5B),** a property consistent with those of the P450 SP_{α} and P450 BS_{β} peroxygenases, both of which have a glutamine in the same position (20,38). The data appear to rule out a key role for His85 in proton donation to reactive iron-oxo species in $OleT_{JE}$, and suggest that the system is robust and that alternative protonation pathway(s) may exist. Mutations to $OleT_{JE}$ Phe79 also diminishes substrate-dependent heme HS conversion and weakens affinity for shorter chain (C10:0-C16:0) fatty acid substrates. This translates into much lower product formation for the F79Y/W mutants from these substrates, although the F79A $OleT_{JE}$ is less severely affected, with between 36-85% overall product formation compared to that of WT $OleT_{JE}$ for C10:0-C20:0 substrates (**Table 3.4**). These data indicate that the more “conservative” F79Y/W mutants are actually more disruptive to active site structure and catalytic efficiency than is the F79A mutation, a conclusion consistent with the greater propensity of the F79Y/W mutants to aggregate/precipitate and their failure to crystallize. These properties are shared with the R245L/E variants, in which the substrate carboxylate tethering Arg245 is mutated. Each of the F79Y/W and R245E/L mutations show some extent of heme depletion, with the R245E variant being the worst affected (**Figure 3.4B**). The red shifted (423 nm) Soret band of the oxidized R245E $OleT_{JE}$ protein suggests that the glutamate may coordinate the heme iron in the ferric state. The R245L/E mutants retain low activity, with stearic acid (C18:0) being the best substrate and forming the greatest amounts of alkene product for both mutants (**Table 3.4**). Crystal structure data for the H85Q and F79A mutants reveal only minor alterations to $OleT_{JE}$ active site structure, suggesting that quite subtle changes in the positions of active site amino acids, water molecule(s) and the substrate carboxylate region may be sufficient to trigger

catalysis when H_2O_2 binds to initiate compound 0 formation. Recent studies by Makris' group have revealed how this could lead to substrate hydroxylation by the radical rebound mechanism, involving hydrogen atom abstraction from the substrate by compound I and subsequent "rebound" of the hydroxyl group to the substrate radical (5). However, through their identification and characterization of the transient ferryl-hydroxo compound II, a novel mechanism for substrate decarboxylation was proposed. In this model, compound II abstracts a further electron from the substrate radical to form a diradical or carbocation intermediate (**Figure 3.1**), which decarboxylates to form CO_2 and the n-1 terminal alkene, with protonation of the ferric-hydroxo species restoring the water-coordinated resting form of the heme iron (15,39). Further protein engineering studies on $OleT_{JE}$ are now clearly needed to improve its stability and catalytic performance as an alkene producing enzyme, and to facilitate its biotechnological application.

3.6. References

1. Munro, A. W., Girvan, H. M., and McLean,K. J. (2007) Variations on a (t)heme – novel mechanisms, redox partners and catalytic functions in the cytochrome P450 superfamily. *Nat. Prod. Rep.* **24**, 585-609.

2. Denisov, I. G., Makris, T. M., Sligar, S. G., and Schlichting, I. (2005) Structure and chemistry of cytochrome P450. *Chem. Rev.* **105**, 2253-2277.

3. Raag, R., Martinis, S. A., Sligar, S. G., and Poulos, T. L. (1991). Crystal structure of the cytochrome P-450CAM active site mutant Thr252Ala. *Biochemistry* **30**, 11420-11429.

4. Rittle, J., and Green, M. T. (2010) Cytochrome P450 compound I: capture, characterization, and C-H bond activation kinetics. *Science* **330**, 933-937.

5. Groves, J. T. (2006) High-valent iron in chemical and biological oxidations. *J. Inorg. Biochem*. **100**, 434-437.

6. Joo, H., Lin, Z., and Arnold, F. H. (1999) Laboratory evolution of peroxide-mediated cytochrome P450 evolution. *Nature* **399**, 670-673

7. Li, Q. S., Ogawa, J., and Shimizu, S. (2001) Critical role of the residue size at position 87 in H_2O_2-dependent substrate hydroxylation activity and H_2O_2-inactivation of cytochrome P450BM-3. *Biochem. Biophys. Res. Commun.* **280**, 1258-1261.

8. Hrycay, E. G., and Bandiera, S. M. (2012) The monooxygenase, peroxidase and peroxygenase properties of cytochrome P450. *Arch. Biochem. Biophys.* **522**, 71-89.

9. Rude, M. A., Baron, T. S., Brubaker, S., Alibhai, M., Del Cardayre, S. B., and Schirmer, A. (2011) Terminal olefin (1-alkene) biosynthesis by a novel P450 fatty acid decarboxylase from *Jeotgalicoccus* species. *Appl. Environ. Microbiol.* **77**, 1718-1727.

10. Belcher, J., McLean, K. J., Matthews, S., Woodward, L. S., Fisher, K., Rigby, S. E., Nelson, D. R., Potts, D., Baynham, M. T., Parker, D. A., Leys, D., and Munro, A. W. (2014) Structure and biochemical properties of the alkene producing cytochrome P450 $OleT_{JE}$ (CYP152L1) from the *Jeotgalicoccus* sp. 8456 bacterium. *J. Biol. Chem.* **289**, 6535-6550.

11. Dennig, A., Kuhn, M., Tassoti, S., Thiessenhusen, A., Gilch, S., Bulter, T., Haas, T., Hall, M., and Faber, K. (2015) Oxidative decarboxylation of short-chain fatty acids to 1-alkenes. *Angew. Chem. Int. Ed. Engl.* **54**, 8819-8822.

12. Liu, Y., Wang, C., Yan, J., Zhang, W., Guan, W., Lu, X., and Li, S. (2014) Hydrogen peroxide-independent production of □-alkenes by $OleT_{JE}$ P450 fatty acid decarboxylase. *Biotechnol. Biofuels* **7**:28.

13. McIver, L., Leadbeater, C. Campopiano, D. J., Baxter, R. L., Daff, S., Chapman, S. K., and Munro, A. W. (1998) Characterisation of flavodoxin $NADP^+$-oxidoreductase and flavodoxin: key components of electron transfer in *Escherichia coli*. *Eur. J. Biochem*. **257**, 577-585.

14. Zachos, I., Gassmeyer, S. K., Bauer, D., Sieber, V., Hollmann, F., and Kourist, R. (2015) Photobiocatalytic decarboxylation for olefin synthesis. *Chem. Commun. (Camb)* **51**, 1918-1921.

15. Grant, J. L., Hsieh, C. H., and Makris, T. M. (2015) Decarboxylation of fatty acids to terminal alkenes by cytochrome P450 compound I. *J. Am. Chem. Soc.* **137**, 4940-4943.

16. Zhang, F., Rodriguez, S., and Keasling, J. D. (2011) Metabolic engineering of microbial pathways for advanced biofuels production. *Curr. Opin. Biotechnol*. **22**, 775-783.

17. Yan, J., Liu, Y., Wang, C., Han, B., and Li, S. (2015) Assembly of lipase and P450 fatty acid decarboxylase to constitute a novel biosynthetic pathway for production of 1-alkenes from renewable triacylglycerols and oils. *Biotechnol. Biofuels* **8**:34.

18. Fujishiro, T., Shoji, O., Nagano, S., Sugimoto, H., Shiro, Y., and Watanabe, Y. (2011) Crystal structure of H_2O_2-dependent cytochrome P450SP□ with its bound fatty acid substrate: insight into the regioselective hydroxylation of fatty acids at the alpha position. *J. Biol. Chem.* **286**, 29941-29950.

19. Matsunaga, I., Ueda, A., Sumimoto, T., Ichihara, K., Ayata, M., and Ogura, H. (2001) Site-directed mutagenesis of the putative distal helix of peroxygenase cytochrome P450. *Arch. Biochem. Biophys.* **394**, 45-53.

20. Lee, D. S., Yamada, A., Sugimoto, H., Matsunaga, I., Ogura, H., Ichihara, K., Adachi, S., Park, S. Y., and Shiro, Y. (2003) Substrate recognition and molecular mechanism of fatty acid hydroxylation by cytochrome P450 from *Bacillus subtilis*. Crystallographic, spectroscopic, and mutational studies. *J. Biol. Chem.* **278**, 9761-9767.

21. Girvan, H.M., Marshall, K.R., Lawson, R.J., Leys, D., Joyce, M.G., Clarkson. J., Smith, W.E., Cheesman, M.R., and Munro, A.W. (2004) Flavocytochrome P450 BM3 mutant A264E undergoes substrate-dependent formation of a novel heme iron ligand set. *J. Biol. Chem*. **279**, 23274-23286.

22. McLean, K. J., Warman, A. J., Seward, H. E., Marshall, K. R., Girvan, H. M., Cheesman, M. R., Waterman, M. R., and Munro A. W. (2006) Biophysical characterization of the sterol demethylase P450 from *Mycobacterium tuberculosis*, its cognate ferredoxin and their interactions. *Biochemistry* **45**, 8427-8443.

23. Perera, R., Sono, M., Sigman, J. A., Pfister, T. D., Lu, Y., and Dawson, J. H. (2003) Neutral thiol as a proximal ligand to ferrous heme iron: implications for heme proteins that lose cysteine thiolate ligation on reduction. *Proc. Natl. Acad. Sci. U. S. A*. **100**, 3641-3646.

24. Driscoll, M. D., McLean, K. J., Levy, C., Mast, N., Pikuleva, I. A., Lafite, P., Rigby, S. E., Leys, D., and Munro, A. W. (2010) Structural and biochemical characterization of *Mycobacterium tuberculosis* CYP142: evidence for multiple cholesterol 27-hydroxylase activities in a human pathogen. *J. Biol. Chem*. **285**, 38270-38282.

25. Matsunaga, I., Yamada, A., Lee, D. S., Obayashi, E., Fujiwara, N., Kobayashi, K., Ogura, H., and Shiro, Y. (2002) Enzymatic reaction of hydrogen peroxide dependent peroxygenase cytochrome P450s: kinetic deuterium isotope effect and analyses by resonance Raman spectroscopy. *Biochemistry* **41**, 1186-1892.

26. Joyce, M. G., Girvan, H. M., Munro, A. W., and Leys, D. (2004) A single mutation in cytochrome P450 BM3 induces the conformational rearrangement seen upon substrate binding in the wild-type enzyme. *J. Biol. Chem.* **279**, 23287-23293.

27. Matsunaga, I., Ueda, A., Fujiwara, N., Sumimoto, T., and Ichihra, K. (1999) Characterization of the ybdT gene product of *Bacillus subtilis*: nove fatty acid beta-hydroxylating cytochrome P450. *Lipids* **34**, 841-846.

28. Matsunaga, I., Yokotani, N., Gotoh, O., Kusunose, E., Yamada, M., and Ichihara, K. (1997) Molecular cloning and expression of fatty acid alpha-hydroxylase from *Sphingomonas paucimobilis*. *J. Biol. Chem*. **272**, 23592-23596.

29. Matsunaga, I., Yamada, M., Kusunose, E., Miki, T., and Ichihara, K. (1998) Further characterization of hydrogen peroxide-dependent fatty acid alpha-hydroxylase from *Sphingomonas paucimobilis*. *J. Biochem*. **124**, 105-110.

30. Amaya, J. A., Rutland, C. D., and Makris, T. M. (2016) Mixed regiospecificity compromises alkene synthesis by a cytochrome P450 peroxygenase from *Methylobacterium populi*. *J. Inorg. Biochem*. **158**, 11-16.

31. Herman, N. A., and Zhang, W. (2016). Enzymes for fatty acid-based hydrocarbon biosynthesis. *Curr. Opin. Chem. Biol*. **35**, 22-28.

32. Raag, R., Martinis, S. A., Sligar, S. G., and Poulos, T. L. (1991) Crystal structure of the cytochrome P-450CAM active site mutant Thr252Ala. *Biochemistry* **30**, 11420-11429.

33. Girhard, M., Schuster, S., Dietrich, M., Dürre, P., and Urlacher, V. B. (2007) Cytochrome P450 monooxygenase from *Clostridium acetobutylicum*: a new alpha-fatty acid hydroxylase. *Biochem. Biophys. Res. Commun*. **362**, 114-119.

34. Daff, S. N., Chapman, S. K., Turner, K. L., Holt, R. A., Govindaraj, S., Poulos, T. L., and Munro, A. W. (1997) *Biochemistry* **36**, 13816-13823.

35. Ost, T. W., Miles, C. S., Munro, A. W., Murdoch, J., Reid, G. A., and Chapman, S. K. (2001) Phenylalanine 393 exerts thermodyamic control over the heme of flavocytochrome P450 BM3. *Biochemistry* **40**, 13421-13429.

36. Ost, T. W., Clark, J., Mowat, C. G., Miles, C. S., Walkinshaw, M. D., Reid, G. A., Chapman, S. K., and Daff, S. (2003) Oxygen activation and electron transfer in flavocytochrome P450 BM3. *J. Am. Chem. Soc*. **125**, 15010-15020.

37. Kapust, R.B., Tozser. J., Fox, J.D., Anderson, D.E., Cherry, S., Copeland. T.D., and Waugh, D.S. (2001) Tobacco etch virus protease: mechanism of autolysis and rational design of stable mutants with wild-type catalytic proficiency. *Protein Eng*. **14**, 993-1000.

38. Imai, Y., Matsunaga, I., Kusunonse, E., and Ichihara, K. (2000) Unique heme environment at the putative distal region of hydrogen peroxide-dependent fatty acid alpha-hydroxylase from *Sphingomonas paucimobilis* (peroxygenase P450$_{SP\square}$). *J. Biochem*. **128**, 189-194.

39. Grant, J. L., Mitchell, M. E., and Makris, T. M. (2016) Catalytic strategy for carbon-carbon bond scission by the cytochrome P450 OleT. *Proc. Natl. Acad. Sci. U. S. A*. **113**, 10049-10054.

40. Morrison, J. F. (1969) Kinetics of the reversible inhibition of enzyme catalysed reactions by tight-binding inhibitors. *Biochim. Biophys. Acta* **185**, 269-286.

Chapter 4

Driving alkene production in the peroxygenase P450 $OleT_{JE}$ using a novel hydrogen peroxide-producing fusion protein system

Sarah Matthews[1], Kang Lan Tee[1], Nicholas J. Rattray[1], Kirsty J. McLean[1], David Leys[1], David A. Parker[2], Richard T. Blankley[3] and Andrew W. Munro[1]*

[1]Manchester Institute of Biotechnology, Centre for Synthetic Biology of Fine and Specialty Chemicals (SYNBIOCHEM), School of Chemistry, The University of Manchester, Manchester M1 7DN, United Kingdom. [2]The Westhollow Technology Center, Houston, Texas 77028-3101, USA. [3]Agilent Technologies UK Ltd., Lakeside, Cheadle Royal Business Park, Stockport, Cheshire SK8 3GR, United Kingdom.

Keywords: $OleT_{JE}$, CYP152L1, cytochrome P450, alkene production, hydrogen peroxide, fusion enzymes

4.1. Abstract

Jeotgalicoccus sp. 8456 $OleT_{JE}$ (CYP152L1) is a fatty acid decarboxylase cytochrome P450 that uses hydrogen peroxide (H_2O_2) to catalyse production of terminal alkenes, which are industrially important chemicals with biofuel applications. We report enzyme fusion systems in which the *Streptomyces coelicolor* alditol oxidase (AldO) is linked to $OleT_{JE}$. AldO oxidizes polyols (including glycerol), generating H_2O_2 as a co-product and facilitating its use for efficient $OleT_{JE}$-dependent decarboxylation of fatty acids. AldO activity is regulatable by polyol substrate titration, enabling control over H_2O_2 supply that minimises oxidative inactivation of $OleT_{JE}$ to prolong activity and increase total alkene production. We also describe novel products from secondary turnover of 2-OH and 3-OH myristic acid primary products, expanding the catalytic repertoire of $OleT_{JE}$.

4.2. Introduction

The *Jeotgalicoccus* sp. 8456 $OleT_{JE}$ (CYP152L1) is a member of the cytochrome P450 (P450 or CYP) enzyme superfamily. P450s bind heme *b*, which is proximally coordinated by a cysteine thiolate and typically has a water ligand in the 6^{th} position in the resting state (4). Substrate binding generally displaces the distal water ligand, converting low-spin (LS) ferric heme iron to the high-spin (HS) state (5). The HS heme has a more positive potential, facilitating heme iron reduction by a redox partner, binding of dioxygen to ferrous iron and subsequent reduction and protonation steps resulting in formation of the ferryl-oxo porphyrin radical species compound I, which is the major substrate oxidizing species in P450s. P450s perform numerous oxidative (and other) reactions, including hydroxylation, demethylation, epoxidation and dehydrogenation of a vast substrate range (6).

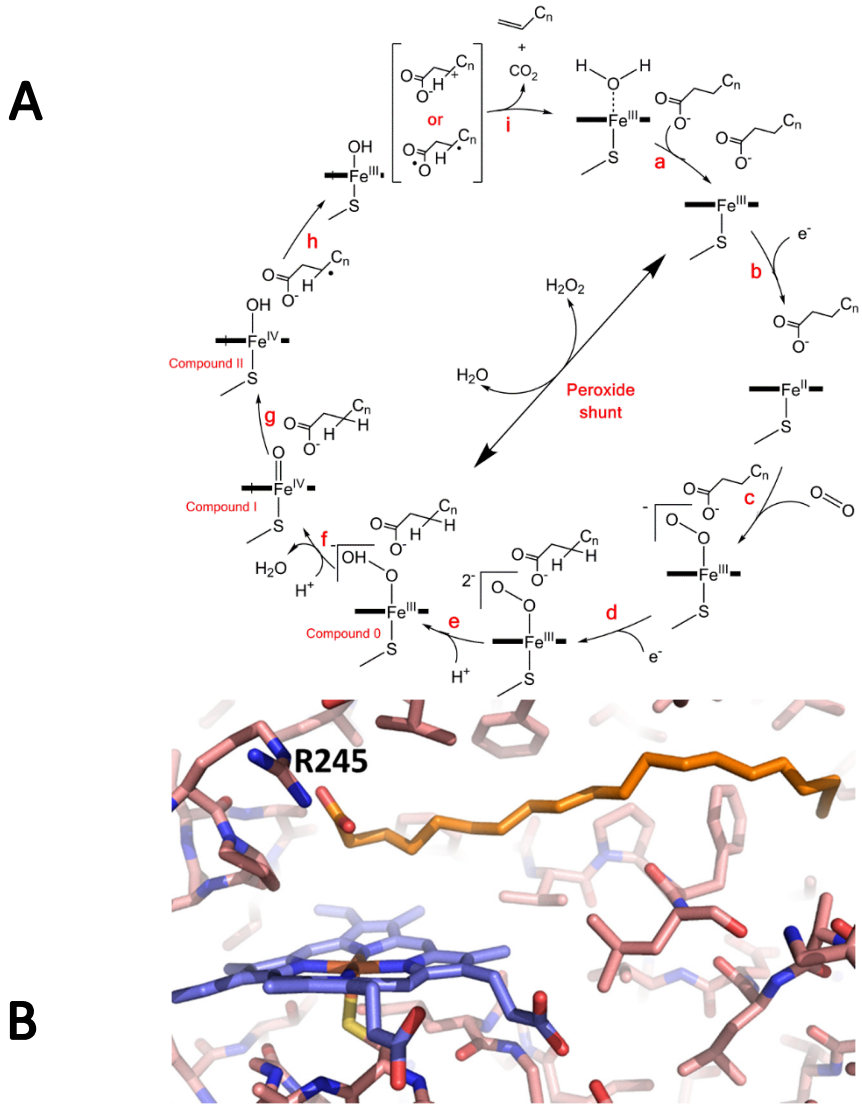

Figure 4.1. P450 catalytic cycle and active site structure of $OleT_{JE}$. **Panel A** shows a cytochrome P450 catalytic cycle, illustrating how $OleT_{JE}$ utilises the peroxide shunt pathway to catalyse fatty acid decarboxylation to form terminal alkenes. In its ferric resting state, the $OleT_{JE}$ heme iron is axially co-ordinated by cysteine thiolate and a water molecule. Upon addition of fatty acid (a), the axial water molecule is displaced, and the heme iron converts from a low spin (LS) to a high spin (HS) state (2). Addition of H_2O_2 to $OleT_{JE}$ initiates the peroxide shunt, forming a ferric-hydroperoxo intermediate (Compound 0, reaction indicated by the arrow crossing the cycle). Protonation and dehydration of Compound 0 (f), yields a reactive ferryl (Fe^{IV})-oxo, porphyrin radical cation (Compound I), which has been observed in $OleT_{JE}$ using single turnover stopped-flow absorption spectroscopy (11). $OleT_{JE}$ then catalyses either decarboxylation of the fatty acid (g-i) to form terminal alkene (the major reaction), or hydroxylates the substrate at the α- or β-position (not shown). Hydroxylation involves Compound I-mediated hydrogen abstraction from a substrate CH group (forming Compound II, Fe^{IV}-OH), and hydroxylation by radical rebound with restoration of the ferric heme (28). However, decarboxylation likely occurs through the further abstraction of an electron from the substrate radical by Compound II (h), producing an unstable substrate carbocation or diradical that decarboxylates to generate the alkene (12). The alkene product then dissociates, releasing CO_2 (i), and a protonation step restores the ferric heme iron to its resting, water ligated form. $OleT_{JE}$ can also function using redox partner systems, in which case two electron transfer steps and one protonation step are required to convert the substrate-bound, ferric species to compound 0 [(b)-(e)] (27) (29). Steps (f)-(i) then occur as described above following the peroxide shunt process (3). **Panel B** shows the active site of $OleT_{JE}$ bound to arachidic acid (C20:0), with substrate shown in orange. The heme is coloured in blue, and is proximally coordinated to Cys365 thiolate. Also shown is arachidic acid (orange) and the interaction between its carboxylate and Arg245.

However, not all P450s are redox partner-dependent. Peroxygenase P450s function efficiently using only hydrogen peroxide (H_2O_2) to drive catalysis. Early studies focused on the peroxygenases P450 BS□ (CYP152A1) from *Bacillus subtilis* and P450 SP_α (CYP152B1) from *Sphingomonas paucimobilis*. Initial studies suggested these enzymes acted as fatty acid hydroxylases, using the "peroxide shunt" mechanism to convert substrate-bound, ferric P450 directly to its ferric-hydroperoxo (compound 0) state, which then undergoes rapid protonation and dehydration to form compound I (7,8) (**Figure 4.1A**). However, Rude et al. subsequently demonstrated that P450 BS□ also produced n-1 terminal alkenes alongside 2-OH and 3-OH fatty acids, suggesting that other CYP152 peroxygenases might also produce alkenes through oxidative decarboxylation of fatty acids (9). The *Jeotgalicoccus* $OleT_{JE}$ P450 was then identified as a more efficient alkene producer, catalysing oxidative decarboxylation of fatty acids from ~C10-C20, generating terminal alkenes as major products and smaller amounts of 1-OH and 2-OH fatty acids formed (9,10). Terminal alkenes have industrial uses in plastics, lubricants and as feedstocks for other compounds, such as alcohols and surfactants (11). Alkenes are also potential fuels, making $OleT_{JE}$ an attractive candidate for production of "drop-in" biofuels (12).The structure and catalytic mechanism of $OleT_{JE}$ have been characterized (13-15), revealing how the fatty acid carboxylate binds close to the P450 heme (**Figure 4.11B**), and the different mechanisms by which $OleT_{JE}$ produces alkenes and hydroxylated fatty acids. $OleT_{JE}$ was reported to catalyse 97% conversion of 200 µM myristic acid (C14:0) in the presence of 500 µM H_2O_2 (10). However, on an industrial scale excess H_2O_2 may inhibit enzymatic activity (16). This phenomenon was demonstrated in the *Clostridium actetobutylicum* peroxygenase P450 CLA (CYP152A2) where, despite high peroxygenase activity (200 min^{-1}) with myristic acid, use of 200 µM H_2O_2 led to enzyme inactivation in 2-4 minutes (17). Also, using H_2O_2 in a bacterial cell-based alkene-producing system may not be viable, as H_2O_2 levels of only 2 µM may cause growth inhibition of *E. coli* (18). Girhard et al. described a novel method of driving peroxygenase catalysis, using light to excite flavin cofactors with ethylenediaminetetraacetic acid (EDTA) as an electron donor. Electron transfer from reduced flavins then converts dioxygen to H_2O_2. The approach was successful with P450 CLA and P450 BS_β, where near-

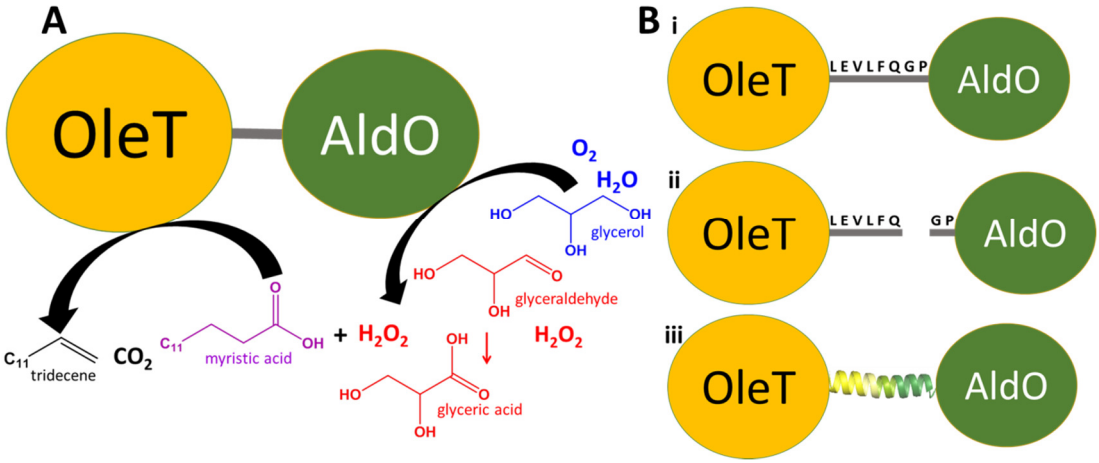

Figure 4.2. Schematic of $OleT_{JE}$/AldO constructs. **Panel A** shows how an $OleT_{JE}$-AldO fusion system can use *S. coelicolor* AldO to oxidise glycerol (or another alditol substrate), forming H_2O_2 as a co-product. H_2O_2 is then used by $OleT_{JE}$ to decarboxylate fatty acids such as myristic acid, producing terminal alkenes as the major product. Terminal alkenes have important industrial uses, including as "drop-in" biofuels. **Panel B** shows the fusion constructs used in this work. (i) $OleT_{JE}$-HRV3C-AldO. $OleT_{JE}$ and AldO are fused by a HRV3C-cleavable linker, enabling stoichiometric production of $OleT_{JE}$ and AldO, as shown in (ii). (iii) $OleT_{JE}$-αhelix-AldO. In this construct $OleT_{JE}$ and AldO are linked by an $A(EAAK)_4LEA(EAAK)_4A$ α-helix.

complete conversion of 200 µM myristic acid was observed using flavin mononucleotide (FMN) (19). The method also worked with $OleT_{JE}$, where 99% of stearic acid (C18:0) substrate was oxidised using the light-driven system, a much higher conversion rate than achieved by direct H_2O_2 addition either at the start of the reaction, or stepwise during the reaction (16). However, this light driven approach produced only low conversion levels for the shorter chain fatty acids lauric acid (C12:0) and myristic acid (16).

In this manuscript, we present novel systems for alkene production in which the H_2O_2-forming alditol oxidase (AldO) from *Streptomyces coelicolor* is fused to $OleT_{JE}$. AldO is a 45.1 kDa flavoprotein containing covalently bound flavin adenine dinucleotide (FAD) (20). AldO catalyses oxidation of the primary alcohol moiety of alditols using molecular oxygen, and forms the aldose product and H_2O_2. AldO oxidizes several polyol substrates, including glycerol, xylitol, sorbitol and diols such as 1,2-propanediol and 1,2-hexanediol (21). Our rationale for creating the $OleT_{JE}$-AldO fusion is that the H_2O_2 coproduct from AldO could be used to drive fatty acid decarboxylation by $OleT_{JE}$ and that the system could be regulated through measured alditol substrate additions to maintain H_2O_2 concentrations compatible with efficient substrate

conversion, while minimising heme destruction by excess H_2O_2. We present catalytic data showing the efficiency of the reactions, as well as using $OleT_{JE}$ and its fusion systems to identify novel products of $OleT_{JE}$-dependent fatty acid oxidation.

4.3. Materials and Methods

4.3.1 Gene Cloning

The $OleT_{JE}$ (*CYP152L1*) gene from *Jeotgalicoccus* sp 8456 was codon optimised for expression in *E. coli*, synthesised (Genscript, Cherwell UK) and cloned into pET15b at NdeI/BamHI sites. The construct contains an N-terminal polyhistidine tag and a TEV cleavage site 5' to the NdeI cleavage site. The alditol oxidase (AldO) gene from *Streptomyces coelicolor* A3(2) with an N-terminal polyhistidine tag and TEV cleavage site was codon optimised for *E. coli* expression and synthesised (Genscript), prior to cloning into pET24b at NdeI/BamHI sites.

Cloning of the $OleT_{JE}$-HRV3C-AldO fusion protein gene construct (linker sequence: GSGLEVLFQGPGSGGGGS with cleavage site underlined) was performed by amplification of $OleT_{JE}$/AldO genes from pET15b/pET24b plasmids using primers $OleT_{JE}$-For: GTA TTT CCA AGG CCA TAT G, $OleT_{JE}$-Rev: CCC CTG GAA CAG AAC TTC CAG ACC AGA ACC GGT GCG GTC CAC AAC (underlined region signifies overhang), AldO-For: GAA GTT CTG TTC CAG GGG CCC GGA TCT GGC GGC GGC, and AldO-Rev: ATT GCG GAT CCT TAT CAG CCG GCC AG using Phusion High Fidelity DNA polymerase (NEB, Hitchin UK). The 5'-$OleT_{JE}$ and AldO-3' genes were then joined with an HRV3C cleavage site by PCR using primers GTA TTT CCA AGG CCAvTAT G (v corresponds to NdeI cleavage site) and ATT GCG GAT CCvT TAT CAG CCG GCC AG (corresponds to BamHI cleavage site), respectively. The $OleT_{JE}$-HRV3C-AldO gene was then cloned into the pET15b-TEV plasmid at NdeI/BamHI sites (**Figure 4.2**).

The $OleT_{JE}$-αhelix-AldO construct was produced using a NEB HiFi DNA assembly Kit (NEB) according to manufacturer's instructions. DNA encoding the $A(EAAAK)_4LEA(EAAAK)_4A$ α-helix was synthesised (Eurofins, Manchester UK). The pET15b $OleT_{JE}$-HRV3C-AldO plasmid

was used as a template, and primers For: ATG TCG GAT ATT ACC GTT ACG and Rev: GGT GCG GTC CAC AAC TTC were used to amplify the backbone. The α-helix insert was amplified with backbone overhangs of 15 bp using primers GTT GTG GAC CGC ACC GCT GAG GCT GCC GCT AAG and ACG GTA ATA TCC GAC ATC GCT TTT GCT GCT GCT TC (**Figure 4.2**).

4.3.2 Gene expression and protein purification

The pET15b-OleT$_{JE}$, pET15b-OleT$_{JE}$-HRV3C-AldO and pET15b-OleT$_{JE}$-αhelix-AldO plasmids were transformed into *E. coli* C41 (DE3) and grown in 500 ml 2xYT cultures. Cultures were shaken at 200 rpm at 37°C until an OD_{600} of 0.5. 500 μM δ-aminolevulinic acid (ΔALA) was then added and gene expression induced with 100 μM isopropyl 1-thio-ß-D-galactopyranoside (IPTG). Temperature was then decreased to 25°C for pET15b-OleT$_{JE}$ transformed cells, and to 20°C for cells transformed with pET15b-OleT$_{JE}$-HRV3C-AldO and pET15b-OleT-αhelix-AldO constructs. Cells were grown for a further 20 hours before harvesting by centrifugation at 6000 rpm at 4°C in a JLA-8.1 rotor using an Avanti J-26 XP centrifuge. Cell pellets were washed with ice-cold 100 mM KPi buffer (pH 8), centrifuged again and stored at -80°C until required for purification.

4.3.3 Purification of OleT$_{JE}$, OleT$_{JE}$-HRV3C-AldO, OleT$_{JE}$-αhelix-AldO and P450 BM3

OleT$_{JE}$ expressing cells were resuspended in 100 mM KPi, 1 M NaCl, 10% glycerol (pH 8) (buffer A). OleT$_{JE}$-HRV3C-AldO and OleT$_{JE}$-αhelix-AldO expressing cells were resuspended in 100 mM KPi, 750 mM NaCl (pH 8) (buffer B). To each cell suspension, SigmaFAST Protease Inhibitor Cocktail Tablets (EDTA-Free), 100 μg/ml DNase I and lysozyme were added (Sigma-Aldrich, Poole UK). Cell suspensions were sonicated for 40 minutes at 10 s on, 50 s off, at 40% amplitude using a Bandelin Sonopuls sonicator. The cell homogenate was then centrifuged at 20,000 rpm for 90 minutes at 4°C using a JA-25.5 rotor.

For $OleT_{JE}$, 5 mM imidazole and nickel-iminodiacetic acid (Ni-IDA) chromatographic medium (Generon, Maidenhead UK) (10 ml/100 g cell pellet) was added to the supernatant and stirred overnight at 4℃. The resin was packed into a column, washed with 20 column volumes (CV) of 50 mM imidazole in buffer C (100 mM KPi, 750 mM NaCl, 10% glycerol [pH 8]) and the flow-through collected. After washing with 2 CV of 150 mM imidazole in buffer C, $OleT_{JE}$ protein was eluted in 175 mM imidazole in buffer C and extensively dialysed into buffer C to remove imidazole and fatty acids retained from *E. coli*. $OleT_{JE}$ was then concentrated using a Vivaspin (30,000 MWCO, GE Healthcare, Little Chalfont UK) and transferred into 100 mM KPi, 750 mM NaCl, 20% glycerol (pH 8) (buffer D) using a PD10 Desalting Column (GE Healthcare). The protein was then flash frozen in liquid nitrogen and stored at -80℃ until required.

For $OleT_{JE}$-HRV3C-AldO and $OleT_{JE}$-αhelix-AldO, 5 mM imidazole and Ni-IDA (5 ml/100 g) was added to cell supernatants and samples stirred at 4℃ for 2 hours. The resin was washed using 20 CV of 50 mM imidazole in buffer B and the flow-through retained. Proteins were eluted with 250 mM imidazole in buffer B, and incubated overnight at 4℃ with ~500 U of a S219V TEV protease variant (expressed using plasmid pRK793 from David Waugh's lab, Addgene plasmid no 8827) (22). The protein was exchanged into buffer B using a desalting column, and added to a bed of Ni-IDA resin. His-tag cleaved protein was eluted with 20 mM imidazole in buffer B, concentrated using a Vivaspin (30,000 MWCO) and exchanged into buffer B using a PD10 desalting column. Aliquots were frozen in liquid nitrogen and stored at -80℃.

The *Bacillus megaterium* P450 BM3 protein was expressed and purified as described previously (23).

4.3.4 Hydrogen peroxide tolerance of P450 enzymes

UV-visible spectroscopy was carried out on a Cary 60 UV-visible spectrophotometer (Agilent, Cheadle UK). Oxidative modification of $OleT_{JE}$ and P450 BM3 heme was measured at H_2O_2 concentrations of 10, 25, 50, 125, 250, 500 and 1000 μM. Stock H_2O_2 concentrations were

prepared at 100x final concentration. After H_2O_2 addition, P450 spectra were recorded every 2 minutes for 1 hour at 10°C. Soret peak intensity (418 nm for $OleT_{JE}$, 419 nm for BM3) was plotted against time. For $OleT_{JE}$, data were fitted accurately using a single exponential decay function, and for BM3 data fitted best using a double exponential decay function.

4.3.5 *In vitro* substrate turnover reactions with fusion proteins

Reactions were carried out in buffer B. To cleave $OleT_{JE}$-HRV3C-AldO, HRV3C (Novagen, Feltham UK) was added at 1 U/100 µg $OleT_{JE}$-HRV3C-AldO, and incubated for 1 hour at 4°C. Proteins were exchanged into buffer B using a PD10 desalting column before starting reactions.

For reactions with $OleT_{JE}$-HRV3C-AldO and $OleT_{JE}$-αhelix-AldO, 0.5 ml reactions were set up with 5 µM enzyme, 500 µM myristic acid and varying concentrations of different AldO substrates. Initial studies tested glycerol (3%, 1%, 0.1% and 0.01%), xylitol (2 mM and 10 mM) and sorbitol (2 mM and 10 mM). Reactions were incubated for 20 minutes. Time dependence studies were also done using 1% glycerol at time points of 0.5, 1, 2, 5, 10, 20 and 30 minutes. Additional reactions were done with 0.1% and 0.01% glycerol with incubations for 20 minutes. Time point experiments and reactions with 0.1% and 0.01% glycerol were done in duplicate with incubation at 27°C and shaking at 700 rpm, using 5 µM enzyme and 500 µM myristic acid in a total volume of 0.5 ml.

All reactions were stopped with 20 µl of 37% HCl. Internal standards 1-pentadecene, palmitic acid (C16:0), 2-OH palmitic acid and 3-OH palmitic acid were added, and reactions were extracted with an equal volume of dichloromethane (DCM). The DCM layer was removed and dried with anhydrous $MgSO_4$. The DCM extract was mixed with an equal volume of N,O-*bis*(trimethylsilyl)trifluoroacetamide (BSTFA) containing 1% trimethylchlorosilane (TMCS) and incubated at 60°C for 45 minutes to derivatise fatty acids.

4.3.6. *In vitro* $OleT_{JE}$ enzymatic reactions with products

To investigate $OleT_{JE}$'s ability to further oxidize initial reaction products, 200 μM 1-tridecene, 200 μM α-OH myristic acid or 200 μM β-OH-myristic acid was incubated with either (i) 1 μM $OleT_{JE}$/500 μM H_2O_2 or (ii) 5 μM $OleT_{JE}$-HRV3C-AldO/1% glycerol. Reaction mixtures were incubated for 30 minutes at 27℃ before acidification with 20 μl 37% HCl, and extraction, drying and derivatisation as described previously.

4.3.7. GC/Q-TOF

After derivatisation, 1 μl of sample was injected onto an Agilent 7200 GC/QTOF with 7890B GC, installed with a VF-5ms 30 m x 250 mm x 0.25 mm column. The front inlet was set at 250℃, and a split ratio of 25:1 was used. Column flow was set at 1.2 ml/min, and the oven was held at 100℃ for 1 minute before being ramped at 25℃/min until 200℃. Ramping was then decreased to 15 ml/min until 325℃, and held for 2 minutes. Electronic ionization was used, and m/z ratios of 40-500 were recorded at 5 Hz, at a temperature of 230℃.

Quantitation of tridecene, myristic acid, α-OH myristic acid and β-OH myristic acid was performed using external standard calibration curves and structural analogue internal standards.

4.3.8. Fusion protein kinetics

To determine reaction kinetics for (i) $OleT_{JE}$-αhelix-AldO and (ii) intact and cleaved forms of $OleT_{JE}$-HRV3C-AldO, the relevant decreases in myristic acid substrate concentration were plotted against reaction time. Data were fitted using a single exponential function.

4.4. Results

4.4.1. Hydrogen peroxide tolerance

The P450 peroxygenase $OleT_{JE}$ uses H_2O_2 to drive the decarboxylation of fatty acids. However, excess H_2O_2 causes oxidative damage to the heme and protein. To investigate this phenomenon, H_2O_2 was added to $OleT_{JE}$ at concentrations of 10, 25, 50, 125, 250, 500 and 1000 μM, and decreases in Soret peak intensity were monitored. To compare the effects of H_2O_2 on $OleT_{JE}$ to those of a typical P450 monooxygenase, the same experiment was

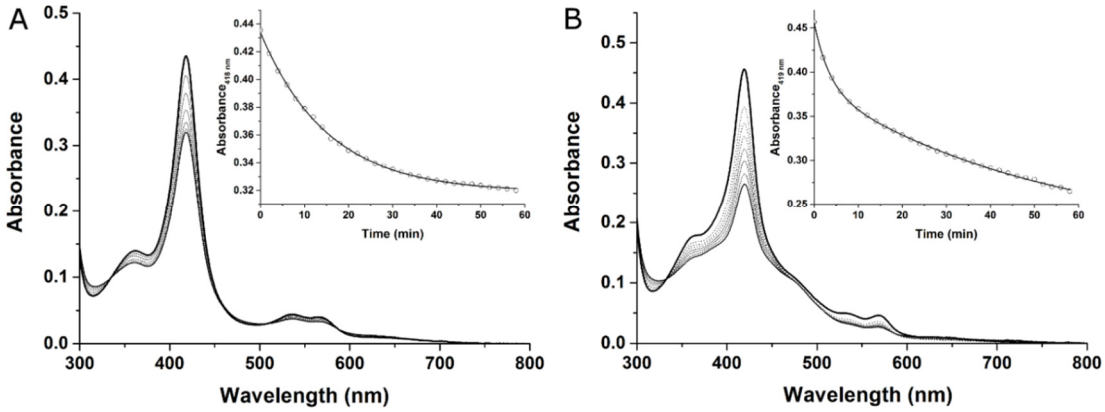

Figure 4.3. P450 H_2O_2 tolerance. Panels A and **B** show the UV-visible spectra of $OleT_{JE}$ and BM3 (4.5 μM and 4 μM, respectively) before (thick solid line) after the addition of 1 mM H_2O_2. These spectra show heme spectral decrease due to H_2O_2-mediated oxidation of the prosthetic group, measured over 1 hour at 2 minute intervals. Rate constants for heme oxidation were obtained for the two proteins at H_2O_2 concentrations of 1, 0.5 0.25, 0.125 and 0.05 mM H_2O_2. For $OleT_{JE}$, data were fitted using a single exponential function, whereas for BM3 data were fitted using a double exponential function. Fitting of the heme absorbance change *versus* time data is shown in panel insets.

performed with P450 BM3 (BM3). Heme modification was measured at intervals over a period of one hour, and at 10°C in order to minimise temperature-dependent effects on protein stability (**Table 4.1**). **Figure 4.3** shows time-dependent changes in UV-visible spectra for $OleT_{JE}$ and BM3, demonstrating Soret band absorbance decreases indicative of heme modification.

H_2O_2 (mM)	$OleT_{JE}$		BM3			
	k (min^{-1})	A	k_1 (min^{-1})	A1	k_2 (min^{-1})	A2
1	(6.55 ± 0.09) x 10^{-2}	(11.5 ± 0.1) x 10^{-2}	(29.0 ± 1.5) x 10^{-2}	(7.2 ± 0.3) x 10^{-2}	(1.9 ± 0.2) x 10^{-2}	(17.6 ± 0.6) x 10^{-2}
0.5	(5.71 ± 0.13) x 10^{-2}	(6.3 ± 0.1) x 10^{-2}	(25.0 ± 2.1) x 10^{-2}	(4.9 ± 0.3) x 10^{-2}	(3.1 ± 0.2) x 10^{-2}	(14.7 ± 0.2) x 10^{-2}
0.25	(5.06 ± 0.28) x 10^{-2}	(5.1 ± 0.1) x 10^{-2}	(14.5 ± 1.3) x 10^{-2}	(3.1 ± 0.3) x 10^{-2}	(1.9 ± 0.2) x 10^{-2}	(11.5 ± 0.3) x 10^{-2}
0.125	(6.83 ± 0.61) x 10^{-2}	(2.2 ± 0.1) x 10^{-2}	(12.4 ± 1.5) x 10^{-2}	(2.7 ± 0.4) x 10^{-2}	(0.3 ± 0.3) x 10^{-2}	(41.9 ± 40.1) x 10^{-2}
0.05	ND	ND	(2.5 ± 0.1) x 10^{-2}	(7.0 ± 0.2) x 10^{-2}	---	---
0.025	ND	ND	ND	ND	ND	ND

Table 4.1. Rates of oxidative modification of $OleT_{JE}$ and P450 BM3 heme by H_2O_2. Rate constants for heme oxidation (k) and associated absorbance amplitudes (A) for heme absorption change are presented for $OleT_{JE}$ and BM3 across a range of H_2O_2 concentrations. $OleT_{JE}$ data were fitted using a single exponential function. BM3 data in most cases were fitted accurately using a double exponential function and the two rate constants (k_1 and k_2) and corresponding amplitudes (A1 and A2) are presented. ND indicates that rate constants could not be determined accurately due to small amplitudes with lower concentrations of H_2O_2. In the case of BM3 at 0.05 mM H_2O_2, data were fitted best using a single exponential function.

The decrease in Soret intensity (418 nm for $OleT_{JE}$, 419 nm for BM3) was plotted against time, and a rate constant (k) was derived for the heme oxidation process. For $OleT_{JE}$, data were fitted using a single exponential function. For BM3, data were fitted accurately using a double exponential function. This is possibly due to retention of lipid in a small proportion of the enzyme, and its influence in shielding the heme.

The heme oxidation rate constant (k) is consistently lower for $OleT_{JE}$ compared to the BM3 k_1, the higher of the two rate constants derived from a biexponential data fit. The difference in H_2O_2 tolerance becomes more apparent at higher H_2O_2 concentrations, and at 1 mM H_2O_2 the rate constant is 4.5 times greater for BM3 than for $OleT_{JE}$. These data indicate that $OleT_{JE}$ has a greater tolerance to H_2O_2 than BM3, consistent with this P450 peroxygenase being able to withstand destructive effects of H_2O_2 better than a typical P450 monoxygenase. However, substantial $OleT_{JE}$ Soret peak loss occurs at 1 mM H_2O_2 (**Figure 4.3**). This concentration of H_2O_2 is typically used in turnover experiments performed with e.g. 0.5 mM fatty acid substrate.

In this respect, more efficient fatty acid oxidation (with less heme destruction) could be achieved in a catalytic system where H_2O_2 is produced (and enzymatically consumed) continuously at a level that is non-destructive to P450 heme.

4.4.2. Construction of $OleT_{JE}$-HRV3C-AldO and $OleT_{JE}$-αhelix-AldO fusion proteins

Two fusion proteins ($OleT_{JE}$-HRV3C-AldO and $OleT_{JE}$-αhelix-AldO) were constructed by linking $OleT_{JE}$ to *Streptomyces coelicolor* AldO. In these systems, AldO produces H_2O_2 from oxidation of substrates including glycerol, sorbitol and xylitol. H_2O_2 then drives fatty acid decarboxylation by $OleT_{JE}$. The $OleT_{JE}$-HRV3C-AldO fusion contains a short peptide linker including a HRV3C cleavage site. The protease cleavage site enables production of stoichiometric amounts of free $OleT_{JE}$ and AldO, allowing for comparative analysis of the activity of the separated enzymes. The $OleT_{JE}$-HRV3C-AldO protein was produced with a yield of ~2.5 mg of protein/L culture. Fusing human growth hormone (hGH) and transferrin (Tf) with a rigid helical linker proved more successful for protein production by comparison to hGH/Tf fusions without a helical linker (24,25). We adopted a similar strategy to produce the $OleT_{JE}$-αhelix-AldO fusion enzyme, which was also purified with a yield of ~2.5 mg/L. **Figure 4.4** shows SDS-PAGE gels of both constructs following purification by nickel affinity chromatography, TEV cleavage of the polyhistidine tag, and separation of the untagged fusion protein using reverse nickel column chromatography.

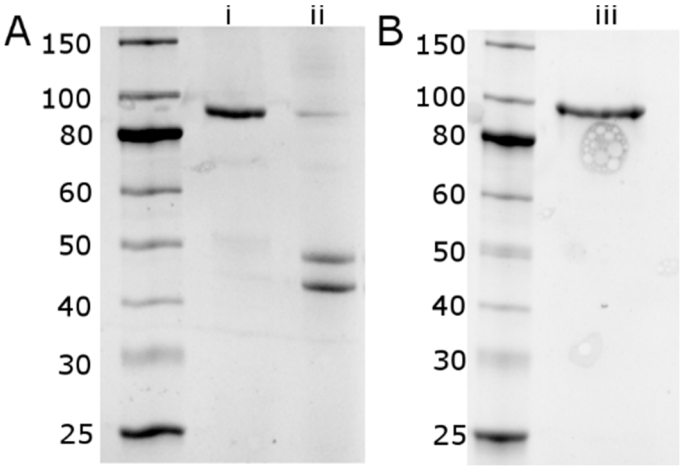

Figure 4.4: SDS-PAGE analysis of purified $OleT_{JE}$ fusion proteins. **Panel A** shows intact $OleT_{JE}$-HRV3C-AldO (i) and cleaved $OleT_{JE}$-HRV3C-AldO (ii), following incubation of the fusion protein with HRV3C protease for 1 hour at 4°C. **Panel B** shows purified $OleT_{JE}$-αhelix-AldO (iii). Samples were resolved by SDS-PAGE using a 10% polyacrylamide gel. The first lane in each case shows protein markers (NEB Broad Range

Figure 4.4A also shows $OleT_{JE}$-HRV3C-AldO following inter-domain cleavage using HRV3C protease.

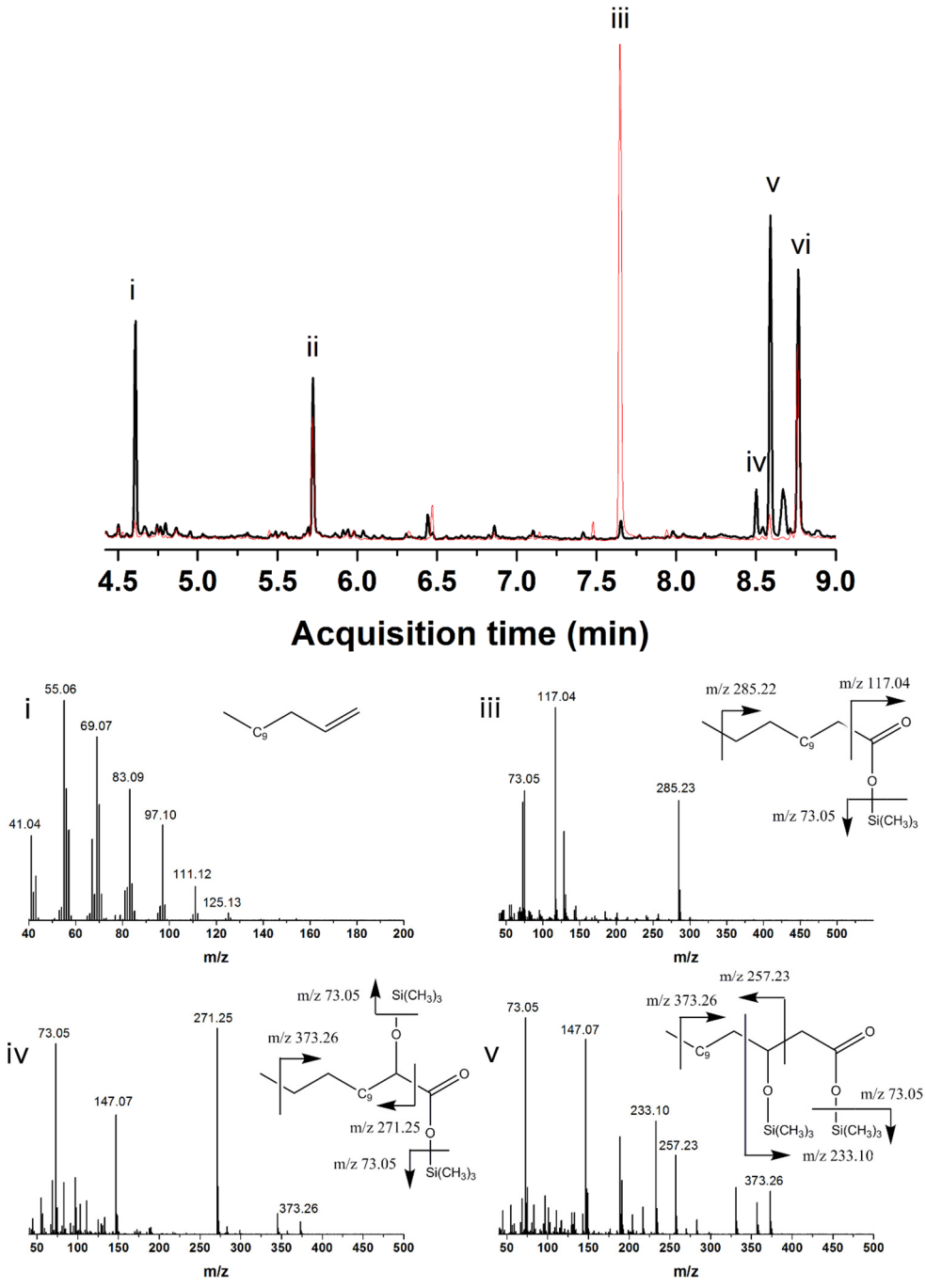

Figure 4.5: GC/MS chromatogram showing products formed by the $OleT_{JE}$-αhelix-AldO fusion protein with myristic acid substrate. The reaction shown was performed at 27 ℃ with shaking at 700 rpm, and with 0.5 mM myristic acid, 5 µM $OleT_{JE}$-αhelix-AldO fusion protein and 0.1% glycerol. The black chromatogram shows reaction products formed with the reaction stopped at 20 minutes. The red chromatogram shows a control reaction containing the same components, but also including catalase (40 units) to remove H_2O_2. The peaks relate to the following compounds: i) tridecene, ii) pentadecene (internal standard), iii) myristic acid, iv) 2-OH myristic acid, v) 3-OH myristic acid and vi) palmitic acid (internal standard).

4.4.3. Driving decarboxylation of fatty acids with different AldO substrates

Reactions were set up with 5 μM $OleT_{JE}$-HRV3C-AldO, 0.5 mM myristic acid and different AldO substrates (glycerol, sorbitol and xylitol). In addition, one reaction was set up with 500 μM H_2O_2 and 5 μM $OleT_{JE}$-HRV3C-AldO. A control reaction in absence of substrate was also set up, including 40 units of catalase to remove any H_2O_2. As shown in **Table 2**, all AldO substrates gave high levels of turnover, facilitating myristic acid oxidation levels of 91-95%, compared to 87% in the case where H_2O_2 was added directly to substrate-bound $OleT_{JE}$. As glycerol gave marginally the highest levels of substrate oxidation, it was used as the AldO substrate for further experiments.

Substrate	Fatty acid conversion (%)
0.5 mM H_2O_2	87
1% glycerol	95
3% glycerol	94
2 mM sorbitol	93
10 mM sorbitol	93
2 mM xylitol	91
10 mM xylitol	92

Table 4.2. $OleT_{JE}$-dependent oxidation of myristic acid with different substrates. The percentage conversion of 0.5 mM myristic acid by the $OleT_{JE}$-HRV3C-AldO fusion enzyme is shown using H_2O_2 and various AldO substrates at different concentrations. A control reaction using 40 units of catalase, myristic acid and $OleT_{JE}$-HRV3C-AldO confirmed that myristic acid oxidation did not occur in the absence of H_2O_2. Myristic acid product analysis was done using GC/MS.

4.4.4. Time-dependent oxidation of fatty acids using fusion proteins

Reactions were set up with 1% glycerol, 0.5 mM myristic acid, and 5 μM of (i) intact $OleT_{JE}$-HRV3C-AldO, (ii) cleaved $OleT_{JE}$-HRV3C-AldO or (iii) $OleT_{JE}$-αhelix-AldO. Myristic acid concentration was plotted against time, and rate constants (*k*) determined for fatty acid conversion. The highest rate was obtained for $OleT_{JE}$-αhelix-AldO (0.48 ± 0.02 min^{-1}). $OleT_{JE}$-HRV3C-AldO and the HRV3C-cleaved forms showed conversion rates of 0.38 ± 0.05 min^{-1} and 0.15 ± 0.01 min^{-1}, respectively, indicating that the fused enzymes have improved activity over their separate entities at the same concentration. **Figure 4.5** shows GC-MS analysis of myristic acid products formed by the $OleT_{JE}$-αhelix-AldO fusion protein.

The formation of products over time was also monitored for the conditions (i)-(iii). In all cases, tridecene was the major product after 20 minutes (**Table 4.3**). However, for both intact and cleaved $OleT_{JE}$-HRV3C-AldO, 3-OH myristic acid is initially produced at high levels, and is the

major product at 1 minute. Levels of 2-OH and 3-OH myristic acid decreased after 2 minutes in all three conditions. We hypothesised that, with continued production of H_2O_2 by AldO-dependent oxidation of glycerol, the hydroxylated fatty acids are further converted into other products. This finding suggests that all the $OleT_{JE}$ constructs used remain active throughout the assays and are able to bind and further oxidise the primary products of the reaction.

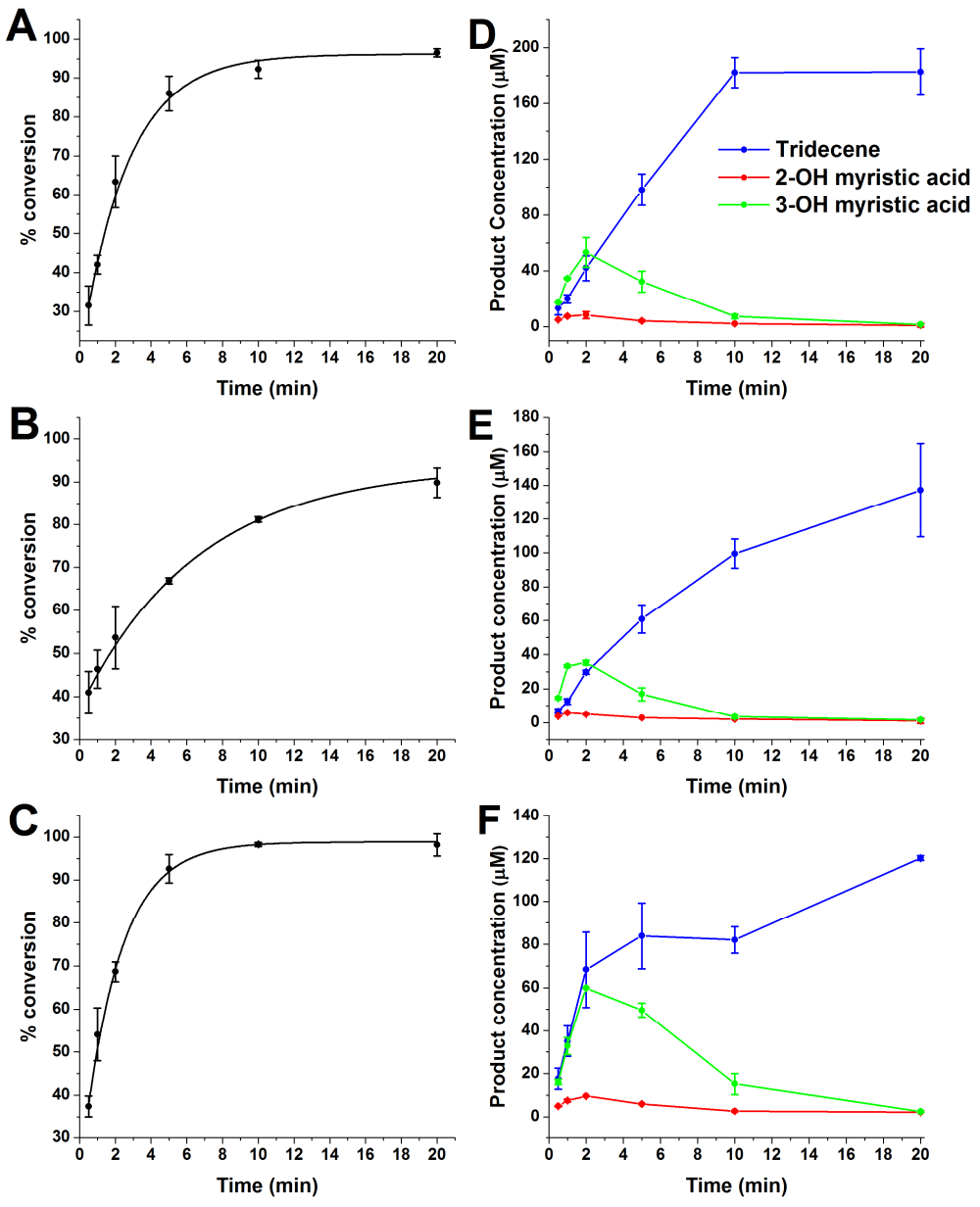

Figure 4.6. Time dependence of myristic acid conversion and product formation at 1% glycerol. **Panels A, B and C** show the extents of myristic acid conversion using GC/MS data collected at 0.5, 1, 2, 5, 10 and 20 minutes for intact $OleT_{JE}$-HRV3C-AldO, cleaved $OleT_{JE}$-HRV3C-AldO and $OleT_{JE}$-αhelix-AldO, respectively. **Panels D, E and F** show concentrations of tridecene, 2-OH myristic acid and 3-OH myristic acid in samples taken over 20 minutes for the same enzymes. Duplicate samples were tested and standard errors are shown.

4.4.5. Optimising glycerol concentration

To establish suitable glycerol concentrations for $OleT_{JE}$/AldO fusion proteins, reactions were also performed with 0.1 and 0.01% glycerol. Reactions were stopped after 20 minutes. **Table 4.3** compares the percentage conversion of myristic acid for (i) intact $OleT_{JE}$-HRV3C-AldO, (ii) cleaved $OleT_{JE}$-HRV3C-AldO, and (iii) $OleT_{JE}$-αhelix-AldO, as well as the concentrations of tridecene, 2-OH myristic acid and 3-OH myristic acid products formed. For all proteins, there was little activity at 0.01% glycerol. However, hydroxylated products were formed at higher levels than alkene at low glycerol concentrations. At 0.1% glycerol, levels of 2-OH and 3-OH myristic acid are higher than at 1% glycerol. This may occur due to limitation of enzymatic activity at the lower glycerol concentration, resulting in less efficient secondary oxidation of the primary hydroxylated reaction products.

Enzyme system	Glycerol (%)	Tridecene (μM)	2-OH myristic acid (μM)	3-OH myristic acid (μM)	% substrate conversion
(i) $OleT_{JE}$-HRV3C-AldO	1	183 ± 17	0.98 ± 1.40	1.6 ± 0.1	96 ± 1
	0.1	175 ± 6	21 ± 1	93 ± 3.3	81 ± 5
(ii) $OleT_{JE}$ + AldO	1	137 ± 38	1.0 ± 1.4	1.7 ± 0.1	88 ± 3
	0.1	209 ± 19	22 ± 2	113 ± 7	97 ± 1
(iii) $OleT_{JE}$-αhelix-AldO	1	120 ± 2	2.1 ± 0.2	2.4 ± 0.5	98 ± 3
	0.1	118 ± 3	27 ± 2	123 ± 6	93 ± 2

Table 4.3. Myristic acid conversion by $OleT_{JE}$ fusion enzymes and products formed. Reactions were performed with 0.5 mM myristic acid using (i) intact $OleT_{JE}$-HRV3C-AldO, (ii) cleaved $OleT_{JE}$-HRV3C-AldO, and (iii) $OleT_{JE}$-αhelix-AldO at 0.1% and 1% glycerol concentrations. Reactions were stopped after 20 minutes.

For intact $OleT_{JE}$-HRV3C-AldO, the 1% glycerol condition yielded a 15% increase in total turnover and 9% increase in alkene production compared to 0.1% glycerol. There was little difference in total turnover and alkene levels for the intact and HRV3C-cleaved forms of $OleT_{JE}$-HRV3C-AldO, suggesting that proteolytic cleavage is effective and does not inactive enzymatic functions.

4.4.6. Secondary turnover of 2-OH myristic acid and 3-OH myristic acid products

Time-course reactions with $OleT_{JE}$/AldO fusion proteins showed that levels of 2-OH and 3-OH myristic acid decreased over time (from ~2 minutes onwards). This suggested that $OleT_{JE}$ can convert 2-OH and 3-OH fatty acids to further products (**Figure 4.6**). 0.5 ml reactions were set up with 1 µM $OleT_{JE}$, 500 µM H_2O_2 and 200 µM of either 2-OH or 3-OH myristic acid.

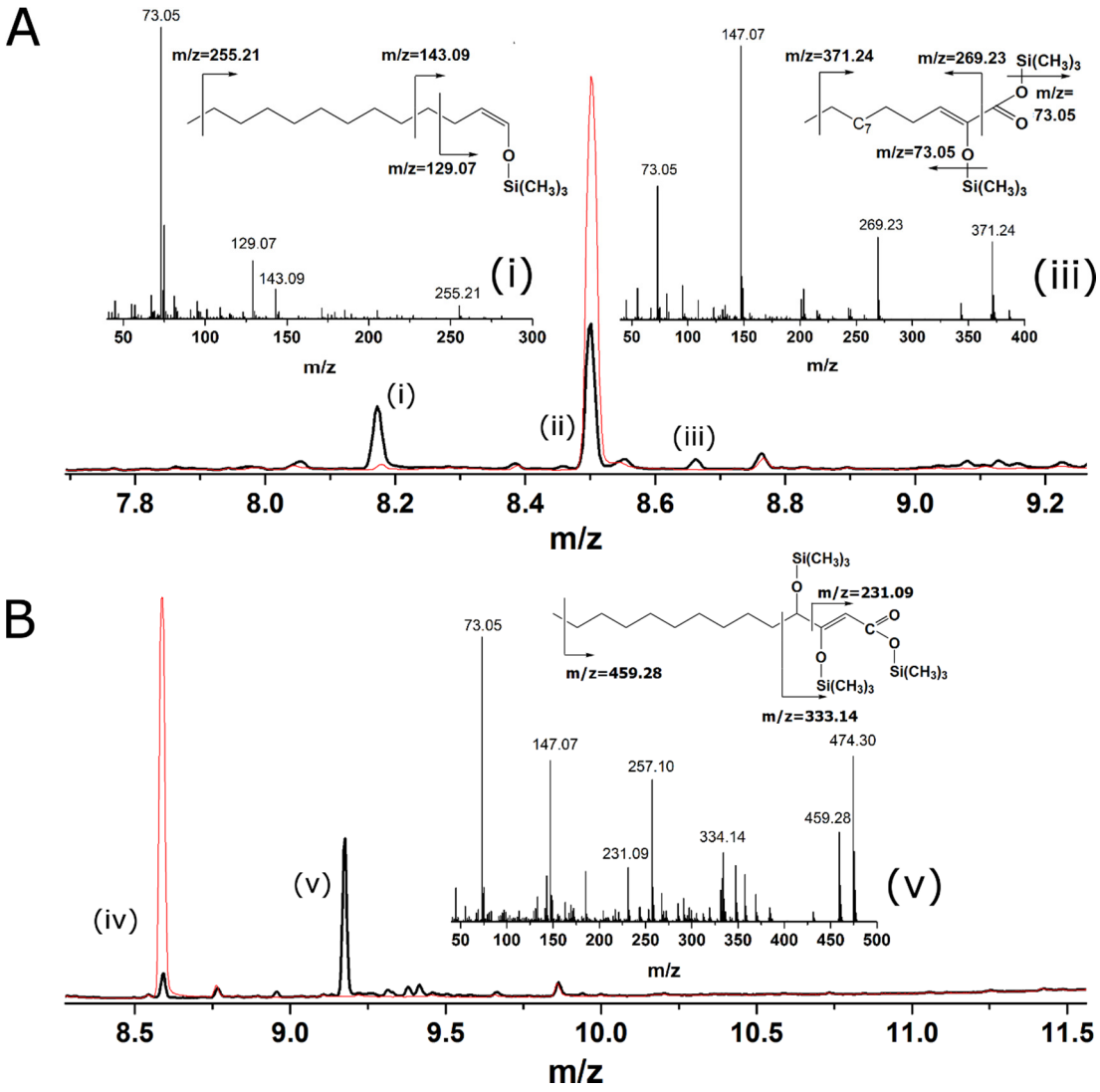

Figure 4.7. Secondary turnover of primary hydroxylated products from $OleT_{JE}$-mediated myristic oxidation. **Panel A** shows chromatograms from a reaction (black) with 1 µM $OleT_{JE}$, 200 µM 2-OH myristic acid and 500 µM H_2O_2, as well as a control sample with no enzyme (red). The reaction shows a decrease in 2-OH myristic acid (ii) and the appearance of peaks (i) and (iii). The ion spectra identify these molecules as (i) tridec-1-en-1-ol and (iii) 2-hydroxytetradec-2-enoic acid. **Panel B** shows reaction (black) and control (red) with 200 µM 3-OH myristic acid (same conditions as for panel A). The data show the disappearance of 3-OH myristic acid (iv), and the appearance of peak (v), which is identified as 3,4 dihydroxytetradec-2-enoic acid.

Reactions were incubated for 30 minutes with mixing at 700 rpm at 27°C. GC/Q-TOF chromatograms were compared to those of control samples where no enzyme was present.

Data showed that both 2-OH myristic acid and 3-OH myristic acid were used effectively as substrates by $OleT_{JE}$, with 3-OH myristic acid reactions showing almost complete turnover (**Figure 4.7**). For the 2-OH myristic acid reaction, two products were identified. One of these products is tridec-1-en-1-ol, indicating that $OleT_{JE}$ can decarboxylate 2-OH myristic acid. The ion spectrum of the second product indicates that it is 2-hydroxytetradec-2-enioc acid. This demonstrates that $OleT_{JE}$ can desaturate 2-OH myristic acid at the C_α-C_β bond. For reactions with 3-OH myristic acid, the product is 3,4 dihydroxytetradec-2-enoic acid, indicating that $OleT_{JE}$ can further hydroxylate as well as desaturate 3-OH myristic acid.

4.5. Discussion

The *Jeotgalicoccus* sp. $OleT_{JE}$ is an efficient P450 peroxygenase that uses H_2O_2 to oxidatively decarboxylate fatty acids to form terminal alkenes. This "peroxide shunt" mechanism (**Figure 4.1**) to form compound 0 is inefficient in many P450s, including BM3, causing heme oxidative damage and giving low product formation. Efforts have been made to enhance peroxide shunt efficiency through protein engineering of BM3 and the camphor hydroxylase P450cam, although improvements were not substantial (26,27). Our data (using heme stability analysis) show that $OleT_{JE}$ is relatively tolerant to H_2O_2 at low levels (<125 μM), and is clearly more resistant to H_2O_2-mediated heme oxidation than is the well-studied P450 BM3 (**Figure 4.3**, **Table 4.1**). However, despite its evolution into a peroxygenase, it remains susceptible to heme modification at higher concentrations of H_2O_2 (e.g. 1 mM), although the enzyme should not encounter such high levels of H_2O_2 in the bacterial cell.

In this study, we report the production and catalytic properties of AldO-$OleT_{JE}$ fusion systems. AldO produces H_2O_2 as a co-product from oxidation of substrates including glycerol, sorbitol and xylitol. The fused $OleT_{JE}$ uses the H_2O_2 effectively to drive decarboxylation and hydroxylation of myristic acid, a good substrate for $OleT_{JE}$ (10). In a system where $OleT_{JE}$ and AldO proteins are fused by a linker containing a HRV3C cleavage site ($OleT_{JE}$-HRV3C-AldO),

addition of 1% glycerol gave an 8% increase in myristic acid conversion compared to addition of 0.5 mM H_2O_2 (following a 20 minute incubation). Glycerol is abundant and inexpensive (28), and is formed as a by-product in the production of biofuels with associated disposal costs (29). This suggests it would be an ideal substrate for the cheap and efficient production of alkenes using AldO-$OleT_{JE}$ fusion enzymes.

The kinetics of myristic acid oxidation and product formation were measured for (i) $OleT_{JE}$-HRV3C-AldO, (ii) $OleT_{JE}$-αhelix-AldO, a construct in which $OleT_{JE}$ and AldO domains are fused by a cleavable alpha helical linker, and (iii) the separated $OleT_{JE}$ and AldO entities produced stoichiometrically by HRV3C-dependent cleavage of the $OleT_{JE}$-HRV3C-AldO linker. The fused proteins showed higher rates of myristic acid turnover than their separated entities, with 97% myristic acid turnover catalysed by $OleT_{JE}$-αhelix-AldO after 20 minutes. Fusion of the partner domains thus enhances product formation in comparison to equal amounts of isolated $OleT_{JE}$ and AldO. The ability to co-express functional and stable $OleT_{JE}$/AldO fusion enzymes is also advantageous in view of issues of regulating expression of the separate enzymes to avoid excessive H_2O_2 production. The proximity of these domains in the fusion enzymes may enhance activity through more efficient channelling of H_2O_2 between the enzyme active sites, and in a cellular context this could be important in ensuring that fatty acid decarboxylation/hydroxylation is well coupled to H_2O_2 production. Ongoing studies involve analysis of product formation from the $OleT_{JE}$/Ado fusion enzymes expressed in *E. coli* cells to establish reaction efficiency and products formed.

Importantly, time-dependent studies of myristic acid product formation from $OleT_{JE}$-AldO fusion enzymes indicated the early formation and then decrease in concentration of 2-OH and 3-OH myristic acid products. Reactions performed with the lower glycerol concentration (0.1%) produced higher levels of hydroxylated myristic acid, possibly due to a reduced level of secondary turnover of the hydroxylated products due to weaker overall enzyme activity with lower glycerol. Incubation of 2-OH myristic acid with $OleT_{JE}$ and H_2O_2, or with $OleT_{JE}$-HRV3C-AldO and 1% glycerol, led to further turnover of 2-OH myristic acid and the formation of 2-hydroxytetradec-2-enoic acid and tridec-1-en-1-ol, indicating that $OleT_{JE}$ is able to decarboxylate 2-OH myristic acid as well as catalysing desaturation of this substrate.

Reactions using $OleT_{JE}$ and H_2O_2, or $OleT_{JE}$-HRV3C-AldO and 1% glycerol showed extensive conversion of 3-OH myristic acid, and formation of 3,4 dihydroxytetradec-2-enoic acid. These data demonstrate that $OleT_{JE}$ can di-hydroxylate the fatty acid, in addition to desaturating the C□-C□ bond. $OleT_{JE}$ was previously shown to produce 2-alkanones from reactions with palmitic acid and stearic acid (C16:0 and 18:0) (30). However, we provide the first examples for the secondary turnover of primary $OleT_{JE}$ reaction products with myristic acid.

In conclusion, we describe the development of novel alditol oxidase-peroxygenase (AldO-$OleT_{JE}$) fusion enzymes that enable production of alkenes using glycerol and other alditol substrates. Further, we use these fusion systems to characterize previously undescribed decarboxylated, hydroxylated and desaturated products formed from primary reaction products (2- and 3-hydroxy myristic acid). These data provide new insights into the catalytic repertoire of the $OleT_{JE}$ enzyme, as well as providing efficient new fusion enzyme systems for alkene production.

4.6. References

1. Luthra, A., Denisov, I. G., and Sligar, S. G. (2011) Spectroscopic features of cytochrome P450 reaction intermediates. *Arch Biochem Biophys* **507**, 26-35
2. Sligar, S. G., and Gunsalus, I. C. (1979) Proton coupling in the cytochrome P-450 spin and redox equilibria. *Biochemistry* **18**, 2290-2295
3. Munro, A. W., Girvan, H. M., and McLean, K. J. (2007) Variations on a (t)heme--novel mechanisms, redox partners and catalytic functions. *Nat Prod Rep* **24**, 585-609
4. Denisov, I. G., Makris, T. M., Sligar, S. G., and Schlichting, I. (2005) Structure and chemistry of cytochrome P450. *Chem Rev* **105**, 2253-2277
5. Rittle, J., and Green, M. T. (2010) Cytochrome P450 compound I: capture, characterization, and C-H bond activation kinetics. *Science* **330**, 933-937
6. Rude, M. A., Baron, T. S., Brubaker, S., Alibhai, M., Del Cardayre, S. B., and Schirmer, A. (2011) Terminal olefin (1-alkene) biosynthesis by a novel p450 fatty acid decarboxylase. *Appl Environ Microbiol* **77**, 1718-1727

7. Liu, Y., Wang, C., Yan, J., Zhang, W., Guan, W., Lu, X., and Li, S. (2014) Hydrogen peroxide-independent production of alpha-alkenes by OleTJE P450 fatty acid decarboxylase. *Biotechnol Biofuels* **7**, 28

8. Wang, W., and Lu, X. (2013) Microbial Synthesis of Alka(e)nes. *Front Bioeng Biotechnol* **1**, 10

9. Herman, N. A., and Zhang, W. (2016) Enzymes for fatty acid-based hydrocarbon biosynthesis. *Curr Opin Chem Biol* **35**, 22-28

10. Belcher, J., McLean, K. J., Matthews, S., Woodward, L. S., Fisher, K., Rigby, S. E., Nelson, D. R., Potts, D., Baynham, M. T., Parker, D. A., Leys, D., and Munro, A. W. (2014) Structure and biochemical properties of the alkene producing cytochrome P450 OleTJE (CYP152L1) from the Jeotgalicoccus sp. 8456 bacterium. *J Biol Chem* **289**, 6535-6550

11. Grant, J. L., Hsieh, C. H., and Makris, T. M. (2015) Decarboxylation of fatty acids to terminal alkenes by cytochrome P450 compound I. *J Am Chem Soc* **137**, 4940-4943

12. Grant, J. L., Mitchell, M. E., and Makris, T. M. (2016) Catalytic strategy for carbon-carbon bond scission by the cytochrome P450 OleT. *Proc Natl Acad Sci U S A* **113**, 10049-10054

13. Zachos, I., Gassmeyer, S. K., Bauer, D., Sieber, V., Hollmann, F., and Kourist, R. (2015) Photobiocatalytic decarboxylation for olefin synthesis. *Chem Commun (Camb)* **51**, 1918-1921

14. Girhard, M., Schuster, S., Dietrich, M., Durre, P., and Urlacher, V. B. (2007) Cytochrome P450 monooxygenase from Clostridium acetobutylicum: a new alpha-fatty acid hydroxylase. *Biochem Biophys Res Commun* **362**, 114-119

15. Seaver, L. C., and Imlay, J. A. (2001) Hydrogen peroxide fluxes and compartmentalization inside growing Escherichia coli. *J Bacteriol* **183**, 7182-7189

16. Girhard, M., Kunigk, E., Tihovsky, S., Shumyantseva, V. V., and Urlacher, V. B. (2013) Light-driven biocatalysis with cytochrome P450 peroxygenases. *Biotechnol Appl Biochem* **60**, 111-118

17. Heuts, D. P., van Hellemond, E. W., Janssen, D. B., and Fraaije, M. W. (2007) Discovery, characterization, and kinetic analysis of an alditol oxidase from Streptomyces coelicolor. *J Biol Chem* **282**, 20283-20291

18. van Hellemond, E. W., Vermote, L., Koolen, W., Sonke, T., Zandvoort, E., Heuts, D. P. H. M., Janssen, D. B., and Fraaije, M. W. (2009) Exploring the biocatalytic scope of alditol oxidase from Streptomyces coelicolor. *Adv Synth Catal* **351**, 1523-1530

19. Kapust, R. B., Tozser, J., Fox, J. D., Anderson, D. E., Cherry, S., Copeland, T. D., and Waugh, D. S. (2001) Tobacco etch virus protease: mechanism of autolysis and rational design of stable mutants with wild-type catalytic proficiency. *Protein Eng* **14**, 993-1000

20. Butler, C. F., Peet, C., Mason, A. E., Voice, M. W., Leys, D., and Munro, A. W. (2013) Key mutations alter the cytochrome P450 BM3 conformational landscape and remove inherent substrate bias. *J Biol Chem* **288**, 25387-25399

21. Amet, N., Lee, H.-F., and Shen, W.-C. (2009) Insertion of the Designed Helical Linker Led to Increased Expression of Tf- based fusion proteins. *Pharm Res* **26**, 523-528

22. Chen, X., Zaro, J., and Shen, W.-C. (2013) Fusion Protein Linkers: Property, Design and Functionality. *Adv Drug Deliv Rev* **65**, 1357-1369

23. Joo, H., Lin, Z., and Arnold, F. H. (1999) Laboratory evolution of peroxide-mediated cytochrome P450 hydroxylation. *Nature* **399**, 670-673

24. Li, Q. S., Ogawa, J., and Shimizu, S. (2001) Critical role of the residue size at position 87 in H2O2- dependent substrate hydroxylation activity and H2O2 inactivation of cytochrome P450BM-3. *Biochem Biophys Res Commun* **280**, 1258-1261

25. Mattam, A. J., Clomburg, J. M., Gonzalez, R., and Yazdani, S. S. (2013) Fermentation of glycerol and production of valuable chemical and biofuel molecules. *Biotechnol Lett* **35**, 831-842

26. Yazdani, S. S., and Gonzalez, R. (2007) Anaerobic fermentation of glycerol: a path to economic viability for the biofuels industry. *Curr Opin Biotechnol* **18**, 213-219

27. Dennig, A., Kuhn, M., Tassoti, S., Thiessenhusen, A., Gilch, S., Bulter, T., Haas, T., Hall, M., and Faber, K. (2015) Oxidative Decarboxylation of Short-Chain Fatty Acids to 1-Alkenes. *Angew Chem Int Ed Engl* **54**, 8819-8822

28. Groves, J. T. (2006) High-valent iron in chemical and biological oxidations. *J Inorg Biochem* **100**, 434-447

29. Fisher, M. T., and Sligar, S. G. (1985) Control of heme protein redox potential and reduction rate: linear free energy relation between potential and ferric spin state equilibrium. *J Am Chem Soc* **107**, 5018-5019

Chapter 5

Catalytic and structural properties of the peroxgenase cytochrome P450 KR from *Kocuria rhizophila*

Kang Lan Tee, Sarah Matthews, Kirsty J. McLean, Hazel M. Girvan, Stephen E. J. Rigby, Dijana Matak-Vinkovic, David Leys, Richard T. Blankley and Andrew W. Munro*

Manchester Institute of Biotechnology, Faculty of Life Sciences, University of Manchester, Manchester M1 7DN, United Kingdom

Keywords: cytochrome P450, decarboxylase, fatty acid, alkene, biofuel, biosynthesis, biophysics

5.1. Abstract

The cytochrome P450 peroxygenases (CYP152 family) are a distinct class of P450s that have evolved to use hydrogen peroxide (H_2O_2) to drive catalysis rather than using redox partner systems. H_2O_2 drives a "peroxide shunt" mechanism by which the substrate-bound peroxygenases are converted directly to the reactive Compound 0 (ferric-hydroperoxo) intermediate, bypassing steps that involve redox partners. The biochemical and catalytic properties of a novel peroxygenase (P450 KR from *Kocuria rhizophila*) are described. KR is readily expressed in *E. coli* and purified in a 3-step process involving nickel affinity, protease cleavage of the affinity tag, and reverse nickel affinity. The highly purified KR has a Soret band at 424 nm, red shifted by comparison with other P450s, and likely reflecting an unusual coordination state in the heme distal pocket. P450 KR binds fatty acids of chain length C10-18, which induce a high-spin shift in the KR heme iron. Longer chain substrates bind tightest, though short chain fatty acids give greater high-spin conversion. EPR spectroscopy indicates heterogeneity of the KR heme iron coordination state, while redox potentiometry reveals little change in the Fe^{III}/Fe^{II} reduction potential on substrate binding, indicative of the different evolutionary pathway taken by the KR and other peroxygenases, including a lack of reliance on any effect of substrate binding in elevating the heme potential to enable electron transfer from redox partners. KR is catalytically active and generates tridecene in excess over 2-hydroxy and 3-hydroxy myristic acid from myristic acid substrate. The P450 KR enzyme thus has potential applications related to fine chemical synthesis and drop-in biofuel production.

5.2. Introduction

Cytochrome P450 monooxygenases (P450s or CYPs) are heme *b*-binding enzymes represented widely in organisms from all of the major domains of life (1). The vast majority of P450 enzymes catalyse the NAD(P)H-dependent activation of molecular oxygen (O_2) bound to the P450 heme iron, resulting in its cleavage and the insertion of a single atom of oxygen into a substrate bound close to the heme, with the other oxygen atom used to form a water molecule (2). Two electrons are transferred from NAD(P)H through one or more redox partners to the P450 heme, where they are used consecutively to reduce resting ferric heme

iron to the ferrous state (which then binds dioxygen), and then to further reduce the ferric-peroxo species formed to the ferric peroxo state. Subsequent protonations produce first the ferric hydroperoxo (compound 0) species, and then (with loss of a water molecule) the reactive ferryl-oxo compound I (3). In the canonical P450 cycle representation, compound I abstracts a hydrogen atom from a substrate to form the ferryl-hydroxo compound II, and then "rebounds" the hydroxyl group to form a hydroxylated product and to return the heme iron to its ferric resting state (4,5). P450s are arguably the most versatile enzymes known, and can use iron-oxo species to facilitate a wide range of chemical transformations of their substrates, including hydroxylation, epoxidation, sulfoxidation, oxidative dealkylation, N-oxidation, decarboxylation, isomerisation and dehalogenation (1,6).

In most eukaryotic P450 systems, electrons from NAD(P)H are delivered to membrane-associated P450s by either the microsomally located diflavin enzyme NADPH-cytochrome P450 reductase (CPR, a class II system), or (in mitochondria) through the NADPH-dependent FAD-binding enzyme adrenodoxin reductase (ADR) and its 2Fe-2S cluster-binding adrenodoxin (AD) partner protein, with AD acting as the 1-electron carrier between the ADR and the P450 (a class I system) (7). In prokaryotic and archaeal systems, the P450s are soluble, cytoplasmic enzymes that interact with soluble class I reductase and ferredoxin partners (8). The best characterized of the bacterial P450 systems is the camphor hydroxylase P450cam (CYP101A1) from *Pseudomonas putida*, which catalyzes the 5-*exo* hydroxylation of camphor in the pathway for its degradation and use as an energy source, using NADH-putidaredoxin reductase and the 2Fe-2S putidaredoxin (9). P450cam was the first of the P450s to have its structure resolved by X-ray crystallography, and remains an important model system in the P450 superfamily (10).

However, recent years have seen the identification of several different types of P450 redox partners, as well non-redox partner enzymes and P450-partner fusion enzymes (11). These include proteins such as cytochrome b_5 (shown to have crucial roles in eukaryotic steroid transformations (12), and the P450 BM3 (CYP102A1, BM3) enzyme from *Bacillus megaterium* – in which soluble P450 and CPR enzymes (both lacking any N-terminal membrane anchor region) are fused in a 119 kDa flavocytochrome enzyme (13). P450 BM3 forms a dimer and

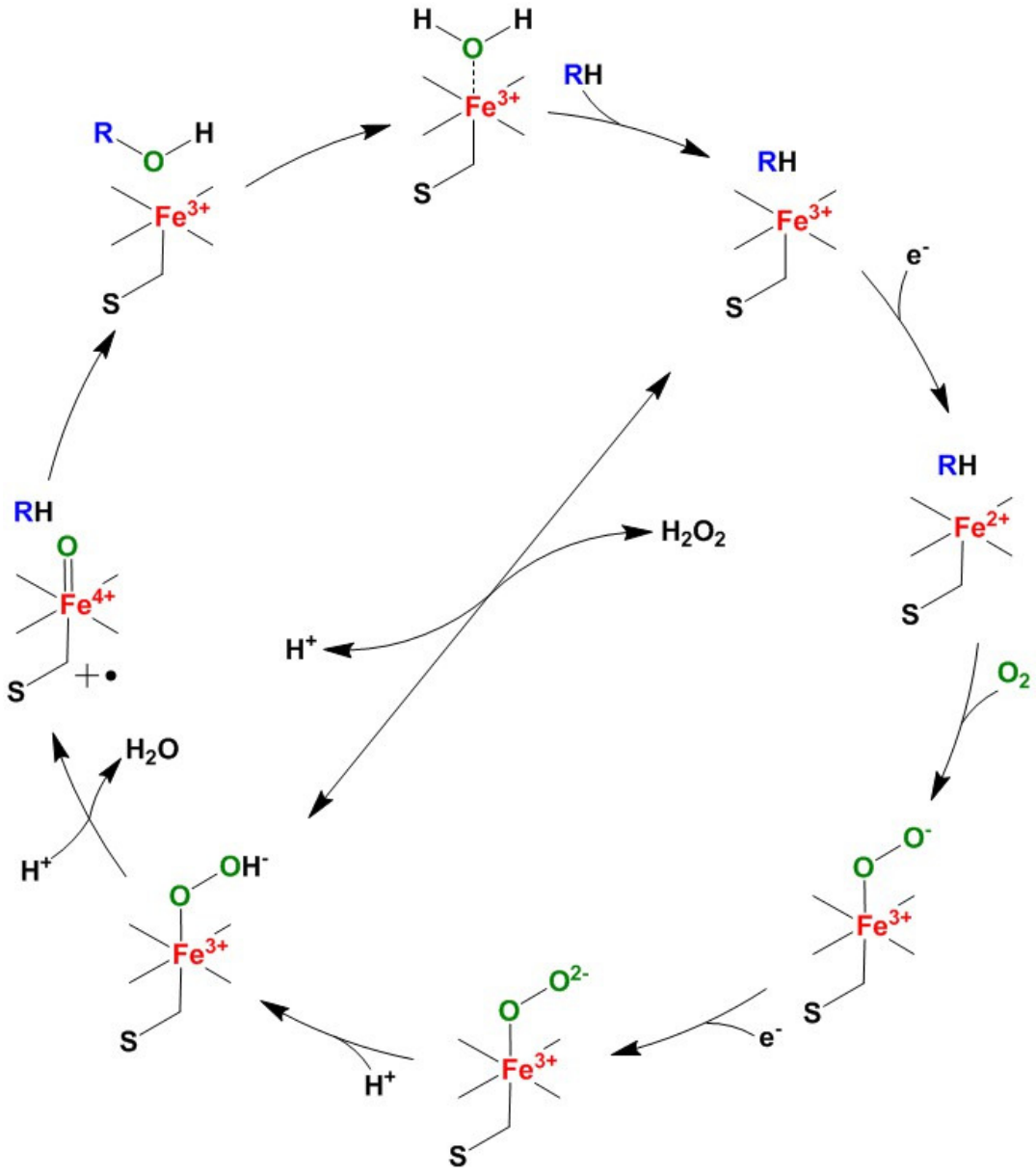

Figure 5.1. The cytochrome P450 catalytic cycle. The peroxide shunt pathway (as utilized by the P450 peroxygenase enzymes, including P450 KR) is shown as a double headed arrow between the ferric, substrate-bound and the ferric-hydroperoxo (Compound I) species.

electron transfer can occurs between the CPR domain of one monomer and the P450 domain of the other to drive hydroxylation of fatty acid substrates (14,15). Various bacterial P450s are found fused to flavodoxin or phthalate dioxygenase redox partners (16,17), while others are fused to non-redox partners. For instance, recent studies revealed a fused P450-aldo-keto reductase (AKR) enzyme system in opium poppy in which the P450 (CYP82Y2) acts as a (*S*)-reticuline dehydrogenase to form 1,2-dehydroreticuline (DR), while its NADPH-dependent AKR fusion partner (1,2-dehydroreticuline reductase, DRR) catalyzes stereospecific reduction

to form (*R*)-reticuline (which then undergoes further conversion to form morphine in several subsequent steps) (18). In the ascomycete fungus *Aspergillus nidulans*, the PpoA (psi factor-producing oxygenase A) enzyme is a fusion between a heme-binding dioxygenase/peroxidase and a P450. The dioxygenase domain oxidizes linoleic acid to (*8R*)-hydroperoxyoctadecadienoic acid, and this molecule is the substrate for the P450 domain, which isomerizes the molecule to 5,8-dihydroxyoctadecadienoic acid (19). However, other P450s bypass requirements for partner enzymes altogether. Examples include the fungal nitric oxide reductase (NOR) P450s that bind NAD(P)H within their active site and perform a reductive reaction whereby two molecules of NO (one bound to the heme iron) are converted to dinitrogen monoxide (N_2O) (20). The peroxide shunt (**Figure 5.1**) was also found to be used naturally by a class of bacterial P450s (peroxygenases) to enable hydroxylation of fatty acids predominantly at the beta-carbon (*B. subtilis* P450 BS□), or exclusively at the alpha-carbon (*Sphingomonas paucimobilis* P450 SP$_\alpha$) (21,22).

Recently, a novel catalytic process was revealed for selected members of the peroxygenase P450s. In studies by Rude *et al*., the OleT$_{JE}$ (CYP152L1) enzyme from *Jeotgalicoccus* sp. ATCC 8456 was shown to catalyze hydrogen peroxide (H_2O_2)-dependent oxidative decarboxylation of long chain fatty acids. *In vitro* turnover studies using isolated OleT$_{JE}$ enzyme showed production of the n-1 terminal alkene from even chain, saturated fatty acids from C14-C20 chain length (23). Parallel studies showed that the P450 BS$_\beta$ enzyme also produced terminal alkenes, though product profiles were dominated by the α- and β-hydroxylated products in this case. Belcher *et al*. described the structural properties of OleT$_{JE}$ and the fact that the P450 active site is "pre-formed" for substrate binding, with little structural change occurring to accommodate the binding of the C20:0 substrate arachidic acid, and that the fatty acid carboxylate is bound to a conserved arginine (Arg245) that is located above the heme plane (24). High affinity binding was demonstrated for a range of saturated fatty acids (C12:0-C20:0), with n-1 alkenes formed from these substrates and the C20:0 fatty acid arachidic acid having a tight K_d = 0.29 μM. Stopped-flow turnover studies revealed a rate constant of 167 s^{-1} for H_2O_2-dependent turnover of arachidic acid-bound OleT$_{JE}$ using 200 μM H_2O_2, indicating an efficient substrate oxidation reaction (24). In other studies, Yan *et al*.

combined lipase and $OleT_{JE}$ enzymes in both cell-free and cell-based systems to generate alkenes from cheap triacylglycerol substrates (25), while Liu *et al*. demonstrated that bacterial NAD(P)H-dependent redox partners could also drive oxidative decarboxylation of fatty acids by $OleT_{JE}$ (26). A photocatalytic method was also described to facilitate H_2O_2 production for $OleT_{JE}$ catalysis (27), while Grant *et al*. presented compelling UV-visible spectroscopic evidence for the formation of the P450 ferryl-oxo compound I species in rapid mixing experiments using perdeuterated arachidic acid-bound $OleT_{JE}$ and H_2O_2, thus implicating this reactive iron-oxo species in $OleT_{JE}$ catalysis (28). Subsequent studies by the same group identified the transient formation of the ferryl-hydroxo (Compound II) species in $OleT_{JE}$, and assigned this species a key role in catalytic events that lead to substrate decarboxylation and terminal alkene production (29).

In their earlier study, Rude et al. identified distinct $OleT_{JE}$-related P450 enzymes from *Kocuria*, *Corynebacterium* and *Methylobacterium* spp. The *Kocuria rhizophila* orthologue shares only 30 % amino acid identity with $OleT_{JE}$, and was thus predicted to have distinctive properties from $OleT_{JE}$. In this study, the *K. rhizophila* P450 (P450 KR) was expressed and purified, and its catalytic and biochemical properties were analyzed. Data collected reveal various properties distinct from those of $OleT_{JE}$ and other peroxygenases characterized to date, and point to its potential applications in production of alkenes. P450 KR also has a propensity to dimerize and its crystal structure was solved in an unusual dimeric state.

5.3. Materials and Methods

5.3.1 P450 KR gene expression

The gene encoding P450 KR from *Kocuria rhizophila* DC2201 (accession no. WP_012399225) was codon optimized for expression in *E. coli*, synthesized with a N-terminal polyhistidine-tag and a TEV cleavage site, and cloned into pET24b(+) at the NdeI and EcoRI restriction sites (GenScript USA Inc.). The *E. coli* strain C41 (DE3) (Lucigen) was used as an expression host. Cells transformed with the pET24b(+)-P450 KR plasmid were cultivated in 500 mL of 2YT broth supplemented with 50 µg/L of kanamycin in a 2 L flask at 37℃ with

shaking at 190 rpm. When the cell culture reached an optical density (OD_{600}) of 0.5–0.6, 450 µM δ-aminolevulinic acid was added and the cultivation temperature was lowered to 25℃. P450 KR expression was then induced using 100 µM isopropyl 1-thio-β-D-galactopyranoside (IPTG) and cells were grown for a further 20 h. Cells were harvested by centrifugation at 6000 rpm and 4 ℃ (Avanti J-26 XP centrifuge and JLA-8.1000 rotor). Pellets were resuspended in phosphate buffered saline (PBS) buffer (10 mM Na_2HPO_4, 1.8 mM KH_2PO_4, 2.7 mM KCl, 137 mM NaCl, pH 7.4), combined and centrifuged as before. The cell pellet was frozen at -20℃ until purification.

5.3.2. Protein purification

Bacterial cells were thawed and resuspended in buffer A (0.1 M potassium phosphate, 0.75 M NaCl, 10 % glycerol, pH 8.0) with 20 mM imidazole, a protease inhibitor tablet (SIGMAFAST™ Protease Inhibitor Cocktail Tablets, EDTA-Free), DNase (10 µg/mL) and lysozyme (10 µg/mL). The cells were disrupted by sonication using 10 s bursts, at 50 s intervals and 40% amplitude for 45 min (Bandelin SONOPULS sonicator with VS 70 T probe). The cell lysate was centrifuged (20000 rpm, 35 min, 4℃) using a Beckman JA25.50 rotor to remove the cell debris. The supernatant was mixed with 10 mL of Ni-IDA agarose resin (Generon) pre-equilibrated using buffer A with 20 mM imidazole. The resin-protein mix was incubated overnight at 4 ℃ on a roller platform before it was transferred to an empty chromatography column. The resin with P450 KR bound was washed using ten column volumes of buffer A with 20 mM imidazole, followed by ten column volumes of buffer A with 40 mM imidazole. P450 KR was eluted using a one-step elution process with 300 mM imidazole in buffer A. TEV protease expressed using pRK793 (a gift from David Waugh, Addgene plasmid # 8827) (30) was added to the eluted P450 KR and left overnight at 4℃. The cleaved P450 KR was exchanged into buffer A using a HiPrep 26/10 Desalting column (GE Healthcare) before protein was applied to Ni-IDA resin pre-equilibrated with buffer A to remove the cleaved tag and TEV protease. The resin was washed with five column volumes of buffer A before the cleaved protein was eluted using buffer A with 10 mM imidazole. Eluted P450 KR was concentrated by ultrafiltration using a Vivaspin with 10 kDa MWCO (Generon).

Concentrated protein was loaded onto a Superdex 200 16/600 gel filtration column (GE Healthcare) equilibrated with buffer B (0.1 M potassium phosphate, 0.75 M NaCl, pH 8.0). The purified P450 KR fractions were analyzed by UV-visible spectroscopy to establish purity and heme content.

Purified P450 KRprotein was concentrated using a VivaSpin and used for crystallography directly, or stored in buffer A at -80℃ for subsequent use for other assays.

5.3.3. UV visible spectroscopy

UV-visible spectroscopy was performed using a Cary 60 UV-Visible spectrophotometer (Agilent). Spectra were recorded using 5-10 µM of P450 KR in buffer B. The NO complex was formed by addition of a few bubbles of NO into the ferric P450 KR sample in anaerobic buffer. To form the CO complex, a few grains of sodium dithionite was added to reduce P450 KR in buffer B before CO was bubbled slowly into the solution until no further spectral change was observed. The concentration of the low-spin form of P450 KR was determined using an extinction coefficient of ε_{424} = 75 $mM^{-1}cm^{-1}$, as determined by using the pyridine hemochromagen method of Berry and Trumpower (31).

5.3.4. Fatty acid and inhibitor binding titration

All spectral binding titrations were performed in 1-cm path length quartz cuvettes at 25℃ using ~5 µM protein in buffer A. Fatty acid substrates used were capric acid (C10:0), lauric acid (C12:0), myristic acid (C14:0), palmitic acid (C16:0) and stearic acid (C18:0) (Sigma-Aldrich). All fatty acids were dissolved in methanol (C12:0, C14:0, C16:0) or ethanol (C10:0, C18:0). Spectra (300–800 nm) was recorded for the ligand-free P450 KR and following stepwise additions (0.1–0.5 µL) of fatty acids using microliter syringes (Hamilton) until no further spectral changes were observed. The total volume of substrate added was always <2 % of the total volume of the sample. Difference spectra at each stage in the titration were computed by subtracting the spectrum of the ligand-free P450 KR from the individual fatty acid-bound

spectra obtained during the titration. ΔA_{max} was calculated as the difference between the maximum and minimum of the difference spectra (using the same wavelength pair throughout each individual titration set) and was plotted against substrate concentration. The data were fitted using the Hill function to derive the substrate dissociation values (K_d). The extent of spin state change induced by substrate addition was estimated based on the $\varepsilon\Delta A_{max}$ = 100 mM^{-1} cm^{-1} (32).

For inhibitor binding, capric acid was first added to ligand-free P450 KR until no further spectral changes were observed. The inhibitors imidazole and 4-phenylimidazole were dissolved in buffer A and ethanol, respectively. Inhibitors were then added stepwise into the capric acid-bound P450 KR until no further spectral changes were observed. The volume of inhibitor was always <3% of the total volume of the assay mixture. Difference spectra and K_d values were computed as described for the substrates. The ΔA_{max} versus [inhibitor] data were fitted using a hyperbolic (Michaelis-Menten) function.

5.3.5. Redox potentiometry

Midpoint potentials for the P450 KR heme Fe^{III}/Fe^{II} couple were determined by spectroelectrochemical redox titrations at 25°C inside an anaerobic glove box (Belle Technology), under a nitrogen atmosphere, with O_2 level maintained below 3 ppm. All solutions were deoxygenated by sparging with nitrogen gas. All titrations were performed using ~10 µM P450 KR in buffer A. For substrate-bound P450 KR, capric acid (400 mM stock in ethanol) was added until no further conversion of the heme iron towards its high-spin state was observed (~4 mM capric acid). Mediators were added to expedite electronic equilibration in the system (2 µM phenazine methosulfate, 7 µM 2-hydroxy-1,4-naphthoquinone, 0.3 µM methyl viologen, and 1 µM benzyl viologen) to mediate in the range from +100 to –480 mV versus the normal hydrogen electrode (NHE). Midpoint potentials were determined by fitting heme absorbance *versus* applied potential data using the Nernst equation (33,34).

5.3.6. EPR analysis of P450 KR

Continuous wave X-band electron paramagnetic resonance (EPR) spectra of the P450 KR heme were obtained at 10 K using a Bruker ELEXSYS E500 EPR spectrometer equipped with an ER 4122SHQ Super High Q cavity. Temperature was controlled using an Oxford Instruments ESR900 cryostat connected to an ITC 503 temperature controller. Microwave power was 0.5 milliwatt, modulation frequency was 100 kHz, and the modulation amplitude was 5 G. EPR spectra were collected from P450 KR (285 µM) in the substrate-free form and when bound to 2.5 mM myristic acid, 0.7 mM lauric acid and 5 mM capric acid. All samples were prepared in buffer A with the EPR spectrum of buffer A recorded and subtracted from the EPR spectra for P450 KR samples in the same buffer. EPR spectra were also collected under the same conditions for P450 KR samples (360 µM) bound to imidazole (250 mM) and to 4-phenylimidazole (5 mM).

5.3.7. Fatty acid biotransformation by P450 KR

The oxidative transformation of fatty acids by P450 KR to facilitate identification of products was done as follows. A 0.5 mL reaction was set up in buffer A for each fatty acid tested (2 mM C10:0, 0.5 mM C12:0, 0.25 mM C14:0, 0.2 mM C16:0 and 0.2 mM C18:0) with P450 KR (4 µM). Each biotransformation was initiated by the addition of 250 µM H_2O_2 and the reaction mixtures were incubated at 27℃, with mixing at 700 rpm for 30 min (using an Eppendorf ThermoMixer® C). After the incubation period, 40 µL of 37% HCL was added to stop the reaction and the product was extracted using 0.5 mL of dichloromethane. The extracted organic phase was dried using anhydrous magnesium sulfate before GC-MS analysis.

To quantify the decarboxylated and hydroxylated product ratio, a biotransformation using P450 KR (4 µM) and C14:0 (0.5 mM) was initiated using 250 µM H_2O_2. To test electron transfer using NADPH with spinach FDX/FDR, P450 KR (1 µM) was combined with C14:0 (0.25 mM) in the presence of NADPH (0.5 mM), FDX (5µM) and FDR (1 µM). Both reactions were performed in the conditions described above, except that 1-pentadecene (250 µM) and lauric acid (250 µM) were added as internal standards before product extraction.

The rates of terminal olefin formation by P450 KR were measured using two different P450 reducing/activating systems. One used added H_2O_2 and the other used *in situ* generated H_2O_2 (via a photochemical system for flavin-mediated reduction of O_2 (27). In both systems, C14:0 (0.5 mM) and P450 KR (1–5 µM) were combined in 10 mL of buffer A. The first system used a stoichiometric addition of H_2O_2 (0.5 mM), while the second system used 5–50 µM FMN and 1–50 mM EDTA. Sample illumination in the second system was done using a Mounted High-Power LED white light (Thorlabs). The reaction mixtures were stirred at 27℃ and products were extracted at various time points by sampling 0.5 mL from the reaction mixtures at time intervals up to 20 h. The reaction progress was stopped in these samples and products extracted as described above. Internal standards 1-pentadecene (250 µM) and lauric acid (250 µM) were added before product extraction.

5.3.8. Analysis of products using GC-MS

Analysis of fatty acid conversion products was carried out by gas chromatography coupled with EI-MS on an Agilent 5977A GC/MSD equipped with a HP-5ms Ultra Inert column (30 m x 250 µm x 0.25 µm, Agilent). The Multi-Mode injector was set at 280℃, with helium as carrier gas at 1.2 mL/min. A 1 µL sample (split ratio 1:10) was derivatized in the injection inlet with 1 µL N,O-bis(trimethylsilyl)trifluoroacetamide (BSTFA) containing 1% trimethylchlorosilane, using a 2-layer sandwich injection. The oven temperature was maintained at 40℃ for 1 min, then ramped at 10℃/min to 290℃ and held at 290℃ for 1 min. For product determination, electronic ionization scan mode was used to detect ions in the range of 40–350 m/z. Additionally, appropriate m/z ion fragments of conversion products were monitored using the EI-MS in Selected Ion Mode (SIM). For product quantification, authentic standards of myristic acid, 1-tridecene, 2-hydroxy- and 3-hydroxy myristic acids were treated in the same way and used to prepare the calibration curves.

5.4. Results

5.4.1. Expression and Purification of P450 KR

The codon optimized P450 KR gene was cloned into the T7 promoter plasmid pET24b(+) for high level expression in *E. coli* strain C41 (DE3). Bacterial cell growth and harvest were done as described in the Materials and Methods section. Both the cell pellet and the lysed cell extract were red in colour, indicative of the production of a substantial quantity of soluble P450 KR. Purification was achieved in three chromatographic stages involving two Ni-IDA affinity chromatography steps (pre- and post- TEV protease-dependent cleavage of the Strep-tag) and one gel filtration chromatography step using a Superdex 200 16/600 column. The 3-step purification yielded approximately 50 mg of P450 KR per liter of 2YT medium. During development of the purification process, we noticed the precipitation of P450 KR in low salt buffer, an observation similar to that made for the P450 $OleT_{JE}$ peroxygenase studied by Belcher *et al*. (24). Subsequently, only high salt buffers (containing 750 mM NaCl) were used with P450 KR.

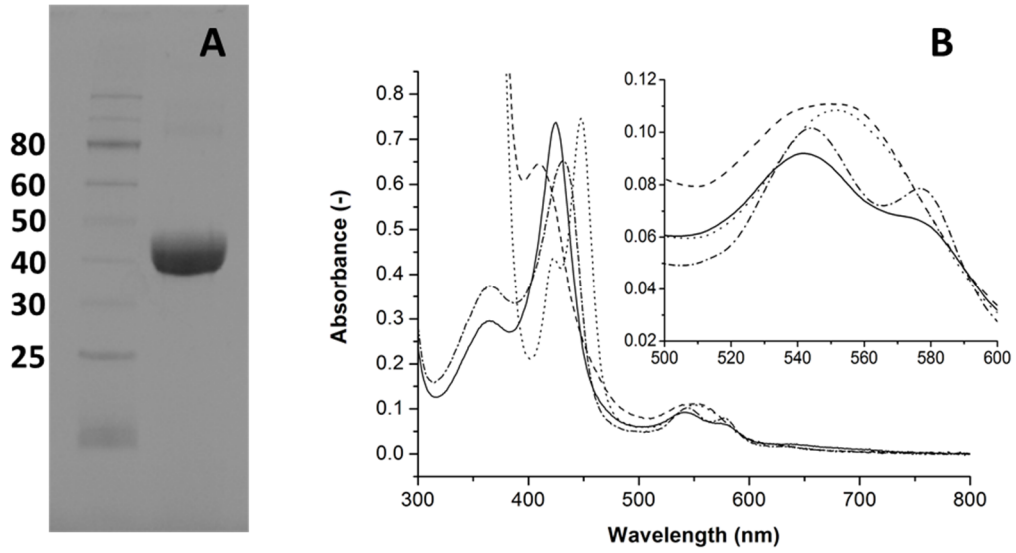

Figure 5.2. Purification and UV-visible spectroscopic characterization of P450 KR. Panel A shows the purification of P450 KR in the second lane, with NEB protein marks in the first lane with their individual masses (kDa) indicated. **Panel B** shows the UV-visible spectroscopic properties of P450 KR (9.7 μM) in its ferric resting state (solid line); in the dithionite reduced (ferrous) state (dashed line); in its Fe^{II}-CO complex (dotted line) and in the ferric, nitric oxide-bound form (dot-dashed line). The inset shows a magnification of the Q-band spectral region, highlighting the different spectral properties of the different forms of P450 KR in this region.

5.4.2. UV-Visible Spectroscopic Analysis of P450 KR

The purified P450 KR was analysed by UV-visible spectroscopy to establish the absorbance features of its heme prosthetic group. **Figure 5.2** shows the characteristic absorption spectra of the pure P450 KR in its oxidized (Fe^{III}), sodium dithionite-reduced (Fe^{II}), ferrous-carbon monoxide bound (Fe^{II}-CO), and ferric-nitric oxide bound (Fe^{III}-NO) forms. The major absorption feature for the ferric resting state of P450 KR is at 424 nm (the Soret band), with smaller α- and β-bands at ~575 nm and 542 nm. The β-band is more pronounced, while the α-band is weaker and appears more as a shoulder on the β-band. These absorption features are all red-shifted compared to those for typical low-spin bacterial P450s (e.g. the fatty acid hydroxylase P450 BM3 from *Bacillus megaterium* at 418, 534, and 568 nm, the *Mycobacterium tuberculosis* cyclodipeptide oxidase CYP121A1 at 416.5, 538 and 568 nm, and the camphor hydroxylase P450cam from *Pseudomonas putida* at 417 nm, 537 nm and 570 nm (35-37). The shift of the Soret band to longer wavelengths (a type II P450 spectral shift) is normally indicative of the replacement of the distal water molecule (the 6th

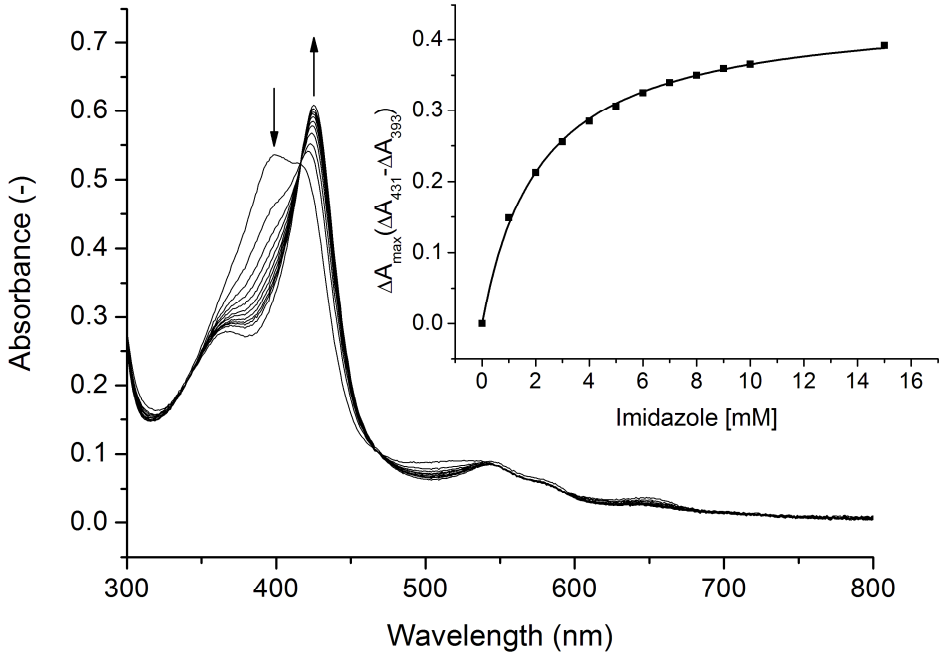

Figure 5.3. Titration of imidazole into capric acid-bound P450 KR. Imidazole was titrated into HS, capric acid-bound P450 KR, giving an apparent binding constant ($K_{d\ app}$) of 2.2 ± 0.1 mM. Using the K_d for binding of capric acid to P450 KR (1.22 ± 0.06 mM) and the quantity of capric acid added (4.8 mM), a P450 KR K_d for imidazole of 445 ± 35 µM was determined.

ligand to the heme iron) with a stronger field ligand, for instance imidazole. In view of the unusual red-shifted Soret spectroscopic feature and the use of imidazole during Ni-IDA affinity chromatography, the affinity of P450 KR for imidazole was investigated. Dialysis of the purified P450 KR in imidazole-free buffer failed to shift the absorption maximum of the P450 KR heme, suggesting that either imidazole binds extremely tightly to the P450 KR heme iron, or that an endogenous ligand (potentially the imidazole side chain of a histidine residue) occupies the distal position on the heme iron. However, imidazole is usually a weak inhibitor of P450s. For instance, the *M. tuberculosis* sterol demethylase CYP51B1 and the orphan *M. tuberculosis* P450 CYP144A1 have K_d values for imidazole of 11.7 ± 0.9 mM and 3.0 ± 0.7 mM, respectively (38,39). Imidazole does bind tightly to the Royal Demolition Explosive (RDX) degrading XplA (CYP177A1), with a K_d of 1.6 ± 0.1 mM (40). However, in this case, the structural organization of the XplA distal pocket enables a near-ideal geometry of heme iron coordination, as well as an extended active site water-mediated hydrogen bonding network to the non-coordinating nitrogen atom of the imidazole (40,41). The binding of imidazole to P450 KR was investigated, but it was found that negligible changes occurred to the heme Soret spectrum, consistent with a model that an internal histidine ligand might ligate the heme iron. To obtain an estimate of affinity for imidazole, a titration was instead done using a capric acid-bound form of P450 KR, resulting in an apparent binding constant ($K_{d\ app}$) of 2.2 ± 0.1 mM (see **Figure 5.3**). Assuming competitive binding and with knowledge of the K_d for the binding of capric acid to P450 KR (1.22 ± 0.06 mM) (**Table 5.1**) and the quantity of substrate added (4.8 mM capric acid), a "true" P450 KR imidazole K_d was determined as 445 ± 35 µM. These data confirm that imidazole binds P450 KR weakly and that the unusually red-shifted P450 KR Soret feature at 424 nm does not result from distal ligation of the heme iron by imidazole retained from the Ni-IDA purification step. For further verification that endogenous heme iron coordination produces the unusual 424 nm Soret feature in P450 KR, we expressed and purified P450 KR using the Strep-tag/Step-Tactin system (IBA GmbH) in the absence of any exogenous imidazole. The Strep-Tactin-purified P450 KR enzyme in its ferric resting state has UV-visible absorption features similar to those observed in the Ni-IDA-purified P450 KR, with the Soret peak at 424

nm and the α- and β-bands at ~575 nm and 542 nm. These data further support the model of an endogenous distal ligand to the heme iron in P450 KR.

The P450 KR heme iron is readily reduced by sodium dithionite to give a Soret band of diminished intensity that is blue shifted to 410 nm, with a single merged peak in the alpha/beta

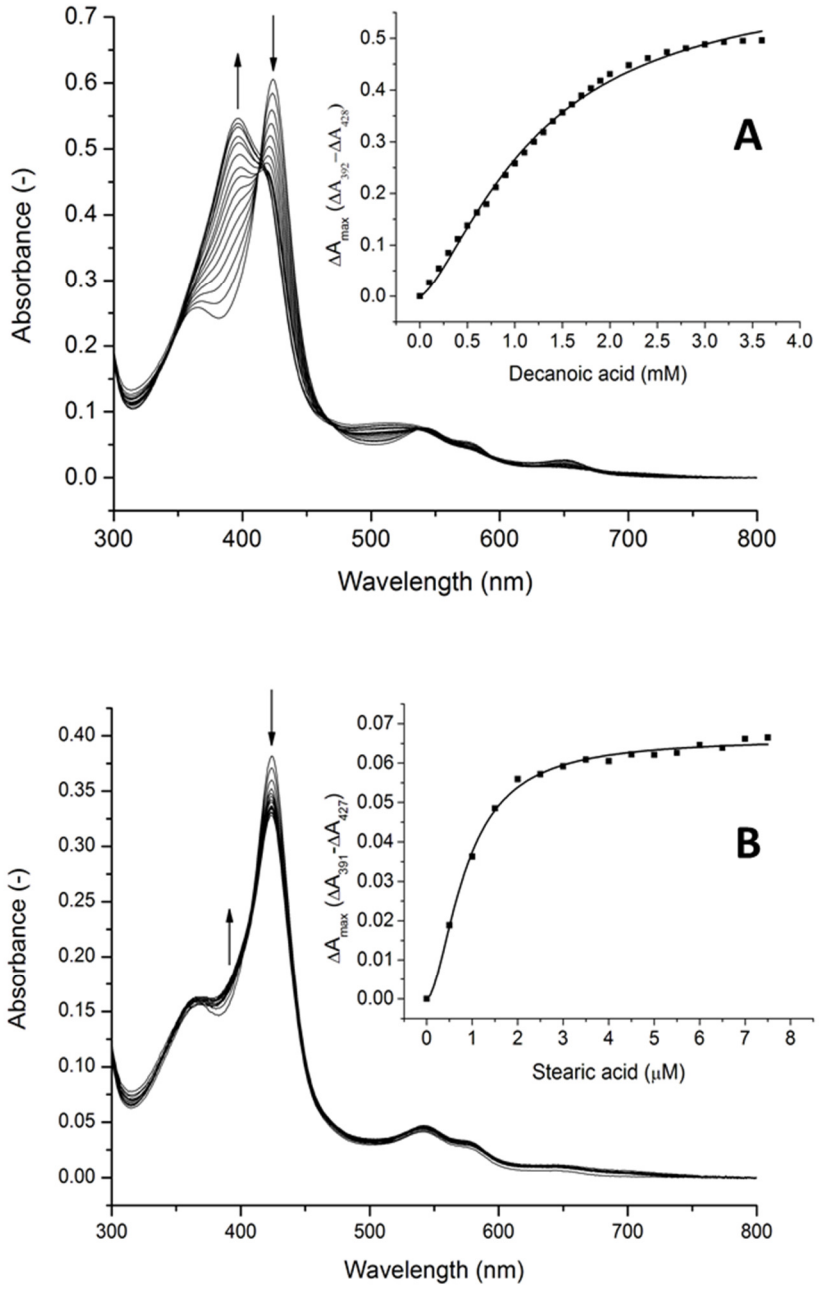

Figure 5.4. Fatty acid binding to P450 KR. Spectral titrations of P450 KR are shown with decanoic acid (8 μM P450 KR, panel A) and stearic acid (5 μM P450 KR, panel B). HS heme accumulation is more substantial with decanoic acid. The insets show fits of binding data using the Hill equation, giving K_d (K_H) values of 1.22 ± 0.06 mM and 0.9 ± 0.1 μM, respectively.

(Q-band) region at ~550 nm, consistent with the retention of cysteine thiolate proximal coordination to the ferrous heme iron. Addition of carbon monoxide produced a characteristic P450 Fe^{2+}-CO heme spectrum, with the Soret band shifted to 448 nm and a merged Q-band feature at 552 nm (**Figure 5.2**). A smaller peak at 423 nm likely indicates a small amount of the P420 form likely arising from cysteine thiol-coordination in a small proportion of the P450 KR Fe^{II}-CO complex. The NO-bound P450 KR also exhibits spectral features typical of other P450-NO adducts, with an asymmetric Soret peak at 431 nm and α- and β-bands with enhanced intensity at 577 nm and 544 nm. Using the method of Berry and Trumpower (31), an extinction coefficient of ε_{424} = 75.5 $mM^{-1}cm^{-1}$ was established for the purified, substrate-free ferric form of P450 KR.

5.4.3. Fatty acid substrate binding analysis

The binding of substrates to low-spin (LS) P450 enzymes generally displaces the weakly bound 6th ligand water and induces a shift of the spin-state of the ferric iron from LS to the high-spin (HS) state. A range of fatty acid substrates of varied chain lengths were investigated for binding to P450 KR, and all were all found to induce a LS-to-HS heme iron transition, with the Soret band shifting from 424 nm to 397 nm (see **Figure 5.4**). The K_d values for fatty acid

Fatty acid substrate	K_d	High-spin heme (%)
C10:0 (capric acid)	1.22 ± 0.06 mM	62
C12:0 (lauric acid)	172.2 ± 11.6 μM	61
C14:0 (myristic acid)	17.4 ± 0.3 μM	62
C16:0 (palmitic acid)	3.1 ± 0.1 μM	36
C18:0 (stearic acid)	0.9 ± 0.1 μM	15

Table 5.1. Dissociation constants (K_d values) for the binding of P450 KR to fatty acids.

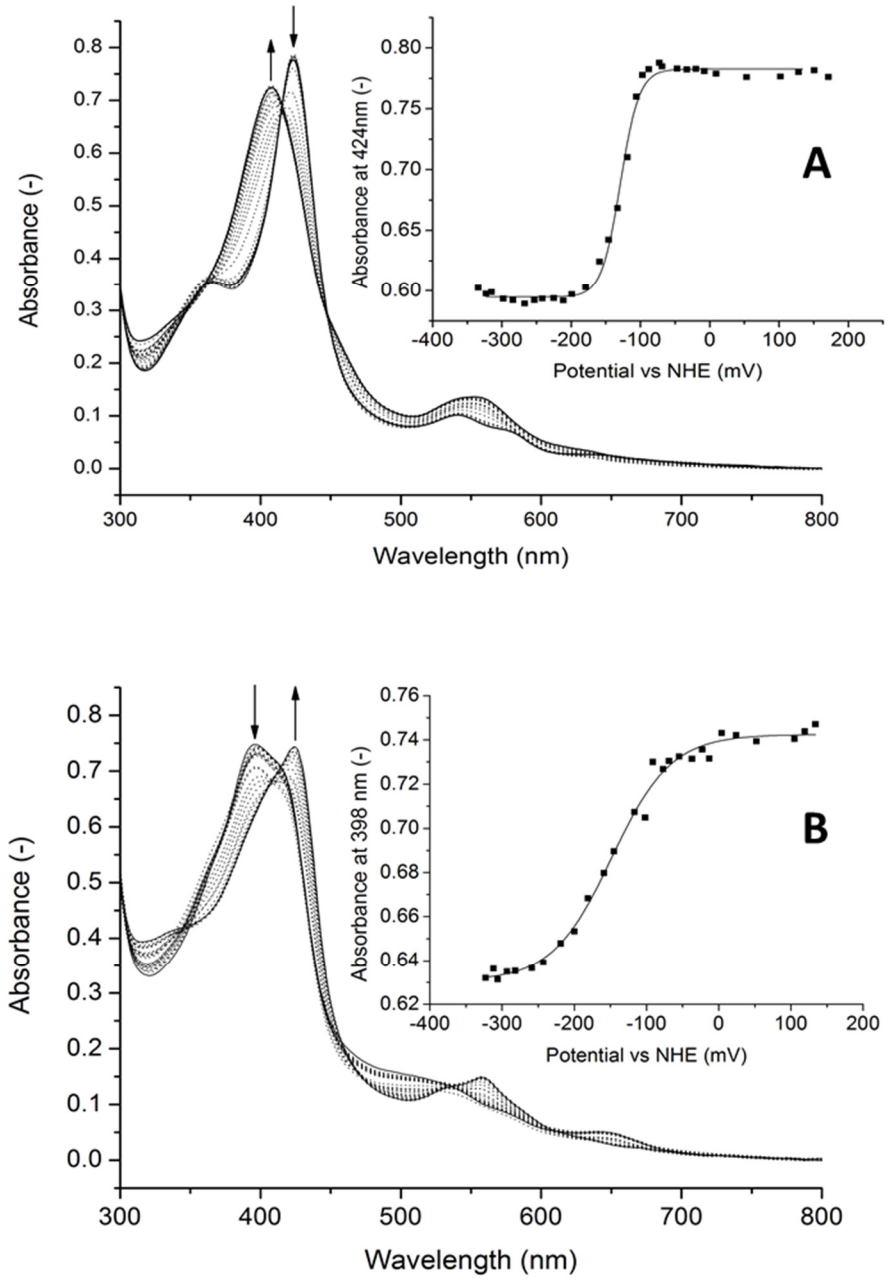

Figure 5.5. Heme iron redox potentials for substrate-free and capric acid-bound forms of P450 KR. In the main panels, arrows indicate directions of Soret band absorbance change during the course of the redox titrations. The insets show plots of heme absorbance change at relevant wavelengths at different applied potentials, with data fitted using the Nernst equation to give midpoint reduction potentials of -129 ± 3 mV vs. NHE for the substrate-free P450 KR (panel A), and -149 ± 4 mV vs. NHE for the capric acid-bound P450 KR (panel B).

binding to P450 KR and the extent of spin-state shift induced by substrates tested are shown in **Table 5.1**. The substrates C10:0 (capric acid), C12:0 (lauric acid) and C14:0 (myristic acid) display similar extents of spin-state shift (61-62%) at apparent saturation, while the extent of HS heme accumulation decreases as chain length increases to C16:0 (palmitic acid, 36%)

and C18:0 (stearic acid, 15%). This extent of spin-state shift induced by saturated fatty acids is generally lower than that observed for the alkene producing peroxygenase $OleT_{JE}$ (27-84%) (24), but it is important to note that $OleT_{JE}$ exhibits its greatest spin-state shift for the longest fatty acid substrate tested (arachidic acid, C20:0) while P450 KR apparently favours binding to the shorter chain length C10:0 to C14:0 fatty acids. The P450 KR K_d values for the tested fatty acids differ by >3 orders of magnitude (from 1.22 mM for capric acid to 0.9 µM for stearic acid). Under similar assay conditions, the K_d range for $OleT_{JE}$ is less extensive (from 2.3 µM with arachidic acid to 59.2 µM with lauric acid). These data suggest that P450 KR is a more selective enzyme compared to $OleT_{JE}$, although its general affinity for fatty acid substrates is slightly lower compared to $OleT_{JE}$.

5.4.4. Heme iron redox potential of P450 KR

Figure 5.5 shows spectra from the spectroelectrochemical (redox) titration of both substrate-free and capric acid-bound forms of P450 KR, illustrating the progressive conversion of the ferric enzymes to their ferrous state with additions of dithionite reductant. Substrate free P450 KR (**Figure 5.5A**) has its ferric heme Soret maximum at 424 nm, with the ferrous form absorbing maximally at 408 nm and with a slightly lower Soret intensity than the oxidized form. The α- and β-bands become merged into a single peak with a maximum at 550 nm and increased intensity by comparison with the oxidized enzyme. The data are consistent with cysteine thiolate coordination of the heme iron being retained in the ferrous state of substrate-free P450 KR (42,43). The capric acid-bound P450 KR in its ferric state is predominantly HS with a Soret peak at 398 nm and a shoulder at ~415 nm, reflecting the incomplete shift of the heme to a HS state. Following reduction by dithionite, the Soret peak is shifted to 424 nm with a shoulder at ~398 nm. The spectral features in the Q-band region are distinct from those seen in the spectrum for substrate-free, ferric P450 KR (**Figure 5.2**) and from those for the reduced, substrate-bound P450 KR (**Figure 5.2B**), The asymmetric Q-band feature has a peak at 558 nm, with a pronounced shoulder at ~530 nm. These spectral data are consistent with the reduced, substrate-bound P450 KR having a mixture of cysteine thiol- and thiolate-

coordination of the ferrous heme iron. The reduction of the capric acid-bound P450 KR is further confirmed by the abolition of the HS ferric heme iron-to-cysteine thiolate charge-transfer (CT) band at ~650 nm at the end of the reductive titration.

The shift in the heme iron spin state equilibrium from LS to HS is often associated with the development of a substantially more positive ferric heme iron potential, to facilitate more efficient electron transfer from the redox partner to the P450 heme. Examples include P450 BM3 (-429 to -289 mV upon arachidonic acid binding) (34) and P450cam (-300 to -170 mV upon camphor binding) (42). However, spectroelectrochemical titrations for both the substrate-free (-129 ± 3 mV vs. NHE) and capric acid-bound (-149 ± 4 mV vs. NHE) forms of P450 KR revealed quite similar midpoint potentials for the heme iron Fe^{III}/Fe^{II} couples in both cases. For P450 KR, there is clearly no substantial increase in heme iron potential associated with the accumulation of the HS ferric form. Indeed, the heme iron potential is slightly more negative in the capric acid-bound P450 KR. While the P450 KR heme iron potential values are more positive compared to those for most other bacterial P450s, they are similar to those for the alkene producing P450 $OleT_{JE}$ (-103 ± 6 mV for the substrate-free enzyme and -105 ± 6 mV for the arachidic acid-bound enzyme) (24). The similarity in the redox properties of the heme irons in these peroxygenase P450s is consistent with their performing the same types of reaction (albeit with some differences in their fatty acid substrate specificity profile). As was postulated for $OleT_{JE}$, the lack of a major change in the heme iron potential on binding capric acid substrate to P450 KR may be due to the proximity of the negatively charged carboxylate group of the substrate to the heme, counteracting any positive shift in potential resulting from accumulation of HS ferric heme iron.

5.4.5. EPR Analysis of P450 KR

Figure 5.6A shows the EPR spectra for substrate-free P450 KR and for the capric acid-, lauric acid- and myristic acid-bound forms. The substrate-free P450 KR exhibits a major set of LS ferric heme g-values at $g_z = 2.55$, $g_y = 2.26$, and $g_z = 1.85$. There is a minor proportion of a second species with $g_z = 2.72$, possibly due to two different conformations of the sixth ligand.

These g-values are distinct from those typically observed for LS microbial P450s, e.g. P450 BM3 (2.42/2.26/1.92) (43) and P450cam (2.45/2.26/1.91) (44). The spectral features of the substrate-free P450 KR may thus be consistent with a nitrogen donor (or other strong donor) as the 6th heme ligand. The high g_z values (g_z = 2.55 (major), 2.72 (minor)) observed are comparable to those for the imidazole adducts of P450 BM3 (2.61/2.25/1.83) (45) and P450cam (2.56, 2.27, 1.87) (46).

The EPR spectra of substrate-bound forms of P450 KR display significant differences to that for the substrate-free form. The spectra are more heterogeneous and composed of 3-4 different LS species (**Figure 5.6B-D**). In addition, there is some enhancement of the HS signal in each case, with some splitting of the HS g_z signal observed in the case of the capric acid (8.19/7.88) and lauric acid (8.16/7.80) complexes. These data suggest that fatty acid binding results in a more complex mixture of protein conformational states compared to the substrate-

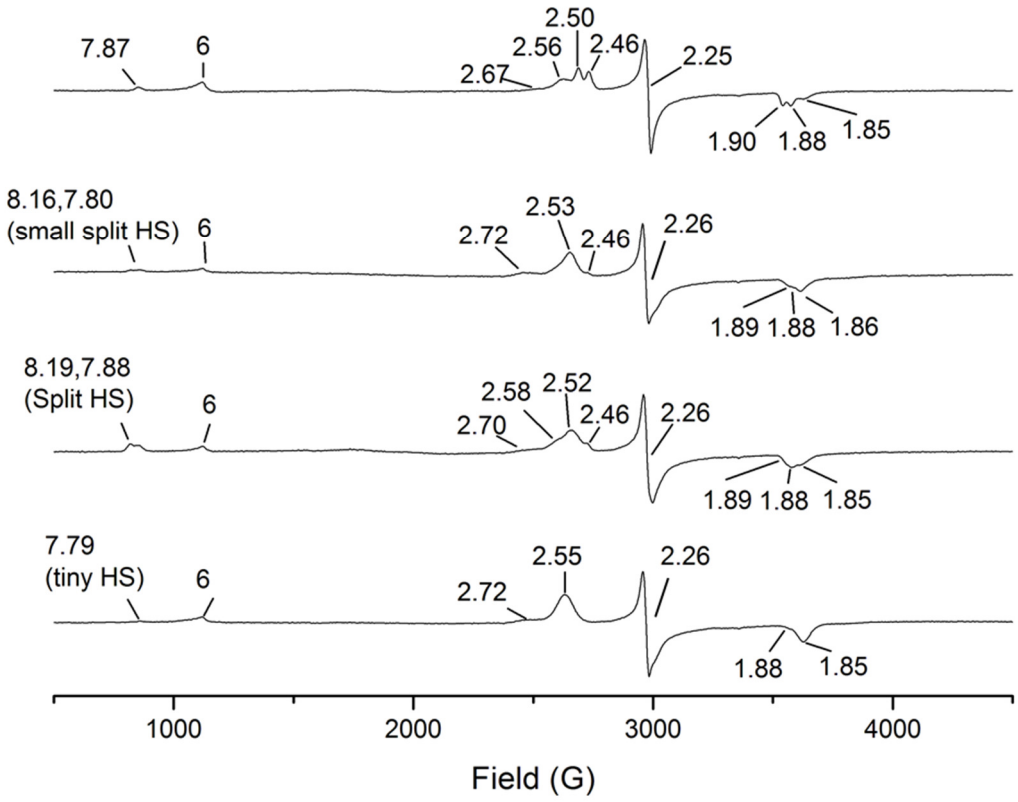

Figure 5.6. EPR spectroscopy of P450 KR. X-band EPR spectra for P450 KR. The samples from bottom to top are P450 KR, P450 KR + C10:0, P450 KR + C12:0 and P450 KR + C14:0. Relevant LS and HS g-values are indicated.

free P450 KR. This behaviour is different to that observed for the $OleT_{JE}$ peroxygenase, where the substrate-free form exhibits considerable heterogeneity with approximately 5 different LS species, whereas the arachidic acid-bound $OleT_{JE}$ has a single major LS form (2.46/2.25/1.89), in addition to a substantial HS rhombic S = 5/2 signal from two major pentacoordinate species (24). A more complex mixture of species for P450 KR in the substrate-bound form is explicable in terms of the displacement of an endogenous distal ligand from the heme iron, enabling greater protein flexibility and enabling P450 KR to explore different conformational states

5.4.6. Fatty acid conversion by P450 KR

Bioconversion of saturated fatty acids (C10-C18) by P450 KR resulted in the generation of the n-1 terminal alkene in each case, as well as amounts of the 2-hydroxylated and 3-hydroxylated carboxylic acids from each fatty acid, as determined by GC-MS analysis. In a 30 min reaction, the combination of P450 KR (4 µM) and myristic acid (0.5 mM) with 250 µM H_2O_2 resulted in

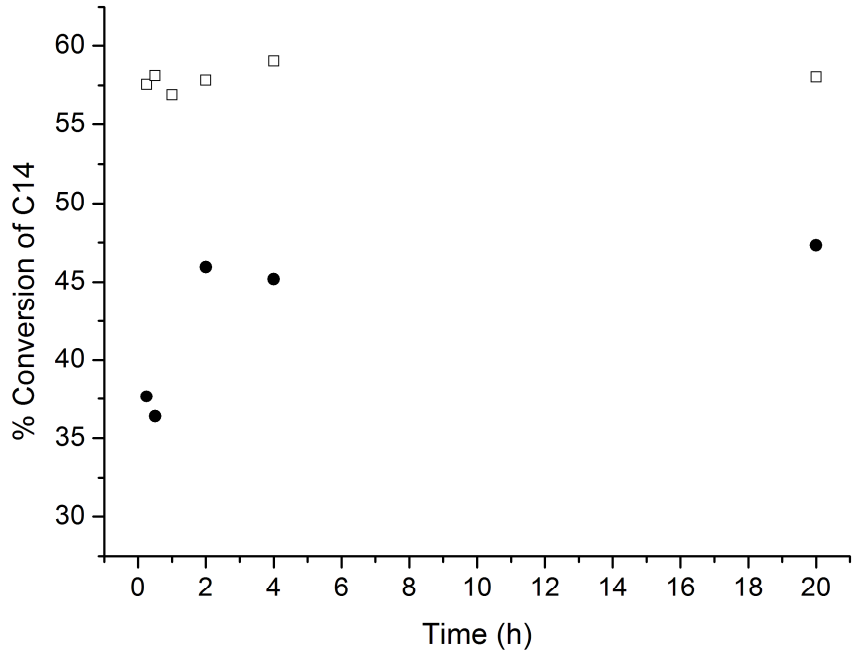

Figure 5.7. Fatty Acid Conversion by P450 KR. Conversion of myristic acid (0.5 mM) by P450 KR using either a stoichiometric amount of H_2O_2 ( ) or a photocatalytic system with FMN (•).

36 % substrate conversion. Performing the reaction using P450 KR (1 μM) and a stoichiometric amount of H_2O_2 and C14:0 (0.5 mM), with samples taken for analysis at different time intervals, showed conversion of 58 % of the substrate within 30 min of initiating the reaction (**Figure 5.7**) and a product ratio of 30% 1-tridecene, 26% 2-OH myristic acid and 44% 3-OH myristic acid. Based on a 58% conversion in 30 min, the P450 KR and H_2O_2 catalytic system exhibited a turnover number (TON) of 295 and a turnover frequency of 2.5 min^{-1}. **Table 5.2** shows comparative data for P450 KR-dependent myristic acid conversion using added H_2O_2 or a photochemical system for generating H_2O_2. Replacing H_2O_2 with the photochemical system (using 50 mM EDTA and 50 μM FMN) and keeping all other reagents constant led to a lower fatty acid conversion of up to 47 % over the same 30 min time course (**Figure 5.7**). This finding is contrary to data indicating an improvement reported for the P450 $OleT_{JE}$ system (27)

Enzyme : substrate	H_2O_2 (mM)	EDTA (mM)	FMN (μM)	Conversion (%)	TON
1:500	0.5	-	-	59	295
1:500	-	50	50	47	235
1:500	-	1	50	68	340
1:500	-	1	5	60	300
1:100	-	1	5	84	84

Table 5.2. P450 KR conversion of myristic acid (0.5 mM) using different hydrogen peroxide delivery systems. Conversion data were all calculated based on products formed after a 20 h reaction. TON indicates turnover number.

However, we considered that the high concentration of EDTA could be inhibitory for P450 KR, and found that decreasing the EDTA concentration to 1 mM improved the conversion to 68%, higher than that achieved using exogenous H_2O_2. By varying reaction conditions, we observed that a higher concentration of FMN (5 μM cf 50 μM) facilitated a slight improvement in substrate conversion (60 to 68%). Increasing the enzyme-to-substrate ratio (5-fold) increased the relative substrate conversion (from 60 to 84%). Complete conversion of

substrate was not achieved under any of the conditions investigated, despite running reactions for up to 20 h.

5.5. Discussion

In this manuscript, we present novel data describing the cloning, expression and purification of P450 KR (CYP152L1), a novel member of the CYP152 family of cytochrome P450 peroxygenase enzymes that have evolved to use hydrogen peroxide (H_2O_2) to drive catalysis using the peroxide shunt mechanism described by John Groves (48) (**Figure 5.1**). P450 KR is readily expressed in *E. coli* and was purified using a 3-step method involving separation using Ni-IDA affinity chromatography, proteolytic cleavage of its His_6-tag, and reverse Ni-IDA affinity chromatography to separate pure, untagged P450 KR from the tagged enzyme.

P450 KR exhibits an unusual P450 UV-visible spectrum with a Soret maximum at 424 nm. This suggest that there is an unusual ligand (potentially a histidine nitrogen) occupying the 6th (distal) position on the heme iron. However, the binding of fatty acids induces the accumulation of HS heme iron in P450 KR and a Soret shift to ~397 nm, suggesting that any unusual distal ligand bound can be easily displaced by substrate association. Studies of the binding of imidazole to P450 KR show that this ligand has weak affinity (K_d ~ 450 mM) and that the 424 nm band does not originate from P450 KR's retention of imidazole used in the purification of the enzyme.

P450 KR binds to fatty acids from C10:0 to C18:0 with HS heme iron formation, enabling K_d values for these substrates to be readily determined by UV-visible titrations. The longer chain C18:0 and C16:0 substrates bind much tighter than do the shorter (C10:0 to C14:0) lipids. However, the shorter substrates produce much larger shifts in the heme iron spin-state equilibrium towards HS. This may be partially explained by the much greater aqueous solubility of the shorter chain fatty acids (overcoming their weaker affinity), but a deeper understanding of these phenomena awaits the determination of P450 KR crystal structures in complex with substrate of different chain lengths. Such structural data may also provide insights into the origin of the unusual 424 nm Sore band in P450 KR.

Catalytic studies show that P450 KR is active in fatty acid substrate oxidation, and that the enzyme can generate tridecene, 2-OH myristic acid and 3-OH myristic acid from myristic acid substrate using the peroxide shunt route, of by using a photochemical system in which EDTA and FMN are used to produce H_2O_2 (49). 44% of the myristic acid was converted to tridecene using the peroxide shunt mechanism. While further research is needed to explore P450 KR catalytic efficiency with different fatty acids, the amount of alkene produced relative to hydroxylated fatty acid is less than that produce by $OleT_{JE}$ with its preferred substrates. However, in both cases protein engineering should open new avenues to fine-tuning these enzymes to make higher amounts of the alkenes, which are sought as valuable molecules for synthetic chemistry as well as potential drop-in biofuels (see section 6.2 *Further Work*).

Analysis of the reduction potentials of P450 KR in its substrate-free and capric acid-bound form revealed very positive potentials for P450 enzymes (-129 mV and -149 mV vs. NHE, respectively), and a lack of any increase in heme iron potential in the presence of a substrate. In enzymes such as the well-studied P450 BM3, a large positive shift in potential occurs on fatty acid substrate binding, and this helps facilitate electron transfer from the redox partner to the catalytically primed, substrate-bound form of this P450. The lack of a P450 KR substrate-induced positive shift in heme iron potential is a property shared with the related $OleT_{JE}$ enzyme, and these findings point to an important evolutionary schism between the monooxygenase and peroxygenase P450s. Through relying on the binding of H_2O_2 to the substrate-bound ferric heme iron in P450 KR/$OleT_{JE}$ in order to trigger catalysis, the peroxygenases have disposed of a widely conserved acid-alcohol amino acid pair (Asp251/Thr252 in P450cam) that is crucial to protonation of iron-oxo species in the typical P450 monooxygenase catalytic cycle. These residues are replaced by Arg244/Pro245 in P450 KR (with the same Arg-Pro motif found in $OleT_{JE}$ and other peroxygenase P450s), and the arginine becomes a pivotal residue for binding to the substrate carboxylate, as shown in the crystal structure of $OleT_{JE}$.

In conclusion, we present a combination of spectroscopic, thermodynamic and analytical data for a new cytochrome P450 peroxygenase enzyme (P450 KR) from the soil bacterium *Kocuria rhizophila*. Ongoing work is focused on the determination of its crystal structure, as well as on

its ability to self-aggregate, where we have shown recently that P450 KR is in a monomer-dimer equilibrium in solution.

5.6. References

1. Guengerich, F. P., and Munro, A. W. (2013) Unusual cytochrome P450 enzymes and reactions. *J. Biol. Chem.* **288**, 17065-17073
2. Denisov, I. G., Makris, T. M., Sligar, S. G., and Schlichting, I. (2005) Structure and chemistry of cytochrome P450. *Chem Rev* **105**, 2253-2277
3. Rittle, J., and Green, M. T. (2010) Cytochrome P450 compound I: capture, characterization, and C-H bond activation kinetics. *Science* **330**, 933-937
4. Groves, J. T. (2006) High-valent iron in chemical and biological oxidations. *J Inorg Biochem* **100**, 434-447
5. Munro, A. W., Girvan, H. M., Mason, A. E., Dunford, A. J., and McLean, K. J. (2013) What makes a P450 tick? *Trends Biochem. Sci.* **38**, 140-150
6. Isin, E. M., and Guengerich, F. P. (2007) Complex reactions catalyzed by cytochrome P450 enzymes. *Biochim. Biophys. Acta* **1770**, 314-329
7. Keizers, P. H., Mersinli, B., Reinle, W., Donauer, J., Hiruma, Y., Hannemann, F., Overhand, M., Bernhardt, R., and Ubbink, M. (2010) A solution model of the complex formed by adrenodoxin and adrenodoxin reductase determined by paramagnetic NMR spectroscopy. *Biochemistry* **49**, 6846-6855
8. McLean, K. J., Luciakova, D., Belcher, J., Tee, K. L., and Munro, A. W. (2015) Biological diversity of cytochrome P450 redox partner systems. *Adv. Exp. Med. Biol.* **851**, 299-317
9. Sevrioukova, I. F., Poulos, T. L., and Churbanova, I. Y. (2010) Crystal structure of the putidaredoxin reductase-putidaredoxin electron transfer complex. *J. Biol. Chem.* **285**, 13616-13620
10. Poulos, T. L., Finzel, B. C., and Howard, A. J. (1987) High-resolution crystal structure of cytochrome P450cam. *J. Mol. Biol.* **195**, 687-700

11. Munro, A. W., Girvan, H. M., and McLean, K. J. (2007) Variations on a (t)heme – novel mechanisms, redox partners and catalytic functions in the cytochrome P450 superfamily. *Nat Prod Rep* **24**, 585-609

12. Storbeck, K. H., Swart, A. C., Goosen, P., and Swart, P. (2013) Cytochrome b_5: novel roles in steroidogenesis. *Mol. Cell. Endocrinol.* **371**, 87-99

13. Narhi, L. O., and Fulco, A. J. (1987) Identification and characterization of two functional domains in cytochrome P450 BM3, a catalytically self-sufficient monooxygenase induced by barbiturates in *Bacillus megaterium*. *J. Biol. Chem.* **262**, 6683-6690

14. Girvan, H. M., Dunford, A. J., Neeli, R., Ekanem, I. S., Waltham, T. N., Joyce, M. G., Leys, D., Curtis, R. A., Williams, P., Fisher, K., Voice, M. W., and Munro, A. W. (2011) Flavocytochrome P450 BM3 mutant W1046A is a NADH-dependent fatty acid hydroxylase: implications for the mechanism of electron transfer in the P450 BM3 dimer. *Arch Biochem Biophys* **507**, 75-85

15. Neeli, R., Girvan, H. M., Lawrence, A., Warren, M. J., Leys, D., Scrutton, N. S., and Munro, A. W. (2005) The dimeric form of flavocytochrome P450 BM3 is catalytically functional as a fatty acid hydroxylase. *FEBS Lett.* **579**, 5582-5588

16. Jackson, R. G., Rylott, E. L., Fournier, D., Hawari, J., and Bruce, N. C. (2007) Exploring the biochemical properties and remediation applications of the unusual explosive-degrading P450 system XplA/B. *Proc Natl Acad Sci U S A* **104**, 16822-16827

17. Warman, A. J., Robinson, J. W., Luciakova, D., Lawrence, A. D., Marshall, K. R., Warren, M. J., Cheesman, M. R., Rigby, S. E., Munro, A. W., and McLean, K. J. (2012) Characterization of *Cupriavidus metallidurans* CYP116B1--a thiocarbamate herbicide oxygenating P450-phthalate dioxygenase reductase fusion protein. *FEBS J.* **279**, 1675-1693

18. Farrow, S. C., Hagel, J. M., Beaudoin, G. A., Burns, D. C., and Facchini, P. J. (2015) Stereochemical inversion of (*S*)-reticuline by a cytochrome P450 fusion in opium poppy. *Nat. Chem. Biol.* **(in press)**

19. Brodhun, F., Gobel, C., Hornung, E., and Feussner, I. (2009) Identification of PpoA from *Aspergillus nidulans* as a fusion protein of a fatty acid heme dioxygenase/peroxidase and a cytochrome P450. *J. Biol. Chem.* **284**, 11792-11805

20. Daiber, A., Shoun, H., and Ullrich, V. (2005) Nitric oxide reductase (P450nor) from *Fusarium oxysporum*. *J Inorg Biochem* **99**, 185-193

21. Fujishiro, T., Shoji, O., Nagano, S., Sugimoto, H., Shiro, Y., and Watanabe, Y. (2011) Crystal structure of H_2O2-dependent cytochrome $P450SP_{alpha}$ with its bound fatty acid substrate: insight into the regioselective hydroxylation of fatty acids at the alpha position. *J. Biol. Chem.* **286**, 29941-29950

22. Lee, D. S., Yamada, A., Sugimoto, H., Matsunaga, I., Ogura, H., Ichihara, K., Adachi, S., Park, S. Y., and Shiro, Y. (2003) Substrate recognition and molecular mechanism of fatty acid hydroxylation by cytochrome P450 from *Bacillus subtilis*. Crystallographic, spectroscopic, and mutational studies. *J. Biol. Chem.* **278**, 9761-9767

23. Rude, M. A., Baron, T. S., Brubaker, S., Alibhai, M., Del Cardayre, S. B., and Schirmer, A. (2011) Terminal olefin (1-alkene) biosynthesis by a novel P450 fatty acid decarboxylase from *Jeotgalicoccus* species. *Appl. Environ. Microbiol.* **77**, 1718-1727

24. Belcher, J., McLean, K. J., Matthews, S., Woodward, L. S., Fisher, K., Rigby, S. E., Nelson, D. R., Potts, D., Baynham, M. T., Parker, D. A., Leys, D., and Munro, A. W. (2014) Structure and biochemical properties of the alkene producing cytochrome P450 $OleT_{JE}$ (CYP152L1) from the *Jeotgalicoccus* sp. 8456 bacterium. *J. Biol. Chem.* **289**, 6535-6550

25. Yan, J., Liu, Y., Wang, C., Han, B., and Li, S. (2015) Assembly of lipase and P450 fatty acid decarboxylase to constitute a novel biosynthetic pathway for production of 1-alkenes from renewable triacylglycerols and oils. *Biotechnol Biofuels* **8**, 34

26. Liu, Y., Wang, C., Yan, J., Zhang, W., Guan, W., Lu, X., and Li, S. (2014) Hydrogen peroxide-independent production of alpha-alkenes by $OleT_{JE}$ P450 fatty acid decarboxylase. *Biotechnol Biofuels* **7**, 28

27. Zachos, I., Gassmeyer, S. K., Bauer, D., Sieber, V., Hollmann, F., and Kourist, R. (2015) Photobiocatalytic decarboxylation for olefin synthesis. *Chem Commun (Camb)* **51**, 1918-1921

28. Grant, J. L., Hsieh, C. H., and Makris, T. M. (2015) Decarboxylation of fatty acids to terminal alkenes by cytochrome P450 compound I. *J. Am. Chem. Soc.* **137**, 4940-4943

29. Grant, J. L., Mitchell, M. E., and Makris, T. M. (2016) Catalytic strategy for carbon-carbon bond scission by the cytochrome P450 OleT. *Proc. Natl. Acad. Sci. U. S. A.* **113**, 10049-10054

30. Kapust, R. B., Tozser, J., Fox, J. D., Anderson, D. E., Cherry, S., Copeland, T. D., and Waugh, D. S. (2001) Tobacco etch virus protease: mechanism of autolysis and rational design of stable mutants with wild-type catalytic proficiency. *Protein Eng* **14**, 993-1000

31. Berry, E. A., and Trumpower, B. L. (1987) Simultaneous determination of hemes a, b, and c from pyridine hemochrome spectra. *Anal. Biochem.* **161**, 1-15

32. Luthra, A., Denisov, I. G., and Sligar, S. G. (2011) Spectroscopic features of cytochrome P450 reaction intermediates. *Arch Biochem Biophys* **507**, 26-35

33. Dutton, P. L. (1978) Redox potentiometry: determination of midpoint potential of oxidation-reduction components of biological electron-transfer systems. *Methods Enzymol* 54, 411-435

34 Daff, S. N., Chapman, S. K., Turner, K. L., Holt, R. A., Govindaraj, S., Poulos, T. L., and Munro, A. W. (1997) Redox control of the catalytic cycle of flavocytochrome P450 BM3. *Biochemistry* **36**, 13816-13823

35. Girvan, H. M., Marshall, K. R., Lawson, R. J., Leys, D., Joyce, M. G., Clarkson, J., Smith, W. E., Cheesman, M. R., and Munro, A. W. (2004) Flavocytochrome P450 BM3 mutant A264E undergoes substrate-dependent formation of a novel heme iron ligand set. *J. Biol. Chem.* **279**, 23274-23286

36. McLean, K. J., Cheesman, M. R., Rivers, S. L., Richmond, A., Leys, D., Chapman, S. K., Reid, G. A., Price, N. C., Kelly, S. M., Clarkson, J., Smith, W. E., and Munro, A. W. (2002) Expression, purification and spectroscopic characterization of the cytochrome P450 CYP121 from *Mycobacterium tuberculosis*. *J Inorg Biochem* **91**, 527-541

37. Murugan, R., and Mazumdar, S. (2005) Structure and redox properties of the haem centre in the C357M mutant of cytochrome P450cam. *ChemBioChem* **6**, 1204-1211

38. Driscoll, M. D., McLean, K. J., Cheesman, M. R., Jowitt, T. A., Howard, M., Carroll, P., Parish, T., and Munro, A. W. (2011) Expression and characterization of *Mycobacterium tuberculosis* CYP144: common themes and lessons learned in the *M. tuberculosis* P450 enzyme family. *Biochim. Biophys. Acta* **1814**, 76-87

39. McLean, K. J., Warman, A. J., Seward, H. E., Marshall, K. R., Girvan, H. M., Cheesman, M. R., Waterman, M. R., and Munro, A. W. (2006) Biophysical characterization of the sterol demethylase P450 from *Mycobacterium tuberculosis*, its cognate ferredoxin, and their interactions. *Biochemistry* **45**, 8427-8443

40. Bui, S. H., McLean, K. J., Cheesman, M. R., Bradley, J. M., Rigby, S. E., Levy, C. W., Leys, D., and Munro, A. W. (2012) Unusual spectroscopic and ligand binding properties of the cytochrome P450-flavodoxin fusion enzyme XplA. *J. Biol. Chem.* **287**, 19699-19714

41. Sabbadin, F., Jackson, R., Haider, K., Tampi, G., Turkenburg, J. P., Hart, S., Bruce, N. C., and Grogan, G. (2009) The 1.5 Å structure of XplA-heme, an unusual cytochrome P450 heme domain that catalyzes reductive biotransformation of royal demolition explosive. *J. Biol. Chem.* **284**, 28467-28475

42. Sligar, S. G., and Gunsalus, I. C. (1976) A thermodynamic model of regulation: modulation of redox equilibria in camphor monoxygenase. *Proc Natl Acad Sci U S A* **73**, 1078-1082

43. Miles, J. S., Munro, A. W., Rospendowski, B. N., Smith, W. E., McKnight, J., and Thomson, A. J. (1992) Domains of the catalytically self-sufficient cytochrome P450 BM3. Genetic construction, overexpression, purification and spectroscopic characterization. *Biochem. J.* **288 (Pt 2)**, 503-509

44. Dawson, J. H., Andersson, L. A., and Sono, M. (1982) Spectroscopic investigations of ferric cytochrome P450cam ligand complexes. Identification of the ligand trans to cysteinate in the native enzyme. *J. Biol. Chem.* **257**, 3606-3617

45. McKnight, J., Cheesman, M. R., Thomson, A. J., Miles, J. S., and Munro, A. W. (1993) Identification of charge-transfer transitions in the optical spectrum of low-spin ferric cytochrome P450 *Bacillus megaterium*. *Eur. J. Biochem.* **213**, 683-687

46. Lipscomb, J. D. (1980) Electron paramagnetic resonance detectable states of cytochrome P450cam. *Biochemistry* **19**, 3590-3599

47 Groves, J. T. (2006) High-valent iron in chemical and biological oxidations. *J. Inorg. Biochem*. **100**, 434-437

48. Girhard, M., Kunigk, E., Tihovsky, S., Shumyantseva, V. V., and Urlacher, V. B. (2013) Light-driven biocatalysis with cytochrome P450 peroxygenases. *Biotechnol. Appl. Biochem.* **60**, 111-118

49. Paul, C. E., Churakova, E., Maurits, E., Girhard, M., Urlacher, V. B., and Hollmann, F. (2014) In situ formation of H_2O_2 for P450 peroxygenases. *Bioorg. Med. Chem.* **22**, 5692-5696

6. Conclusions

6.1. Summary

Since the isolation of $OleT_{JE}$ from *Jeotgalicoccus sp*. 8456 in 2011(1), this enzyme has attracted considerable interest as a candidate for a synthetic approach to producing drop-in biofuels (2-5). This thesis describes structural and biochemical characterisation of this alkene-producing P450 peroxygenase. Initial characterisation highlighted three residues believed to be crucial for catalysis: His85, Phe79 and Arg245. To further probe the mechanics of the enzyme, I characterised several mutants: H85Q, F79A, F79W, F79Y, R245L and R245E. I then characterised the $OleT_{JE}$ homologue P450 KR from *Kocuria rhizophila* in order to compare the properties of these two related enzymes, and to evaluate their individual effectiveness in catalysing fatty acid decarboxylation. Lastly, I generated two different $OleT_{JE}$ fusion systems, in which $OleT_{JE}$ was linked to alditol oxidase (AldO) from *Streptomyces coelicolor*.

Based on its sequence, Schirmer and coworkers assigned $OleT_{JE}$ to the CYP152 family of P450 peroxygenases (1). In this thesis, I report the further classification of $OleT_{JE}$ as CYP152L1. The amino acid sequence of $OleT_{JE}$ shows less than 40% identity to most CYP152 sequences, and slightly over 40% identity to CYP152A1 (P450BSβ) from *Bacillus subtilis* (41%) and CYP152A2 (P450CLA) from *Clostridium acetobutylicum* (40%). $OleT_{JE}$ was assigned to a distinct CYP152 clade based on its position within the phylogenetic tree. $OleT_{JE}$ was thus assigned as CYP152L1.

$OleT_{JE}$ was expressed in *E. coli* and purified by nickel-affinity chromatography. One interesting aspect of $OleT_{JE}$ is its propensity to aggregate in low salt conditions. When $OleT_{JE}$ was dialysed into low salt buffer, the protein aggregated. However, it could be resolubilised effectively into solution by addition of buffer containing 1 M NaCl. This behaviour probably relates to the halotolerant/halophilic nature of the *Jeotgalicoccus* genus from which $OleT_{JE}$ has originated (6). These properties were exploited in order to prepare the enzyme to a high degree of purity. The UV-visible spectrum of $OleT_{JE}$ resembles that of a typical P450 enzyme in its ferric low spin (LS) form, with a Soret maximum at 418 nm, and alpha and beta bands at

~566 nm and ~535 nm. Reduction of $OleT_{JE}$ with sodium dithionite results in decreased intensity of the Soret peak, and its movement to a lower wavelength of 414 nm, which is typical for formation of ferrous (Fe^{II}), cysteine thiolate-coordinated heme (7). Formation of a ferrous-carbon monoxy complex led to a shift in the Soret peak to shift to a wavelength of 449 nm, definitively establishing the enzyme as a cytochrome P450 (8,9).

Binding of fatty acid substrates to $OleT_{JE}$ was analysed by UV-visible spectroscopy. Fatty acid binding resulted in Soret peak shifts to a lower wavelength (~389 nm for arachidic acid, C20:0). This absorbance shift indicates displacement of the distal water molecule on the heme iron, resulting in the formation of a high spin (HS) heme (10). This phenomenon was not observed in the related P450 peroxygenases P450 SPα (36% sequence similarity) and P450 BSβ (41% sequence similarity), where addition of substrate did not result in any spectral change in comparison to the resting state of the enzyme (11,12). It was hypothesised that, in P450 SPα and P450 BSβ, H_2O_2 binding was responsible for displacement of the water molecule (11). The fact that $OleT_{JE}$ undergoes such extensive HS formation upon addition of several substrates suggests that it may have a different reaction mechanism to P450 SPα and P450 BSβ. The extent of heme iron spin-state shift is dependent upon the fatty acid chain length, with longer chain fatty acids inducing a higher amount of spin-state change. For example, arachidic acid binding results in ~95% HS conversion, whereas lauric acid (C12:0) binding results in only a 52% spin state shift.

Binding of inhibitors to $OleT_{JE}$ was also studied. Imidazole and cyanide were both found to shift the Soret peak to a longer wavelength (433 nm for cyanide and 424 nm for imidazole), giving type II spectral shifts (13). The reducing agent dithiothreitol (DTT) was also shown to bind to $OleT_{JE}$ in a similar manner to that described in the Royal Demolition Explosive (RDX) degrading enzyme XplA (14). DTT binding to $OleT_{JE}$ results in the appearance of Soret spectral features at 372 nm and 423 nm, with an additional shoulder at appearing at 460 nm. In this case the peak at 423 nm relates to distal coordination of the heme by DTT in its thiol form, whereas the outer (372 nm and 460 nm) “split Soret” features relate to DTT thiolate co-ordination of the heme iron (15).

Heme iron redox potentials were determined for $OleT_{JE}$ in substrate-free and substrate-bound forms by spectroelectrochemical titration, using sodium dithionite as a reductant. The heme iron Fe^{III}/Fe^{II} couple midpoint redox potential of substrate-free $OleT_{JE}$ was determined as -103 ± 6 mV vs. NHE. This value is relatively positive for a typical P450 monoxygenase (e.g. P450cam in its substrate-free state has a heme iron potential of -300 mV vs. NHE (16), and P450 BM3 has a potential of -429 mV vs. NHE (17)). The more positive potential of $OleT_{JE}$, is likely related to the environment around the cysteine-thiolate bond and to the active site structure of the heme distal pocket in $OleT_{JE}$ .Typical P450s also usually have a more positive redox potential on binding substrate and undergoing HS formation. This is often a way in which they regulate the transfer of electrons from their redox partner to the P450 heme. In P450cam for example, the heme iron potential shifts from -300 to -170 mV upon binding of camphor, allowing the transfer of electrons from the ferredoxin putidaredoxin which has a potential of -240 mV vs. NHE (16). The lack of change of redox potential upon substrate binding in $OleT_{JE}$ could be attributed to the proximity of the negatively charged fatty acid carboxylate group to the $OleT_{JE}$ heme. As $OleT_{JE}$ is a P450 peroxygenase, where catalysis is preferentially driven by H_2O_2, it is not surprising that the electrochemical properties of this enzyme differs from those of typical P450 monooxygenases. Despite these differences, $OleT_{JE}$ has been reported to act as a typical P450 monooxygenase, and fatty acid oxidation/decarboxylation reactions can be driven in a NAD(P)H-dependent manner using spinach ferredoxin and ferredoxin reductase, as well as *Pseudomonas putida* putidaredoxin and putidaredoxin reductase (CamAB) redox partner systems (5,18). However, in these cases it may be the case that heme reduction and dioxygen binding could not be as tightly regulated by substrate binding as in other P450s that have evolved to function as well coupled systems in conjunction with their native redox partners.

Stopped-flow kinetic analyses were performed with arachidic acid-bound $OleT_{JE}$, in order to determine a rate constant for the single turnover reaction of peroxide driven substrate oxidation. The rate constants for the recovery of $OleT_{JE}$ LS heme iron absorbance were measured over a range of H_2O_2 concentrations, with the highest peroxide concentration of 200 μM giving a rate constant of 167 s^{-1}. There was a linear dependence of H_2O_2 concentration

on the rate constants determined. From these data, a second order rate constant (k_{on}) of 8.0 ± 0.2 x 10^5 M^{-1} s^{-1} and a k_{off} rate constant of 8.32 ± 1.96 s^{-1} were derived. This gave a k_{off}/k_{on} ratio of 10.40 ± 2.71 μM, which describes the K_d for H_2O_2 binding.

Electron paramagnetic resonance (EPR) spectroscopy was performed in order to characterise the heme coordination environment of $OleT_{JE}$. In its substrate free form, $OleT_{JE}$ showed several LS species exhibiting rhombic anisotropy. These relate to LS ferric heme iron with proximal cysteine thiolate ligation heme, and likely with a distally ligated water molecule, although this water may interact with surrounding waters and/or residues to produce the complex LS EPR spectrum. $OleT_{JE}$ species display a range of g-values. While species with g_z values of 2.43 and 2.48 reflect species typical of LS ferric, thiolate coordinated P450s (7), those with higher g_z values (e.g. 2.55, 2.61 and 2.70) are consistent with g-values seen in P450SPα and chloroperoxidase (CPO) (12,19). The presence of multiple low spin species suggests that $OleT_{JE}$ has a large water-filled active site, and there are multiple co-ordination geometries related to the hydrogen bonding network. Substrate binding with arachidic acid lead to the formation of a rhombic HS signal indicative of a pentacoordinated heme with g-values of g_z = 7.76, g_y =3.76 and g_x =1.75. These g-values differ from EPR data reported for P450 SPα, which shows no formation of HS heme iron on fatty acid substrate binding.

Schirmer and coworkers previously published both *in vivo* and *in vitro* turnover data showing that $OleT_{JE}$ is capable of decarboxylating fatty acids of chain lengths C14:0 to C22:0 (1). Our data demonstrated *in vitro* turnover of arachidic acid to form 1-nonadecene, and in addition to existing data, showed that $OleT_{JE}$ was also capable of decarboxylating lauric acid to form 1-undecene.

Crystal structures of substrate-free and arachidic acid-bound $OleT_{JE}$ were solved to 2.3 Å and 2.5 Å, respectively. The overall structure of $OleT_{JE}$ resembles that of a typical P450 enzyme.

There is little variation in the overall fold of the substrate-free and arachidic acid-bound forms of $OleT_{JE}$, indicating that substrate binding does not induce any large structural changes. The structure of $OleT_{JE}$ is also very similar to that of P450 BSβ (r.m.s.d of 0.99 Å for 379 Ca atoms). $OleT_{JE}$ differs from P450 BSβ most significantly in the fatty acid binding channel, where the

binding pocket of $OleT_{JE}$ is elongated compared to that in P450 BSβ. The elongated pocket of $OleT_{JE}$ is due mainly to three point mutations: Ile25/Thr24, Leu41/Ala40 and Leu315/Ala317 for P450BSβ/$OleT_{JE}$ These residue changes allow extra space for $OleT_{JE}$, to accommodate longer chain fatty acids.

Three key active site region residues were highlighted from the $OleT_{JE}$ structures: His85, Phe79 and Arg245. The Arg245 residue binds to the fatty acid carboxylate, and is orientated perpendicular to the heme plane. This residue places the fatty acid in close proximity to the heme with substrate Cα and Cβ distances of 5.1 Å and 5.7 Å, respectively. In the fatty acid-bound structure, the heme is pentacoordinate, which is in accordance with UV-visible and EPR spectroscopic data. Mutagenesis of this conserved Arg residue in P450SPα (R242K and R242A variants) was reported to reduce the catalytic efficiency of the enzyme, decreasing the V_{max}/K_m values 48 fold in the R242K and 300000 fold in R242A mutants with respects to WT P450SPα (12).

The His85 residue in $OleT_{JE}$ is replaced by a glutamine residue in P450BSβ and P450 SPα. This is the most prominent amino acid substitution in the active site of $OleT_{JE}$, which led to the hypothesis that the compound II (ferryl-hydroxo) is formed from compound I (ferryl-oxo) following its protonation by His85 and the abstraction of an electron from the carboxylic acid to form a carboxylate radical. Following this, compound II could then abstract a further electron from the fatty acid substrate Cα position, leading to the formation of a diradical, with subsequent homolytic scission of the C-Cα bond. This would ultimately lead to formation of terminal alkene and CO_2 products. In P450 SPα and P450 BSβ this histidine is not present to act as a proton donor, and so Compound I would more likely abstract a hydrogen from either Cα or Cβ, and radical rebound would then lead to hydroxylation of the fatty acids in these positions as the preferred reactions (20).

His85 is sandwiched between Phe79 and the heme. Phe79 (also Phe79 in P450 BSβ) is replaced by Leu78 in P450 SPα, and was thought to play a role in the regioselectivity of fatty acid hydroxylation in P450 SPα (100% α-OH) and P450 BSβ (40% α-OH:60% β-OH)(11). Mutagenesis studies have shown that the P450 BSβ F79L mutant produces higher proportions

of α-hydroxylated fatty acid, with levels of α-OH myristic acid increasing from 43% in WT P450 BSβ to 75% in the P450 BSβ F79L mutant (12). Despite this, P450 SPα L78F did not show altered regioselectivity of hydroxylation with respect to WT P450 SPα (12). Phe79 appears to be important for catalysis in P450 BSβ and, considering its close proximity to His85, I postulated that this residue may affect the product profile of $OleT_{JE}$.

Following the initial characterisation of the wild-type enzyme, we chose to focus on the roles of the $OleT_{JE}$ active site residues His85, Phe79 and Arg245. I employed a mutagenesis strategy, and created the following mutants: H85Q, F79A, F79W, F79Y, R245L and R245E.

In this thesis, I reported the product profiles for $OleT_{JE}$ WT as well as for the H85Q, F79A, F79W, F79Y, R245L and R245E mutants. These data included total substrate conversions as well as the proportions of alkene, 2-OH fatty acid and 3-OH fatty acid products. For wild type $OleT_{JE}$, total substrate conversion was highest for shorter chain length fatty acids (C10:0, C12:0 and C14:0). These data are in accordance with data published by Li and coworkers (5). Product yield decreased as the chain length increased from C16:0 to C20:0, which is presumably due to a decrease in fatty acid solubility. For all chain lengths, the major product was the alkene, showing that decarboxylation is the major reaction catalysed by $OleT_{JE}$. 2-OH and 3-OH fatty acids were also produced in reactions with C10:0 to C18:0 substrates, with the 3-OH fatty acid being the dominant hydroxylated product for all chain lengths with the exception of stearic acid (C18:0). Interestingly, nonadecene is the only product formed from $OleT_{JE}$ reactions with arachidic acid, indicating that the product profile of the enzyme is influenced by the fatty acid chain length. A similar phenomenon is observed in P450MP from *Methylobacterium populi*, where the regioselectivity of hydroxylation is affected by the fatty acid substrate chain length (21).

Schirmer and colleagues reported that a Q85H mutation in P450BSβ led to an increase in the ratio of decarboxylation to hydroxylation from 0.19 to 0.30 (1). Despite this, our data show that the $OleT_{JE}$ H85Q mutant has a similar level of activity and product profile to WT $OleT_{JE}$. However, my data show that, upon substrate binding, the same extensive HS shift in the UV-visible spectrum seen for WT $OleT_{JE}$ does not occur in $OleT_{JE}$ H85Q. This behaviour

resembles that of P450 SPα and P450 BSβ, which also do not show significant HS conversion upon substrate binding (11,12). This finding indicates that the H85Q mutation alters the heme environment so that substrate binding does not effectively displace the distal water ligand. Alterations in the heme environment of the H85Q mutant were confirmed by EPR spectroscopy. Binding of arachidic acid to $OleT_{JE}$ H85Q produces a much smaller HS signal (g_z = 7.8, g_y = 3.75) than that induced by arachidic acid binding to WT $OleT_{JE}$. In addition, the substrate-free LS EPR spectrum of $OleT_{JE}$ H85Q is less complex than that of the substrate-free WT $OleT_{JE}$. This suggests that the H85Q mutation alters the hydrogen bonding network around the distal water molecule in $OleT_{JE}$.

A 1.8 Å resolution crystal structure was solved for the $OleT_{JE}$ H85Q mutant. Compared to WT $OleT_{JE}$, little structural change was observed upon mutagenesis of the His85 residue. However, the structure did show ligation of a distal water molecule in the presence of arachidic acid, and this water molecule was not present in the WT arachidic acid-bound structure. The presence of this water molecule in the $OleT_{JE}$ H85Q structure is consistent with UV-visible and EPR data that indicate minimal HS heme accumulation on substrate binding.

From these data it would appear that His85 does not act as a proton donor to compound I in order to catalyse decarboxylation of the fatty acid substrate. Structural data have shown that, for the WT $OleT_{JE}$ and the $OleT_{JE}$ H85Q mutant, there is a water molecule positioned in between His85 and the arachidic acid carboxylate (at distances of 3.3 and 2.7 Å respectively). It may be possible that this water molecule could act as a proton donor in the absence of His85, or in the cases of both WT $OleT_{JE}$ and the $OleT_{JE}$ H85Q mutant. Alternatively, Makris and colleagues have provided an alternative mechanism for fatty acid decarboxylation, where compound I abstracts a hydrogen atom from the fatty acid substrate, leading to the formation of compound II and a substrate radical. It has been postulated that reduction of compound II by the substrate radical could then form a carbocation species or diradical that decomposes rapidly to form the alkene product (22,23).

Structural data have shown that Phe79 sandwiches the His85 residue and the heme. This residue has also been shown to play a role in the regioselectivity of fatty acid hydroxylation in P450 BSβ (11). Makris and colleagues have also speculated that Phe79, in combination with

Phe172, may be responsible for anchoring the fatty acid substrate in a conformation that is conducive to decarboxylation (21). This assumption is based on the fact that the absence of these residues in the $OleT_{JE}$ homologue P450MP may be associated with decreased alkene formation (21). In order to further explore the role of Phe79 in $OleT_{JE}$, I generated $OleT_{JE}$ F79A, F79W and F79Y mutants.

Mutagenesis of Phe79 led to an overall decrease in activity compared to WT $OleT_{JE}$ for all of the mutants constructed. For example, WT $OleT_{JE}$ showed a total myristic acid conversion of 100%, whereas for $OleT_{JE}$ F79A this was reduced to 42%, and for $OleT_{JE}$ F79W and F79Y the percentage conversion was only 6.5% and 6.1%, respectively. Product formation was also altered, and despite the fact that 1-nonadecene remained the only product of arachidic acid turnover, the overall levels of hydroxylation increased with respect to WT $OleT_{JE}$ for other substrates. This increase in hydroxylation was less obvious for $OleT_{JE}$ F79A, where the ratio of decarboxylation to hydroxylation decreased from 2.5 to 1.1. However, no tridecene was produced from myristic acid substrate in reactions with $OleT_{JE}$ F79W and F79Y. Despite this, decarboxylase activity appeared to be restored for the $OleT_{JE}$ F79W and F79Y mutants at higher chain lengths (decarboxylase:hydroxylase ratio of 12 for F79W and 6.8 for F79 compared to a WT value of 5.4). However, decarboxylation activity was still low for F79A (decarboxylation:hydroxylation ratio of 1.5). These data indicate the importance of the Phe79 residue for effective decarboxylation of fatty acids to make terminal alkenes.

Similarly to the $OleT_{JE}$ H85Q mutant, all three Phe79 mutants showed little HS shift when titrated with fatty acid substrate, indicating that substrate binding does not induce displacement of the distal water molecule. EPR data also show a lack of HS heme iorn formation upon addition of arachidic acid substrate to $OleT_{JE}$ F79A and F79W, and only a small HS signal was observed (g_z = 7.79) for arachidic-acid bound $OleT_{JE}$ F79Y. For all Phe79 mutants, the substrate free EPR spectra are less complex than that of the substrate-free WT $OleT_{JE}$. Binding of arachidic acid does perturb the g-values for the substrate-free forms of all three Phe79 mutants, indicating that that the presence of fatty acid substrate has an effect on the hydrogen bonding network in the heme distal pocket. $OleT_{JE}$ F79W and F79Y mutants

both show a large axial HS signal relating to free iron. This highlights the instability of these two mutants, which are also prone to aggregation, especially at higher concentrations.

A 1.95 Å crystal structure of the $OleT_{JE}$ F79A mutant in complex with arachidic acid showed that there is little structural difference between $OleT_{JE}$ F79A and WT $OleT_{JE}$. Similarly to $OleT_{JE}$ H85Q, the $OleT_{JE}$ F79A structure shows that a distal water molecule is ligated to the heme (this water is not present in the WT $OleT_{JE}$ structure), which confirms that substrate binding does not displace this distal water molecule in the F79A variant.

The crystal structure of $OleT_{JE}$ showed that the Arg245 residue is crucial for the binding of the carboxylate group of the fatty acid substrate. In P450 BSβ and P450 SPα, it has also been proposed that the salt bridges formed between Arg245 and the fatty acid carboxylate are crucial for the heterolytic scission of the peroxide O-O bond (11). I prepared $OleT_{JE}$ R245L and R245E variants in order to investigate the role of this conserved residue.

Mutagenesis of Arg245 had an effect on the stability and the heme incorporation of the mutant enzymes, and both $OleT_{JE}$ R245L and R245E mutants showed decreased heme incorporation and a propensity for aggregation. Both $OleT_{JE}$ R245L and R245E showed highly diminished catalytic activity. For example, reactions with myristic acid showed a total conversion of 0.1 and 1.1% for $OleT_{JE}$ R245L and R245E mutants, respectively. At lower chain length fatty acids (C10:0 to C14:0) hydroxylation was the dominant reaction. However, the level of decarboxylation increased with C16:0 and C18:0 substrates, with 1-heptadecene being the only product from reactions with stearic acid.

The oxidised UV-visible spectrum of $OleT_{JE}$ R245E contains a Soret maximum at 423 nm, which is probably indicative of a glutamate co-ordinated heme iron (24). No spectral change was noted upon addition of fatty acids from C12:0 to C20:0 to $OleT_{JE}$ R245E. However, addition of capric acid (C10:0) to $OleT_{JE}$ resulted in ~40% HS heme iron formation. I postulated that the binding of shorter chain length fatty acids may displace a ligated glutamate more effectively than longer fatty acids. Consistent with studies on P450 BSβ, in which mutagenesis of the conserved Arg residue resulted in compromised catalysis (25), my data show that mutagenesis of this residue has a drastic effect on the stability and activity of $OleT_{JE}$.

Several terminal-alkene forming P450s were identified by Schirmer and colleagues including $OleT_{JE}$ homologues from *Corynebacterium efficiens, Methylobacterium populi and Kocuria rhizophila* (1). P450 MP from *M. populi* was subsequently characterised by Makris and colleagues (21). We have characterised P450 KR from *K. rhizophila*, which shows a 30% sequence identity to $OleT_{JE}$ and shares the His85 residue (as His89) that was previously investigated in $OleT_{JE}$.

When purified, P450KR has a ferric LS resting state with a Soret maximum at 424 nm, and alpha and beta bands at ~575 and 542 nm, respectively. The Soret band properties are typical of a P450 type II spectral shift, suggesting heme ligation by a nitrogen-containing compound, or by another strong ligand (13). This red shifted spectrum was also observed in P450 MP, which showed a Soret maximum at 422 nm with alpha and beta bands at 575 and 545 nm, respectively (21). These observations may indicate that these unusual spectral features are related to an altered co-ordination environment around the heme in these enzymes.

Reduction of P450 KR with sodium dithionite caused the Soret peak to shift to a wavelength of 410 nm with a merging of the features in the Q-band region at 550 nm. Binding of reduced P450 KR to carbon monoxide led to the formation of a ferrous carbon-monoxy complex with a Soret maximum at 448 nm, and with a much smaller peak at 420 nm consistent with cysteine thiol coordination of the heme iron in a minor proportion of the enzyme. Fatty acid binding studies using UV-visible spectroscopy also showed that fatty acids from C10:0 to C18:0 induced a HS shift, with the greatest extent of HS shift being produced by the addition of capric acid.

Heme iron redox potentials were obtained by spectroelectrochemical titrations of P450 KR in its substrate-free and capric acid-bound forms. The substrate-free form of the enzyme had a Fe^{III}/Fe^{II} midpoint reduction potential of 129 ± 4 mV vs. NHE, whereas the capric acid-bound P450 KR had a potential of -149 ± 6 mV vs. NHE. The slightly more negative potential shown by the capric acid bound P450 KR is atypical of a P450 enzyme, where substrate binding often makes the heme iron potential more positive in order to facilitate electron transfer from the redox partner to enable oxidative catalysis. P450 KR is similar to $OleT_{JE}$ in this respect, as $OleT_{JE}$ also does not undergo a significant change in redox potential in its substrate-bound

form. This behaviour is likely due to the presence of the substrate carboxylate in the heme distal pocket and its effect in offsetting any reduction potential increase associated with HS heme formation.

P450 KR is capable of converting capric acid, lauric acid, myristic acid, palmitic acid and stearic acid to products, with each fatty acid substrate producing the corresponding alkene, 2-OH fatty acid and 3-OH fatty acid. Reactions set up with 1 mM P450 KR, 0.5 mM myristic acid and 0.5 mM H_2O_2 led to a 58% conversion of the substrate, with products comprised of 30% tridecene, 26% 2-OH myristic acid and 44% 3-OH myristic acid. These data indicate that P450 KR primarily hydroxylates myristic acid, and is less effective at decarboxylating fatty acids than is $OleT_{JE}$, which has a myristic acid product profile of 72% tridecene, 3.3% 2-OH myristic acid and 25% 3-OH myristic acid. We have also used a photochemical method of driving P450 KR turnover by *in situ* generation of H_2O_2 by flavin-mediated reduction of O_2 (26,27). In this system, light was shone on a reaction mixture containing 5 μM P450 KR, 1 mM EDTA, 50 μM FMN and 0.5 mM myristic acid, this led to an 84% conversion of the substrate. In this case it would appear that using a photochemical method to slowly produce H_2O_2 may enable a more complete oxidative conversion of the fatty acid substrates than when peroxide is added directly to the reaction mixture.

Despite the fact that $OleT_{JE}$ efficiently functions as a P450 peroxygenase, using H_2O_2 to drive the decarboxylation of fatty acids, little is known about $OleT_{JE}$'s tolerance to peroxide. I performed heme stability studies on $OleT_{JE}$ in the presence of various concentrations of H_2O_2 (10-1000 μM), and compared the results to those obtained for P450 BM3. My data showed that, at low concentrations of H_2O_2 (<125 μM), $OleT_{JE}$ is relatively resistant to destructive oxidation of the heme prosthetic group, and appears to be more tolerant to the effects of H_2O_2 than is the P450 monoxygenase BM3. Despite this, at high H_2O_2 concentrations $OleT_{JE}$ undergoes substantial heme oxidative modification. This is in agreement with other studies on $OleT_{JE}$ that have shown that high concentrations of hydrogen peroxide can compromise catalysis (26).

I also reported the development of a novel enzymatic system that would allow slow and controlled release of H_2O_2 to drive catalysis by $OleT_{JE}$, thus limiting damage to the enzyme, and optimising substrate conversion. In this system, alditol oxidase (AldO) from *Streptomyces coelicolor* A3(2) was fused to $OleT_{JE}$. AldO is a polyol oxidase that produces H_2O_2 as a co-product from reactions with substrates that include glycerol, sorbitol, xylitol and diols such 1,2-hexanediol and 1,2 propanediol (28,29). The rationale for this fusion was that addition of an AldO substrate to the $OleT_{JE}$/AldO fusion enzyme would lead to controlled formation of H_2O_2, which would in turn drive the decarboxylation of fatty acids to form terminal alkenes. I prepared two constructs: $OleT_{JE}$-HRV3C-AldO and $OleT_{JE}$-αhelix-AldO. In $OleT_{JE}$-HRV3C-AldO, the presence of a HRV3C specific site allowed proteolytic cleavage of the linker in order to produce stoichiometric amounts its $OleT_{JE}$ and AldO components. This allowed for the comparison of the activity of the fused system with that for of the separate $OleT_{JE}$ and AldO entities. In $OleT_{JE}$-αhelix-AldO, $OleT_{JE}$ and AldO are fused by a rigid α-helical linker, which has previously been shown to increase the expression of human growth hormone (hGH)/transferrin (Tf) fusion proteins (30,31). I showed that glycerol, sorbitol and xylitol can be used to drive the decarboxylation of myristic acid in the $OleT_{JE}$/AldO fusion system, and that these reactions led to higher levels of substrate conversion than when H_2O_2 was directly added to the system. Glycerol is an inexpensive waste product from biofuel production, making it an industrially viable substrate (32,33).

I also performed kinetic analyses with 1% glycerol and 0.5 mM myristic acid, and found that the rate of fatty acid oxidation was highest for the $OleT_{JE}$-αhelix-AldO (k = 0.48 ± 0.02 min^{-1}), which showed a 98 ± 3% conversion of myristic acid. The rate of fatty acid conversion was also higher for fused $OleT_{JE}$-HRV3C-AldO (0.38 ± 0.05 min^{-1}) than when the two domains were cleaved by incubation with HRV3C protease (0.15 ± 0.01 min^{-1}), suggesting that there is a catalytic advantage to fusing the $OleT_{JE}$ and AldO proteins.

During kinetic analysis of the $OleT_{JE}$/AldO system, I observed the disappearance of 2-OH and 3-OH myristic acid products shortly after (~2 minutes) the start of the incubation. I hypothesised that this was due to the secondary turnover of 2-OH myristic acid and 3-OH myristic acid primary products. To investigate this possibility, I prepared reactions using either

i) 1 μM $OleT_{JE}$/500 μM H_2O_2 or ii) 5 μM $OleT_{JE}$-HRV3C-AldO/1% glycerol and added 2-OH myristic acid or 3-OH myristic acid as substrates. After 30 minutes incubation, the concentration of 2-OH myristic acid had drastically decreased, with GC/Q-TOF analysis showing the formation of two further products. One of the products was assigned as tridec-1-en-1-ol, indicating that $OleT_{JE}$ is capable of decarboxylating the 2-OH myristic acid. The other peak corresponded to the formation of 2-hydroxytetradec-2-enoic acid, showing that $OleT_{JE}$ is able to desaturate the Cα-Cβ bond. $OleT_{JE}$ also catalysed the complete conversion of 3-OH myristic acid, and appeared to perform Cα-Cβ desaturation and further hydroxylation at the Cγ position to yield the 3,4 dihydroxytetradec-2-enoic acid product.

6.2. Further Work

Industrial utilisation of $OleT_{JE}$ for the production of biofuels

$OleT_{JE}$ has been expressed and used to produce alkene titres of 97.6 mg/L and 3.7 mg/L in *E.coli* and *Saccharomyces cerevisiae* respectively (5,34). However, these levels fall far below those required for industrial use. For comparison, specific pentadecane yields of 80 mg/L (with a total alkane yield of 300 mg/L) have already been achieved in *E.coli* by Schirmer et al (35), corresponding to a pentadecene yield of 0.0027 g/g glucose (36). This accounts for <1% of the maximum theoretical yield of 0.3 g pentadecene/g glucose, as calculated by i*n silico* predictions of *E.coli* optimised for the production of alkanes (37). The economic viability of generating hydrocarbons from microorganisms is dependent upon the cost of the carbon source required. Considering this maximum predicted yield, Pfleger et al predicted that glucose would have to cost ≤$0.18/Lb in order to cover the cost of the raw materials, based on the price of biodiesel in January 2014 at $0.64 (37).

Further development is required to achieve an effective $OleT_{JE}$-based system. In order to develop such a system, several metabolic engineering strategies could be applied, including: blocking competing pathways; optimizing enzyme activity or expression; balancing cofactor synthesis; balancing reducing power; deregulating fatty acid biosynthesis; driving fatty acid biosynthesis; and removing or sequestering products to avoid toxicity (37).

Altering $OleT_{JE}$ substrate specificity and enabling use of shorter chain length fatty acids

Studies reported in this thesis have demonstrated that $OleT_{JE}$ is a robust and catalytically efficient alkene-producing fatty acid decarboxylase that would be suited to a synthetic biology approach to generating “drop in biofuels”. However, as highlighted in this thesis, $OleT_{JE}$ also functions as a fatty acid hydroxylase, producing 2-OH and 3-OH fatty acids, and the amount of alkene production only represents 63-85% of the total product (based on analysis of the turnover of fatty acids C10:0 to C16:0). Hence, there is scope for improvement of this system and in order to improve the catalytic activity of $OleT_{JE}$ further towards decarboxylation of fatty acids.

The active site structure of $OleT_{JE}$ is very similar to that of the fatty acid hydroxylase P450 BSβ, and it is likely that that the greater decarboxylase activity in $OleT_{JE}$ is attributed to subtle secondary structure changes that we are unable to detect by medium resolution X-ray crystallography, or other subtle changes that alter e.g. active site composition, positions of water molecules and molecular interactions. In this case, it would seem appropriate to use a directed evolution approach to order $OleT_{JE}$ through random mutagenesis in order to identify mutants that have improved decarboxylase activity. To achieve this outcome, it would be necessary to employ a robust and efficient method of screening candidate mutants. This could be done by performing GC/MS analysis on Fad D deletion strain of *E. coli* that has been transformed with candidate genes. Alternatively a flourescence *in situ* biosensor system could be used to screen quickly for increased levels of alkenes made by $OleT_{JE}$ mutant transformants (38). Substrate conversion studies highlighted that $OleT_{JE}$ produces a larger proportion of alkene product compared with P450 KR. Therefore, it would be reasonable to focus engineering efforts soley on $OleT_{JE}$ rather than performing mutagenesis with P450 KR.

As I have reported, $OleT_{JE}$ is only capable of performing peroxide-mediated decarboxylation of fatty acids in the range from C10:0 to C20:0 (Although C22:0 was also described as a substrate by Schirmer and colleagues (1). Although these mid-chain length alkenes have uses within the petrochemical industry as lubricants and fuel additives, there is an industrial demand for shorter chain terminal-alkenes. The crystal structure of $OleT_{JE}$ highlights that the fatty acid binding pocket in this P450 in long and is comprised of hydrophobic residues that are favourable to the binding of mid- and long-chain fatty acids. It may be possible to rationally engineer the $OleT_{JE}$ substrate binding channel to enable the substrate chain length preference to switch towards shorter chain substrates. However, mutating hydrophobic residues to amino acids with a more hydrophilic nature might simply disfavour binding of all fatty acid chain lengths. In this respect, a directed evolution approach would appear to be the best option.

In chapter 4, I described $OleT_{JE}$/AldO fusion protein systems that were effective at driving the decarboxylation of fatty acids through the addition of glycerol as an alditol oxidase substrate that leads to H_2O_2 production. The *in vitro* data that I presented showed that these were efficient systems that performed high levels of fatty acid conversion. To test whether this

system would be viable in an industrial setting, it would also be necessary to perform *in vivo* studies in order to establish the effectiveness of the systems in a bacterial (likely *E. coli*) host organism. In addition it would be beneficial to further engineer the $OleT_{JE}$/AldO fusion systems in order to improve their expression in *E. coli*. This could be done by e.g. altering the length and amino acid composition of the linker regions, investigating other promoter/polymerase expression systems and looking at different host strains. Some previous studies have also found that domain order is more important than the composition of the linker region for designing an effective fusion protein, and therefore swapping the domain order (N-terminal AldO and C-terminal $OleT_{JE}$ system) may also improve expression (39).

Alternatively, a SpyTag/SpyCatcher system could be used to increase the proportion of covalently bound $OleT_{JE}$/AldO(40). The SpyTag/SpyCatcher system was developed by Howarth and colleagues (40), and is based on the *Streptococcus pyogenes* second immunoglobulin-like collagen adhesion domain (CnaB2) from the fibronectin binding protein FbaB (40). Engineering of the CnaB2 domain led to the formation of a 15 kDa SpyCatcher domain, and a small 13 amino acid peptide "SpyTag", which are able to covalently bind to one another through the spontaneous formation of an isopeptide bond. It may be possible to fuse SpyCatcher to either $OleT_{JE}$ or AldO, and express the other domain (either either $OleT_{JE}$ or AldO) with the SpyTag. These constructs could be expressed separately, and then covalently attached post-translationally in the cell.

This thesis has described the initial characterisation of $OleT_{JE}$ as well as the $OleT_{JE}$ homologue P450 KR. In addition, a novel fusion system has been reported that utilises glycerol in order to drive the decarboxylation of fatty acids. Further, $OleT_{JE}$ was used in studies of the oxidation of primary fatty acid metabolites (2- and 3-OH fatty acids) to identify novel desaturated, decarboxylated and dihydroxylated secondary metabolites; simultaneously explaining the unexpected decrease in the amounts of the primary metabolites that occurs in the early stages of the reaction. These studies have enabled a greater understanding of the catalytic versatility of $OleT_{JE}$, highlighting its further potential applications in fine chemical synthesis. As an industrially useful enzyme, $OleT_{JE}$ has attracted considerable interest since its discovery in 2011, and there is clearly much scope for further engineering of $OleT_{JE}$ to improve its stability,

productivity and fatty acid chain length selectivity; as well as for the development of a suitable host system to allow $OleT_{JE}$ to produce terminal alkenes *in vivo* and for these systems to be utilised in the production of "drop-in" biofuels.

6.3. References

1. Rude, M. A., Baron, T. S., Brubaker, S., Alibhai, M., Del Cardayre, S. B., and Schirmer, A. (2011) Terminal olefin (1-alkene) biosynthesis by a novel p450 fatty acid decarboxylase. *Appl Environ Microbiol* **77**, 1718-1727

2. Zhang, F., Rodriguez, S., and Keasling, J. D. (2011) Metabolic engineering of microbial pathways for advanced biofuels production. in *Curr Opin Biotechnol*, 2011 Elsevier Ltd, England. pp 775-783

3. Wang, W., and Lu, X. (2013) Microbial Synthesis of Alka(e)nes. *Front Bioeng Biotechnol* **1**, 10

4. Yan, J., Liu, Y., Wang, C., Han, B., and Li, S. (2015) Assembly of lipase and P450 fatty acid decarboxylase to constitute a novel biosynthetic pathway for production of 1-alkenes from renewable triacylglycerols and oils. *Biotechnol Biofuels* **8**, 34

5. Liu, Y., Wang, C., Yan, J., Zhang, W., Guan, W., Lu, X., and Li, S. (2014) Hydrogen peroxide-independent production of alpha-alkenes by OleTJE P450 fatty acid decarboxylase. *Biotechnol Biofuels* **7**, 28

6. Yoon, J. H., Lee, K. C., Weiss, N., Kang, K. H., and Park, Y. H. (2003) Jeotgalicoccus halotolerans gen. nov., sp. nov. and Jeotgalicoccus psychrophilus sp. nov., isolated from the traditional Korean fermented seafood jeotgal. *Int J Syst Evol Microbiol* **53**, 595-602

7. Luthra, A., Denisov, I. G., and Sligar, S. G. (2011) Spectroscopic features of cytochrome P450 reaction intermediates. *Arch Biochem Biophys* **507**, 26-35

8. Omura, T. (2011) Recollection of the early years of the research on cytochrome P450. *Proc Jpn Acad Ser B Phys Biol Sci* **87**, 617-640

9. Omura, T., and Sato, R. (1964) The carbon monoxide-binding pigment of liver microsomes. I. Evidence for its hemoprotein nature. *J Biol Chem* **239**

10. Munro, A. W., Girvan, H. M., and McLean, K. J. (2007) Variations on a (t)heme--novel mechanisms, redox partners and catalytic functions. *Nat Prod Rep* **24**, 585-609

11. Lee, D. S., Yamada, A., Sugimoto, H., Matsunaga, I., Ogura, H., Ichihara, K., Adachi, S., Park, S. Y., and Shiro, Y. (2003) Substrate recognition and molecular mechanism of fatty acid hydroxylation by. *J Biol Chem* **278**, 9761-9767

12. Fujishiro, T., Shoji, O., Nagano, S., Sugimoto, H., Shiro, Y., and Watanabe, Y. (2011) Crystal structure of H2O2-dependent cytochrome P450SPalpha with its bound fatty. *J Biol Chem* **286**, 29941-29950

13. Denisov, I. G., Makris, T. M., Sligar, S. G., and Schlichting, I. (2005) Structure and chemistry of cytochrome P450. *Chem Rev* **105**, 2253-2277

14. Bui, S. H., McLean, K. J., Cheesman, M. R., Bradley, J. M., Rigby, S. E., Levy, C. W., Leys, D., and Munro, A. W. (2012) Unusual spectroscopic and ligand binding properties of the cytochrome P450-flavodoxin fusion enzyme XplA. in *J Biol Chem*. pp 19699-19714

15. Sono, M., Andersson, L. A., and Dawson, J. H. (1982) Sulfur donor ligand binding to ferric cytochrome P-450-CAM and myoglobin. Ultraviolet-visible absorption, magnetic circular dichroism, and electron paramagnetic resonance spectroscopic investigation of the complexes. *J Biol Chem* **257**, 8308-8320

16. Sligar, S. G., and Gunsalus, I. C. (1976) A thermodynamic model of regulation: modulation of redox equilibria in camphor monoxygenase. *Proc Natl Acad Sci U S A* **73**, 1078-1082

17. Miles, J. S., Munro, A. W., Rospendowski, B. N., Smith, W. E., McKnight, J., and Thomson, A. J. (1992) Domains of the catalytically self-sufficient cytochrome P-450 BM-3. Genetic construction, overexpression, purification and spectroscopic characterization. *J Biochem* **288**, 503-509

18. Dennig, A., Kuhn, M., Tassoti, S., Thiessenhusen, A., Gilch, S., Bulter, T., Haas, T., Hall, M., and Faber, K. (2015) Oxidative Decarboxylation of Short-Chain Fatty Acids to 1-Alkenes. *Angew Chem Int Ed Engl* **54**, 8819-8822

19. Hollenberg, P. F., Hager, L. P., Blumberg, W. E., and Peisach, J. (1980) An electron paramagnetic resonance study of the high and low spin forms of chloroperoxidase. *J Biol Chem* **255**, 4801-4807

20. Groves, J. T. (2006) High-valent iron in chemical and biological oxidations. *J Inorg Biochem* **100**, 434-447

21. Amaya, J. A., Rutland, C. D., and Makris, T. M. (2016) Mixed regiospecificity compromises alkene synthesis by a cytochrome P450 peroxygenase from Methylobacterium populi. *J Inorg Biochem* **158**, 11-16

22. Grant, J. L., Mitchell, M. E., and Makris, T. M. (2016) Catalytic strategy for carbon-carbon bond scission by the cytochrome P450 OleT. *Proc Natl Acad Sci U S A* **113**, 10049-10054

23. Grant, J. L., Hsieh, C. H., and Makris, T. M. (2015) Decarboxylation of fatty acids to terminal alkenes by cytochrome P450 compound I. *J Am Chem Soc* **137**, 4940-4943

24. Girvan, H. M., Marshall, K. R., Lawson, R. J., Leys, D., Joyce, M. G., Clarkson, J., Smith, W. E., Cheesman, M. R., and Munro, A. W. (2004) Flavocytochrome P450 BM3 mutant A264E undergoes substrate-dependent formation of a novel heme iron ligand set. *J Biol Chem* **279**, 23274-23286

25. Matsunaga, I., Ueda, A., Sumimoto, T., Ichihara, K., Ayata, M., and Ogura, H. (2001) Site-Directed Mutagenesis of the Putative Distal Helix of Peroxygenase Cytochrome P450. *Arch Biochem Biophys* **394**, 45-53

26. Zachos, I., Gassmeyer, S. K., Bauer, D., Sieber, V., Hollmann, F., and Kourist, R. (2015) Photobiocatalytic decarboxylation for olefin synthesis. *Chem Commun (Camb)* **51**, 1918-1921

27. Girhard, M., Kunigk, E., Tihovsky, S., Shumyantseva, V. V., and Urlacher, V. B. (2013) Light-driven biocatalysis with cytochrome P450 peroxygenases. *Biotechnol Appl Biochem* **60**, 111-118

28. van Hellemond, E. W., Vermote, L., Koolen, W., Sonke, T., Zandvoort, E., Heuts, D. P. H. M., Janssen, D. B., and Fraaije, M. W. (2009) Exploring the biocatalytic scope of alditol oxidase from Streptomyces coelicolor. *Adv Synth Catal* **351**, 1523-1530

29. Heuts, D. P., van Hellemond, E. W., Janssen, D. B., and Fraaije, M. W. (2007) Discovery, characterization, and kinetic analysis of an alditol oxidase from Streptomyces coelicolor. *J Biol Chem* **282**, 20283-20291

30. Chen, X., Zaro, J., and Shen, W.-C. (2013) Fusion Protein Linkers: Property, Design and Functionality. *Adv Drug Deliv Rev* **65**, 1357-1369

31. Amet, N., Lee, H.-F., and Shen, W.-C. (2009) Insertion of the Designed Helical Linker Led to Increased Expression of Tf- based fusion proteins. *Pharm Res* **26**, 523-528

32. Mattam, A. J., Clomburg, J. M., Gonzalez, R., and Yazdani, S. S. (2013) Fermentation of glycerol and production of valuable chemical and biofuel molecules. *Biotechnol Lett* **35**, 831-842

33. Yazdani, S. S., and Gonzalez, R. (2007) Anaerobic fermentation of glycerol: a path to economic viability for the biofuels industry. *Curr Opin Biotechnol* **18**, 213-219

34. Chen B, Lee DY, Chang MW. (2015) Combinatorial metabolic engineering of Saccharomyces cerevisiae for terminal alkene production. *Metabolic engineering* **30**, 53-61

35. Schirmer A, Rude MA, Li X, Popova E, Del Cardayre SB. (2010) Microbial biosynthesis of alkanes. *Science* **30**, 559-62

36. d'Espaux L, Mendez-Perez D, Li R, Keasling JD. (2015) Synthetic biology for microbial production of lipid-based biofuels. *Current opinion in chemical biology* **31**, 58-65

37. Pfleger BF, Gossing M, Nielsen J. (2015) Metabolic engineering strategies for microbial synthesis of oleochemicals. *Metabolic engineering* **31**,1-1

38. Wu, W., Zhang, L., Yao, L., Tan, X., Liu, X., and Lu, X. (2015) Genetically assembled fluorescent biosensor for in situ detection of bio-synthesized alkanes. *Sci Rep* **5**, 10907

39. Bakkes, P. J., Biemann, S., Bokel, A., Eickholt, M., Girhard, M., and Urlacher, V. B. (2015) Design and improvement of artificial redox modules by molecular fusion of flavodoxin and flavodoxin reductase from Escherichia coli. *Sci Rep* **5**, 12158

40. Zakeri, B., Fierer, J. O., Celik, E., Chittock, E. C., Schwarz-Linek, U., Moy, V. T., and Howarth, M. (2012) Peptide tag forming a rapid covalent bond to a protein, through engineering a bacterial adhesin. *Proc Natl Acad Sci U S A* **109**, E690-697